

Northern Power NW 1500 Direct-Drive Generator

April 12, 2001 — September 30, 2006

G. Bywaters, P. Mattila, D. Costin, J. Stowell,
V. John, S. Hoskins, J. Lynch, T. Cole, A. Cate,
C. Badger, and B. Freeman
Northern Power Systems, Inc.
Waitsfield, Vermont

Subcontract Report
NREL/SR-500-40177
October 2007

NREL is operated by Midwest Research Institute • Battelle Contract No. DE-AC36-99-GO10337



Northern Power NW 1500 Direct-Drive Generator

Subcontract Report
NREL/SR-500-40177
October 2007

April 12, 2001 — September 30, 2006

G. Bywaters, P. Mattila, D. Costin, J. Stowell,
V. John, S. Hoskins, J. Lynch, T. Cole, A. Cate,
C. Badger, and B. Freeman
Northern Power Systems, Inc.
Waitsfield, Vermont

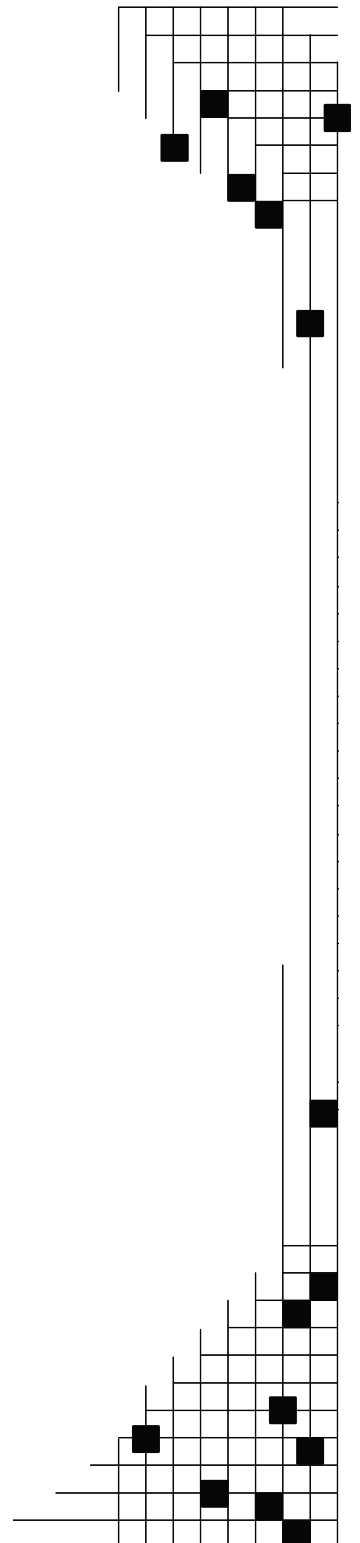
NREL Technical Monitor: Scott Schreck

Prepared under Subcontract No. YCX-1-30209-02

National Renewable Energy Laboratory
1617 Cole Boulevard, Golden, Colorado 80401-3393
303-275-3000 • www.nrel.gov

Operated for the U.S. Department of Energy
Office of Energy Efficiency and Renewable Energy
by Midwest Research Institute • Battelle

Contract No. DE-AC36-99-GO10337



NOTICE

This report was prepared as an account of work sponsored by an agency of the United States government. Neither the United States government nor any agency thereof, nor any of their employees, makes any warranty, express or implied, or assumes any legal liability or responsibility for the accuracy, completeness, or usefulness of any information, apparatus, product, or process disclosed, or represents that its use would not infringe privately owned rights. Reference herein to any specific commercial product, process, or service by trade name, trademark, manufacturer, or otherwise does not necessarily constitute or imply its endorsement, recommendation, or favoring by the United States government or any agency thereof. The views and opinions of authors expressed herein do not necessarily state or reflect those of the United States government or any agency thereof.

Available electronically at <http://www.osti.gov/bridge>

Available for a processing fee to U.S. Department of Energy and its contractors, in paper, from:

U.S. Department of Energy
Office of Scientific and Technical Information
P.O. Box 62
Oak Ridge, TN 37831-0062
phone: 865.576.8401
fax: 865.576.5728
email: <mailto:reports@adonis.osti.gov>

Available for sale to the public, in paper, from:

U.S. Department of Commerce
National Technical Information Service
5285 Port Royal Road
Springfield, VA 22161
phone: 800.553.6847
fax: 703.605.6900
email: orders@ntis.fedworld.gov
online ordering: <http://www.ntis.gov/ordering.htm>

This publication received minimal editorial review at NREL



Executive Summary

The National Renewable Energy Laboratory's (NREL) Wind Partnerships for Advanced Component Technologies (WindPACT) project sought to advance wind turbine technology by exploring innovative concepts in drivetrain design. A team led by Northern Power Systems (Northern) of Waitsfield, Vermont, was chosen to perform this work under subcontract YCX-1-30209-02. The team set project objectives to identify, design, and test a megawatt (MW)-scale drivetrain with the lowest overall life-cycle cost. The project comprised three phases:

- Preliminary study of alternative drivetrain designs (Phase I)
- Detailed design development (Phase II)
- Proof of concept fabrication and test (Phase III).

This report summarizes the results of all three phases of this project.

Participants

The WindPACT project was conducted under directive from NREL, with active participation from personnel at the National Wind Technology Center (NWTC) at Golden, Colorado. Northern Power Systems, the prime subcontractor, assembled a highly experienced team for the WindPACT project. The following table identifies team members (in bold) and contributing consultants, along with their major roles.

Company	Location	Role
Northern Power Systems	Waitsfield, VT	Prime contractor, project management, turbine systems design, power electronics design, modeling, and integration
General Dynamics Electric Boat	Groton, CT	Generator design and costing
TIAX (formerly Arthur D Little, Inc.)	Cambridge, MA	Operations and maintenance analysis and modeling
Gear Consulting Services of Cincinnati (formerly Cincinnati Gear Company)	Cincinnati, OH	Gearing design and costing
Cantarey	Reinosa, Spain	Generator Manufacturing
Adept Engineering	Glen Cove, NY	System layout and structural design
Catamount Engineering	Waitsfield, VT	System layout and structural design
Comprehensive Power	Shrewsbury, MA	Generator scaling model

Trade Study

In Phase I, the Northern team assessed current technology, studied proposed drivetrain designs, and evaluated trade-offs among proposed designs to identify a megawatt-scale drivetrain for development and testing in subsequent phases of the project (Bywaters 2004). The preliminary study evaluated each design to determine size, weight, and probable cost of energy (COE) over a range of sizes. The study considered all major components of drivetrain design. The proposed designs considered all loading conditions identified by NREL in the statement of work (SOW). Manufacturing, tooling, and transportation costs were also considered.

We began by selecting the blades and rotor size, and developed a conceptual baseline turbine design. The baseline design was used to calculate turbine loads. After developing conceptual designs for each drivetrain type, we designed the gearing and generators. Next we completed the structural design of the main load-carrying members. Finally, we determined costs for each configuration, including the balance of turbine cost.

The original NREL subcontract stipulated examining drivetrain configurations over a range of sizes from 1 MW to 10 MW. NREL modified the range to focus on drivetrains at the 1.5-MW and 3-MW levels. The Northern team used a similar approach for both the 1.5-MW and 3-MW levels. Scaling laws *were not* used in the course of the analysis. We believe that the use of scaling laws is prone to large errors, and with efficient design and analysis techniques, more accurate costing can be achieved.

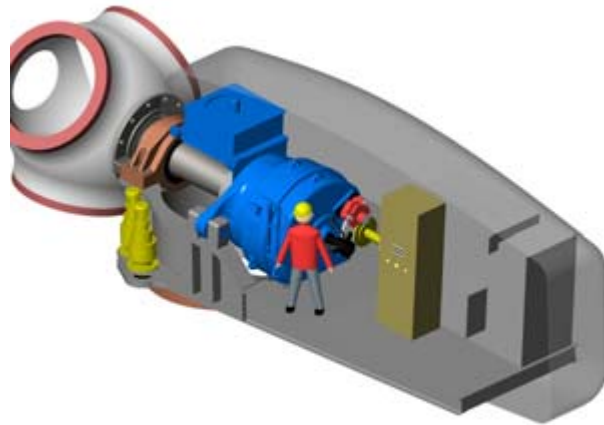
Estimates for component and manufacturing costs were supported by detailed rationale or vendor data. Manufacturing costs were based on the production of 200 MW of capacity per year on an ongoing basis. The designs were optimized for variable speed operation, characterized by high efficiencies at a wide range of rotational speeds and power levels.

We began the analysis methodology by establishing criteria for evaluating drivetrain options. Sets of primary and secondary criteria were developed. The primary evaluation metrics included first cost and COE. Our secondary evaluation metrics included part count, weight, size (envelope), and operations and maintenance (O&M) costs.

The WindPACT statement of work (SOW) describes a number of alternative drivetrain configurations for consideration in Phase I. With input from NREL, the Northern team divided the SOW system design alternatives into the following four subsets for in-depth evaluation.

Baseline multiple-stage, gear-driven, high-speed, wound-rotor induction generator (Baseline) The baseline drivetrain, so-called because of its widespread commercial installed base, employs a Cincinnati Gear multiple-stage hybrid gear speed increaser with a compound planetary low-speed front end, followed by a helical parallel shaft stage to achieve a nominal output speed suitable for a six-pole (1,200-rpm), wound-rotor-induction generator (WRIG). The baseline drivetrain uses an industry-standard power electronics package.

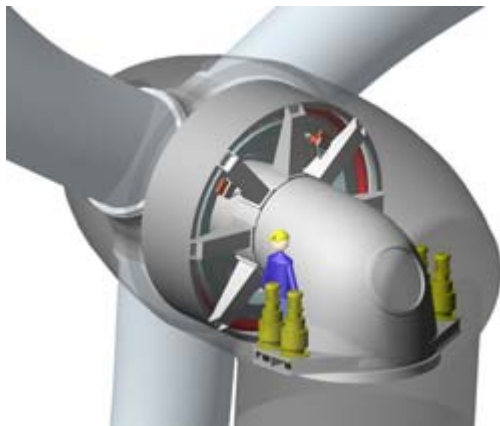
The arrangement of the complete drivetrain is shown in the figure to the right. The rotor hub drives the gearbox through a main shaft-bearing arrangement. The main bearing is a pillow-block-mounted, double-row spherical bearing. The gearbox is supported on a three-point suspension. The gearbox drives the generator through a flexible coupling, which has an integral brake disk and mechanical fuse, and which provides electrical isolation. The generator package includes the rotor slip rings and heat exchanger. Provisions are made for a slip ring, which feeds power to the blade pitch system.



1.5-MW baseline drivetrain

Because the baseline drivetrain was the benchmark for evaluating alternative designs, the Northern team strove to make the drivetrain design reflect the latest component technology in a well-established industry configuration with a documented record of performance.

Direct-drive, low-speed, permanent magnet generator (PMDD) Direct-drive generators offer significant potential because they eliminate the gear-speed increaser, which is susceptible to significant accumulated fatigue torque loading, related reliability issues, and maintenance costs. Employing a synchronous field permanent magnet generator, the PMDD configuration is gaining strong interest because it offers simplicity and potential reduction in size, weight, and cost compared with a drivetrain incorporating a wound-field generator rotor.



1.5-MW PMDD drivetrain

The figure to the left shows the arrangement of the complete PMDD drivetrain and associated tower-top structure. The figure shows an integrated single-bearing design composed of a low-speed, permanent-magnet (PM) generator; turret with yaw drives; and nacelle housing. The generator assembly is composed of the main bearing, stator and rotor electromagnetics, spindle, stator ring and frame, brake system, water jacket, and associated hardware.

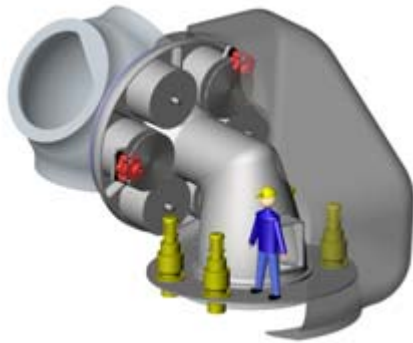
The rotor hub and generator rotor are connected directly to the outer race of the main bearing. The inner race of the main bearing is pressed onto the spindle. The stator frame is connected to the base of the spindle, and the stator ring is bolted to the outside diameter (OD) of the arms. The spindle is bolted to the turret, which provides the structural path to the tower top. A slip ring, which feeds the blade pitch system, and a rotor lock are provided.

Gear-driven, medium-speed, single-output generator (MS-1) Wind turbines using a single-stage gearbox coupled with a low- to medium-speed generator combine the benefits of both gearing and specialty generators. Single-stage gearing, which decreases the size of the generator, can use either a wound rotor synchronous generator or a permanent magnet generator. For our drivetrain study, the Northern team chose the PM generator for its performance advantages and relative simplicity when compared with the wound rotor generator.



1.5-MW MS-1 drivetrain

The integrated drivetrain, which we refer to as MS-1 (see figure), is composed of a 13.89:1 compound planetary helical box with a medium-speed PM generator. (In the figure, the nacelle and rotor hub are removed for clarity.) The drivetrain is composed of the compound planetary helical gearbox, medium-speed generator, turret, brake system, and yaw system. The rotor hub is connected directly to the inner race of the main bearing. The inner race of the main bearing is mounted to the gearbox carrier, and its outer race to the gearbox casing. The generator is mounted to the gear case using flanges on the gearbox and generator housings. The turret design brings the moment loading of the turbine rotor directly from the main bearing into the turret structure, with minimal impact on the gear alignments. Located on the back of the generator, the parking brake system is composed of a brake disk, calipers, and hydraulic system. A slipring, which feeds the blade pitch system, is provided.

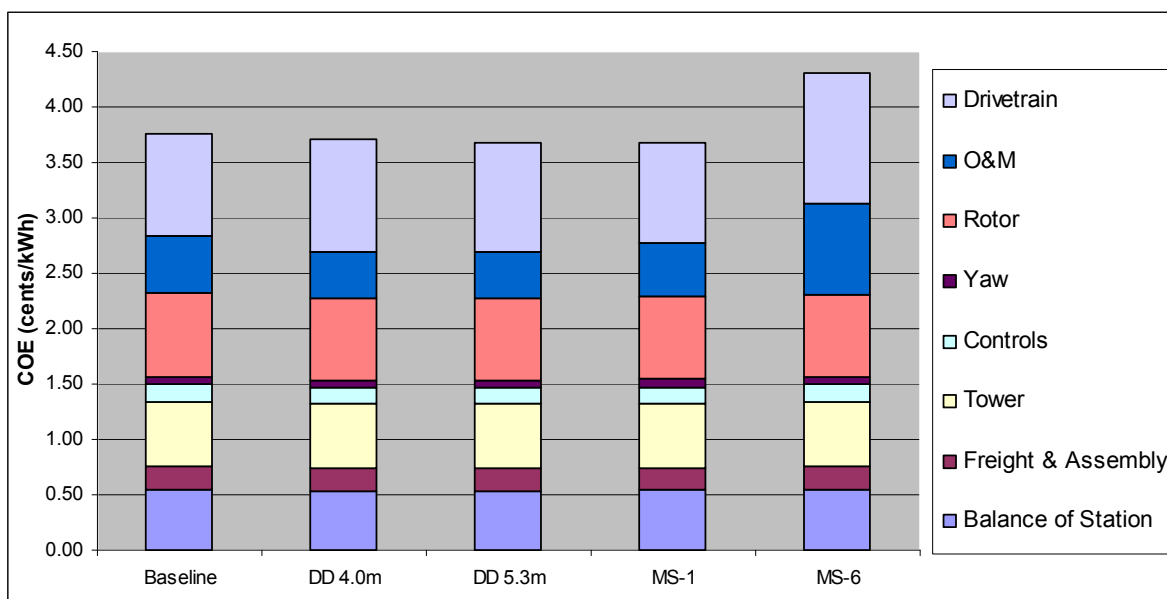


1.5-MW MS-6 drivetrain

Gear-driven, medium-speed, six-output generator (MS-6). The MS-6 configuration is an integrated drive composed of a large-diameter bull gear driving six pinions, which interface with six medium-speed PM generators. This configuration, shown in the figure to the left, is favored by some because of the possibility of using smaller generators for power production. The drive unit is composed of the main bearing, bull gear, pinions, spindle, generators, brake system, and associated hardware. The rotor hub and bull gear are connected directly to the outer race of the main bearing.

The inner race of the main bearing is pressed onto the spindle, which is composed of the central tube that provides the main load path, and the disk, which provides the mounting frame for the generators. The six generator housings are directly connected to the disk and interface the bull gear through the pinions. The pinions are cantilevered off the generator bearings. The spindle is bolted to the turret, which provides the structural path to the tower top. A parking brake system composed of disks and calipers is used. A slip ring, which feeds the blade pitch system, and a rotor lock, which interfaces with the bull gear, are provided.

The results of the Phase I drivetrain study show commercial potential for two configurations: the MS-1 design and the PMDD design. Both configurations appear competitive at the 1.5-MW and 3-MW power levels with the industry state-of-the-art baseline turbine.



Cost of energy: 1.5-MW configurations

Inherent design characteristics of the PMDD drivetrain make its performance more favorable as the generator diameter increases. The main limitation on maximum diameter is shipping constraints in the target markets. As our report describes, two diameters—5.3 m and 4 m—are appealing for the U.S. and European markets, respectively. As part of Phase I, we considered machine designs at both diameters.

Our analysis in Phase I predicted a reduction in COE for both the 4-m diameter PMDD (1.5% reduction) and the MS-1 (2.2% reduction) configurations compared with the 1.5-MW baseline turbine. The 5.3-m diameter 1.5-MW PMDD shows the lowest COE of all configurations—2.3% below the baseline turbine. Economies of scale favored all turbines at increased power levels. All 3-MW designs show a downward trend in COE compared with the 1.5-MW designs.

In selecting a drivetrain configuration for further development, the Northern team also considered factors unaccounted for in the COE calculations, such as technology and industry trends that impact future competitiveness and market acceptance. Of major importance is the maturity level of the intrinsic technology—evolving technologies have inherently greater

potential for improvement. *With this in mind, it is far more likely that technological improvements will reduce costs for new PMDD designs than for mature baseline/gearbox designs.* Magnet and power electronics costs, which are major factors in the capital cost of the PMDD configuration, continue to decline steadily. The same cannot be said of the gearbox costs that dominate the gear-based drivetrains.

Industry and market trends also support the selection of the PMDD configuration. The team identified strong industry interest in an integrated turbine with a PM generator. The commercial wind turbine market is dominated by large, megawatt-scale machines. Direct-drive systems, both with and without PM generators, are becoming popular in this size range. At least six wind industry players are exploring and implementing direct-drive configurations at various levels. These industry players include manufacturers and research and design companies.

Therefore, the Northern team recommended the PM generator applied in a direct-drive configuration for detailed design, manufacturing, and testing in Phases II and III of the WindPACT project.

Design

The permanent magnet direct-drive concept was chosen for detailed design. General Dynamics performed detailed design on the active materials of the generator, and Northern Power Systems performed detailed design on the balance of the generator and auxiliary systems for dynamometer testing. Northern Power Systems also performed detailed design on the power electronics.

The critical mechanical design challenges were as follows:

- 1) The maintenance of a tight tolerance on the air gap. The efficiency, durability, and power quality all depend on a small and uniform air gap between the rotor and the stator. The gap is very small compared to the overall dimensions of the parts. Stackup analysis and operational deflection calculations were performed to ensure the design would work.
- 2) The main bearing between the spindle and rotor. This joint needs to carry a lot of moment and torque. Installation is difficult because of magnetic forces on the rotor. The potential for field replacement of the bearing had to be considered. Also, the tolerances of these parts affect the gap.
- 3) The water-cooling of the generator had to be performed at minimum cost. This depended on the exact way to fit the stator to the water jacket and the water jacket to the outer frame of the generator.
- 4) The spindle and the spider had to be made at minimum cost, while maintaining small gap deflections. Also, the configuration had to allow winding the stator without interference.
- 5) The choice between cast and welded structures had to be reviewed for lowest cost and best performance.

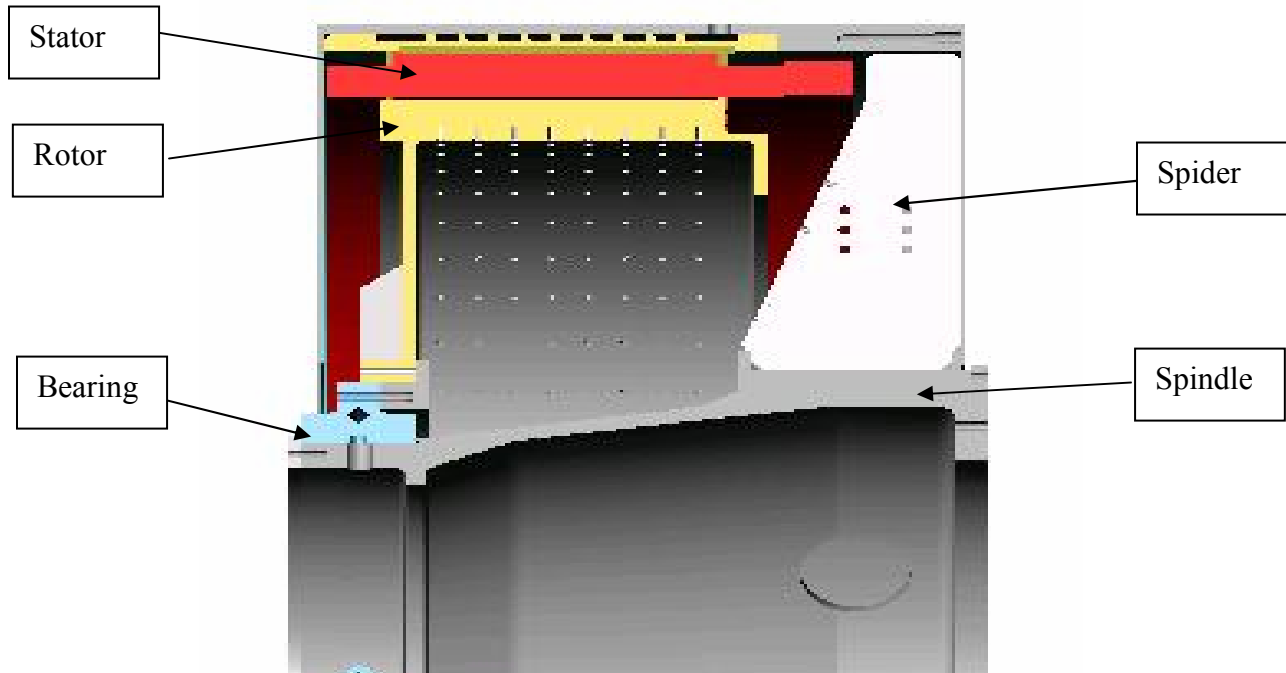
The critical electromagnetic design challenges were as follows:

- 1) The choice of the winding configuration to optimize cost, performance, and reliability
- 2) The choice of insulation to provide adequate insulation without sacrificing heat transfer
- 3) The choice of impregnation of the stator to maximize heat transfer and durability without sacrificing heat transfer
- 4) The choice of magnet material and size to obtain required power at minimum cost
- 5) The choice of rotor hub material and pole fastening method.

The critical power electronics design challenges were as follows:

- 1) Choice of power electronics architecture
- 2) Methods to ensure system safety during first installation
- 3) Cooling method
- 4) Modularity
- 5) Modulation techniques to reduce voltage spikes
- 6) Filtering methods to reduce voltage spikes
- 7) Power factor manipulation.

The resulting design was characterized by a single bearing configuration, with a set of spider arms supporting the stator from the downwind side. A hollow spindle supports the generator rotor and the blade rotor. The connections of the generator stator come out the front of the generator.



The 1.5-MW generator design is characterized by a spindle supporting a single bearing and rotor. The stator is supported by spider arms.

Fabrication

During the prototype fabrication process, several lessons were learned that were critical to the planning of serial production of the generator.

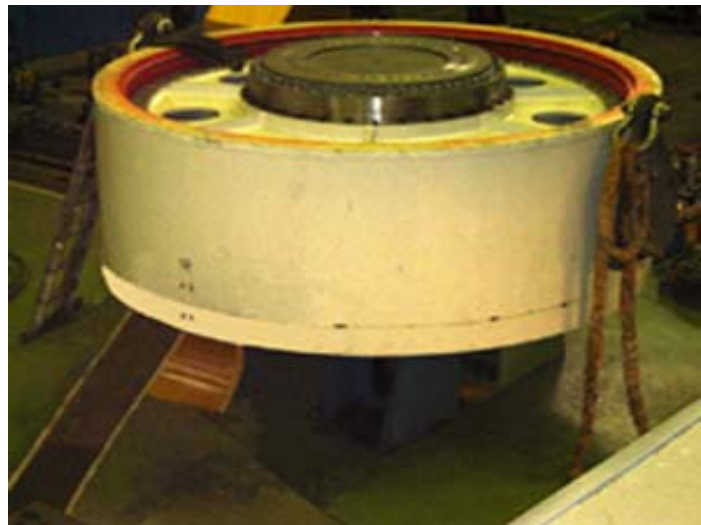
First, the method of creating the connections to the windings was changed to match the capabilities of the vendor. This change was necessary because we used a single-turn coil, which is optimal for this large diameter, but is very rare for smaller generators. A single-turn coil does not make a complete loop, but instead is U-shaped.

Second, we learned that the tight tolerances on the stator diameter (particularly the roundness) were very difficult to obtain. The main problem was not the accuracy of machining, but the inherent flexibility of the stator. The stator was originally analyzed with the spider attached. The spider, however, had to be taken off during the stator winding process. Once the spider is taken off, the stator (before winding and impregnation) is too flexible to reliably hold tolerance. A special spider and stiffening ring was made to hold the stator round during winding and impregnation.

Another issue that had to be addressed was the detailed cost calculation. We found that a few parts were significantly more expensive than predicted. The biggest cost increase was that of the stainless-steel generator rotor hub. Note that this part is inside the generator and is not the rotor hub that supports the wind turbine blades. The outside ring of this part needs to be nonmagnetic for the rotor poles to have the desired magnetic properties.

Still another issue was increased cost incurred by the difficult assembly of the stator. We recommend that more space for end turns and connections be provided to make the assembly process go more smoothly. Magnet insertion was less complicated than expected. Insertion of the rotor into the stator was difficult, however, because the insertion tool was too flexible, and because there was tight clearance between the generator rotor and a stiffening ring on the generator that was added. It is expected that these problems will be rectified on the next generator design.

Finally, no vacuum pressure impregnation tank could be found for a stator of this size. A dip varnish was used for the prototype, which is known to have a less favorable heat transfer capability.



Two challenges, the permanent magnet assembly process, and the assembly of large components were addressed during the 1.5-MW fabrication.

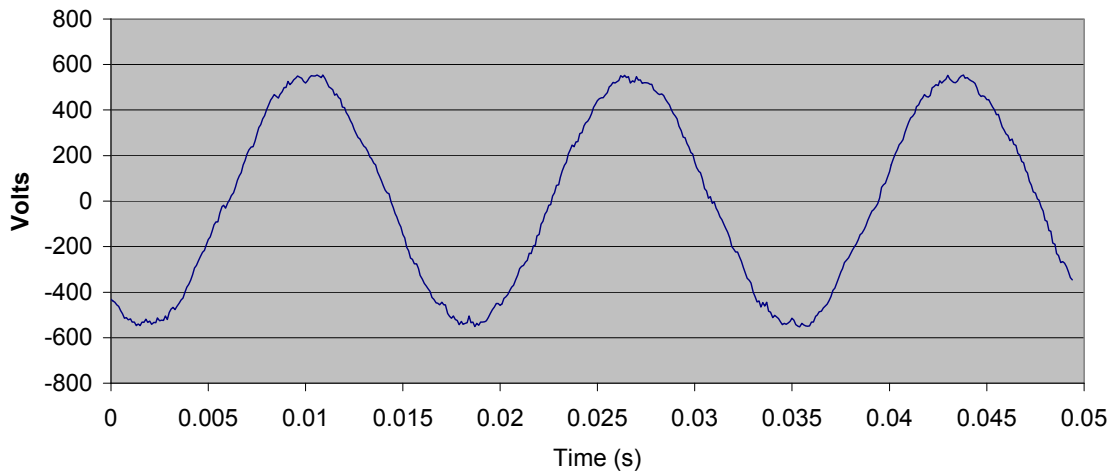
Dynamometer Test

The dynamometer test was done at the NWTC in Colorado. This test program consisted of a series of individual tests done to check out the generator, converter, and control system. During testing, two shorts between the windings and the stator laminations occurred. These were repaired. Once this was done, the generator was run at rated power conditions. The results are shown in the following table and charts. An accidental dynamometer overspeed and subsequent power converter failure occurred, however, and the testing was terminated before tests were performed at steady-state temperature conditions. The estimated performance at rated temperature shows that stator temperatures slightly above specification will occur, but this situation should improve with a stator that has been through the vacuum pressure impregnation process.

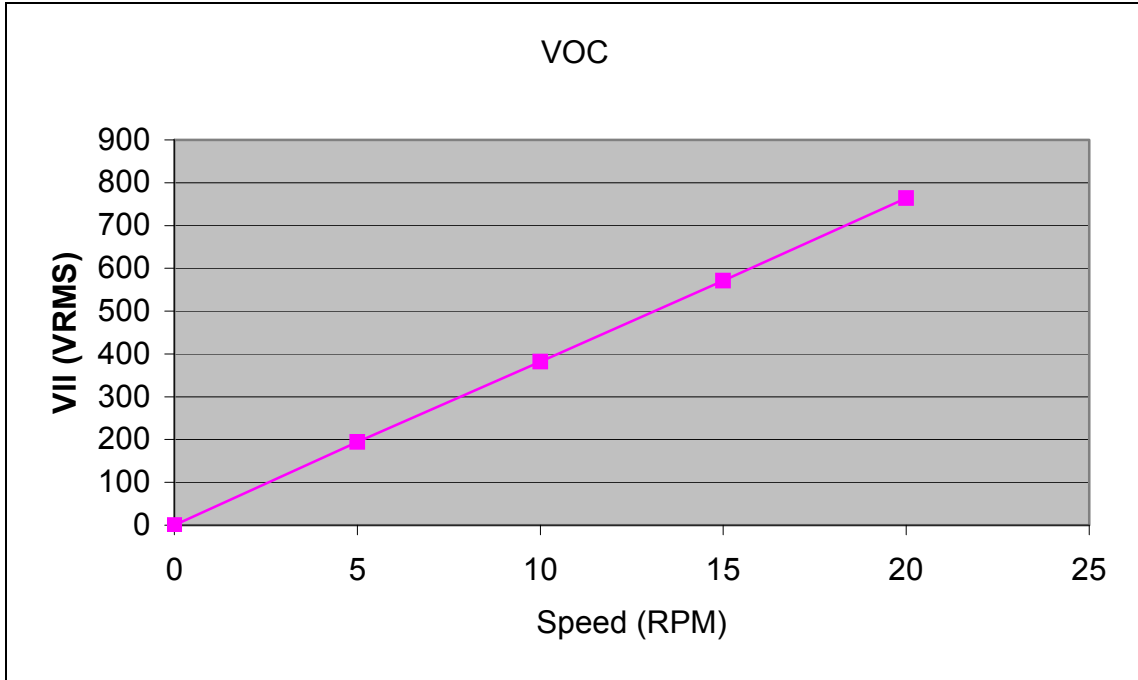
The Generator and Converter Functioned Well at Rated Power Conditions.

Measurement	Value
D-Axis Current Command (A)	-337
Q-Axis Current Command (A)	-1.914
Power to Grid	1.503.5 kW
Shaft Speed	19.0 rpm
Generator Voltage Total Harmonic Distortion (THD)	7.12 %
Utility Inverter Current (Arms) Average of Three Phases	1.301.5
Active Rectifier Current (Arms) Average of Three Phases	1.369.1
Active Rectifier Voltage (Vllrms)	722.8
DC Voltage Average (V DC)	1.149.0
Converter Line-Line Voltage (THD)	3.15%
Generator Peak Temperature (°C)	58.9
IGBT Peak Temperature (°C)	61.0
Coolant Peak Temperature (°C)	28.4

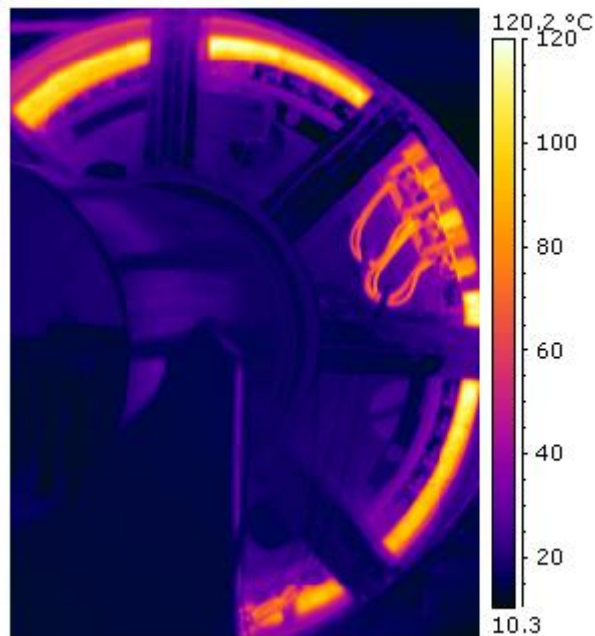
Converter Phase Voltage V2
1500 kW, 19 rpm, 1/4/06



The converter output voltage was very smooth at rated power.



The generator open-circuit voltage increased linearly with rpm, and reached the predicted value at rated speed.



The generator was viewed with a thermal imaging camera and the stator winding temperatures were very uniform.

Conclusion

Wind turbines with gearboxes continue to have gearbox failures. The exact extent of the problem is difficult to determine because turbine manufacturers do not advertise their failures, but an alternative design solution is available. A permanent-magnet, direct-drive generator eliminates the gearbox and all possibilities of this common failure mode. The design, fabrication, and test of the prototype 1.5-MW generator are important steps forward in the development of this design. Trade studies indicated that the COE for the permanent-magnet, direct-drive wind turbine is lower than the COE for the baseline turbine.

Many lessons were learned in the process of completing this study. The critical dimensions, manufacturing processes, and assembly procedures have been identified. Areas for cost reduction have been found. The design has been demonstrated, and with some improvements, will be ready for commercialization.

The next step is to build a second prototype incorporating the lessons learned under the WindPACT program, and install it on a wind turbine. This will be done with a commercialization partner.

Acronym & Abbreviation List

Acronym/ Abbreviation	Full Term	First Occurrence
A	current amperes	ix
AC	alternating current	4-9
AEP	annual energy production	2-5
AGMA	American Gear Manufacturers Association	2-4
ANSI	American National Standards Institute	2-4
AOM	Annual Operation and Maintenance	2-5
Asx, Asy, Asz	stator acceleration in x, y and z directions	5-27
Arx, Ary, Arz	Rotor acceleration in x, y, and z directions	5-27
AWEA	American Wind Energy Association	2-4
baseline	baseline multiple-stage, gear-driven, high-speed, wound-rotor induction generator	ii
COE	cost of energy	ii
Cp	coefficient of performance	2-1
CW	clockwise	3-7
d	displacement	5-6
DC	direct current	ix
DD 4.0 m	direct drive, 4.0 m OD	2-45
DD 5.3 m	direct drive, 5.3 m OD	2-45
DFIG	doubly-fed induction generator	2-6
di/dt	rate of change of current	5-2
DLC	design load case	2-24
DSP	digital signal processing	2-12
dv/dt	rate of change of voltage	5-2
ECD	extreme coherent gust with direction change	2-24
EDC	extreme direction change	2-24
ECG	extreme coherent gust	2-24
EOG	extreme operating gust	2-24
EM	electromagnetic	2-18
EMF	electromagnetic force	5-1
EMI	electromagnetic interference	3-14
EWS	extreme wind shear	2-24
F	Force	5-6
FAST	Fatigue, Aerodynamics, Structures, and Turbulence program	2-4
FCR	Fixed Charge Rate	2-5
FEA	Finite Element Analysis	2-1
GCSC	Gear Consulting Services of Cincinnati	2-14
GDEB	General Dynamics Electric Boat	1-1
GPM	gallons per minute	3-27
hr	hour	3-25

Acronym/ Abbreviation	Full Term	First Occurrence
ICC	initial capital cost	2-5
IEC	International Electrotechnical Commission	2-24
ID	inside diameter	4-15
IEEE	Institute of Electrical and Electronics Engineers	3-14
IEGT	injection-enhanced gate transistor	2-11
IGBT	insulated gate bipolar transistor	2-4
IGCT	integrated gate commutated thyristors	2-11
IP	ingress protection	3-10
I _q	Q-axis current	5-15
ISC	short circuit current	5-7
kHz	kilohertz	2-21
kN	kilonewton	3-25
kNm	kilonewton meters	5-7
kVA	kilovolt ampere	2-12
kW	kilowatt	ix
L10	life at 10% failure probability	C-13
LRC	levelized replacement cost	2-5
ll	line to line	ix
mH	millihenry	5-36
mOhm	milliohm	5-16
MOhm	megaohm	5-7
MPa	megapascal	3-3
MS-1	gear-driven, medium-speed, single-output generator	iv
MS-6	gear-driven, medium-speed, six-output generator	iv
MTFB	mean time between failures	2-12
MW	megawatt	i
N	newton	5-6
NA	not applicable	5-9
NdFeB	Neodymium Iron Boron	2-10
NEMA	National Electrical Manufacturers Association	3-10
Northern	Northern Power Systems	i
NREL	National Renewable Energy Laboratory	i
NTM	normal turbulence model	2-24
NWTC	National Wind Technology Center	i
O&M	operations and maintenance	ii
OD	outside diameter	iii
PDF	portable document format	3-5
PE	power electronics	2-32
Pk	peak value	3-28

Acronym/ Abbreviation	Full Term	First Occurrence
PLC	programmable logic controller	3-9
PM	permanent magnet	iii
PMDD	direct-drive, low-speed, permanent magnet generator	iii
PMSM	permanent magnet synchronous machines	2-16
psi	pounds per square inch	5-6
PU	per unit	3-8
rms	root mean squared	ix
rpm	revolutions per minute	ii
RTD	resistance temperature detector	3-8
s	seconds	5-7
SCR	semiconductor controlled rectifier	2-20
SOW	statement of work	ii
THD	total harmonic distortion	ix
V	volts	ix
V _{mean}	wind velocity mean	2-25
VOC	volts open circuit	x
VPI	vacuum pressure impregnated	3-8
WindPACT	Wind Partnerships for Advanced Component Technologies	i
WRIG	wound rotor induction generator	ii
X _d	D-axis impedance	5-1
X _q	Q-axis impedance	5-1
μs	microseconds	5-19

Table of Contents

Executive Summary.....	i
Participants	i
Trade Study	ii
Design.....	vi
Fabrication	viii
Dynamometer Test	ix
Conclusion	xi
Acronym & Abbreviation List.....	xiii
1 Introduction	1-1
1.1 Project team.....	1-1
1.2 Trade Study	1-2
1.3 Design.....	1-3
1.4 Fabrication	1-4
1.5 Dynamometer Testing.....	1-4
2 WindPACT Drivetrain Study.....	2-1
2.1 Drivetrain Study Parameters	2-1
2.1.1 Drivetrain Design Criteria	2-1
2.1.2 Drivetrain Matrix	2-2
2.2 Design and Analysis Methodology	2-4
2.3 Technology Assessment.....	2-5
2.3.1 Commercial Wind Turbines	2-6
2.3.2 Previous Drivetrain Studies	2-7
2.3.3 Industry Trends	2-8
2.3.4 Technology Trends.....	2-10
2.3.5 Drivetrain Component Reliability	2-12
2.3.6 Drivetrain Technology Options	2-14
2.4 Design Specifications and Parameters	2-21
2.4.1 Drivetrain Specifications.....	2-21
2.4.2 Turbine Safety and Operation	2-21
2.4.3 Power Curves.....	2-22
2.4.4 Power Electronics.....	2-23
2.4.5 Loads	2-24
2.5 Drivetrain Designs.....	2-26
2.5.1 Baseline Design	2-26
2.5.2 Permanent Magnet Direct-Drive Design.....	2-28
2.5.3 Medium-Speed/Single-Output Design	2-33
2.5.4 Medium-Speed/Six-Output Design	2-36
2.6 Drivetrain Study Results	2-42
2.7 Drivetrain Study Conclusions	2-50
3 Design.....	3-1
3.1 Design Methodology	3-1
3.1.1 Turbine Specification.....	3-1
3.1.2 Generator Active Material.....	3-1
3.1.3 Power Electronics.....	3-1
3.1.4 System, Structural, and Mechanical Design.....	3-2

3.1.5	Design Control	3-3
3.2	Design Goals	3-4
3.2.1	Turbine	3-4
3.2.2	Generator	3-5
3.2.3	Power Electronics.....	3-9
3.3	Design Issues	3-11
3.3.1	Structural.....	3-11
3.3.2	Mechanical	3-11
3.3.3	Electromagnetic	3-12
3.3.4	Power Electronics.....	3-13
3.3.5	Design Control	3-16
3.4	Detailed Design Verification	3-16
3.4.1	Structural.....	3-16
3.4.2	Mechanical	3-24
3.4.3	Electromagnetic	3-26
3.4.4	Power Electronics.....	3-32
3.5	Cost Estimation.....	3-35
3.6	Dynamometer Assembly Design	3-36
3.7	Detailed Design Summary	3-39
4	Fabrication	4-1
4.1	Generator.....	4-1
4.1.1	Generator Component Issues	4-1
4.1.2	Generator Quality Control	4-8
4.2	Power Electronics	4-9
4.2.1	Power Electronics Component Issues.....	4-9
4.2.2	Power Electronics Quality Control.....	4-10
4.3	Dynamometer Installation	4-11
4.3.1	Dynamometer Installation Issues	4-11
4.3.2	Dynamometer Quality Control.....	4-14
4.4	Conclusions and Recommendations.....	4-15
5	Dynamometer Testing.....	5-1
5.1	Test objectives	5-1
5.1.1	Structural Objectives	5-1
5.1.2	Cooling Objectives	5-1
5.1.3	Electrical Objectives.....	5-1
5.2	Test Milestones.....	5-2
5.3	Description of the Test Article	5-3
5.4	Test Results	5-5
5.4.1	Gap Deflection Test.....	5-5
5.4.2	Cooling System Test	5-6
5.4.3	Generator High Pot Test	5-6
5.4.4	Generator Free Spinning Tests	5-7
5.4.5	Voltage Waveforms.....	5-7
5.4.6	Brake Run-In and Bearing Tests	5-10
5.4.7	Accelerometer Ramp Test.....	5-10
5.4.8	Generator Short Circuit Test	5-13

5.4.9	Bearing Impedance Test	5-14
5.4.10	Converter No Load Test	5-15
5.4.11	Generator Converter Integration Test 1	5-15
5.4.12	Generator Converter Integration Test 2	5-15
5.4.13	Generator Short Circuit Thermal Test	5-15
5.4.14	Generator Converter Integration Test 3	5-17
5.4.15	Natural Frequency Test	5-26
5.4.16	Thermal Image Test	5-28
5.4.17	Frequency Response Test	5-35
6	Conclusions and Recommendations	6-1
6.1	Trade Study	6-1
6.2	Generator Performance	6-1
6.3	Generator Recommendations	6-2
6.4	Power Converter Recommendations	6-3
6.5	Dynamometer Assembly and Test Recommendations	6-4
6.6	Final Comments	6-4
7	References	7-1
Appendix A	– Generator Design Drawing	A-1
Appendix B	– Dynamometer Test Assy Drawing	B-1
Appendix C	- Detailed Design Document	C-1
C.1	Generator Structural Design	C-1
C.1.1	Structural Analysis	C-1
C.1.2	Stackup and Deflection Analysis	C-7
C.1.3	Bolted Joint Analysis	C-10
C.1.4	Vibration Analysis	C-11
C.1.5	Main Bearing Analysis	C-13
C.1.6	Generator Cooling Analysis	C-14
C.2	Dynamometer Structural Design	C-15
C.2.1	Test Turret Stress Analysis	C-16
C.2.2	Hub Adapter Stress Analysis	C-17
C.2.3	Lifting Plate Stress Analysis	C-18

Table of Figures

Figure 2-1. Advantages of direct-drive turbines.....	2-9
Figure 2-2. Disadvantages of direct-drive turbines.....	2-10
Figure 2-3. Rare-earth magnet cost has been falling as production has been increasing.....	2-11
Figure 2-4. Development and integration of power semiconductors and modules.....	2-12
Figure 2-5. Axial and transverse flux configurations were considered.	2-17
Figure 2-6. 1.5-MW baseline power curve	2-22
Figure 2-7. 3.0-MW baseline power curve	2-23
Figure 2-8. 1.5-MW 70-m baseline design	2-26
Figure 2-9. 1.5-MW compound planetary helical gearbox.....	2-27
Figure 2-10. PMDD drivetrain.....	2-28
Figure 2-11. PMDD generator.....	2-29
Figure 2-12. PMDD (and MS-1) power electronics schematic	2-32
Figure 2-13. MS-1 drivetrain design.....	2-33
Figure 2-14. 1.5-MW MS-1 Drivetrain (Gearbox and Housings Cut Away)	2-35
Figure 2-15. MS-1 generator section view	2-35
Figure 2-16. MS-6 design.....	2-37
Figure 2-17. MS-6 generator section view	2-39
Figure 2-18. (A) Power electronics for MS-6 design. (B) Power electronics for individual generator.	2-41
Figure 2-19. Component initial capital cost centers: 1.5-MW	2-42
Figure 2-20. Component initial capital cost centers: 3-MW configurations.....	2-43
Figure 2-21. O&M cost centers: 1.5-MW configurations.....	2-45
Figure 2-22. COE cost centers: 1.5-MW configurations.....	2-48
Figure 2-23. COE cost centers: 3-MW configurations.....	2-48
Figure 2-24. Relative drivetrain weights	2-49
Figure 2-25. Drivetrain specific cost.....	2-49
Figure 3-1. Schematic of the power electronics design.....	3-10
Figure 3-2. The power electronics system was made from three 500-kW modules.	3-15
Figure 3-3. Power electronics protection 1-line.	3-15
Figure 3-4. A common-mode circuit model of the generator and power electronics determined the magnitude of voltages in the system caused by the IGBT switching noise.	3-16
Figure 3-5. The spindle was analyzed using finite element analysis to determine the correct thickness and geometric details to carry blade rotor moment loads.....	3-17
Figure 3-6. The summary of structural analysis shows that margins of safety were adequate (Safe designs >1). .	3-18
Figure 3-7. The deflection of the rotor was calculated to determine the effect on the gap.	3-19
Figure 3-8. Analysis shows that the deflections are within specified limits when manufacturing tolerances are neglected.....	3-20
Figure 3-9. The stackup analysis of the gap showed the major sources of variation.	3-21
Figure 3-10. The bolted joints for all major structural connections were safe.....	3-22
Figure 3-11. The normal modes analysis of the stator showed a torsional natural frequency of 46.5 Hz.....	3-23
Figure 3-12. The normal modes analysis of the rotor showed a torsional natural frequency of 149.9 Hz.	3-23
Figure 3-13. The crossed roller bearing was used instead of the double-tapered roller bearing to reduce the cost of the dynamometer prototype.....	3-25
Figure 3-14. Electromagnetic finite element analysis was used to determine the operating characteristics of the generator.	3-27
Figure 3-15. The no-load torque of the generator was calculated for input into dynamic analysis of generator components.....	3-27
Figure 3-16. The harmonic content of the unskewed no-load cogging torque is at the 12 th and 24 th , relative to the electrical fundamental frequency.	3-28
Figure 3-17. The unskewed torque at rated conditions and 0.9 power factor had a larger ripple than the no-load cogging torque.....	3-28
Figure 3-18. The torque harmonics at rated conditions and 0.9 power factor were similar to no-load harmonics...	3-29

Figure 3-19. The unskewed open circuit voltage had some distortion due to the cogging effects.....	3-29
Figure 3-20. The harmonic content of the open-circuit voltage showed the most distortion at the 5 th , 7 th , and 11 th harmonics.....	3-30
Figure 3-21. The predicted voltage magnitude at rated condition and 0.9 power factor exceeded the specification requirement.....	3-31
Figure 3-22. Total harmonic distortion of the line voltage at rated conditions was dominated by 5 th , 7 th , 11 th , and 13 th order harmonics.....	3-32
Figure 3-23. Thermal models were used to calculate the temperatures of critical components and the resulting efficiency of the power converter.....	3-33
Figure 3-24. The power electronics produces a voltage stress in the generator of 4 kV/mm, but little data exists to accurately predict NOMEX insulation life for the generator.....	3-34
Figure 3-25. The generator cost breakdowns showed significant cost increases for the stator spider, rotor hub, spindle, and water jacket.....	3-35
Figure 3-26. The generator mass breakdowns showed significant mass increases for the water jacket, stator arms, spindle, and generator rotor.....	3-36
Figure 3-27. Dynamometer test layout.....	3-37
Figure 3-28. Finite element analysis was performed on the dynamometer test turret to ensure it would survive test loads.....	3-37
Figure 3-29. The static and fatigue reserves of components in the dynamometer assembly were acceptable (Reserve > 1.0).....	3-38
Figure 4-1. The weldment vendor, Felguera, has equipment such as this vertical lathe for machining large parts....	4-2
Figure 4-2. Distortion of the outer frame was aligned with the lifting bosses. These values are for the stator inner diameter after assembly into the water jacket and outer frame.....	4-4
Figure 4-3. A special spider and front ring was attached to the stator to keep it round during winding and impregnation.....	4-5
Figure 4-4. The stator winding process was more time consuming than expected.....	4-6
Figure 4-5. The magnets were inserted into the rotor using a proprietary method developed by General Dynamics.....	4-7
Figure 4-6. A final acceptance test was performed at the generator manufacturing facility, but the generator was too large for the facility's dynamometer.....	4-9
Figure 4-7. The IGBT's were attached to a water-cooled heat exchanger.....	4-10
Figure 4-8. Each 500-kW section of the power electronics was tested at full current and all temperatures were within specifications.....	4-11
Figure 4-9. The generator was rolled into the dynamometer facility on a cart, which was pulled by cables connected to the gantry crane.....	4-12
Figure 4-10. The generator was rotated into position using a three-point lift, to be as safe as possible.....	4-13
Figure 4-11. The coupling was installed after the generator and dynamometer shafts were aligned.....	4-13
Figure 4-12. Droop loops were hung from the cable tray to take up the slack.....	4-14
Figure 5-1. NW1500 actual test schedule.....	5-3
Figure 5-2. Dynamometer test article.....	5-3
Figure 5-3. The generator was attached to the bedplate with a turret, and had removable covers for access to the active materials.....	5-4
Figure 5-4. The generator connects to the dynamometer using a long shaft and coupling, as shown here viewed from the control room.....	5-4
Figure 5-5. The power electronics connected to the generator via overhead trays, and connected to the grid via trays on the floor.....	5-5
Figure 5-6. The line-to-line voltage for free spinning test was linear.....	5-8
Figure 5-7. The open circuit voltage at 20 rpm was well balanced, and the neutral voltage was near zero.....	5-8
Figure 5-8. The phase voltage spectrum at 20 rpm showed a small amount of harmonic distortion.....	5-9
Figure 5-9. The bearing temperature for free spinning test (18 rpm) stayed low, indicating that the drag torque of the bearing is small.....	5-10
Figure 5-10. The stator had high y-accelerations at rotor speeds of 1.6, 3.6, and 6.1 rpm, when the shaft was accelerating and decelerating.....	5-11
Figure 5-11. The stator had high z-accelerations at rotor speed 3.6 rpm as the rotor speed increased, and at 5.0 rpm as the rotor speed decreased.....	5-12
Figure 5-12. The rotor x acceleration (in shaft direction) did not indicate any natural frequencies, because the vibrations did not occur while the shaft was both accelerating and decelerating.....	5-13

Figure 5-13. The torque in the two phase short circuit test was severe, so the test was terminated.....	5-14
Figure 5-14. The coolant inlet temperature was controlled to maintain a 40°C temperature.....	5-16
Figure 5-15. The temperatures measured in the thermal test were within the limits of a class H insulation system (155 °C), but they caused some out-gassing of vapors due to incomplete curing of the varnish.....	5-17
Figure 5-16. The generator phase voltage is jagged because of neutral-point-modulation, which decreases peak voltage.....	5-18
Figure 5-17. The generator phase voltage dv/dt was less than 6V/μs.	5-19
Figure 5-18. The generator line-to-line voltage was noisy due to active rectifier switching effects.....	5-19
Figure 5-19. The spectrum of the generator line-to-line voltage is dominated by 2.5 kHz switching noise.	5-20
Figure 5-20. The phase current was also noisy, but this did not affect the function of the generator.	5-21
Figure 5-21. The phase current spectrum shows very little harmonic distortion.....	5-21
Figure 5-22. The converter phase waveform at rated conditions was very smooth.....	5-22
Figure 5-23. The converter phase voltage spectrum showed little harmonic distortion and switching noise.....	5-23
Figure 5-24. Stator temperatures during 1500 kW power production reached about 55 °C.	5-24
Figure 5-25. In the ramp test, the current in the rectifier was kept at 313 Amps, while the speed was increased from 10 to 19 rpm.	5-26
Figure 5-26. In the ramp test, the rotor and stator acceleration was small, but increased with rotor speed.	5-27
Figure 5-27. At 19 rpm, the rotor and stator accelerations were small, but increased with increased power production.	5-27
Figure 5-28. At 1,500-kW power production, the largest acceleration was an 18-Hz vibration of the rotor in the x-direction. This is twice the electrical frequency.....	5-28
Figure 5-29. The first generator thermal image test was done with the covers off, and reached a hot-spot temperature of about 120°C.	5-29
Figure 5-30. The coolant temperature was controlled manually to an inlet temperature of about 40°C.	5-30
Figure 5-31. The thermal test was repeated with the covers on and reached a hot-spot temperature of 120°C.....	5-30
Figure 5-32. When the test was repeated, coolant temperature at the generator inlet was about 40°C.....	5-31
Figure 5-33. The thermal image of the end turns at the downwind end showed slightly hotter temperatures (121.6°C) at 12:00.....	5-31
Figure 5-34. The thermal image of the short circuit jumpers shows a hot spot of 123.5°C.	5-32
Figure 5-35. A thermal image of the downwind end of the generator shows a hot spot of 112.6°C.	5-32
Figure 5-36. A hot spot (121.7°C) is visible at 12:00 on the downwind end of the generator.	5-33
Figure 5-37. The upwind end turn temperatures were partially obscured by the front ring of the generator (103.7°C).	5-33
Figure 5-38. The hottest spot on the upwind end of the generator (118.3°C) was about 5°C less than the hottest spot on the downwind side.	5-34
Figure 5-39. The stator housing temperature was very uniform at the temperature of the coolant.	5-34
Figure 5-40. The hottest spot (111.5°C) on the upwind end of the generator was near 12:00.	5-35
Figure 5-41. The hot spot temperatures were similar with the covers on (117.8°C), and a close-up shows that the rotor was at approximately the same temperature as the housing.	5-35
Figure 5-42. The D-axis impedance was obtained from 0.001 Hz to 10 Hz.	5-36
Figure 5-43. The DC D-axis inductance was 2.9 millihenry (mH).....	5-37
Figure 5-44. The Q-axis impedance was recorded up to 4.4 Hz to avoid noise caused by resonance near 10 Hz.	5-37
Figure 5-45. The DC Q-axis inductance was 5.9 mH.....	5-38
Figure 5-46. The common mode impedance was sufficiently large at the switching frequency and at the first several harmonics of the switching frequency.....	5-39
Figure C-1. The spindle was analyzed using finite element analysis to determine the correct thickness to carry blade rotor moment loads.....	C-2
Figure C-2. The generator frame was sized based on the stresses due to lifting.....	C-3
Figure C-3. The rotor was analyzed using finite element analysis to determine the proper sizing of the structure.	C-4
Figure C-4. The spider was analyzed using finite element analysis to determine proper sizing of the spider arms.	C-5
Figure C-5. The brake system was analyzed with finite element analysis to determine proper sizing of the brackets and spider arms.....	C-6
Figure C-6. The summary of structural analysis shows that static and fatigue reserves were adequate (Safe designs >1).	C-7

Figure C-7. The deflection of the rotor was calculated to determine the effect on the gap..... C-8

Figure C-8. Analysis shows that the deflections are within specified limits when manufacturing tolerances are neglected..... C-9

Figure C-9. The stackup analysis of the gap showed the major sources of variation..... C-10

Figure C-10. The bolted joints for all major structural connections were safe..... C-11

Figure C-11. The normal modes analysis of the stator showed a torsional natural frequency of 46.5 Hz..... C-12

Figure C-12. The normal modes analysis of the rotor showed a torsional natural frequency of 149.9 Hz..... C-12

Figure C-13. The crossed roller bearing was used instead of the double-tapered roller bearing to reduce the cost of the dynamometer prototype..... C-14

Figure C-14. Dynamometer test layout..... C-16

Figure C-15. Finite element analysis was performed on the dynamometer test turret to ensure it would survive test loads..... C-17

Figure C-16. Displacement and rotation of the turret was extrapolated to the end of the shaft to determine coupling misalignment..... C-17

Figure C-17. The hub adapter analysis was dominated by fatigue loading from the overhung mass of the main shaft..... C-18

Figure C-18. The lifting plate was analyzed and is safe, even including unbalanced loading due to nonvertical rigging..... C-19

Figure C-19. The static and fatigue reserves of components in the dynamometer assembly were acceptable (Safe Designs > 1.0). C-20

Table of Tables

Table 2-1. Drivetrain Configuration Matrix.....	2-2
Table 2-2. Drivetrain Configurations of Nonstandard Commercial Turbines	2-6
Table 2-3. “High Potential” Direct-Drive Projects.....	2-7
Table 2-4. Reliability Comparison of Gearbox and Direct-Drive Configurations.....	2-13
Table 2-5. Estimated O&M Costs for Gear-Driven 650–900-kW Turbines	2-14
Table 2-6. Estimated Gearbox Costs for 650- to 900-kW Turbines.....	2-15
Table 2-7. Types of Generators for Megawatt-Scale Turbines.....	2-16
Table 2-8. Distinguishing Features of Radial, Axial, and Transversal Flux Generators.....	2-17
Table 2-9. Radial Flux Generator Architectures	2-18
Table 2-10. Normalized Weight and Cost of Materials of Favorable Generators	2-19
Table 2-11. Turbine Drivetrain Specifications	2-21
Table 2-12. Power Electronics Specification	2-23
Table 2-13. Design Loads Cases	2-24
Table 2-14. Partial Loads Factors	2-25
Table 2-15. Cooling Method Tradeoff in 1.5-MW PMDD Generator.....	2-30
Table 2-16. PMDD Generator Specifications	2-31
Table 2-17. MS-1 Drivetrain Specifications	2-34
Table 2-18. MS-1 Gearbox Specifications.....	2-34
Table 2-19. MS-1 Generator Specifications	2-36
Table 2-20. MS-6 Drivetrain Specifications	2-38
Table 2-21. MS-6 Gearing Specifications.....	2-38
Table 2-22. MS-6 Generator Specifications	2-39
Table 2-23. Relative Initial Capital Cost Comparison: 1.5-MW Configurations	2-43
Table 2-24. Relative Initial Capital Cost Comparison: 3-MW Configurations	2-43
Table 2-25. Summary of Operation and Maintenance Costs ^a	2-44
Table 2-26. Annual Energy Production: 1.5-MW Configurations.....	2-45
Table 2-27. Annual Energy Production: 3-MW Configurations.....	2-45
Table 2-28. COE Summary: 1.5-MW Configurations ^a	2-46
Table 2-29. COE Summary: 3-MW Configurations ^a	2-46
Table 2-30. Relative COE: 1.5-MW Configurations.....	2-47
Table 2-31. Relative COE: 3-MW Configurations.....	2-47
Table 3-1. Design Load Cases for 1.5-MW Wind Turbine Design.....	3-2
Table 3-2. Components were Designed with Commonly Available Materials with Known Static and Fatigue Properties	3-3
Table 3-3. Turbine Specification.....	3-4
Table 3-4. Preliminary Specification for the Permanent Magnet Generator	3-6
Table 3-5. Generator Power, Current, Voltage, and Power Factor Data Points	3-7
Table 3-6. Power Electronics Design Specification.....	3-10
Table 3-7. Forcing and Torsional Natural Frequencies at Rated Conditions.....	3-24
Table 3-8. The Avon Bearing Was Analyzed to Determine that the Life Would Be Adequate for the Duration of the Dynamometer Test.	3-24
Table 3-9. The Timken Double-Row, Tapered Roller Bearing Was Designed to Meet the 20-year Life Requirements of the Turbine Application.....	3-25
Table 3-10. The Generator Cooling System was Designed to Keep the Winding Temperatures Lower than 155°C. . 3-26	3-26
Table 3-11. The Total Harmonic Distortion of the Unskewed Open-Circuit Voltage was 5.1%.	3-30
Table 3-12. The Predicted Efficiency of the Generator was Very Close to the Target of 93.8%.	3-32
Table 3-13. Power Electronics Cooling System (Rated Conditions).....	3-34
Table 4-1. The As-Manufactured Gap was Smaller and had More Variation than Originally Specified, but was Considered Acceptable for the First Article.....	4-8

Table 5-1. Air Gap Measurements	5-6
Table 5-2. Cooling Loop Test Results	5-6
Table 5-3. Generator High Pot Test Results	5-7
Table 5-4. Generator Free Spinning Test - Voltage	5-7
Table 5-5. Harmonic Distortion of Open Circuit Voltage at 20 rpm.....	5-9
Table 5-6. Voltage Imbalance of Open Circuit Voltage at 20 rpm.	5-9
Table 5-7. Short Circuit Current (Three Phase Short).....	5-13
Table 5-8. Short Circuit Current (Two Phase Short).....	5-13
Table 5-9. The Bearing Resistance was Low, and Independent of Rotor Position.....	5-14
Table 5-10. Total Harmonic Distortion of the Generator Line-to-Line Voltage at 1,500 kW was Dominated by Switching Noise at 2.5 kHz.	5-20
Table 5-11. The Total Harmonic Distortion of the Phase Current was 1.26%.....	5-22
Table 5-12. The total Harmonic Distortion of the Converter Phase Voltage at 1,500 kW was 3.15%.	5-23
Table 5-13. Generator/Converter Data at 19 rpm, 1,500 kW	5-24
Table 5-14. The Generator Efficiency was Calculated Using the Estimated Converter Efficiency, Because the Generator Voltage Transducer was Damaged.	5-25
Table 5-15. The Generator Efficiency at Rated Temperature Conditions was Estimated by Calculating Winding Resistance at 120 °C.....	5-25
Table 6-1. Test Results Showed that Measured Values were Close to Design Predictions.....	6-2
Table C-1. Forcing and Torsional Natural Frequencies at Rated Conditions	C-13
Table C-2. The Avon Bearing was Analyzed to Determine that the Life Would be Adequate for the Duration of the Dynamometer test.	C-13
Table C-3. The Timken Double-row Tapered Roller Bearing was Designed to Meet the 20-year-life Requirements of the Turbine Application.....	C-14
Table C-4. The Generator Cooling System was Designed to Keep the Winding Temperatures Lower than 155° C	C-15

1 Introduction

The National Renewable Energy Laboratory (NREL) Wind Partnerships for Advanced Component Technologies (WindPACT) project seeks to advance wind turbine technology by exploring innovative concepts in drivetrain design. A team led by Northern Power Systems (Northern) of Waitsfield, Vermont, was chosen to perform this work. Conducted under subcontract YCX-1-30209-02, project objectives were to identify, design, and test a megawatt-scale drivetrain with the lowest overall life-cycle cost. The project comprised three phases:

- Preliminary study of alternative drivetrain designs (Phase I)
- Detailed design development (Phase II)
- Proof of concept fabrication and test (Phase III).

This report summarizes the results of the entire project.

1.1 Project team

The project team was composed of Northern (prime subcontractor), subcontractors, and consultants. The following sections identify the principal participants and their major roles.

- Prime subcontractor and major subcontractors:

Northern Power Systems, Waitsfield, Vermont

Tasks: Project management, subcontract administration, turbine systems design, power electronics design, modeling and integration

Principal contributors: Northern's team is led by Mr. Jonathan Lynch, principle investigator. Mr. Lynch has responsibility for technical performance under the contract. The lead engineer is Mr. Garrett Bywaters. Project management was provided by Mr. Gary Norton and Mr. Peter Mattila. Other contributors include Mr. Chris Badger, Mr. Trevor Cole, Dr. Dan Costin, Mr. Chris Bevington, Mr. Bill Danforth, Mr. Steve Hoskins, Dr. Vinod John, Mr. Hector Hurtado, Mr. Jeff Petter, Mr. Rob Rolland, and Mr. Jesse Stowell.

TIAX (formerly Arthur D. Little Inc.), Cambridge, Massachusetts

Tasks: Operations and maintenance (O&M) analysis and modeling, technology assessment, market analysis

Principal contributors: Mr. David Hablanian, Dr. Allan Chertok, Mr. Michael Morris, and Ms. Lisa Frantzis

General Dynamics Electric Boat (GDEB), Groton, Connecticut

Tasks: Phase I and II generator design and costing, modeling and integration, power electronics support

Principal contributors: Mr. Scott Forney, Mr. Jack Kelley, Mr. Spyro Pappas, Mr. Mike Salata, Mr. Greg Kudrick, Mr. Jack Chapman, and Mr. Al Franco

Gear Consulting Services of Cincinnati (formerly Cincinnati Gear), Cincinnati, Ohio

Tasks: Phase I gearing design and costing

Principal contributors: Mr. Octave Labath and Mr. Dennis Richter

Cantarey Reinoso, Reinoso, Spain

Tasks: Phase III generator fabrication

Principal contributors: Mr. Damian Perez de Larraya, Mr. Rafael Rodriguez Rodriguez

ShinEtsu, Eden Prairie, Minnesota

Tasks: Phase I magnet cost estimation and Phase III magnet fabrication.

Principal contributors: Mr. Bob Buettner

- Other consultants:

Adept Engineering, Glen Cove, New York

Tasks: Phase I system layout and structural design

Principal contributor: Mr. Matthew Hayduk

Catamount Engineering, Waitsfield, Vermont

Tasks: Phase I system layout and structural design

Principal contributor: Mr. Timothy Cosentino

Comprehensive Power, Shrewsbury, Massachusetts

Tasks: Phase I generator cost modeling

Principal contributor: Dr. Frank Jones

Windward Engineering, Salt Lake City, Utah

Tasks: Phase I and II Turbine loads modeling

Principal contributor: Dr. Craig Hansen

The Timken Company, FAG Bearings, LM GlasFiber, EUROS GmbH, Svendborg and other vendors supplied component quotes for costing.

1.2 Trade Study

For the drivetrain configuration study, we classified the proposed design alternatives as follows:

- *Baseline configuration.* The baseline drivetrain employs a multiple-stage hybrid gear speed increaser with a planetary low-speed front-end followed by two helical parallel shaft stages to achieve a nominal output speed suitable for a six-pole (1,200 rpm) wound

rotor induction generator. The baseline configuration uses a partial rating power converter on the generator rotor circuit to allow variable speed operation.

- *Direct-drive configuration.* Direct-drive generators offer significant potential because they eliminate the gear-speed increaser, a well-known source of maintenance cost and significant accumulated fatigue torque loading. The permanent magnet (PM) synchronous direct-drive configuration employs PM field poles in a radial field internal configuration. The PM design offers simplicity and potential reduction in size, weight, and cost compared with a wound-field design. The direct-drive configuration requires a full rating power converter on the generator output to allow variable speed operation.
- *Gear-driven, medium-speed configuration.* A single-stage gearbox coupled with a low- to moderate-speed generator combines the benefits of both gearing and specialty generators. Single-stage gearing decreases the size of the generator and can use either a wound rotor synchronous generator or a permanent magnet generator. For our drivetrain study, we chose the single-stage PM generator for its performance advantages and relative simplicity compared with the wound rotor generator. The gear-driven, low speed configuration requires a full rating power converter on the generator output to allow variable speed operation.
- *Gear-driven, six-output configuration.* Multiple-path drivetrain configurations can range from multiple, low-speed paths where multiple generators are driven off a single-stage gear path, to multiple higher-speed generators driven by multiple, separate gear paths. The number of generators can range from two to twelve. After evaluating many options, we found that a gear-driven, medium-speed, six-generator configuration using PM generators was the most promising of the multiple-path design alternatives. The multiple-path configuration requires a full rating power converter on the generator output to allow variable speed operation.

To identify an optimized megawatt-scale drivetrain configuration for development in Phases II and III, the Northern project team evaluated the four drivetrain options. Preliminary designs were produced, and cost of energy (COE) was calculated for each. On the basis of our evaluation, the Northern project team recommended a direct-drive, permanent-magnet drivetrain design for development and testing in Phases II and III.

1.3 Design

The objective of Phase II, was to design a 1.5-MW, direct-drive generator. Northern and GDEB cooperated to complete the majority of this work. The goals of the design process were stated in a specification. The specification included the power level, voltage, environmental conditions, cooling method, power quality requirements, efficiency requirements, design life, and overall dimensions. We started with the preliminary design from Phase I. This was a permanent-magnet, water-cooled design. We worked with our suppliers and consultants to resolve design issues. We developed a means to insert the rotor into the stator. We did many finite element models to ensure the structural integrity of the design. GDEB did electromagnetic analysis to ensure that the power and efficiency would meet targets. We then worked with generator manufacturers to refine the design and select a supplier. In addition, we designed a power

converter to control the generator and connect it to the grid. Components for connecting the generator to the dynamometer were designed as well.

1.4 Fabrication

The objective of Phase III, was to build the 1.5 MW-direct-drive generator. Most of the work was done at Cantarey in Reinoso, Spain. We were in frequent contact with the vendor to resolve issues that came up during manufacturing. We incorporated many of Cantarey's suggestions in the design. Some issues arose during manufacturing. During this process we learned some lessons about how to manufacture this type of generator more efficiently. The result of this work was a good prototype, and many ideas of how the manufacturing can be further improved. In addition, we fabricated a power electronics system, and components for dynamometer testing.

1.5 Dynamometer Testing

During Phase III, we tested the 1.5-MW generator on the dynamometer at NWTC. The objective of the test was to verify the power performance and efficiency of the generator. Because the generator and power electronics are so closely interconnected, we learned about our power electronics as well. The following tests were performed.

- Gap Deflection Test
- Cooling System Test
- Generator Insulation Resistance Test
- Generator Free-Spinning Test
- Generator Short-Circuit Test
- Converter Hi-Pot Test
- Generator/Converter Integration Test
 - 1,500 kW Power Production
- Natural Frequency Test
- Thermal Image Test
- Frequency Response Test.

Many of these tests were needed only to verify the safe performance of subcomponents prior to the full-power test. The 1,500-kW power test was used to determine if the generator met the original design goals. Originally, more extensive testing at 1,500 kW was planned, but an accidental overspeed of the dynamometer caused damage to the power converter, and the test was discontinued. The measured results at 1,500 kW occurred at less than rated temperature, so results at rated temperature conditions were estimated and compared to original specifications and predictions.

2 WindPACT Drivetrain Study

The goal in Phase I of the WindPACT project was to identify an optimized megawatt-scale drivetrain configuration for development in Phases II and III. The details of the study were included in the document *Northern Power Systems Alternative Drivetrain Design Study Report* (Bywaters et al., 2004).

Upon establishing drivetrain configuration options, the Northern team conducted a comprehensive assessment of drivetrain technology. On the basis of our assessment, we narrowed our configuration options and selected the most promising component technologies for each option.

The drive components were then integrated into a complete structural design. Structural analyses were performed using finite element analysis (FEA) techniques with loads calculated using dynamic simulation models. After integrating the balance of turbine components (rotor, yaw drives, tower, controller, etc.), we determined the cost of each design.

The same approach was employed for the 1.5-MW and 3-MW machines. We did not use scaling laws to “project” the design to larger sizes; rather, we developed actual designs. We believe this approach estimates the probable costs of larger machines more accurately than does scaling smaller designs.

2.1 Drivetrain Study Parameters

To guide drivetrain analysis and design, NREL defined design requirements, prospective wind turbine site criteria, and the loading envelope accommodated by the drivetrain to set a common basis for estimating the cost of energy.

2.1.1 Drivetrain Design Criteria

Following are the design criteria established by NREL:

- System specifications:
 - Variable speed operation with maximum $C_p = 0.5$
 - Maximum tip speed = 85 m/s
 - Turbine hub height = $1.3 \times$ rotor diameter
 - Rated wind speed = $1.5 \times$ hub height annual average wind speed
 - Cut-out wind speed = $3.5 \times$ hub height annual average wind speed.
- Design wind class:
 - WTGS Class II.
- Performance wind definition for evaluating the design:
 - Air density = 1.225 kg/m^3 (sea level)
 - 10-meter wind speed = 5.8 m/s (annual average)
 - Rayleigh distribution

- Power law = 0.143.

In addition, the following system design criteria were considered:

- Market relevance
- Simplicity of design
- Ease of assembly
- Reliability
- Serviceability
- Shipping.

2.1.2 Drivetrain Matrix

For the drivetrain configuration study, we divided the proposed design alternatives into four subsets (Table 2-1). Each configuration was brought to the preliminary design stage and evaluated according to the methodology described in Section 2.2.

Table 2-1. Drivetrain Configuration Matrix

Concept	Definition	Geartrain	Generator configuration	Characteristics
1	Baseline	Multiple stage	I (See Below)	Multiple stage planetary/helical or helical
2	Direct-drive	None	II(a) and II(b)	No gearbox; very slow generator
3	Medium speed	Single stage	III	Planetary gear speed increaser
4	Multiple path	Single stage	III	Multiple options—two or more generators
Generator		Speed	Type and options	Characteristics
I	Baseline	1,200 rpm	Wound rotor induction	Off the shelf
II(a)	Low speed	20 rpm	Wound rotor synchronous	New design
II(b)	Low speed	20 rpm	PM synchronous	New design
III	Medium speed	100 rpm	PM synchronous	New design

We assessed drivetrain configurations as point designs at the 1.5- and 3-MW power levels. Our team carefully examined the point designs and drew conclusions about the relative merits of each component-system configuration.

Concept 1: Baseline Configuration

So-called because it has been the dominant solution installed by wind turbine manufacturers worldwide, the baseline generator employs a multiple-stage gear speed increaser with a planetary low-speed front-end followed by one or two helical parallel shaft stages to achieve a nominal output speed suitable for a six-pole (1,200 rpm) wound rotor induction generator. Variable

frequency, variable voltage rotor power is converted to utility frequency and voltage by an electronics unit at the base of the tower.

Concept 2: Direct-drive Configuration

Direct-drive configurations offer significant potential for the wind industry because they eliminate the gearbox. The direct-drive configuration is already establishing a presence in the marketplace (via Enercon, Lagerwey, and Northern). The two types of direct-drive generators are the (1) wound-rotor synchronous generator and (2) PM rotor synchronous generator. Early in our evaluation of drivetrain configurations, both Northern and GDEB performed comparative studies of the two direct-drive generator options. In both cases, the permanent magnet topology was superior. Therefore, we considered only the PM synchronous direct-drive design.

The PM synchronous direct-drive configuration selected by the project team employs PM field poles in a radial field internal configuration. Only radial field designs were analyzed in detail because they are superior to axial field designs in terms of voltage induction, and are commonly used in electrical machinery. We analyzed a number of PM direct-drive tower-top configurations.

Concept 3: Gear-driven, Medium-speed Configuration

The concept of a single-stage gearbox coupled with a medium (100 rpm) speed generator has gained attention because it combines the benefits of a higher (than direct-drive) generator speed and a lower number of gear parts. The single-stage gearbox configuration can use either a wound rotor synchronous generator or a PM generator. For our drivetrain study, we chose the single-stage PM generator for its cost and performance advantages and relative simplicity compared with the wound rotor configuration.

Concept 4: Multiple-path Configuration

The options for multiple-path drivetrain configurations are many, ranging from multiple, medium-speed paths where multiple generators are driven off a single-stage gear path, to multiple higher-speed generators driven by separate, multiple gear paths. The number of generators could range from two to possibly as many as twelve. We evaluated many of these options. Initially we considered both specially made wound rotor and PM synchronous generators. However, the most promising multiple-path drivetrain configuration proved to be a gear-driven, medium-speed, six-generator configuration using PM generators.

The arrangement allows a number of pinion meshes with a common bull gear to share the total gear load, much like a planetary speed increaser. However, this advantage comes at the expense of more parts and the associated reliability and maintenance concerns. We considered these factors when evaluating this concept.

2.2 Design and Analysis Methodology

Generator. The generator design is based on GDEB's embedded permanent magnet technology. GDEB produced conceptual generator designs for all configurations. Its design process included defining generator parameters and developing conceptual designs (electrical and magnetic). Design analysis was performed using GDEB-proprietary and commercial software.

A parametric generator design and costing tool was developed to determine cost trends and to select design points for the GDEB effort. Power, speed, and life requirements were set by Northern.

Power Electronics. The power electronics designs utilized conventional insulated gate bipolar transistor (IGBT) systems, similar to that used for commercial PM motor drives. Instead of purchasing a standard drive, a custom drive was designed to have flexibility to optimize the control system for the generator. Simulations of the control system and generator were used to validate the designs.

Gears. Gear and bearing life requirements used in this study were based on limits set in *Standard for Design and Specification of Gearboxes for Wind Turbine Generator Systems* (ANSI/AGMA/AWEA 6006-A03 2003) and *Fundamental Rating Factors and Calculation Methods for Involute Spur and Helical Gear Teeth* (ANSI/AGMA 2001-C95). Gearing was designed to a minimum of 175,000 hours of life using duty cycles supplied by Northern. The bearing lives were calculated using the basic rating life L10, and minimum lives were held to limits set forth in Table 5-1 of the ANSI/AGMA/AWEA 6006-A03 specification.

Rotor. The SOW specifies a three bladed, pitch-controlled, rigid rotor. A standard design was implemented using currently available blade designs, electrically actuated pitch drives, an industry-standard pitch control system, and a spherical cast-iron hub. Windward Engineering developed and tuned the pitch controller for the 1.5-MW rotor. The same controller kernel was used for the 3-MW turbine. Northern tuned the control parameters to achieve the desired operational characteristics.

Tower. The SOW largely dictates the tower design. Tubular steel towers with the specified hub height were designed for each turbine.

Loads. We used the Fatigue, Aerodynamics, Structures, and Turbulence (FAST) program to calculate turbine loads under normal turbulence and extreme wind cases. Loads were calculated according to (IEC 61400-1 1999) and (Germanischer Lloyd 1999) standards and processed to yield the loads most useful for designing each component (bearings, gears, etc.). Windward Engineering developed the 1.5-MW baseline turbine model, and Northern developed the 3-MW model. The following loads were calculated for design purposes:

- Shaft torque duration loading
- Bearing load duration histograms
- Shaft-end extreme loads
- Shaft-end fatigue load histograms.

A reduced set of design load cases was analyzed to eliminate load cases that were not critical to the sizing of drivetrain components. Windward developed a program to create multidimensional histograms useful for bearing design.

Structural Design and Analysis. An FEA of major load-carrying components was conducted and the components were dimensioned according to (Germanischer Lloyd 1999) standards. As required by IEC 61400-1, structural design conforms to *General Principles on Reliability for Structures* (ISO 2394 1998). Reserve factors were calculated for both extreme loads and fatigue loads.

Cost Estimation. For this study, our primary evaluation metrics were first cost and COE. Under the WindPACT SOW, the COE calculation attempts to quantify the overall life cycle costs by applying the design to a 200-MW wind farm based on the chosen technology. Because some developers buy turbines based on first cost and others based on COE calculations, we present both.

The development of first cost and COE is described as follows:

1. Develop the capital costs of turbine components. (Costs are based on quotes for both standard and custom components.)
2. Include the costs associated with transportation and assembly of components.
3. Develop a sale price based on an assumed profit margin.
4. Determine the annual energy production based on the mechanical power curve and drive efficiencies.
5. Determine the annual operation and maintenance costs.
6. Determine the COE as follows:

$$\text{COE} = (\text{FCR} \times \text{ICC} + \text{AOM}) / \text{AEP}$$

where

FCR = fixed charge rate
ICC = initial capital cost
AOM = annual operation and maintenance
AEP = annual energy production

Note that the AOM includes the levelized replacement cost (LRC).

2.3 Technology Assessment

To ensure the technical success and market relevance of the WindPACT project, we conducted a comprehensive assessment of drivetrain technology.

The project team:

- Examined commercial wind turbines
- Reviewed previous drivetrain studies in journals, trade publications, and reports
- Examined industry and technology trends
- Studied advances in drivetrain component reliability
- Examined drivetrain technology options for gearboxes, generators, and power electronics.

2.3.1 Commercial Wind Turbines

Our technology assessment first focused on standard commercial wind turbines. We studied the following types of turbine designs:

- Industry-standard, gear-driven, doubly-fed induction generator (DFIG)
- Single-stage gearbox with PM generator
- Direct-drive with PM and wound rotor generators.

The majority of commercial wind turbines being installed are standard, gear-driven, DFIG configurations. However, a number of nonstandard wind turbine configurations are gaining prevalence in the industry. The commercial success of German wind turbine supplier Enercon, which captured 15.2% of the world market in 2001 (ranked second worldwide) with direct-drive wind turbine solutions, proves the commercial viability of nonstandard drivetrain configurations. The success of Enercon and the choice of direct-drive technology for product development by other industry players, such as Jeumont, Lagerwey, Mitsubishi and M. Torres, are solid proof that direct-drive designs can be the basis for megawatt-class turbines that compete successfully with gear-driven models. Other nonstandard drivetrain configurations, such as WinWind (based on MultiBrid technology), are also considerations. Table 2-2 shows a selection of nonstandard turbine drivetrains in use or under development.

Table 2-2. Drivetrain Configurations of Nonstandard Commercial Turbines

Manufacturer	Rated power (kW)	Drivetrain type
Lagerwey	750	Direct-drive, wound rotor
Jeumont	750	Direct-drive, permanent magnet, axial flux
Enercon	850; 1,500	Direct-drive, wound rotor
Mitsubishi	2000	Direct-drive, permanent magnet

According to the *WindStats Newsletter* (Autumn 2002), “the PMG [permanent magnet generator] has become a first preference for new manufacturers eager to make a direct drive market entry” (Table 2-3).

Table 2-3. “High Potential” Direct-Drive Projects

Model	Capacity (MW)	Generator type	Technology	Status
Lagerwey LW58	0.75	External excitation	VS/pitch	Prototype (2002)
Vensys Energiesysteme	1.2	Permanent magnet	VS/pitch	NA
M. Torres TWT1500	1.5	External excitation	VS/pitch	Prototype (2002)
Jeumont J70/J77	1.5	Permanent magnet	VS/pitch	Prototype (2003)
NPS NW1.5/70	1.5	Permanent magnet	VS/pitch	NA
Lagerwey LW72	2.0	Permanent magnet	VS/pitch	Prototype (2002)
ScanWind	3.0	Permanent magnet	VS/pitch	NA
Leitwind LTW62	1.2	Permanent magnet	VS/pitch	Prototype (2003)

Source: WindStats Newsletter (Autumn 2002).

2.3.2 Previous Drivetrain Studies

Our investigation of drivetrain options benefited from reports in technical and trade journals. We reviewed previous and current drivetrain studies and technological advances in drivetrain materials and components. Following are the major findings from our review of drivetrain studies.

- Most direct-drive assessments focused on innovative measures to reduce size, weight, and cost of generator.
- Direct-drive generators must attain a very high torque capacity (mass-specific) to compete with high-speed squirrel cage or doubly-fed wound rotor induction generators.
- (Bohemeke and Boldt 1997) reported “a clear advantage for the gear-driven configuration” and concluded that direct-drive configurations can compete economically only if very high failure rates are assumed for geared drive configurations.
- (Grauers 1994) analyzed annual average efficiency as a function of wind distribution and found a small efficiency advantage for direct-drive configurations.

2.3.3 Industry Trends

The trend toward alternative drivetrain configurations, and more specifically direct-drive configurations, is evidenced through predictions in wind industry market reports, research papers, and trade journals.

“2005 technology: variable speed, direct drive permanent magnet generator . . .” (*Renewable Energy Technology Characterizations*, Electric Power Research Institute, 1997).

“While it would appear optimistic to expect large mass or cost savings in large wind turbines purely by the introduction of a direct drive system, it is likely that in a fully integrated design . . . the simplification of design, provision of wide range variable speed and elimination of gearbox maintenance will all favour the continuing development of direct drive systems.” (*Gardner*, 1998).

“Another trend is the increased focus on direct drive machines, even though it is not yet reflected in commercial sales other than those from Enercon and Lagerwey.” (BTM Consult, 2001).

“Elimination of the gearbox by using variable speed generators will increase through use of permanent magnetic generators on larger turbines increasing the need for magnetic materials.” (*Anacona*, 2001).

“ . . . direct drive has become a well-established concept—established enough that a growing number of companies are working on systems of their own. ABB and Siemens . . . envisage considerable market growth for direct drive systems in the future.” (*WindStats Newsletter*, Autumn 2002).

Each month, editorials in leading industry trade journals tout the bright future of nonstandard turbine designs, particularly direct-drive technology. Historic barriers to new technology in the wind industry are easing as acceptance of wind power grows. The wind industry has blossomed into a business that grosses more than US\$14 billion per year. (*Pullen*, 2006)

Turbine subsystem designs, including controls, yaw drives, blade pitching systems, gearboxes, generators, and blades, are no longer proprietary. Increasingly, turbine manufacturers are integrators because they can introduce turbines with innovative drivetrains without “reinventing” the balance of the system. Component suppliers can sell drivetrain products without becoming turbine manufacturers. In short, many turbine components are becoming commodities.

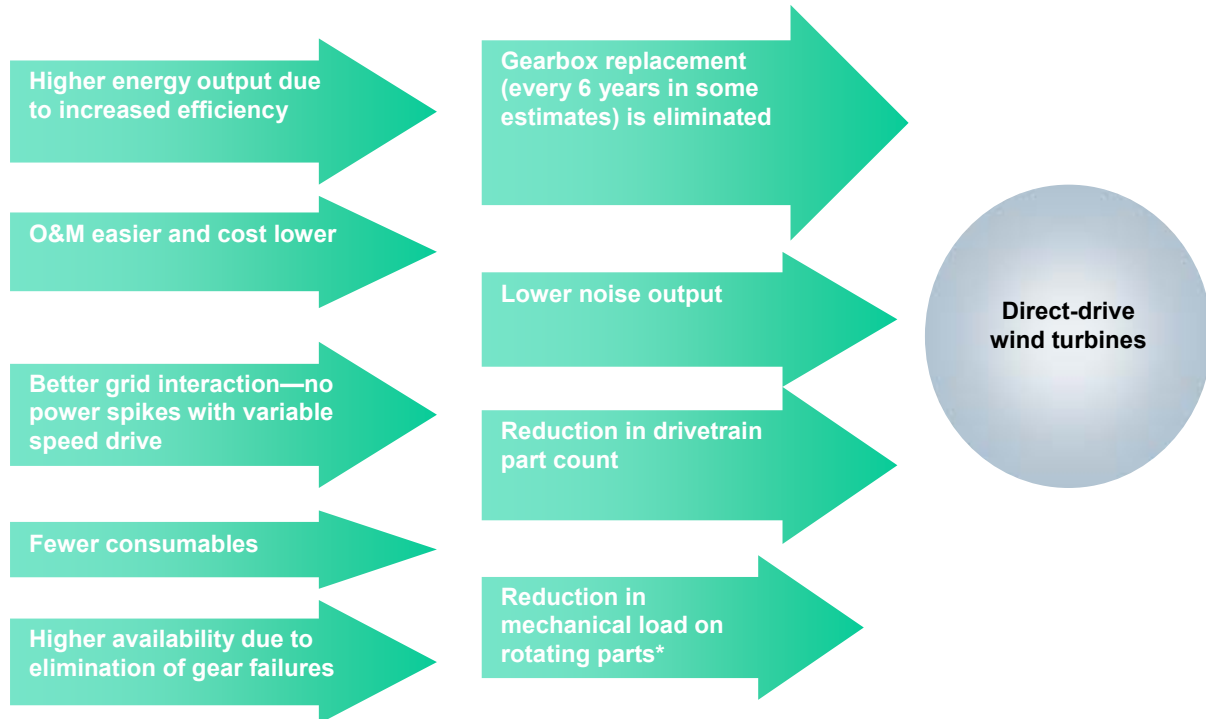
Although our research confirmed the trend toward alternative drivetrain configurations, we sought further verification by surveying wind farm developers, operators, and major international turbine suppliers. Conducted for the WindPACT project by TIAX in June 2001, the survey focused on the following:

- Industry perception of direct-drive versus gear-driven turbines
- Gearbox maintenance requirements and costs

- Primary factors affecting turbine procurement choices.

Following are the two key findings of the survey accompanied by illustrative figures:

- Direct variable-speed drive wind turbines likely will see increased market penetration over the next few years (Figure 2-1).



*Compared with constant-speed, gear-driven wind turbines.

Figure 2-1. Advantages of direct-drive turbines.

- To achieve greater market penetration, minor hurdles must be overcome (Figure 2-2).

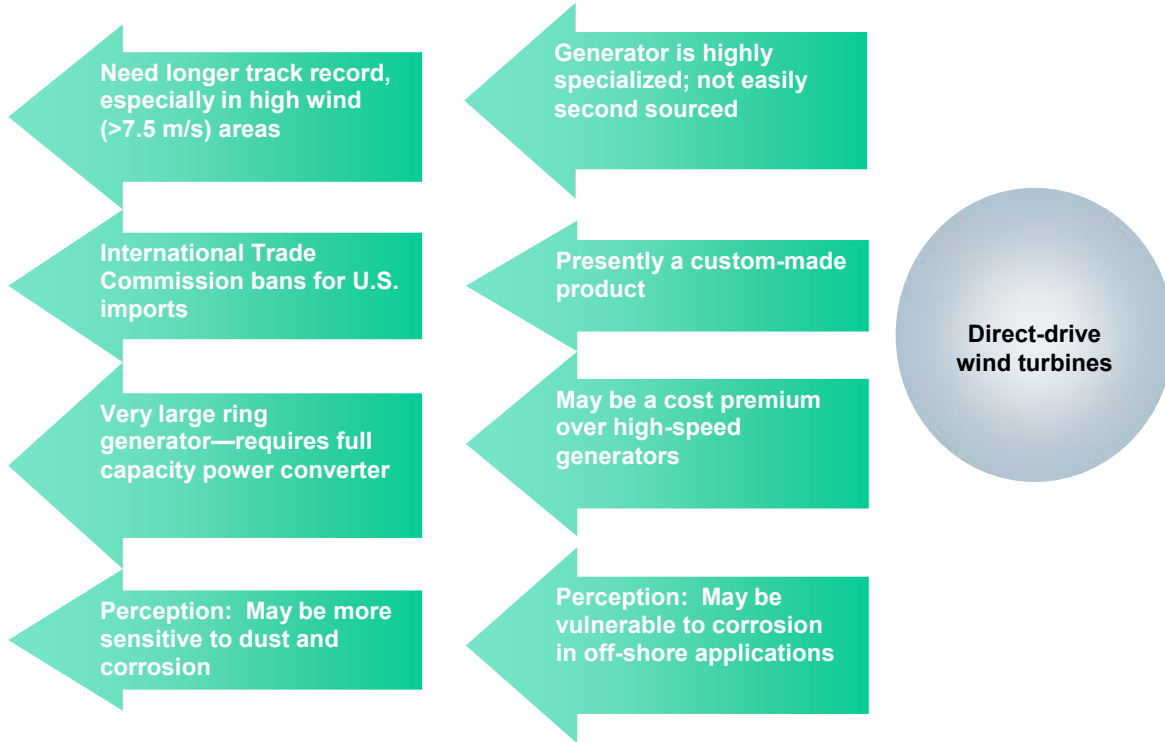
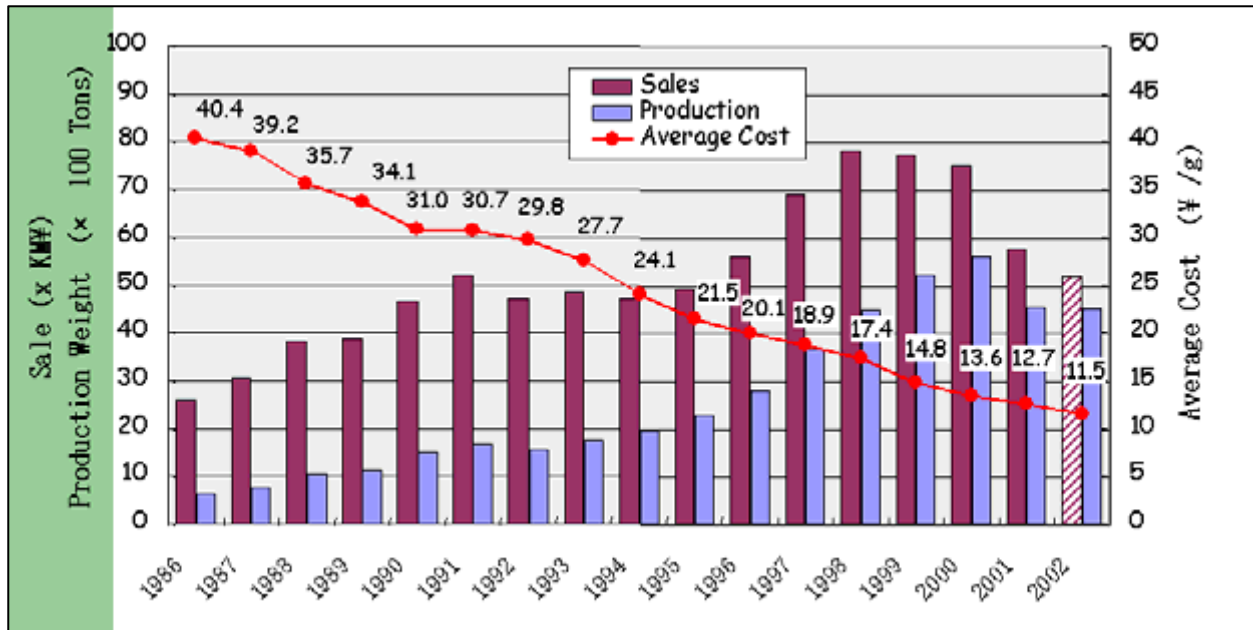


Figure 2-2. Disadvantages of direct-drive turbines.

2.3.4 Technology Trends

Rare-Earth Magnets. Historically, the high cost and limited availability of high-strength, rare-earth, permanent magnets inhibited the commercial viability of motors and generators based on PM design topologies. Over the last decade, the cost of these magnets has dropped significantly, in part due to their use in motors of computer hard drives and other electronic devices. Rare-earth magnets, such as Neodymium Iron Boron (NdFeB), now have the combination of high-energy density and relatively low cost based on the availability of constituent ores. Figure 2-3 depicts the historical trends of rare-earth magnet production and pricing in Japan, which are indicative of the worldwide trends. The currency shown is the Japanese yen.



Courtesy of Shin-Etsu Magnetics

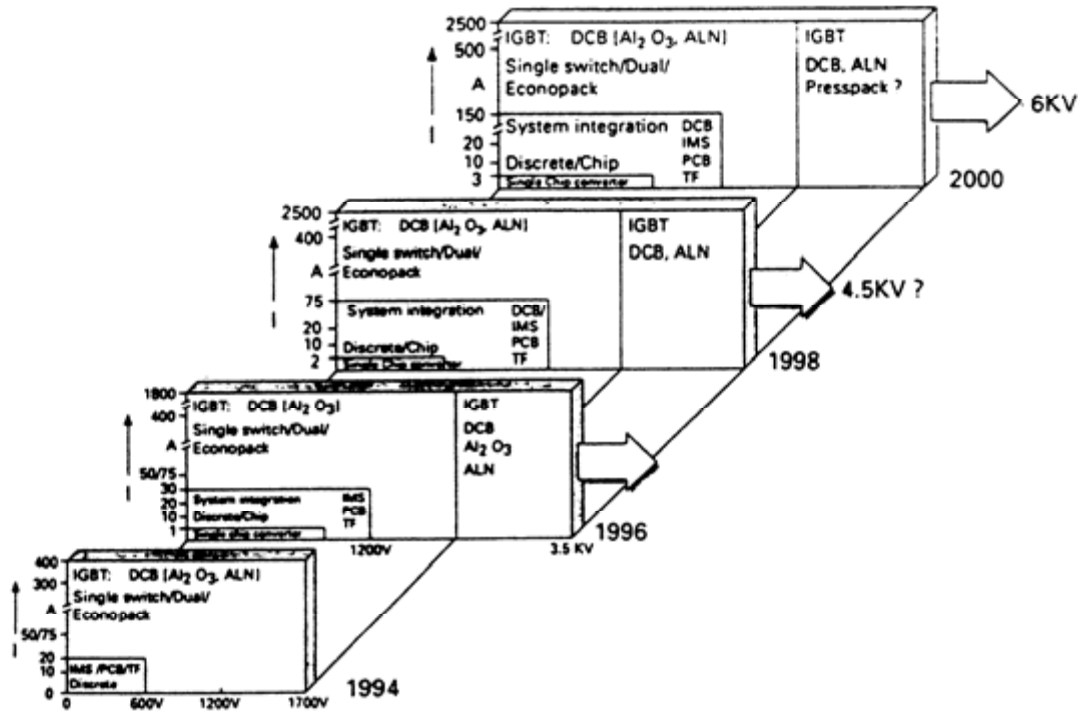
Figure 2-3. Rare-earth magnet cost has been falling as production has been increasing.

For the WindPACT project, we solicited quotes from magnet vendors that reflect shorter-term competitive prices, which further supports the use of these materials in commercial electromagnetic machinery. Because magnets constitute a major cost in a large-scale PM generator, even minor reductions in magnet costs can impact the overall cost significantly.

PM machines, which once carried a premium price because of the cost of magnets, are now cost-competitive with conventional wound rotor motors and generators. Also, for very large machines, such as those considered in this study, magnet vendors will price very aggressively based on the size of the order. Where these magnets may have cost more than US\$100 per pound 10 years ago, a final burdened cost of less than US\$20 per pound is possible today.

Semiconductor Technology. Semiconductor technology has improved greatly in terms of cost, size, and power capabilities. These improvements have a beneficial impact on the cost of wind turbines, especially those using full-rated power electronics (Jaecklin 1997). The research implies it is possible to build megawatt-range power electronics with the three types of semiconductor switches. A mature technology, thyristor’s rate of growth (with respect to power handling) has stagnated over time. Newer technologies, such as injection-enhanced gate transistors (IEGT) and integrated gate commutated thyristors (IGCT), can potentially achieve much higher power-handling capability (Akagi 2002).

Component integration is another emerging trend in the field of power semiconductors. Power switches are available as packaged components that integrate gate circuits, multiple switches for the power-circuit topology, insulation, voltage current and temperature sensing elements, and fault protection. Figure 2-4 shows these packaged Insulated Gate Bipolar Transistor (IGBT) modules are available in higher voltages and current ratings (Lorenz 1997).



Source: Lorenz (1997).

Figure 2-4. Development and integration of power semiconductors and modules

Packaged modules lend themselves to simple mechanical and thermal design, which leads to lower system cost. The reduced cost of power semiconductor devices is reflected in the 50% cost reduction of standard drive units in the 30 hp range between 1990 and 2000 (Kerkman et al. 1999). Newly emerging power switching and packaging technologies indicate that the cost reduction trend will continue.

The cost of power semiconductor devices is decreasing, while the performance of power semiconductor devices is improving (higher voltage ratings and lower switching losses). Increased control capability from the latest digital signal processing (DSP) technology enables complex switching methods and higher bandwidth control. These advances are leading to decreased cost per kilovolt ampere (kVA) for power conversion equipment.

2.3.5 Drivetrain Component Reliability

We obtained data about the reliability of drivetrain components from the Allianz Center for Technology, W.A.Vachon and Associates, and Betreiber-Datenbasis. Since the mid-1990s, the Allianz Center for Technology has analyzed causes of damage to wind turbine components. A recent article states, “the main center of damage is in the gear train—teeth, roller bearings, oil—and the generator bearings” (Bauer 2001). The Allianz Center for Technology provided us cost data for replacement and repair of drivetrain components.

Wind industry consultant W.A.Vachon and Associates predicted a mean time between failures (MTBF) of 12 to 15 years for well-maintained gearboxes, and an MTBF of 10 years for high-speed generators.

Experienced in wind turbine O&M, both the Allianz Center for Technology and W.A.Vachon and Associates confirmed that the gearbox is a major contributor to downtime and O&M costs.

To assess the difference in O&M costs between gearbox and direct-drive configurations, we obtained data from Betreiber-Datenbasis, the source of *WindStats Newsletter* data for turbines operating in Germany. We wanted to compare failure rates, downtime, and other characteristics of direct-drive configurations with baseline configurations over several years.

However, because direct-drive is the only alternative to multiple-stage gearbox-based designs with any operating history, data for alternative configurations other than direct-drive did not exist (Table 2-4). Furthermore, almost all direct-drive configuration data were for Enercon turbines. The lack of diversity in data for alternative configurations, as well as inconsistently reported data, made it difficult to quantify O&M costs for alternative drivetrains.

Table 2-4. Reliability Comparison of Gearbox and Direct-Drive Configurations

Rated power	500–900 kW		>999 kW	
	Gearbox	Direct-drive	Gearbox	Direct-drive
Drivetrain configuration				
Availability (%)	98.83	98.69	97.07	98.43
Average turbine age (months)	46	36	17.5	22.5

Source: Betreiber-Datenbasis (1999–2000).

We decided to build a model “from the ground up” to quantify O&M costs for each drivetrain configuration. The model includes both costs affected by the type of drivetrain configuration and costs independent of the drivetrain configuration.

O&M costs ranged from US\$6,500 to US\$9,000 per turbine during warranty. After warranty, costs ranged from US\$10,000 to US\$20,000 per turbine (Table 2-5).

Developers and suppliers were questioned about wind turbine O&M costs. Most commercial wind turbine manufacturers sell a service plan to cover turbine maintenance for the first 5 years. According to respondents, after the first 5 years (i.e., post-warranty), O&M costs generally increase.

Table 2-5. Estimated O&M Costs for Gear-Driven 650–900-kW Turbines

	US\$/Turbine/Yr (during warranty)	US\$/Turbine/Yr (after warranty)	Cents/kWh (during warranty)	Cents/kWh (after warranty)
Developer P	\$8,500	NA	0.4	NA
Developer Q	\$6,500–\$8,500	NA	NA	NA
Manufacturer R	\$6,500	\$11,000–\$12,000		
Manufacturer S	NA	NA	0.5	0.75
Manufacturer T	\$8,000			
Consultant U	\$9,000	\$20,000 ^a	0.6	1.0
Vendor V^b	\$8,000	\$10,000		

^a\$400,000/MW over 20 years with inflation and crane costs.

^b75%–80% of costs are associated with gearbox and cooling.

2.3.6 Drivetrain Technology Options

2.3.6.1 Gears

Reviewing current gearbox technology, Gear Consulting Services of Cincinnati (GCSC) found the following types of gearing applied to wind turbines:

- Multistage parallel
- Multistage/multipath parallel
- Single-stage epicyclic/two-stage parallel
- Multiple-stage epicyclic/single-stage parallel
- Compound planetary/single-stage parallel
- Single-stage epicyclic/two-stage parallel.

Prior to working on this project, GCSC designed a MW-scale gearbox for a major wind turbine manufacturer. On the basis of the team’s expertise and experience, we determined that the compound planetary technology was the most suitable gearbox technology for our study. This technology has the lowest cost due to reduced tooth loading.

Gearbox Reliability. Because of widespread gearbox failures, many steps have been taken to improve wind turbine gearboxes, including:

- *Monitoring gearbox vibrations and condition of gearbox oil.* The NEG Micon retrofit program upsized gearbox bearings and improved bearing lubrication in more than 1,200 turbines.
- *Improved oil filtration systems.* According to C.C. Jensen, supplier of gearbox oil filtration systems to Bonus Energy, NEG Micon, Vestas, and Gamesa, “When you change the filter size from 40 microns to 10 microns, you double the lifetime of the [gearbox] roller bearings.”

Today wind turbine gearboxes are built to a stricter, more robust AGMA standard. This is consistent with our market survey, in which some European manufacturers reported customers increasingly willing to pay a premium for “heavy duty” gearboxes.

Gearbox Costs. Our market survey of wind farm developers, operators, and major international turbine suppliers revealed that gearbox replacement for a 660- to 900-kW machine is typically between US\$50,000 and US\$75,000 per turbine. Repairs range from US\$10,000 to US\$30,000 but vary greatly depending on turbine location and crane requirements (Table 2-6).

Table 2-6. Estimated Gearbox Costs for 650- to 900-kW Turbines

	Costs (US\$)	Comments
Developer X	≈\$50,000–\$60,000 Repair: ≈\$30,000 minimum	Costs vary greatly depending on turbine placement and crane requirements ≈\$10,000 minimum to transport crane to site
Manufacturer R	Replacement: \$50,000–\$70,000 Repair: \$10,000–\$20,000	High-end costs includes crane
Manufacturer W	≈\$60,000	NA
Consultant U	Replacement: \$75,000	Additional \$35,000 for crane

2.3.6.2 Generators

Table 2-7 describes the types of generators used for megawatt-scale wind turbines.

Table 2-7. Types of Generators for Megawatt-Scale Turbines

Type of generator	Description
High-speed induction—fixed speed with no power electronics	Simple, proven generator design Current inrush each time the machine is connected to grid Efficiency is poor
Wound rotor high-speed induction—variable speed	Proven generator configuration Slip rings and rotor winding add to rotor complexity Efficiency slightly better than cage rotor induction machines Usage of wound rotor avoids need for compromising efficiency (like in cage machines) since no induced slip current losses in wound rotor machines (induction between stator/rotor causes slip currents and related losses in cage machines); also power electronics can be connected in series with rotor windings for greater torque from minimum to maximum speed and reduced current transient overshoot at an improved power factor in wound rotor machines
Wound field synchronous machines—direct-drive with power electronics	Proven generator configuration Requires full-size power electronics Machine is large due to low-speed design Possible efficiency improvement over the wound field induction machine Slip rings or separately coupled excitations system necessary
Permanent magnet synchronous machines (PMSM)—direct-drive with power electronics	Relatively new generator configuration Requires full-size power electronics Machine is large due to low-speed design Efficiency better than synchronous machines because rotor excitation is eliminated
Medium-speed PMSM—single stage with power electronics	Requires full-size power electronics All machine design advantages of preceding generator types, plus reduction in size due to higher speed of operation
Multiple-generator drive	Individual medium-speed generators operate at a fraction of turbine rated power Components, such as bearings, housing, and terminations, must be duplicated

We performed a comprehensive assessment of generator technology and evaluated candidates. TIAX assessed generator technology and presented its findings to the team. On the basis of the TIAX assessment and the expertise of the WindPACT team, we determined the most suitable configurations for our study.

Generator configurations can be classified as axial, radial, or transversal flux. Table 2-8 lists the distinguishing features of each class.

Table 2-8. Distinguishing Features of Radial, Axial, and Transversal Flux Generators

Class of generator configuration	Torque productive armature current path	Torque productive field flux path	Winding	Phases
Radial flux	Parallel with respect to rotation axis	Radial with respect to rotation axis	Distributed or concentrated	Typically 3
Axial flux	Radial with respect to rotation axis	Parallel with respect to rotation axis	Distributed or concentrated	Typically 3
Transverse flux	Circumferential with respect to rotation axis	Toroidal with respect to current axis	Concentrated	2 or 3

Radial Flux Configuration. The radial flux configuration is the most widely used in electrical machinery in general and wind turbine generators in particular. The ABB Windformer™ generator is a typical radial flux configuration.

Axial Flux Configuration. Envisioned at the dawn of the electrical age, axial flux configurations have sustained academic interest; however, until the introduction of Jeumont’s J-48 axial flux direct-drive wind turbine, commercial units were found only in highly specialized applications, such as computer disk drives and industrial servomotors. Analysis by Grauers (1994) found the axial flux configuration deficient: The field at the inner portion of the machine contributes less to voltage induction than the field at the outermost station. (By contrast, all portions of the field in a radial flux configuration have an equally effective impact on voltage induction.)

Transverse Flux Configuration. The high torque density potential of the transverse flux machine and its modular, although complex, construction recommends this concept for a large direct-drive wind turbine generator if potential shortcomings can be overcome. Unfortunately, since the scale of designs investigated and tested to date is small (<10 kW), exploiting this concept for generator sizes envisioned by the WindPACT project entails excessive technical and programmatic risks.

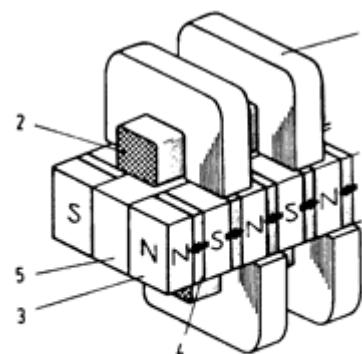
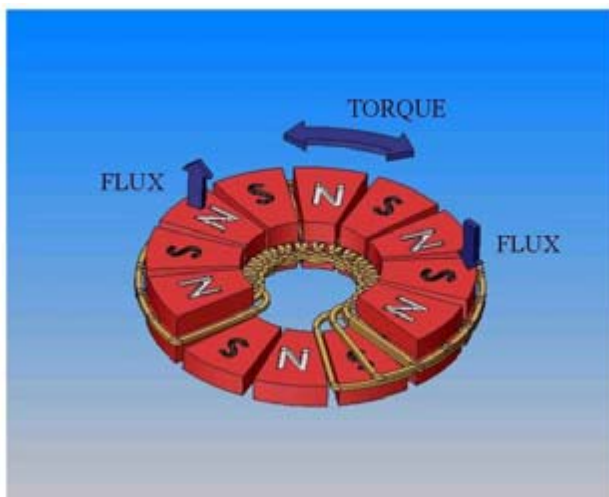


Fig. 5: Proposed transverse flux generator concept
 1...stator core elements
 2...armature winding
 3...rotor
 4...permanent magnets
 5...nonmagnetic material

Figure 2-5. Axial and transverse flux configurations were considered.

Generator Architectures. A number of generator architectures fall within the broad classification of radial flux and axial flux configurations. Heffernan and colleagues (1996) studied the radial flux generator architectures in Table 2-9.

Table 2-9. Radial Flux Generator Architectures

Generator architectures	Variations	Notes
Doubly-salient PM	Single- and three-phase Ferrite or NdFeB magnets	Unconventional concept Magnets located on the armature core
PM field synchronous	Surface NdFeB magnets Buried ferrite or NdFeB magnets	Well-established concept GDEB-patented technology
Wound field synchronous	—	Well-established concept Enercon direct-drive generator configuration
Squirrel cage induction	—	Classic design for high speed
Doubly-fed induction (brushless)	Without power electronics With power electronics	Brushless configuration unconventional
Switched reluctance	—	Unconventional concept at this size

Although the most successful direct-drive generator to date is the wound field synchronous architecture employed by Enercon, the current focus of academic and commercial development is the PM field synchronous machine. Other candidates have been examined in previous studies, the most comprehensive being that by Heffernan and colleagues (1996) in which they examined less promising candidates, including the squirrel-cage machine, the doubly-fed brushless generator (both with and without electronics), the switched reluctance generator, and the doubly-salient PM generator.

Heffernan and colleagues favored only two architectures for a direct-drive generator in the power ratings of interest: wound field synchronous and PM synchronous. Table 2-10 shows weight and cost estimates of electromagnetic (EM) material for seven PM synchronous generator concepts they considered, normalized to weight and cost estimates for the proven direct-drive wound synchronous generator (first row of Table 2-10) exemplified by the Enercon configuration. All the radial field designs achieved an efficiency of 93% (presumably at their rated power of 500 kW and rated power speed of 50 rpm). Because efficiency is not stated for the transverse flux designs, weight and cost comparisons may not be valid.

Table 2-10. Normalized Weight and Cost of Materials of Favorable Generators

Generator configuration	Material weight (lb)	Material cost (US\$)
144-pole wound field synchronous—baseline for PM-relative weights and costs	6,700.00	\$3,600.00
144-pole radial flux PM—buried ferrite magnet	6,499	\$3,708
144-pole radial flux PM—buried rare-earth (NdFeB) magnet	6,432	\$9,756
144-pole radial flux PM—surface ferrite magnet	8,844	\$4,968
144 pole radial flux PM—surface NdFeB magnet	6,566	\$9,504
48-pole transverse flux PM—ferrite magnet ^a	5,360	\$3,852
58-pole transverse flux PM—NdFeB magnet ^b	3,752	\$6,228
96-pole axial flux PM—ferrite magnet ^c	3,350	\$2,736

^{a,b}Weh and May (1988).

^cIdentified as axial field.

Source: Heffernan et al. (1996).

From a cost, size, and weight perspective, Heffernan and colleagues concluded that the differences between the buried ferrite magnet and wound field synchronous designs were small and that the buried ferrite magnet design was more suitable. Except for using ferrite instead of NdFeB magnet material, General Dynamics presented the same embedded design at the WindPACT project kickoff meeting. The experience of Cantarey Reinoso (a former ABB plant located in Spain) enabled us to compare the proposed PM configuration to a commercial wound field machine. Significant cost decreases in recent years have made PM machines more commercially viable.

Although the advantages of the 96-pole axial flux generator were acknowledged, concern was expressed about the structural integrity of the disk-like PM field structure. Moreover, tools to analyze its 3D field and current distributions were unavailable.

Comparing PM with wound field, the following are advantages of PM:

- Higher operating efficiency—from 6% to 8%
 - Permanent magnets rather than excited field
 - Elimination of field losses.
- Smaller, lighter
 - Higher torque density
 - 50% lower internal heat generation.
- Simpler—less to manufacture, QA, and assemble
 - No slip rings or brushes
 - No field coils, wiring, or excitation control
 - Substantially smaller thermal dissipation system.
- Inherent design features
 - Fail-safe and parking brake.

Comparing embedded magnets with surface mount magnets, the following are advantages of embedded magnets:

- Concentrated and directed flux field
- No eddy currents in magnet face
- Easy to fabricate and install
- Magnets are not subject to mechanical stresses in operation.

2.3.6.3 *Power Electronics*

Power electronics options were limited to commercially available systems because the WindPACT statement of work did not include power electronics research and design. Thus, TIAX conducted a survey of commercially available power electronics technology for use in wind turbine configurations. These technologies options are also focused on permanent magnet generators. Following are three commercially available power electronics topologies for the wind turbine drivetrain:

- Insulated gate bipolar transistor (IGBT) rectifier and inverter
- Diode rectifier–IGBT inverter
- Semiconductor controlled rectifier (SCR)–based topology.

The generator cost is approximately 44% higher with a diode rectifier or SCR-based power electronics due to the restricted power factor for a given power, DC link voltage, and current. Also, integrated IGBT modules, as described in Section 2.3.4, are available at reasonable prices that are decreasing over time. Therefore, we selected the IGBT rectifier and inverter for the WindPACT project, because it provided the lowest cost of the combined generator and power electronics system.

IGBT power converter hardware is unaffected by generator speed at frequencies for direct-drive and medium-speed wind turbines. The IGBT rectifier is referred to as an “active rectifier” to differentiate it from the traditional, diode-bridge rectifier. There is no difference in power electronics cost between the direct-drive and the single-stage, single-output configurations with gearboxes. However, in the multiple-generator configuration with parallel power paths, each generator requires an active rectifier. A comparison of air- and water-cooling costs indicates that water-cooling is less expensive in the 1-MW power range when using switching frequencies greater than 2 kHz. On the basis of cost, we chose a water-cooled power converter.

2.4 Design Specifications and Parameters

2.4.1 Drivetrain Specifications

Table 2-11 shows typical specifications for the 1.5- and 3-MW turbine designs.

Table 2-11. Turbine Drivetrain Specifications

Electrical power rating	1.5 MW	3 MW
Low-speed shaft speed		
Minimum	12.0 rpm	8.5 rpm
Rated	19.7 rpm	15.3 rpm
Maximum design	27.8 rpm	19.1 rpm
IEC WTGS Design Class	II	II
Cut-in wind speed	3 m/s	3 m/s
Rated wind speed	12 m/s	12 m/s
Cut-out wind speed	25 m/s	25 m/s
Rotor diameter	70.5 m	94.8 m
Hub height	84.0 m	112.0 m
Operating Environment	-15°C to 50°C Ambient Air 0 to 100% Humidity, Condensing	-15°C to 50°C Ambient Air 0 to 100% Humidity, Condensing
Design life	20 yr	20 yr
Power control	Independent Pitch	Independent Pitch
Safety System	Pitch Control	Pitch Control

Values for the baseline configurations are derived from turbine simulations and Germanischer Lloyd recommendations.

Rated electrical power values assume 94% drivetrain efficiency at converter output.

2.4.2 Turbine Safety and Operation

Three independently pitching blades compose the turbine safety system. Normal and emergency shutdowns are achieved by pitching the three blades simultaneously. Redundant safety is inherent in this design because the turbine can be brought to a safe condition despite the failure

of one pitch drive. In either case, the rotor can be brought to rest by applying the shaft disk brake after the rotor is slowed by the pitching action of the blades. During normal operation, the controller supervises all turbine operations. Only the transition to the maintenance state is initiated through human-machine interface.

2.4.3 Power Curves

Figure 2-6 shows the power curve for the 1.5-MW baseline turbine and Figure 2-7 shows the power curve for the 3-MW turbine. There will be slight variations in the power curve for different drivetrain configurations due to variations in drive efficiency.

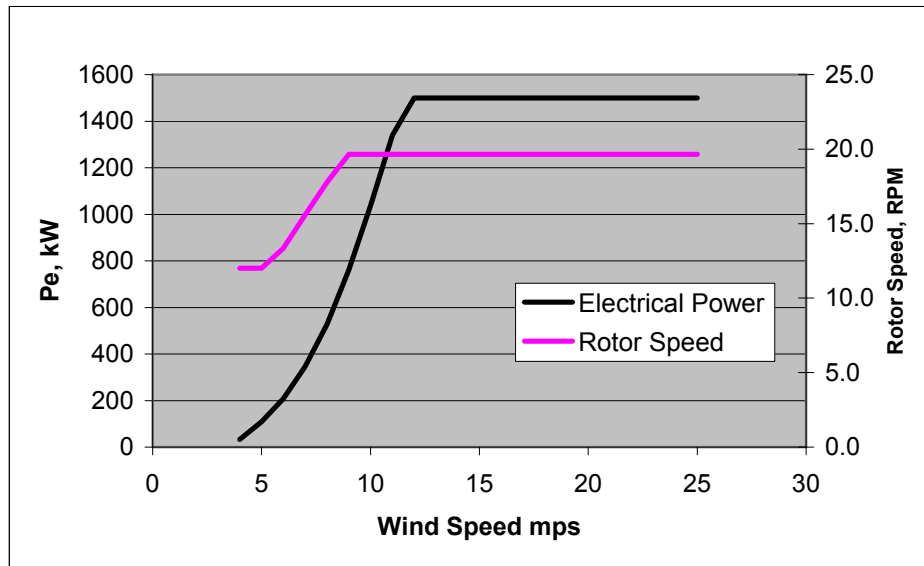


Figure 2-6. 1.5-MW baseline power curve

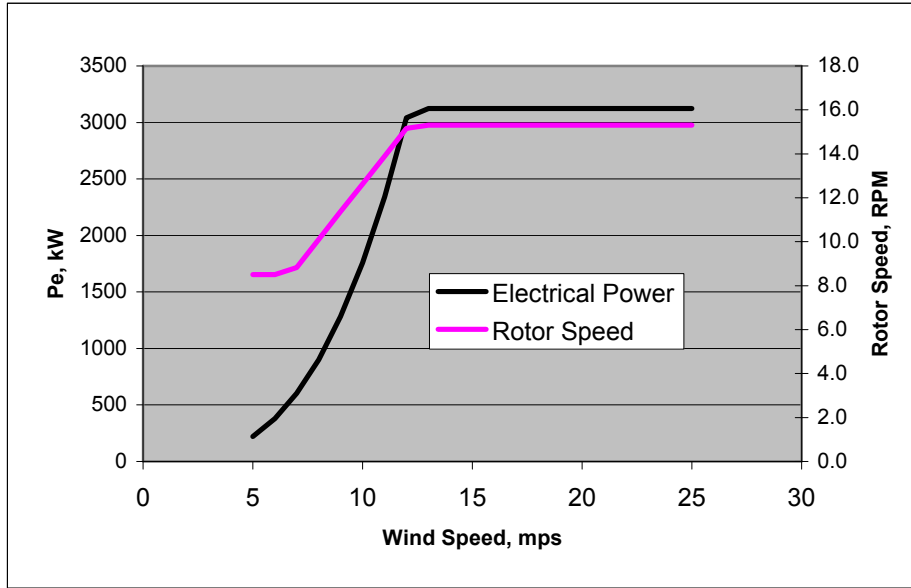


Figure 2-7. 3.0-MW baseline power curve

2.4.4 Power Electronics

The power electronics specification is shown in Table 2-12. Electrical output from the power electronics conforms to *IEEE Recommended Practices and Requirements for Harmonic Control in Electrical Power Systems* (IEEE Std 519-1992). Voltage tolerances adhere to *Electrical Power Systems and Equipment—Voltage Ratings (60Hz)* (ANSI C84.1-1995). The wind turbine incorporates anti-islanding standards, both meeting UL1741 Sec. 46.3 requirements and protecting from typical grid faults such as voltage, frequency, or current issues.

Table 2-12. Power Electronics Specification

Attribute	Description
Output surge power	120% of rated power for 30 seconds
Frequency	50/60 Hz; programmable
Switching frequency	Minimum 5 kHz
Efficiency	>95% from 50% to 100% of rated power
Displacement power factor	>0.95 from 50% to 100% of rated power
Operating Environment	-20°C to 50°C Ambient Air 0 to 100% Humidity, Condensing

2.4.5 Loads

Table 2-13 shows the loads cases used as the basis for sizing components for the 1.5-MW and 3-MW turbines. The *Northern Power Systems Alternative Drivetrain Design Study Report* (Bywaters, 2004) contains the actual computed loads. Table 2-14 shows the partial loads factors used in our analysis.

Table 2-13. Design Loads Cases

Design situation	IEC DLC	Wind condition	Type of analysis	Comments	
Power production	1.1	NTM 8 to 24 mps	Ultimate		
	1.2	NTM 8 to 24 mps	Fatigue		
	1.3	ECD 12 mps	Ultimate	Negative Direction	
	1.3	ECD 12 mps	Ultimate	Positive Direction	
	1.6	EOG 12 and 24 mps	Ultimate		
	1.7	EWS 12 and 24 mps	EWS 12 and 24 mps	Ultimate	Negative Direction, Horizontal Shear
					Positive Direction, Horizontal Shear
					Negative Direction, Vertical Shear
					Positive Direction, Vertical Shear
	1.8	EDC 12 and 24 mps	EDC 12 and 24 mps	Ultimate	Negative Direction
					Positive Direction
1.9	ECG 12 mps	ECG 12 mps	Ultimate		
Parked	6.1	NTM 42.5 mps	Ultimate		

Source: IEC (1999).

Design situation	DLC	Wind condition	Type of analysis	Comments
Power production	1.1	NTM	U	6 seeds each at 8, 12, 16, 20, and 24 mps
	1.2	NTM	F	6 seeds each at 8, 12, 16, 20, and 24 mps
	1.3	ECD_0	U	1 run at 12 mps
	1.3	ECD_00PR	U	1 run at 12 mps
	1.6	EOG_01_	U	2 runs total at 12 and 24 mps
		EOG_50_	U	2 runs total at 12 and 24 mps
	1.7	EWSH00N	U	2 runs total at 12 and 24 mps
		EWSH00P	U	2 runs total at 12 and 24 mps
		EWSV00	U	2 runs total at 12 and 24 mps
		EWSV00p	U	2 runs total at 12 and 24 mps
	1.8	EDC_50N	U	2 runs total at 12 and 24 mps
		EDC_50P	U	2 runs total at 12 and 24 mps
		EDC_01N	U	2 runs total at 12 and 24 mps
		EDC_01P	U	2 runs total at 12 and 24 mps
	1.9	ECG_00_R	U	1 run at 12 mps
				3 seeds total
Parked	6.1	NTM, $V_{\text{mean}} = 42.5$ mps	U	

Table 2-14. Partial Loads Factors

Applied to	Value
Extreme loads	1.35
Fatigue loads	1.00

Source: IEC (1999).

2.5 Drivetrain Designs

2.5.1 Baseline Design

The baseline design is based on a compound-planetary/parallel-shaft helical gearbox, industry-standard doubly-fed wound rotor induction generator, and power electronics package (Figure 2-8).

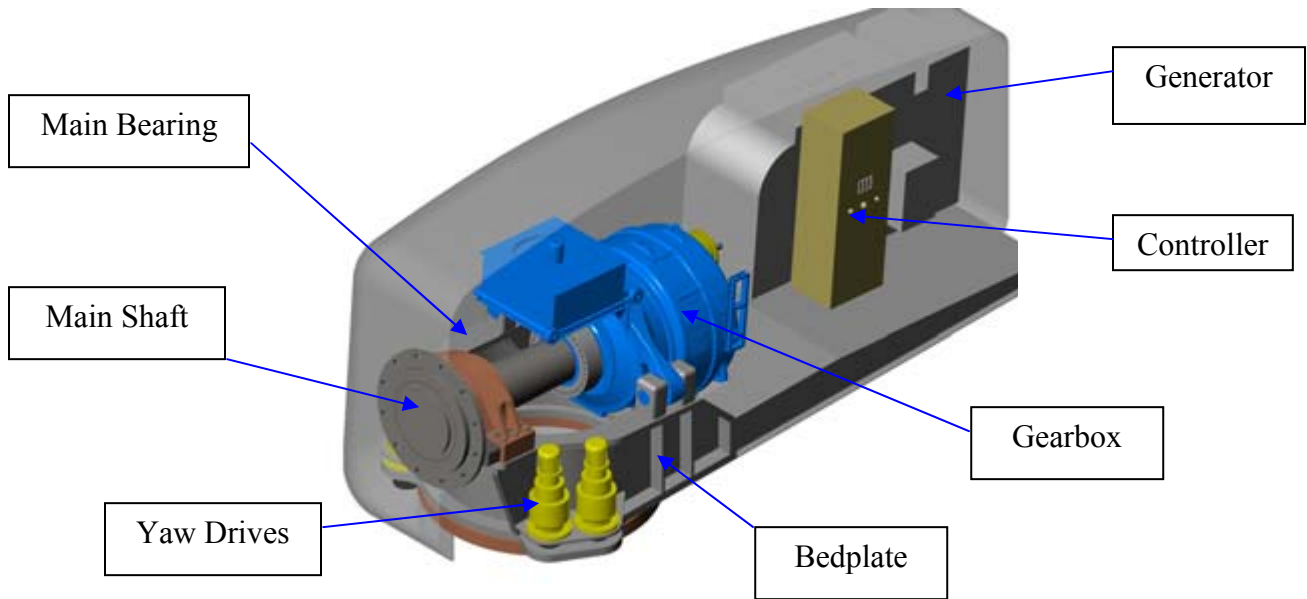


Figure 2-8. 1.5-MW 70-m baseline design

The rotor hub drives the gearbox through a modular main shaft-bearing arrangement, with shrink disk-style coupling at the gearbox input. The main bearing is a pillow block-mounted, double-row, spherical bearing. Compliant elastomer mounts support the gearbox. The gearbox drives the generator through a flexible coupling. The generator system, which includes the generator rotor sliprings and heat exchanger, is also flexibly mounted. Provisions are made for a slipring that feeds the blade pitch system. Rotor loads are taken by the main bearing and gearbox mounts into the bedplate weldment.

Designed by GCSC according to a major manufacturer's specifications, the original gearbox had a compound planetary input section and parallel output stage. The compound system was chosen over a conventional planetary arrangement because it was less expensive and lighter. Helical gearing has become the industry norm due to lower noise and better load-carrying capability, leading to a more compact gearbox.

Figure 2-9 shows the solid-model image of the 1.5-MW compound helical gearbox.



Figure 2-9. 1.5-MW compound planetary helical gearbox

The 3-MW gearbox is also based on GCSC planetary helical technology.

Developed by a major manufacturer, the generator and power converter are an industry-standard design.

Bedplate. The bedplate weldment is composed of a front section that supports the main bearing, shaft, and gearbox, and transmits rotor loads to the tower, and a rear section that supports the generator and ancillary hardware. A bolted joint connects the two sections.

Main Shaft. The main shaft has a forged flange that connects to the rotor hub and accommodates the rotor locking ring. The opposite end of the shaft interfaces with the gearbox input. The shaft and gearbox are joined by a shrink disk connection.

Main Bearing. A double-row, spherical main bearing is mounted in a pillow block. Rotor lock pistons are integrated into the pillow block feet and are actuated by a hydraulic hand pump.

Flexible Coupling. A flexible coupling is mounted between the gearbox and generator. The coupling includes an integral brake disk, mechanical overload protection, and provides electrical isolation.

Brake. The spring-applied, hydraulically released caliper brake is used primarily as a parking brake. Its hydraulic control system allows programming the brake torque for smooth stops.

The structural configuration of the bedplate was based on an industry leader's design. FEA was used to qualify the design under fatigue and extreme loads cases.

Our cost estimate of the baseline design was verified by a major European wind farm developer. The baseline design could be further investigated and optimized:

- The bedplate was designed as a welded structure; however, a cast bedplate might be lighter and more economical.
- An integrated design might be less costly, but component lifting/service considerations might offset any gains.

2.5.2 Permanent Magnet Direct-Drive Design

The PMDD design is based on liquid-cooled PM synchronous generator technology. The generator design essentially determines the design of the drivetrain (Figure 2-10).

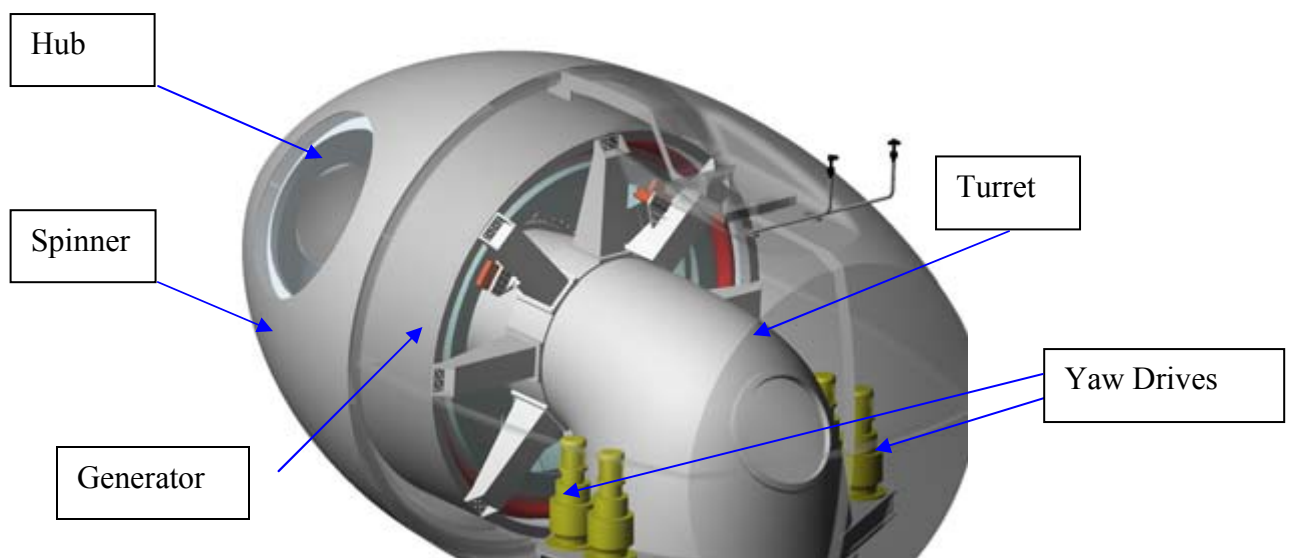


Figure 2-10. PMDD drivetrain

Mechanical Layout. The generator is composed of a single main bearing, stator and rotor electromagnetics, water jacket, spindle, stator ring and frame, brake system, and associated hardware. The rotor hub and generator rotor are connected directly to the outer race of the main bearing. The inner race of the main bearing is pressed onto the spindle. The stator frame is connected to the base of the spindle, and the stator ring is fastened to the stator spider, composed of eight arms. The spindle is bolted to the turret, which provides the structural path to the tower top. Composed of four calipers, the brake system acts on the generator's rotor disk. A slipping, which feeds the blade pitch system, and a rotor lock are provided.

In our PMDD design, the generator is an integrated unit, which makes it possible to ship a fully assembled and tested generator to the site. There it can be mounted to the turret in one operation. Another feature of the design is the capability to lock the generator rotor to the stator frame, which allows servicing the main bearing without removing the generator from the tower. Bearing seals are accessible, and the design allows repairing or replacing the seals without removing the bearing.

Figure 2-11 shows the unitized generator assembly.

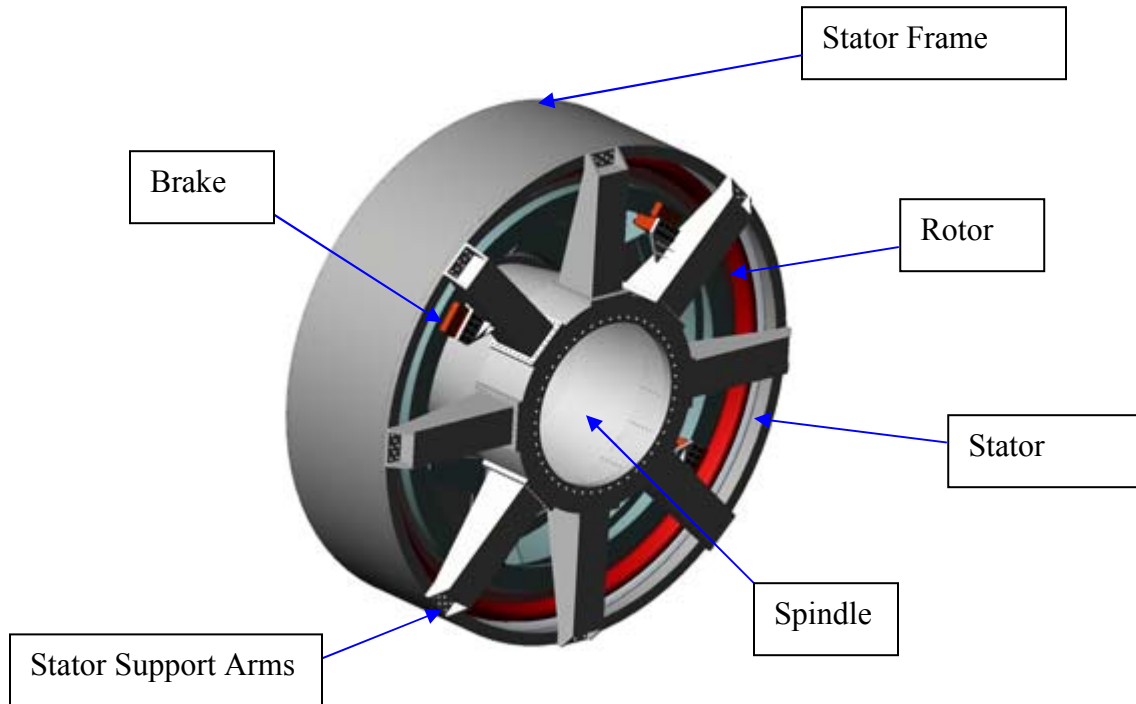


Figure 2-11. PMDD generator

Main Bearing. The single-bearing design simplifies the design of the generator. It allows a direct load path, simple assembly, and ease of service. A unitized component, the main bearing is a two-row, tapered roller with integral seals and an automatic lubrication system. The rotor hub is fastened to the outer race of the bearing. The inner race is pressed onto the spindle.

Spindle. The cast-iron spindle is the main load path from the rotor to the turret. It carries all rotor and generator loads, and its fixed design takes advantage of the lower fatigue loads in the stationary frame. The dimensions of the bearing and spindle allow a crawl-through feature: service technicians can access the rotor pitch system through the center of the spindle. The bearing seals are also easily accessed.

Stator Support. The stator structure is a weldment consisting of the outer ring and eight tapered arms.

Brake. The parking brake acts through the generator rotor hub drum. The calipers and rotor lock, which acts between the generator rotor and stator support, are mounted off the stator support arms.

Outside Diameter and Cooling Method. For the PMDD generator, two critical factors are OD and cooling method.

Outside Diameter. PMDD generator costs are reduced as the OD of the generator is increased. Although the rationale for increasing the diameter is clear, returns diminish above approximately 5.5 meters, primarily because of the increased number of poles, fixed costs of coil fabrication, and to a lesser extent, increased structural costs.

We produced specifications for two PMDD generators: one for the European market and one for the American market.

For the European market (and Phase II design), we chose a liquid-cooled generator with a 4-meter OD. Based on a Danish shipping specification, the diameter is the largest practicably transported in Europe.

For the American market, we chose a liquid-cooled generator with a 5.3-meter OD. We found that this increase in diameter led to a 6.6% reduction in generator cost. For long hauls within the United States, the low-cost mode of transportation is barge and rail. A major shipping agent informed us that a load shipped by rail with an overall height of 6 meters could get within 50 miles of 95% of U.S. sites. Considering the rail truck height, we arrived at our overall diameter specification of 5.3 meters. For loads of this size, a rail-mounted arrangement, which allows transporting the generator vertically with its rotation axis perpendicular to the direction of travel, will resolve any transportation issues.

Cooling method. The cooling method affects both capital costs and efficiency. To determine the best choice, the capital cost and COE for each design must be compared. For a given diameter, a liquid-cooled generator can be made more compact and with lower magnet mass. Efficiency can be sacrificed to reduce the magnet mass—with a loss in annual energy production. Generally an air-cooled generator must be made more efficient to ensure adequate heat rejection—at the expense of higher active materials mass. The PMDD generator is a water-cooled design based on a trade-off among natural air, forced air, and water. Table 2-15 shows the results of our trade-off study.

Table 2-15. Cooling Method Tradeoff in 1.5-MW PMDD Generator

	Water-Cooled	Air-Cooled
Production cost	\$1,100,289	\$1,139,365
Profit margin	15%	15%
Purchase price	\$1,265,332	\$1,310,270
Balance of station cost	\$247,500	\$247,500
Initial capital cost	\$1,512,832	\$1,557,770
Fixed charge rate	10.56%	10.56%
Annual operation and maintenance cost	\$20,315	\$20,315
Annual energy production	4,872,746 kWh	4,903,269 kWh
Cost of energy	3.70¢/kWh	3.77¢/kWh

Because of the higher capital cost and COE of the more efficient air-cooled design, the liquid-cooled design was chosen. Table 2-16 shows the PMDD generator specifications, the basis for the detailed design in Phase II of the WindPACT project.

Table 2-16. PMDD Generator Specifications

Rating	1.5 MW	1.5 MW	3 MW
Generator OD	4.0 m	5.3 m	5.3 m
Stator OD	3.79 m	4.82 m	5.0 m
Air gap mean diameter	3.48 m	4.46 m	4.46 m
Generator speed	19.65 rpm	19.65 rpm	15.3 rpm
Number of poles	56	78	78
Voltage	725 V	725 V	725 V
L/D ratio	0.19	0.11	0.26
Cooling method	Liquid	Liquid	Liquid

Figure 2-12 shows the power-converter required for the direct-drive design. (The same hardware configuration for power electronics is required for the MS-1 design.) The power converter consists of an insulated gate bipolar transistor (IGBT)-based active rectifier on the generator side of the DC link, and a conventional IGBT-based inverter on the utility side. The high current ratings required by the power converter IGBTs are achieved by using parallel devices.

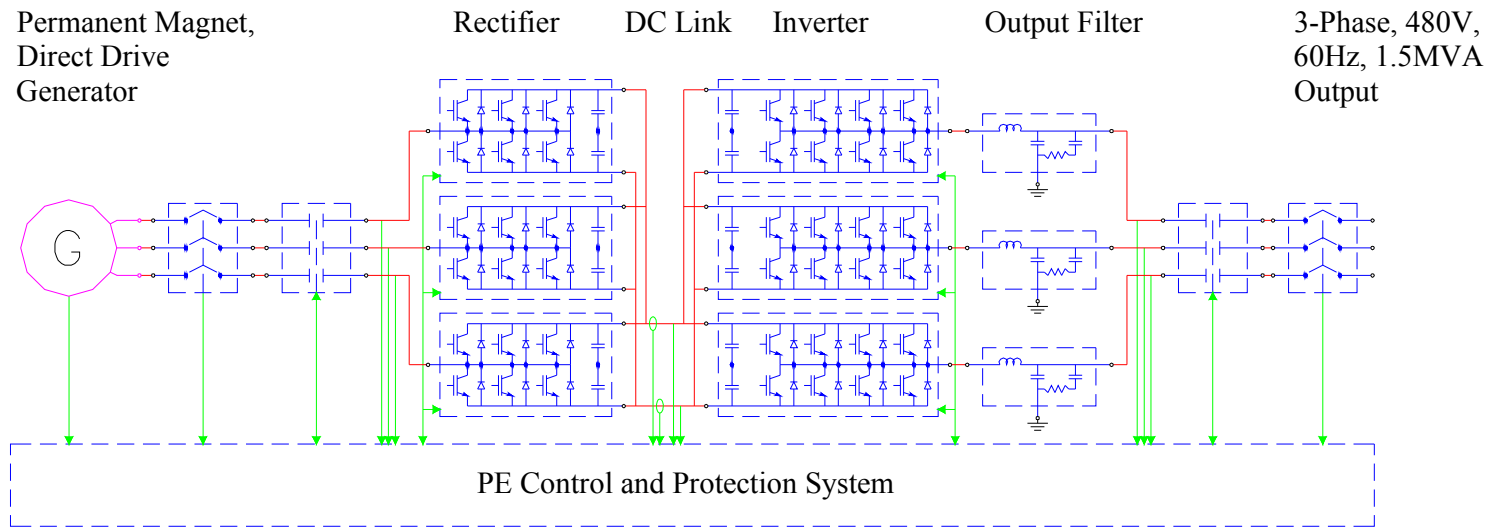


Figure 2-12. PMDD (and MS-1) power electronics schematic

Rotor moment loads are transmitted to the spindle through the main bearing races and into the turret, yaw bearing, and tower top. Rotor torque loads are transmitted directly into the generator rotor spider, across the air gap, through the stator and frame, and back into the spindle base, turret, and yaw bearing.

We investigated a number of bearing configurations during the course of the Phase I activities. The main tradeoff was between systems using one and two bearings. The two-bearing class offers many possibilities, with a main tradeoff being the choice of a non-rotating axle or rotating shaft. Bearings can be in front of, straddled, or behind the generator. In route to choosing the singlebearing, stationary-spindle configuration, alternative configurations were studied.

Evaluation criteria were cost, weight, risk, shipping, assembly, and serviceability. Solid models were created of all of the designs. Preliminary sizing calculations were performed to estimate the masses of the various structural components, and specific costing data were used to estimate the costs of each configuration. Technical risks, shipping, and serviceability issues were also evaluated. The single bearing configuration was chosen due to lower part count and ease of bearing service.

2.5.3 Medium-Speed/Single-Output Design

The medium-speed/single-output (MS-1) integrated design is composed of a compound planetary helical gearbox coupled with a medium-speed PM generator. The front section of the gear casing is integrated with the tower top structure (Figure 2-13).

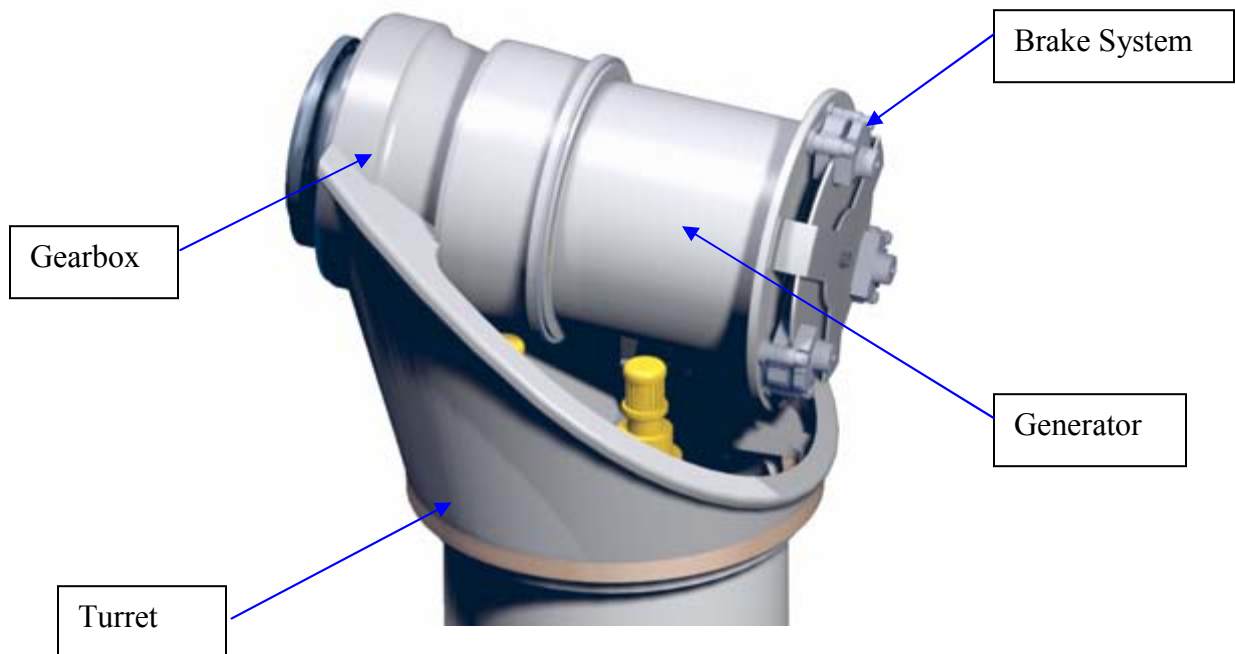


Figure 2-13. MS-1 drivetrain design

The drivetrain is composed of the compound planetary helical gearbox, medium-speed generator, turret, and brake system. The rotor hub is connected directly to the inner race of the main bearing. The inner race of the main bearing is mounted to the gearbox carrier, and its outer race to the gearbox casing. The generator is mounted to the gear case using flanges on the gearbox and generator housings. The turret design brings the moment loading of the turbine rotor directly from the main bearing into the turret structure, with minimal impact on the gear alignments. Located on the back of the generator, the brake system is composed of a brake disk, calipers, and hydraulic system. A slipring, which feeds the blade pitch system, is provided. Table 2-17 shows the MS-1 drivetrain specifications.

Table 2-17. MS-1 Drivetrain Specifications

Power rating	1.5 MW	3 MW
Gearbox type	Compound epicyclic	Compound epicyclic
Gear ratio	13.89:1	16:1
Ring-gear pitch diameter	1.09 m	1.43 m
Generator speed	272.9 rpm	244.8 rpm
Generator cooling method	Liquid	Liquid

The MS-1 gearbox is based on the GCSC compound planetary helical gear technology. The GCSC compound box gives a high ratio—13.89:1 for the 1.5-MW gearbox and 16:1 for the 3-MW gearbox. The technology is ideal for the application because of its high gear ratio, low part count, and balanced internal bearing loads. The compound helical design gives a double reduction with one set of pinion bearings and allows balancing the bearing thrust loads by carefully selecting opposing helix angles. A high ratio is very advantageous because the cost of a PM generator depends greatly on generator speed.

Among integrated designs, we compared the saddle mount and overhung mount carrier configurations. A saddle mount carrier has a bearing at both ends. An overhung mount carrier has a single bearing at one end. We chose the overhung mount configuration because it eliminates one bearing. However, either could be implemented for roughly the same cost.

Table 2-18 shows the MS-1 gearbox specifications.

Table 2-18. MS-1 Gearbox Specifications

Rating	1.5 MW	3 MW
Gear ratio	13.89:1	16:1
Ring-gear pitch diameter	1.09 m	1.43 m
LS mesh face width	0.222 m	0.305 m
LS mesh helix angle	8.75°	8.75°
HS mesh face width	7.5	7.5
HS mesh helix angle	19.25°	19.25°

Figure 2-14 shows a section view of the MS-1 drivetrain.

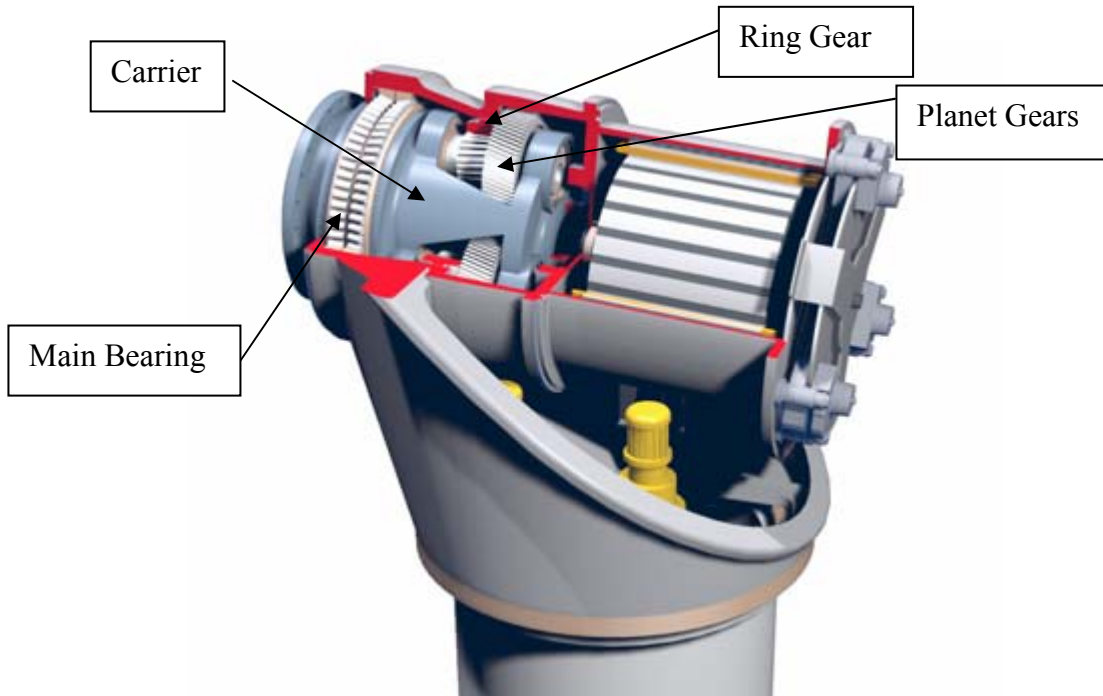


Figure 2-14. 1.5-MW MS-1 Drivetrain (Gearbox and Housings Cut Away)

Mechanical Layout. Totally enclosed, the generator's cast-iron housing contains the water jacket and stator. The generator rotor is supported by two bearings whose outer races are mounted in the housing. Flange-mounted to the gearbox, the generator can be removed as a unit. The rear flange mounts the brakes. Figure 2-15 is a section view of the generator.

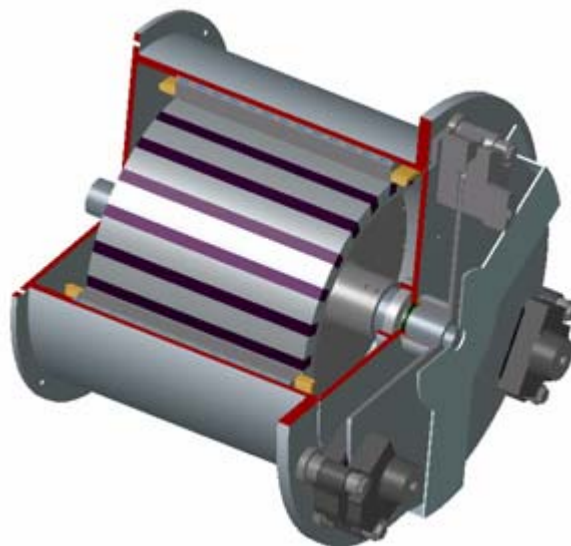


Figure 2-15. MS-1 generator section view

Electrical Design. The MS-1 design is based on GDEB’s liquid-cooled PM generator technology. The mechanical design of the turret accommodates a large generator. We conducted a study to determine the most effective generator diameter.

Table 2-19 shows the MS-1 generator specifications.

Table 2-19. MS-1 Generator Specifications

Rating	1.5 MW	3 MW
Generator OD	1.450 m	2.526 m
Stator OD	1.76 m	2.36 m
Air gap mean diameter	1.48 m	2.026 m
Generator speed	273.6 rpm	244.8 rpm
Number of poles	28	84
Voltage	725 V	725 V
L/D ratio	0.35	0.38
Cooling method	Liquid	Liquid

Figure 2-12 shows the power converter configuration required for the MS-1 design. (The same power converter configuration is required for the PMDD design.) The high current ratings required by the power converter IGBTs are achieved by using parallel devices.

2.5.4 Medium-Speed/Six-Output Design

The medium speed/six-output (MS-6) integrated design is composed of the drive unit, which includes the main bearing, bull gear, pinions, spindle, generators, brake system, and the turret structure, which completes the structural connection to the tower top (Figure 2-16).

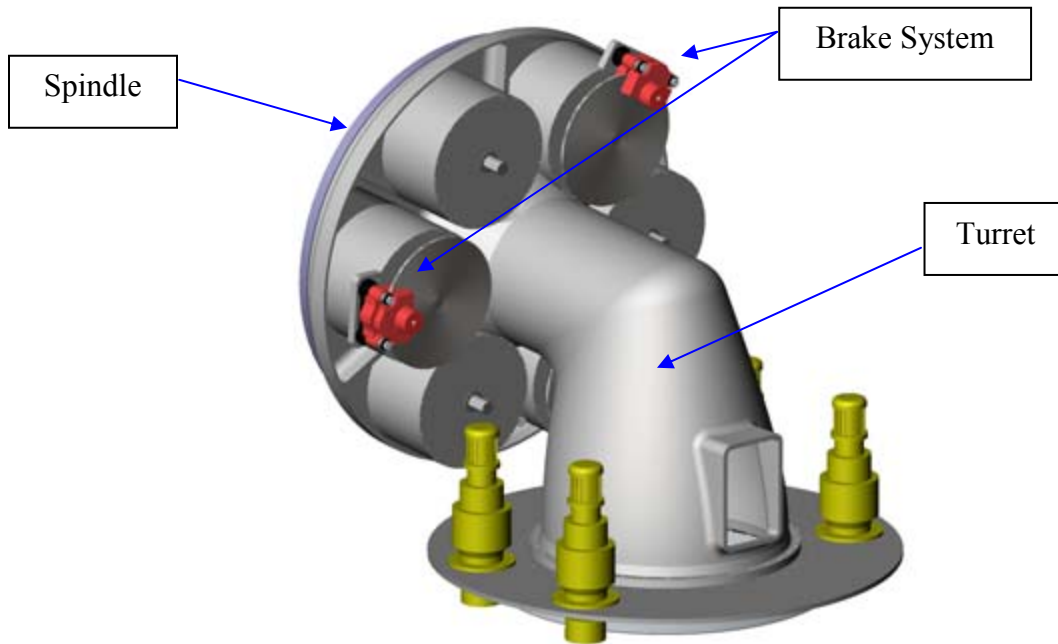


Figure 2-16. MS-6 design

The rotor hub and bull gear are connected directly to the outer race of the main bearing. The inner race of the bearing is pressed onto the spindle, which can be structurally decomposed into two functional parts: (1) a central tubular structure that provides the main load path to the turret and (2) the stiffened disk structure to which the generators are mounted. The pinions are integral with the generator shafts and are cantilevered off of the generator bearings. The generator housings are connected directly to the disk structure. The spindle is fastened to the turret, which provides the structural path to the tower top. Located on the back of the generator, the brake system is composed of three brake disks and calipers. The design includes a slipring, which feeds the blade pitch system, and a rotor lock, which interfaces with the bull gear at the six o'clock position.

To optimize the MS-6 design, we developed drives of several gear ratios and made preliminary estimates of the complete drive costs. Drive cost is at minimum at the 14:1 ratio and rises greatly at the 8:1 ratio. These results show the strong dependence of PM generator costs on speed. Based on these analyses, the 14:1 design was chosen for further development. Table 2-20 shows the MS-6 specifications.

Table 2-20. MS-6 Drivetrain Specifications

Gearing ratio	14:1
Gearbox type	Helical parallel
Bullgear pitch diameter	2.0 m
Generator outside diameter	0.94 m
Generator speed	275 rpm
Generator cooling	Liquid

Mechanical Layout. The “gearbox” is composed of the main bearing, bull gear, six pinions, and spindle. The main bearing stiffens the large-diameter bull gear to reduce operating deflections. Because the pinions are cantilevered off of the generator bearings, all six generators must be mounted to complete the gearbox. This design reduces the number of bearings while allowing removal of the assembled generator, thus easing maintenance. Directed oil spray lubricates the mesh and bearings.

More detailed evaluation would be required to ensure the mesh operates within acceptable tolerances. An alternative design would include separate generator and pinion bearings, with the spline connection allowing removal of the generator as a unit. We attempted to reduce the number of bearings to reduce capital and O&M costs, while keeping serviceability in mind. Either design could be implemented at somewhat higher risk and engineering cost and lower capital cost for the chosen configuration.

Table 2-21 shows the MS-6 gearing specifications.

Table 2-21. MS-6 Gearing Specifications

Gearing ratio	14:1
Bullgear pitch diameter	2.0 m
Pinion pitch diameter	0.143 m
Face width	0.143 m
Helix angle	15.0°

The generator for the MS-6 design is based on GDEB’s liquid-cooled PM technology. The mechanical design of the generator was driven by service requirements: the generator is flange-mounted to allow removing it as a unit. The generator bearings support the overhung load on the pinion. Figure 2-17 shows a section view of the MS-6 generator.

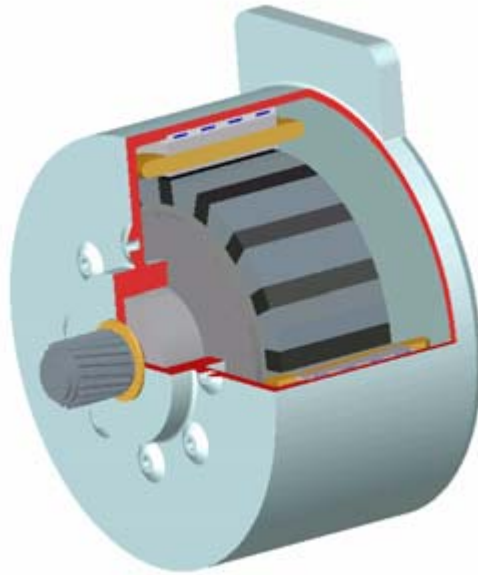


Figure 2-17. MS-6 generator section view

Electrical Design. The MS-6 electrical design is based on GDEB’s liquid-cooled PM generator technology. The generator diameter and bullgear diameter are closely linked—gearing costs rise as the bullgear diameter increases, but in general, generator costs fall as the diameter is increased. We conducted a study to determine the most effective generator diameter. The study showed a local minimum in generator cost at the 0.95-meter diameter. The increase in cost above the 0.95-meter diameter is due to the combination of increased pole and coil count with associated fixed costs in coil and pole fabrication. Table 2-22 shows the MS-6 generator specifications.

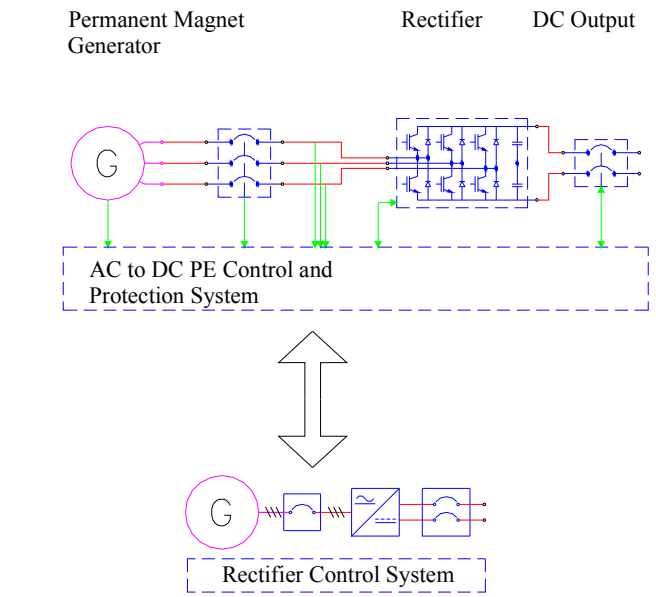
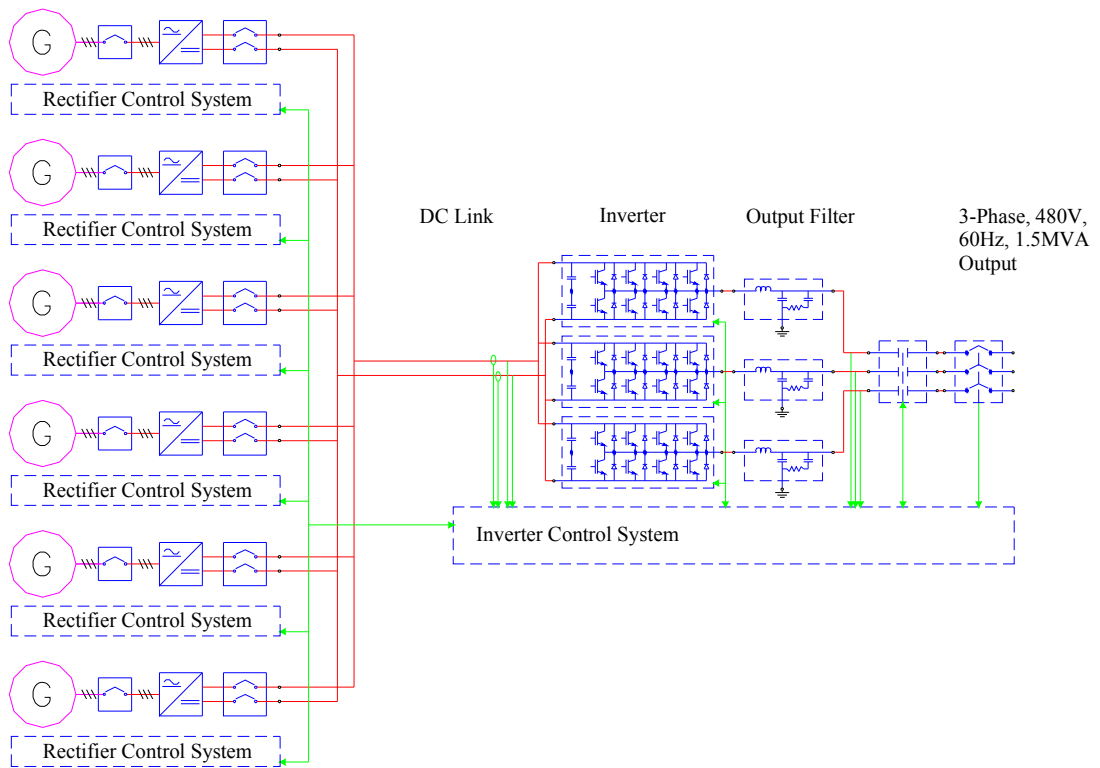
Table 2-22. MS-6 Generator Specifications

Rating	250 kW
Generator OD	1.016 m
Stator OD	0.94 m
Air gap mean diameter	0.772 m
Generator speed	275.8 rpm
Number of poles	16
Voltage	725 V
L/D ratio	0.33
Cooling method	Liquid

Figure 2-18 shows the power electronics schematic for the multiple-output PM generator. The utility-side inverter is similar to a direct-drive’s power converter. The generator-side active

rectifier is duplicated for each parallel path in the system, which increases the cost of the power electronics required by the multiple-output generator.

After investigating several structural configurations for MS-6, we chose a design similar to that of the direct-drive configuration. An FEA of the turret was conducted to prove the integrity of the design. In addition, an FEA of the spindle and generator mounting disk was conducted to prove the structural integrity of the load bearing tube and the stiffness of the disk structure under operating loads.



(B)

(A)

Figure 2-18. (A) Power electronics for MS-6 design. (B) Power electronics for individual generator.

2.6 Drivetrain Study Results

Figures 2-19 and 2-20 show the initial capital cost of major turbine components for each 1.5-MW and 3-MW configuration.

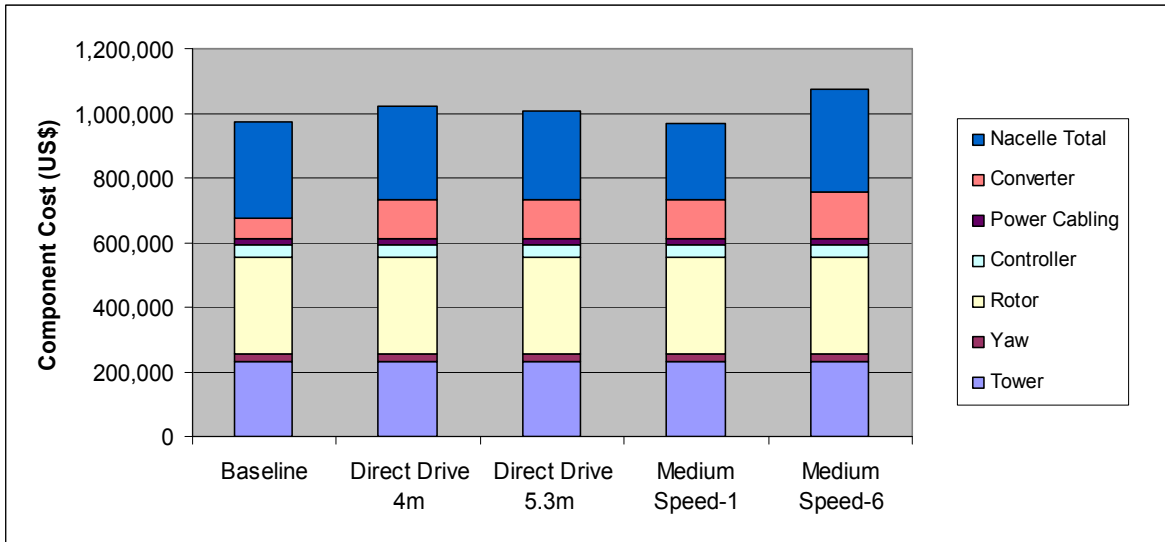


Figure 2-19. Component initial capital cost centers: 1.5-MW

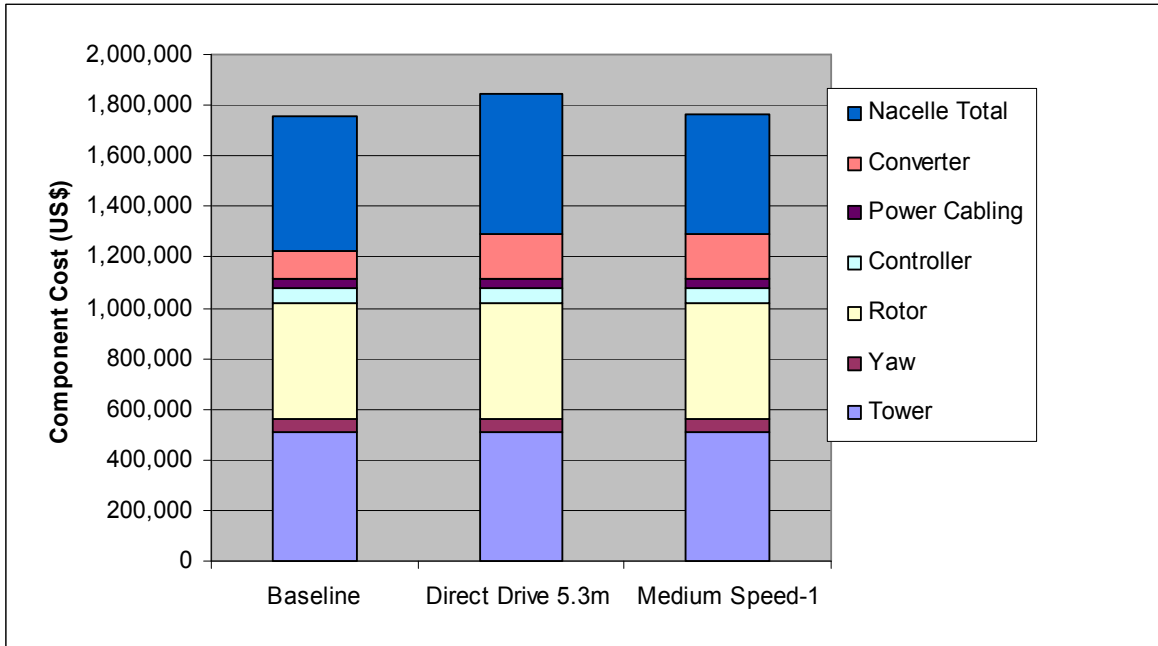


Figure 2-20. Component initial capital cost centers: 3-MW configurations

Tables 2-23 and 2-24 illustrate the relative difference between the initial capital cost of the baseline configuration and alternative configurations.

Table 2-23. Relative Initial Capital Cost Comparison: 1.5-MW Configurations

	Baseline	DD 4 m	DD 5.3 m	MS-1	MS-6
Percentage baseline drivetrain cost	100%	113%	109%	99%	127%
Percentage baseline turbine cost	100%	105%	104%	99%	109%

Table 2-24. Relative Initial Capital Cost Comparison: 3-MW Configurations

	Baseline	DD 5.3 m	MS-1
Percentage baseline drivetrain cost	100%	114%	101%
Percentage baseline turbine cost	100%	105%	100%

Table 2-25 shows the results of the O&M cost analysis. O&M costs are presented in cents per kilowatt-hour produced. Figures 2-21 and 2-22 illustrate the contribution of certain cost centers to total O&M costs. Of note is the very high cost due to unscheduled drivetrain materials for the

MS-6 design. This cost can be attributed to the higher part count and, therefore, greater number of failures (especially relatively expensive generator failures).

Also noteworthy is the O&M savings predicted for the direct-drive designs because of less costly scheduled materials (i.e., no gearbox oil), as well as fewer failures (i.e., lower unscheduled materials cost). As expected, an economy of scale was present: all 3-MW configurations were predicted to be less costly to operate and maintain on a per kilowatt-hour basis than their 1.5-MW counterparts. See *Bywaters (2004)* for a full discussion of the O&M analysis methodology, input parameters, and results. Note that O&M models are subjective to some degree and as a result, they can have relatively higher uncertainties than the other cost models presented in this report.

Table 2-25. Summary of Operation and Maintenance Costs^a

Rating Design	1.5 MW				3 MW		
	Baseline	DD	MS-1	MS-6	Baseline	DD	MS-1
Cost center							
Scheduled burdened labor	0.037	0.037	0.037	0.037	0.034	0.034	0.034
Unscheduled burdened labor	0.039	0.039	0.039	0.039	0.036	0.036	0.036
Scheduled materials	0.041	0.011	0.041	0.041	0.022	0.006	0.022
Unscheduled materials—drivetrain	0.133	0.050	0.098	0.193	0.109	0.058	0.091
Unscheduled materials—other	0.029	0.029	0.029	0.029	0.026	0.026	0.026
Unscheduled spares—drivetrain	0.057	0.057	0.057	0.088	0.050	0.049	0.050
Unscheduled spares— other	0.069	0.069	0.069	0.069	0.056	0.056	0.056
Equipment	0.105	0.105	0.105	0.105	0.070	0.070	0.070
Equipment maintenance	0.030	0.030	0.030	0.030	0.027	0.027	0.027
G&A	0.057	0.057	0.057	0.057	0.053	0.053	0.053
Totals	0.60	0.48	0.56	0.69	0.48	0.42	0.47
Per unit cost wrt 1.5 MW baseline	100%	81%	94%	115%	81%	70%	78%
Per unit cost wrt 3 MW baseline	123%	100%	116%	142%	100%	86%	96%

^aCosts in cents/kWh.

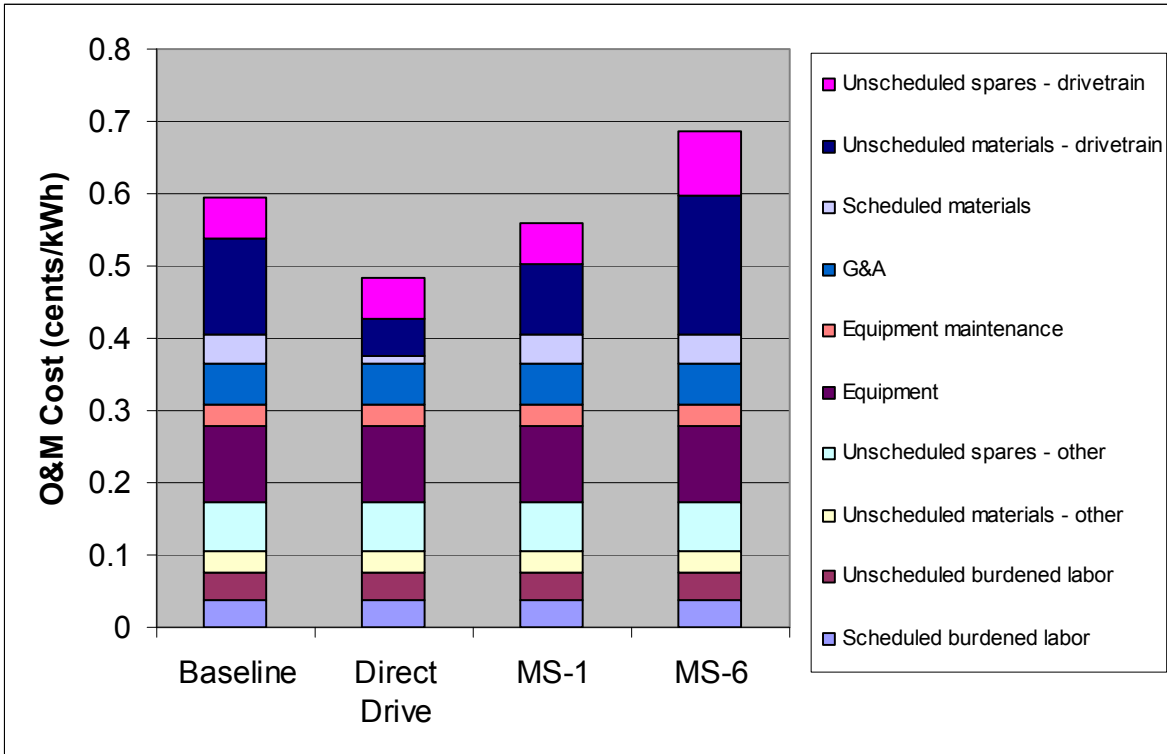


Figure 2-21. O&M cost centers: 1.5-MW configurations

Tables 2-26 and 2-27 show predictions of annual energy production (AEP) for each 1.5-MW and 3-MW configuration. Differences in AEP reflect corresponding differences in predicted drivetrain efficiencies. The gain in energy production realized with a permanent magnet generator and no gearbox (i.e., PMDD) is more than 2%.

Table 2-26. Annual Energy Production: 1.5-MW Configurations

	Baseline	DD 4 m	DD 5.3 m	MS-1	MS-6
AEP (MWh)	4,769	4,873	4,873	4,812	4,776
% 1.5 MW baseline production	100.00%	102.17%	102.17%	100.91%	100.15%

Table 2-27. Annual Energy Production: 3-MW Configurations

	Baseline	DD 5.3 m	MS-1
AEP (MWh)	9,765	9,951	9,841
% 3 MW baseline production	100.00%	101.90%	100.78%

Tables 2-28 and 2-29 show COE for each 1.5-MW and 3-MW drivetrain configuration. Included are values for the major inputs used to calculate COE. As a whole, the predicted COE was lower for the 3-MW designs than for the 1.5-MW designs.

Table 2-28. COE Summary: 1.5-MW Configurations^a

	1.5-MW baseline	1.5-MW DD 4.0 m	1.5-MW DD 5.3 m	1.5-MW MS-1	1.5-MW MS-6
Production cost	\$1,056,068	\$1,106,204	\$1,093,353	\$1,047,719	\$1,154,599
Profit margin	15%	15%	15%	15%	15%
Purchase price	\$1,214,478	\$1,272,135	\$1,257,357	\$1,204,877	\$1,327,789
Balance of station	\$247,500	\$247,500	\$247,500	\$247,500	\$247,500
ICC	\$1,461,978	\$1,519,635	\$1,504,857	\$1,452,377	\$1,575,289
FCR	10.56%	10.56%	10.56%	10.56%	10.56%
AOM	25,226	\$20,315	\$20,315	\$23,805	\$32,787
AEP (kWh)	4,769,243	4,872,746	4,872,746	4,812,485	4,776,373
COE (cents/kWh)	3.77	3.71	3.68	3.68	4.17

^aCosts in US\$ unless stated otherwise.

Table 2-29. COE Summary: 3-MW Configurations^a

	3-MW baseline	3-MW DD 5.3 m	3-MW MS-1
Production cost	\$1,932,264	\$2,029,018	\$1,937,357
Profit margin	15%	15%	15%
Purchase price	\$2,222,104	\$2,333,371	\$2,227,961
Balance of station	\$495,000	\$495,000	\$495,000
ICC	\$2,717,104	\$2,828,371	\$2,722,961
FCR	10.56%	10.56%	10.56%
AOM	\$46,872	\$41,485	\$46,255
AEP (kWh)	9,764,952	9,950,531	9,841,388
COE (cents/kWh)	3.42	3.42	3.39

^aCosts in US\$ unless stated otherwise.

Tables 2-30 and 2-31 show the relative difference in COE for a turbine with each configuration compared with a baseline turbine of the same rated power. The 1.5-MW direct-drive and MS-1 configurations show a lower predicted COE than the baseline design. The 5.3-meter direct-drive configuration offers the greatest predicted savings in COE at 2.3% below the baseline design.

Conversely, the COE predicted for a turbine with the MS-6 configuration is more than 14% more expensive than for the baseline configuration. This is the result of a number of factors. The generator diameter is limited by the allowable spacing around the bull gear. This increases costs in two ways: through a less optimal length-to-diameter ratio of the generator relative to the MS-1 design, and also by reducing the shear stress at which the generator can run due to a less

efficient heat conduction path. Both of these factors increase the cost of the generators. In addition, Northern found that the cost of buying several smaller generators is much greater than the cost of buying one large one. This data is based on manufacturers' quotes for generators in mass production. In addition, we found that our cost for the 250-kW generator was approximately equal to the cost of a wound rotor generator of the same size. The power electronics cost is higher because of the parallel topology. The efficiency is also lower than the MS-1 design, and the consequent reduction in AEP is not offset by running the turbine a partial power as a result of a generator failure.

The relative COE predictions for the 3-MW configurations show a smaller difference in COE between configurations, with the MS-1 showing the greatest savings in predicted COE.

Table 2-30. Relative COE: 1.5-MW Configurations

	Baseline	DD 4.0 m	DD 5.3 m	MS-1	MS-6
% of baseline	100.0%	98.5%	97.7%	97.8%	110.7%
Total (cents/kWh)	3.77	3.71	3.68	3.68	4.17

Table 2-31. Relative COE: 3-MW Configurations

	Baseline	DD 5.3 m	MS-1
% of baseline	100.0%	100.0%	99.2%
Total (cents/kWh)	3.42	3.42	3.39

Figures 2-22 and 2-23 show the cost center contributions to the overall COE for each turbine configuration.

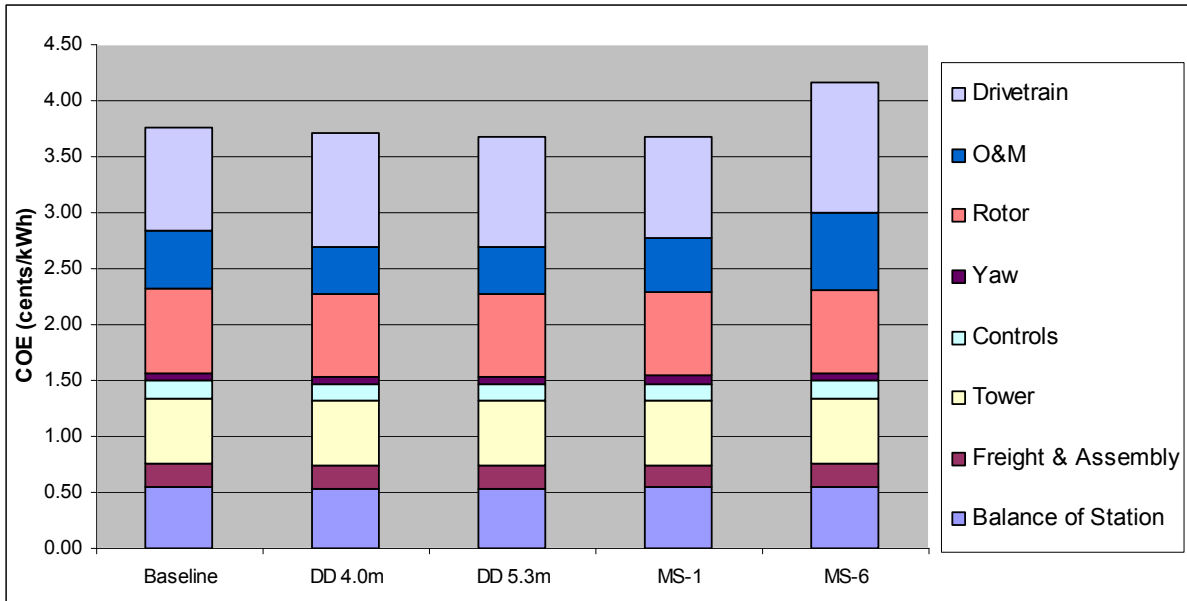


Figure 2-22. COE cost centers: 1.5-MW configurations

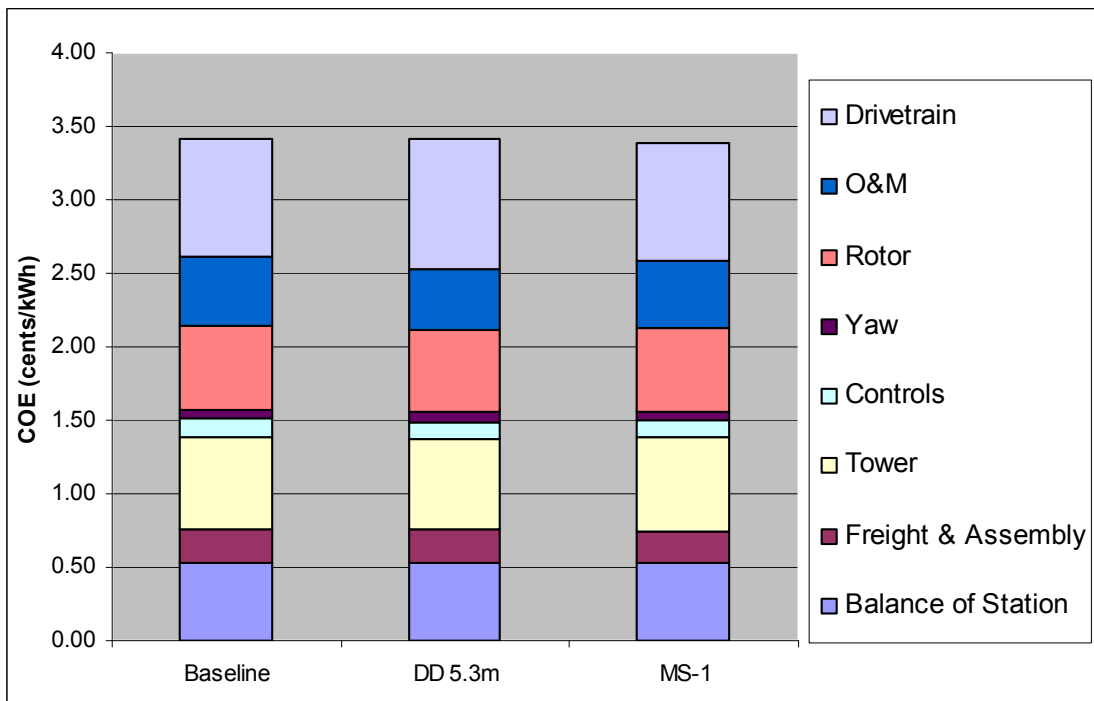


Figure 2-23. COE cost centers: 3-MW configurations

Figure 2-24 illustrates the relative difference in drivetrain weight between each of the configurations. Figure 2-25 shows the specific capital cost (\$ per rated kilowatt) for each configuration. The economy of scale for the 3-MW drivetrains is easily observed from this graph, when comparing the 1.5-MW configurations to the corresponding 3-MW versions.

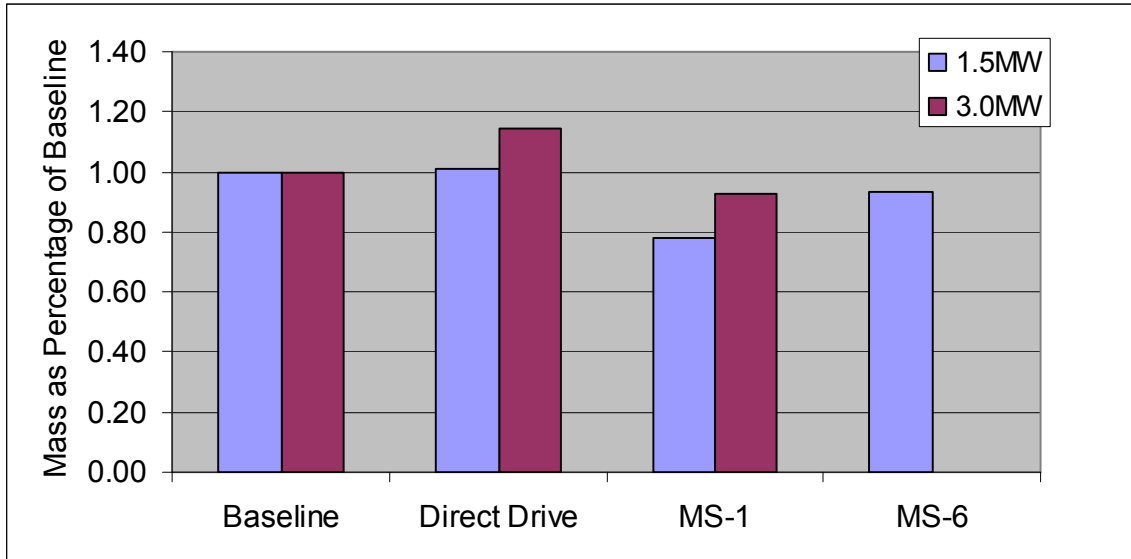


Figure 2-24. Relative drivetrain weights

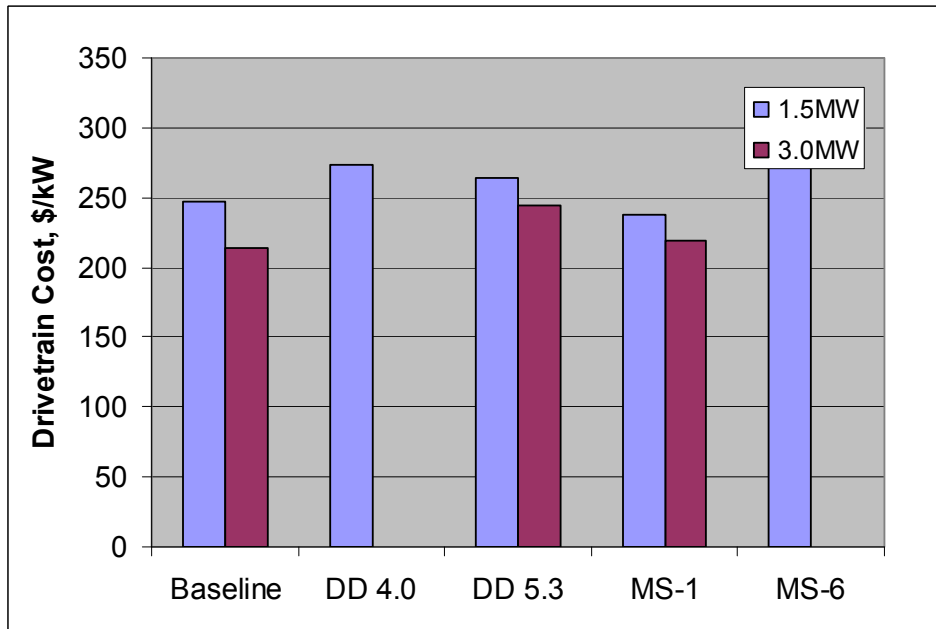


Figure 2-25. Drivetrain specific cost

2.7 Drivetrain Study Conclusions

In Phase I of the study, the mandate was to evaluate multiple innovative drivetrain topologies, compare these designs with a commercially available baseline configuration, and identify the drivetrain configuration with the most potential to reduce COE and become commercially viable in the marketplace. A mature wind turbine design that has a significant installed base and a known track record was used as a baseline configuration. Our results in Phase I show strong potential for two advanced drivetrain configurations: the medium-speed/single-output (MS-1) design and the permanent magnet direct-drive (PMDD) design. Both configurations appear to be competitive with the baseline turbine at the 1.5-MW and 3-MW power levels. A third configuration investigated in this study, the medium-speed/six-output design, proved noncompetitive due to both high equipment and O&M costs, a product of the large number of generators and resultant high component count.

Inherent design characteristics of the PMDD drivetrain make its COE economics more favorable as the generator diameter increases. The main limitation on maximum diameter is the shipping constraints in the target markets. Two diameters—5.3 meters and 4 meters—are appealing for the United States and European markets, respectively. As part of Phase I, we considered machine designs at both diameters.

Our analysis in Phase I predicted a reduction in COE for both the 4-meter diameter PMDD (1.5% reduction) and the MS-1 (2.2% reduction) configurations compared with the 1.5-MW baseline turbine. The 5.3-meter diameter 1.5-MW PMDD shows the lowest COE of all configurations—2.3% below the baseline turbine. Economies of scale favored all turbines at increased power levels. All 3-MW designs show a downward trend in COE compared with the 1.5-MW designs.

In selecting a drivetrain configuration for further development, the Northern team also considered factors unaccounted for in the COE calculations, such as technology and industry trends that impact future competitiveness and market acceptance. Of major importance is the maturity level of the technologies utilized in the different configurations. It is far more likely that technological improvements will reduce costs for new PMDD designs than for mature baseline/gearbox designs. Magnet and power electronics costs, which are major factors in the capital cost of the PMDD configuration, continue to decline steadily. The same cannot be said of the gearbox costs. In fact, it is possible that gearbox costs will rise as a result of modifications made to prevent high failure rates, such as “upsizing.”

Industry and market trends support the selection of the PMDD configuration for the megawatt-scale wind turbine market. The team identified strong interest in a commercial PMDD turbine design from wind project developers and owners, as well as from manufacturers looking for a competitive advantage. Direct-drive wind turbine drivetrain designs, both with and without PM generators, are seen by many in the industry as a commercially viable and attractive option. The Northern team has become convinced of the competitiveness and commercial viability of the PMDD wind turbine drivetrain configuration, and selected this configuration for detailed design, manufacturing, and testing in Phases II and III of the WindPACT project.

3 Design

The goal of Phase II of the WindPACT project was to design a 1.5-MW PMDD drivetrain. This section describes our design process, goals, issues, verification results, and cost estimation.

The design process started with the direct-drive PM configuration of the Phase I design trade study. The roles and responsibilities of the team members were determined, and overall decisions on design methodology were made. A generator specification was written to determine the desired design goals. Issues resulting from the conflicting objectives of low cost and high performance were discussed and resolved. The design was reviewed and discussed to determine the details of the design. Stress analysis was performed to ensure structural integrity of the design in wind turbine service and in the dynamometer test. Stackup analysis was performed to determine that parts would fit correctly, and that the gap between the rotor and stator would be maintained. Electromagnetic and thermal analysis was performed by GDEB to determine the power performance of the generator. Calculations were performed to determine the expected life of the generator and power electronics. Life calculations were performed on mechanical components, such as the main bearings and brakes. Discussions were held with our generator manufacturer to ensure that the design was manufacturable, and detailed cost estimations were made. Various component configurations were evaluated to determine the best to meet the requirements of the design.

3.1 Design Methodology

3.1.1 Turbine Specification

The original specification for the 1.5-MW Phase I turbine was retained. Detailed specifications of the generator, power electronics, and structural systems were based on the turbine specification.

3.1.2 Generator Active Material

The generator active material design was based on GDEB's embedded permanent magnet technology. The GDEB design utilized a distributed-wound stator. Its design process included defining generator parameters and developing a detailed design (electrical and magnetic). Design analysis was performed using GDEB-proprietary and commercial software. This analysis included thermal and electromagnetic analysis, and life calculations. Additional electromagnetic calculations were done at Northern to double-check the design.

3.1.3 Power Electronics

Originally, a standard, off-the-shelf motor regenerative drive was targeted as the power electronics for the wind turbine generator. However, off-the-shelf drives have limited control flexibility, which affects the cost of the PM generator, because drives and controls are sold as a

package. While the hardware of the Northern WindPACT power electronics is similar to that of a standard, commercial PM motor drive, its control system has been designed by Northern to provide greater flexibility.

3.1.4 System, Structural, and Mechanical Design

Loads. We used the FAST program to calculate turbine loads under normal turbulence and extreme wind cases. Loads were calculated according to International Electrotechnical Commission (IEC) standards (1999) and processed to yield the loads most useful for designing each structural component. Load cases are shown in Table 3-1. Windward Engineering developed the 1.5-MW direct-drive turbine model. Windward also developed a program to create multidimensional histograms useful for bearing design. Special-purpose spreadsheets were used to calculate fatigue rainflows and damage equivalent loads. For dynamometer test component design, a separate extreme and fatigue loads were calculated based on the rated torque and the overhanging moments due to the weight of the main shaft.

Table 3-1. Design Load Cases for 1.5-MW Wind Turbine Design.

Design situation	IEC DLC	Wind condition	Type of analysis	Comments	
Power production	1.1	NTM 8 to 24 mps	Ultimate		
	1.2	NTM 8 to 24 mps	Fatigue		
	1.3	ECD 12 mps	Ultimate	Negative Direction	
	1.3	ECD 12 mps	Ultimate	Positive Direction	
	1.6	EOG 12 and 24 mps	Ultimate		
	1.7	EWS 12 and 24 mps		Ultimate	Negative Direction, Horizontal Shear
					Positive Direction, Horizontal Shear
					Negative Direction, Vertical Shear
					Positive Direction, Vertical Shear
	1.8	EDC 12 and 24 mps		Ultimate	Negative Direction
					Positive Direction
1.9	ECG 12 mps		Ultimate		
Parked	6.1	NTM 42.5 mps	Ultimate		

Structural Design and Analysis. An FEA of major load-carrying components was conducted and the components were dimensioned according to Germanischer Lloyd (1999) standards. Reserve factors were calculated for both extreme loads and fatigue loads. Fatigue reserve factors were based on a Miner’s sum of damage due to a load spectrum. Load spectrums were available for pitch, yaw, and rotor torque. Materials were selected based on the availability of published static and fatigue material properties, which are shown in Table 3-2.

Table 3-2. Components were Designed with Commonly Available Materials with Known Static and Fatigue Properties.

Process	Material	Tensile (MPa)	Yield (MPa)	Endurance (MPa)
Casting	60-40-18	414	276	Not Available
	GGG40.3	390	275	205
Weldments	A36	400	250	71
	St37	340	225	71
Bolts	8.8	800	640	50
	10.9	1000	900	50

Mechanical Design and Analysis. Critical bolts were evaluated using the VDI 2230 standard. This is a conservative standard that is recommended by Germanischer Lloyd. Note that in Table 3-2, the endurance limit of 50 MPa is a typical quantity, based on a particular thread type and bolt diameter. The actual endurance limit varies per formulas in the VDI 2230 document. The production bearing was evaluated for 20-year life at a reliability of 95%. To reduce the cost of the prototype, another bearing was designed for minimum 2-year life, subjected to dynamometer loads only. Bearing life calculations were performed by the bearing suppliers. Stackup of tolerances was calculated to determine the required manufacturing precision needed to obtain acceptable performance. The brake system was analyzed to ensure that it had the capacity to hold the rotor during service operation.

3.1.5 Design Control

The design control system used for the design of the generator and power electronics was based on two major review processes. First, the overall design was reviewed by Northern, GDEB, and NREL engineers during the detailed design review. Second, each individual Northern drawing was reviewed and signed by appropriate personnel at Northern. Also, each individual GDEB drawing was reviewed and signed by appropriate personnel at GDEB. For particular drawings of joint interest, GDEB and Northern personnel reviewed the drawings.

After the initial release of the drawings for production, a document change order was required to make any changes to the drawing. In this case, a new drawing was released with all the appropriate signatures. In many cases, however, only minor changes were required by the

manufacturer. For example, one manufacturer requested a material change to a very similar alloy. In this case, a deviation request was processed and signed by the project manager only. All released drawing hard copies were kept in a physical file maintained by the Northern quality department. PDF files of the released drawings were made available in a read-only directory on the Northern computer system.

3.2 Design Goals

3.2.1 Turbine

The detailed turbine design was not within the scope of this project. However, to create a realistic context for a generator design, a turbine was specified for 1.5-MW power production. The turbine specifications are shown in Table 3-3.

Table 3-3. Turbine Specification

Parameter	Value
Electrical power rating	1.5 MW
Low-speed shaft speed	
Minimum	12.0 rpm
Rated	19.65 rpm
Maximum design	27.8 rpm
IEC WTGS Design Class	II
Cut-in wind speed	3 m/s
Rated wind speed	12 m/s
Cut-out wind speed	25 m/s
Rotor diameter	70.5 m
Hub height	65.0 m
Design life	20 yr (150,000 hr)
Tip Speed	72.7 mph (32.5 m/s)
Power control	Independent Pitch
Safety System	Pitch Control
Other	Service Brake, Rotor Lock Pin

This specification represents a standard, class II turbine model for a wind resource with an annual average wind speed of 7.5 to 8.5 m/s. It is probable that the same generator would be used for a class III turbine model, with an annual average wind speed less than 7.5 m/s. For lower wind speeds, the optimum design has a larger rotor and taller tower. The rotor speed and rated power would be lower. COE was calculated based on a 5.8-m/s annual average wind speed.

The overall objectives of the design are as follows:

- Low first cost
- Low COE
- Simplicity
- Low weight
- High efficiency
- High reliability
- Good service-ability
- Easy to ship
- Easy to install on site

3.2.2 *Generator*

The goal of the generator design process was expressed in a specification, shown in Table 3-4. This specification covers the power, voltage, operating conditions, dimensions, cooling, etc. It was used to guide the design process.

Table 3-4. Preliminary Specification for the Permanent Magnet Generator

Parameter	Value
Generator Type	Radial Airgap, PM Synchronous
Excitation	Rare Earth Permanent Magnet
Rotor Configuration	Embedded Magnet (Spoke Design)
Rated Power	1,550 kW (1,722 kVA)
Rated Voltage	724.5 V
Power Factor	0.9
Phases	Three
Speed	Variable (9-20 rpm) normal operation. 25 rpm maximum allowed. Mechanical systems capable of 30 rpm.
Direction	CW looking downwind
Frequency	Variable (5.3 to 11.7 Hz)
Harmonic Distortion (Open Circuit at Rated Speed)	Total distortion < 5% Individual distortion < 3% Voltage imbalance <1% Deviation factor <5%
Efficiency	93.8% (50% to 100% rated power)
Maximum dimensions	4-m diameter, 1.6-m axial length
Operating Environment	-15 to 50°C ambient air 0-100% relative humidity, condensing
Design Life	20 years
Insulation Class	H (180°C Max Temp – 20,000 Hours)
Temperature Rise	F (155°C C Max Temp)
Rated Ambient Air Temperature	30°C
Rated Coolant Temperature	40°C
Cooling	Water Cooled
Braking	Hydraulic Parking Brake, Rotor Lock Pin
Construction and Mounting	Horizontal Axis

The generator was designed to operate at temperatures ranging from -15°C to 50°C . It was designed for exposure to conducting or abrasive dust, and blowing snow. It was designed to withstand exposure to 0 to 100% relative humidity. Loads included those caused by Zone 4 seismic activity, and mechanical loads from the blade rotor hub. At temperatures between rated ambient air temperature (30°C) and maximum ambient air temperature (50°C) the power shall be reduced to no less than 84% of rated power. Power output will be curtailed and cooling flow increased to limit stator temperatures during operation above rated temperature conditions.

The generator electric system was rated on a continuous duty basis. Thus it was designed to run continuously for 20 years under rated conditions. The design point rating is expressed in

kilovolt-amperes (kVA) required to deliver rated kilowatts (kW), at a power factor determined by the power electronics load, at the generator’s base speed and rated terminal voltage. The generator was rated at an ambient temperature of 30 °C. The generator mechanical systems were designed for a minimum operating life of twenty (20) years, based on Class II wind loads transmitted to the generator. All hub loads are transferred to the spindle. Hub thrust, shear, and bending moments are transferred directly to the spindle by the main bearing. Shaft torque is transferred through the main bearing to the generator rotor, stator, and support arms. The support arms transfer the torque to the spindle.

The power electronics load presented to the generator was specified to be a balanced, sinusoidal three-phase load. The load capability of the generator is the highest continuous loading (kVA) through the full range of speed, terminal voltage, and power factor as shown in the operating profile of Table 3-5 below:

Table 3-5. Generator Power, Current, Voltage, and Power Factor Data Points

Speed	Power	Current	Voltage	Power factor
RPM	kW	A rms	V rms	
8.95	72	121	341.5	0.998
11.19	141	189	427.3	0.994
13.34	244	274	511.4	0.988
15.57	388	374	601.2	0.978
17.79	579	488	695.9	0.963
19.18	823	669	713.6	0.982
19.37	1,113	914	718.7	0.960
19.57	1,431	1,202	723.1	0.926
19.65	1,550	1,320	724.5	0.909
22.60	1,550	1,263	724.5	0.964

The generator was specified not to exceed the specified steady state performance requirements when operated with an open circuit and at rated speed. The specifications ensure that the power quality to the grid will meet power customer requirements.

The generator was designed to meet the following transient performance requirements when operated at rated speed and under the conditions specified: The generator must be capable of withstanding, without mechanical damage, a three-phase short circuit at its terminals when operating initially at rated kVA, power factor, and speed. In the case of stator windings, the criteria for no mechanical damage is that the windings can satisfactorily withstand a normal maintenance high-potential test. There shall be no visible abnormal deformation or damage to the winding coils and connections. The overcurrent duration is intended to only be momentary and the generator isolated under a fault condition. Because this overcurrent condition will result in

increased temperatures and a reduction in insulation life, the generator shall not be subjected to these conditions more than a few times in its life.

The specification called for stator windings of the generator to be insulated with an epoxy based, global vacuum pressure impregnated (VPI) or equivalent system adequate for the usual service conditions defined. All insulating material was specified to be consistent with the insulation class of the generator and selected to meet the generator design life requirements.

The generator was specified to have embedded temperature detectors. When operated at load corresponding to the rated ambient temperature and rated speed, the observable temperature rise of the generator stator winding insulation shall not exceed 140°C. Because the rated coolant temperature is 40°C, this corresponds to a maximum temperature of 180°C. The embedded temperature detectors were specified to be of the resistance temperature detector (RTD) type. At least six RTDs were specified, suitably distributed around the circumference, located between the coil sides, and in positions having normally the highest temperature along the length of the stator slot. They were in contact with the insulation of the upper coil side (the coil side nearest the airgap). There were four RTDs located on end turns of the generator with two on each side. The generator leads were specified to have sufficient ampacity such that the total temperature of the conductor will not exceed 130°C when the generator is operating at rated conditions.

The generator efficiency was specified to be equal to or greater than 93.8% from 50% of rated load to 100% of rated load at base speed. Higher efficiencies were a design goal if possible without an increase in generator capital cost.

The stator winding insulation system of the generator may be exposed to stresses due to power electronics switching and to steep-fronted transient voltage surges of high amplitudes. Voltages of high magnitude stress the ground insulation. The steep-fronted voltage surges also stress the turn insulation. If the rise time of the surge is steep enough (0.1 to 0.2 μ s), most of the surge could appear across the first coil and its distribution in the coil could be nonlinear.

The steep-fronted surges appearing across the terminals may be caused by lightning strikes, circuit breaker operation, switching transients of the power electronics, etc. The crest value and rise time of the surge at the generator depends on the transient event taking place, on the electrical system design, and on the number and characteristics of all other devices in the system. These include but are not limited to, the generator, the cables connecting the generator to the power electronics, switching transients of the power electronics, and the number and sizes of all other loads connected to the generator.

Stator winding insulation was designed to have a surge withstand capability of 2.5 PU at a rise time of 0.19 μ s, or 2.6 PU at 1.0 μ s and longer. 1 PU is defined as the crest of the generator rated line to neutral voltage, or $1 \text{ PU} = (\sqrt{2/3}) V_{L-L}$.

The maximum allowable outside diameter of the generator frame was 4.0 m. The maximum allowable overall length of the generator from the generator-mounting flange to the rotor hub-mounting flange was 1.6 m. Generator enclosures or end bells were specified to not protrude beyond the attachment flanges. The allowable air gap deflection was 0.45 mm (10% of nominal

air gap) during normal operation. The allowable air gap deflection was 2.25 mm during extreme wind conditions, where the rotor is not turning.

The generator was specified to have an integral parking brake with the capability to bring the rotor to a standstill after the feathered blades bring the speed to 1 rpm. The maximum torque requirement was 520 Nm, which corresponds to the maximum wind speed for service (33.6 m/s). The brakes are normally released, and are applied with hydraulic pressure. Thus they will remain released if the grid is lost.

The generator was specified to be indirect liquid cooled. The stator is specified to have channels between the stator core and stator frame forming a water jacket. Stator core and frame materials in contact with the liquid coolant are specified to be compatible with a mixed solution of water and glycol. The water jacket is specified to be hydrostatically tested to 150% of the cooling system design operating pressure of 1.38 MPa (200 psi).

The generator was specified to be capable of withstanding, without injuries to any mechanical part, a momentary overspeed to 30 rpm. The maximum allowable speed on the turbine is 25 rpm. It is recognized that the generator's internal voltage may approach or exceed the specified limits, and therefore this capability is only intended for mechanical survivability during emergency conditions.

The wind turbine blade rotation is specified to be clockwise when viewed from the front of the turbine and with the phase sequence of the generator terminals A, B, and C such that the voltage is positive sequence.

3.2.3 *Power Electronics*

Originally, a standard, off-the-shelf motor regenerative drive was targeted as the power electronics for the wind turbine generator. However, limited control flexibility, which affects the cost of the PM generator, required purchasing Northern-built power electronics because drives and controls are sold as a package. While the hardware of the Northern power electronics is identical to that of a standard, commercial PM motor drive, its control system has been designed by Northern to provide greater flexibility. Specifications are shown in Table 3-6. A schematic of the power electronics is shown in Figure 3-1.

The power specified for the electronics was larger than that of the generator because this project was mainly a test for the generator. The design of the electronics was more conservative. The grid voltage of 690 V was chosen to match the voltage capabilities of the best value, commercially available IGBT modules. A water-cooling system was chosen because fewer IGBTs are needed, and the physical size of the electronics is smaller as compared to an air-cooled system. Also, it matches well with a water-cooled generator. The components' power electronics were designed to be modular, so that if a larger electronics system is needed in the future, another module can be added without alteration of the rest of the design. Control was chosen to be with a Programmable Logic Controller (PLC) for convenience in programming, overall operation, and safety functions. The PLC is not fast enough to control the IGBTs, however, so DSP boards were used for this purpose. They are used for generator-side, grid-side,

and dynamic-brake control. The DSP boards are slaves to the PLC. The enclosures for the power electronics were specified as IP54/NEMA 12, which corresponds to the normal factory requirements. The enclosures protect the electronics from dust and noncorrosive drips.

Table 3-6. Power Electronics Design Specification

Parameter	Value
Power Rating (To Grid)	1,500 kW
Surge Power	120% for 30 seconds
Grid Voltage	690 V
Phases	3
Generator Side Frequency	Variable (5.3 to 11.7 Hz)
Grid Side Frequency	60 Hz
Switching Frequency	5 kHz Minimum
Efficiency at Rated Conditions	97%
Power Factor	>0.95 from 20% to 100% Rated Power
Environment	-15 to 50 °C ambient air
Cooling	Water Cooled
Generator Side Power Electronics	1,700 V IGBT, AC-DC
Grid Side Power Electronics	1,700 V IGBT, DC-AC
Modularity	Three 500-kW units
Control	PLC with Slave DSPs
Enclosure Protection	NEMA 12/IP54 (Indoor Factory Environment)
Remote Interface	MODBUS over RS485
Design Life	3 years
Control Power	Grid Power with Battery Backup
Dynamic Brake	Included in First Article Only

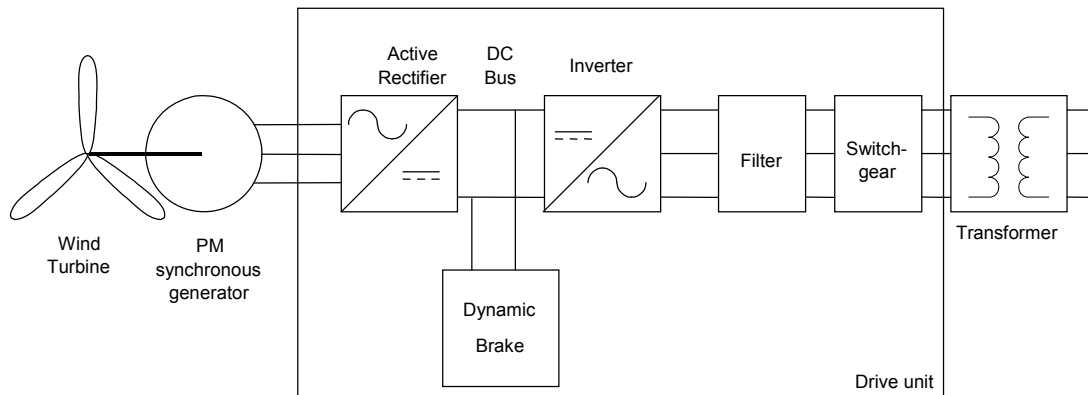


Figure 3-1. Schematic of the power electronics design.

3.3 Design Issues

In the course of the detailed design, several issues arose because of the conflicting requirements. These issues are categorized in the following way:

- Structural
- Mechanical
- Electromagnetics
- Power Electronics
- Design Control.

3.3.1 Structural

The structure of the generator had to be strong and stiff. Most of the structural design issues dealt with tradeoffs needed to maximize strength and stiffness while minimizing cost. The strength requirement was due to safety. The stiffness requirement was due to the gap between the stator and the rotor. When the wind turbine blades are loaded unevenly, a moment is applied to the spindle and main bearing that causes deflections of the generator rotor. These rotor deflections cause potentially problematic variations in the gap. For this reason, many of the structural components are mainly sized based on the deflections, rather than stress.

The torque transfer design from the stator to the water jacket to the outer frame was of concern because of the uncertainties of a large-diameter press fit. There were four major design alternatives: welding, press fit, mechanical fastener, or using a key. A press fit arrangement between the stator and water jacket was used, mainly because it provides good heat transfer. Because of transient changes in temperature, there is a slight possibility that there would not always be enough capacity in the press-fit joint to carry rated torque. Thus a single key along the full length of the stator was used as well. Between the water jacket and the outer frame, a clearance fit was used, and the two parts welded in a continuous seam. A continuous seam is needed for sealing purposes. This was chosen because we felt the weld would be strong enough to carry the torque.

The material chosen for the main structural parts was welded A36 steel. This is the most economical choice for prototype design, because excessive tooling cost is avoided. Castings, however, have better fatigue resistance. It is expected that in production, the welded spindle would be replaced with a cast spindle, which would be lighter than the welded version. A cast spider was also considered, but the required bending stiffness of the arms was difficult to accomplish with a cast configuration.

3.3.2 Mechanical

The mechanical systems, bearings, bolts, brakes, and cooling system had issues that were resolved during the course of detailed design.

The main bearing had to be designed to carry the main loads from the blade rotor while rotating continuously. A sealing system had to be designed to keep grease in the bearing and out of the generator windings. The large diameter of the single bearing made sealing more difficult. Also, the fits between the bearing and rotor were troublesome. Press fits were desired to minimize gap

variation, but were more difficult to assemble. Removal of the bearing, including field removal, was considered. Bolt attachments and clamping attachments to the bearing were considered. The rotor was designed with a single web on the upwind side. This allowed the bearing to be placed upwind and mate directly with the blade rotor hub. Bearing grease ports are on the inner diameter of the spindle. Also, if the bearing needs to be removed, a system for applying a hydraulic force from the spindle is included. A double-tapered roller bearing was selected for the production main bearing. This bearing has excellent load and speed capabilities. Also, it is becoming the more common choice for this application. The tooling of a new bearing of this type is very expensive, however, so a cheaper crossed roller bearing was used for the prototype.

Service and inspection of the rotor pole bolts, main bearing, and electrical connections is done from the downwind side in this design. The front seal on the bearing is accessible through the large holes in the rotor web. The front v-ring seal (a weather seal between the blade rotor hub and the front of the generator) is serviced from the front.

The brakes were designed to carry only parking loads. Compatibility of the brake fluid and the windings was considered. A system for caliper braking, and a backup rotor lock pin were designed. At first, the caliper was going to clamp on a drum; however, this would require special contoured brake pads. A disk was added to the end of the rotor. This allowed the use of a standard brake caliper, made the rotor stiffer, and allowed the use of a rotor lock pin. Methods for routing the brake system piping were evaluated.

The design team resolved several issues concerning the cooling system. First, the cooling fluid, 50% propylene-glycol in water was chosen. The water jacket material was chosen in light of the cooling fluid. An aluminum water jacket would have severe thermal expansion issues. Stainless steel would be corrosion-proof, but very expensive. Carbon steel was chosen because it will not significantly corrode with 50% propylene-glycol, and it will not have thermal expansion problems. Second, a method for corrosion protection during manufacturing was chosen. Oil is to be sprayed into the open cooling paths and washed out prior to connection to the glycol system in operation. Cooling paths and fittings were designed to provide adequate flow for cooling. Analysis was performed to determine the ideal operating temperature of the air. At first we tried to design the generator to run continuously at an ambient air temperature of 50°C. This led to a very expensive generator however, because the magnets degrade at higher temperatures. There was no good reason to stick to this requirement, as the degradation of the magnet material at 50°C was not permanent. The temperature at which damage occurs to the magnet is much higher. The solution was to design the generator to run continuously at rated power with a 30°C ambient air temperature. At temperatures from 30°C to 50°C, the output of the generator, running continuously, would be reduced. At 50°C ambient air temperature, the output is still 86% of nominal power. This provides a more reasonably priced generator at minimal loss of energy.

3.3.3 *Electromagnetic*

There were several electromagnetic issues resolved in the design process. These concerned magnet selection, attachment of rotor poles, rotor materials, and winding connections.

The magnets were sized to obtain the correct torque during operating conditions. The magnets were chosen based on interactions with suppliers to find the best magnet value. The design was evaluated for demagnetization safety. The size of the magnets was changed at one point in the design process. The first size was based on preliminary calculations. Then GDEB performed a finite element analysis, and it was determined that a 10% increase in magnet mass was needed to obtain the specified torque.

The method of attachment of the rotor poles was studied to determine the most appropriate method for this design. Compared to most other generator designs, this one operates at a very low speed. Centrifugal forces are minimal. Thus the number of fasteners required for the rotor poles can be reduced. Also, many generators have machined flats on the outer surface of the rotor hub to provide a good mating surface to the poles and magnets. The diameter of this generator is very large, so machined flats are not necessary. The laminated poles were stamped with a curvature to match that of the rotor hub.

The rotor material options were aluminum and stainless steel. These nonmagnetic materials are needed in the region of the hub by the active materials (magnets and laminated poles) to prevent flux leakage. The aluminum rotor is inexpensive, but has severe thermal expansion issues for the environmental conditions of the wind turbine. Stainless steel has higher material cost, but a stainless outer ring can be welded to a carbon steel inner hub portion. The stainless coefficient of thermal expansion is similar to that of carbon steel, so the air gap tolerance can be maintained even with temperature extremes.

There were two possible positions for the electrical connections of the windings. They could be connected on the upwind side, away from the spider, or on the downwind side, next to the spider. The problem with the upwind side is that there is no convenient place to run the wires between the generator and the tower. A large conduit for the wires would have to extend beyond the 4-m outer diameter. The disadvantage of connections near the spider is that the spider gets in the way of the connection manufacturing process. The connection at the spider end was chosen because the spider could be removed for this manufacturing operation.

The resulting active material geometry is shown in Figure 3-14.

3.3.4 Power Electronics

The power electronic system design selection is based on the objective to minimize the drivetrain cost. The direct-drive generator cost is relatively higher than that of the power electronics. Hence, it was possible to evaluate a higher performance power electronics topology that leads to lower generator cost. The choices for the power electronics system were between a passive rectifier an SCR-based switching system, and an IGBT-based switching system on the generator side. A preliminary study indicated that the use of the IGBT-based system provided control of the generator that fully utilizes its active materials. As the cost savings in the generator justified the increased cost of the IGBT power electronics over the SCR or diode bridge topologies, the IGBT voltage source system was the final topology that was selected.

The power system was made in modular 500-kW units, as shown in Figure 3.2. This simplified the design and made it scalable to larger or smaller power levels. Connections and controls are located in a cabinet on the left in Figure 3.2.

The switching frequency of the power electronics was selected based on meeting the IEEE-519 (1992) standard and to keep generator torque ripple to an acceptable level. The losses in the semiconductors and other components in the power electronics, along with the water-cooled thermal management that is utilized in the power electronics, resulted in expected efficiency of at least 97% at rated conditions. It is possible to further improve the efficiency and the overall system cost with advanced IGBT power electronics technologies. However, as the focus of the project was on the generator and the overall drive train, a simple six-switch voltage source inverter topology was selected for the power electronics.

One concern in an IGBT power electronics unit is the magnitude of the voltage spikes caused by IGBT switching. The generator was designed with enough insulation to survive 20 years with filtered voltage spikes from the IGBTs. The design method is to develop a circuit model (Figure 3.3) of the power electronics and generator, and using the input noise of the IGBTs, calculate the resulting voltage spike in the generator. At first, estimated generator parameters were used in the model, to be replaced with measured data after fabrication. It was assumed that filters would be designed that would reduce the magnitude of the voltage spikes to the level that would lead to a 20-year generator life. Filters were eliminated, however, due to cost constraints. The insulation is sufficient to survive the expected test program, unfiltered, on the dynamometer. Another result of IGBT switching noise is electromagnetic interference (EMI). The filter design and the mounting of the IGBTs on a back plane in each cabinet is designed to keep the high frequency switching noise contained within the power converter enclosure. The circuit model included characteristics of parasitic components and packaging. Simulations indicate that the EMI emissions would be within acceptable limits. Also, a filter at the generator output was designed to damp cable resonance. The length of cable (80 m) was investigated to effectively simulate the condition of a power electronics unit at the base of a tower. A shorter length of cable was chosen for the dynamometer test to reduce cost.

The cooling system for the power converter could either be a water-cooling or air-cooling system. Water-cooling resulted in a lower incremental system complexity as it was already used in the generator. Also, the reduction in IGBT cost with the use of a water-cooling system led to it as the preferred cooling method for the power electronics. The resulting design is a fully sealed power electronics unit with IP54 rating, leading to its improved reliability. The water-cooling system has been easy to implement on the major components of the system. The IGBTs are mounted on a water-cooled heat sink and the remaining components within the power electronics cabinet are cooled by air-water heat exchangers. Fans are used to circulate air over the heat exchanger and other devices in the power electronics cabinet.

The power electronics control design is compatible with the Safe Operating Procedure for testing at the NREL dynamometer. The control and protection one-line drawing is shown in Figure 3.4. The engineering controls incorporated in the design include:

- Protection system in the controller: Over current, ground fault, controller alarms, fusing protection, over temperature monitoring.

- E-stop protection
- Door locks and fully enclosed system

In terms of the controls, the power electronics will not clear any fault signal until the turbine stops running. The power converter has door locks to prevent access to the power circuit section when the power electronics unit is operating. The direct current (DC) bus is discharged before the controller unlocks the DC bus.

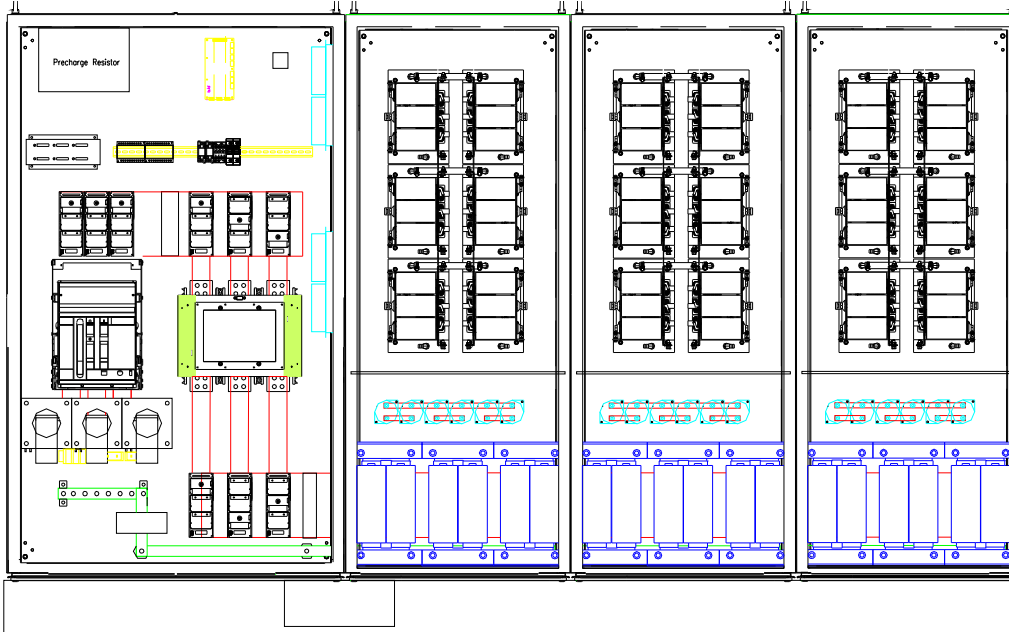


Figure 3-2. The power electronics system was made from three 500-kW modules.

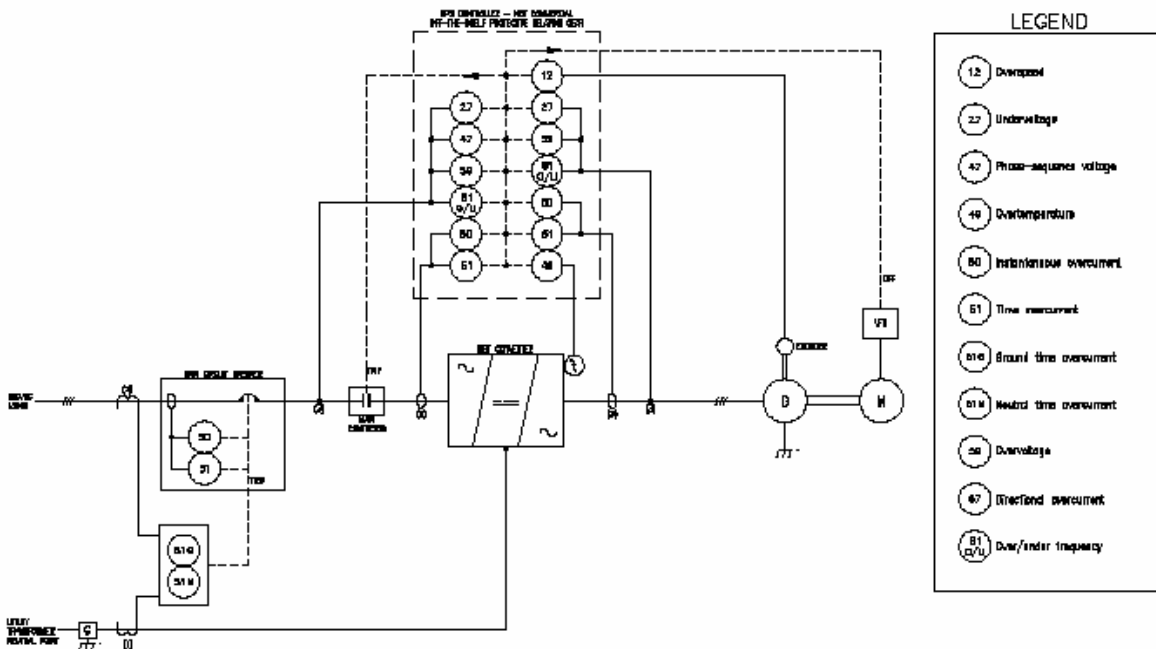


Figure 3-3. Power electronics protection 1-line.

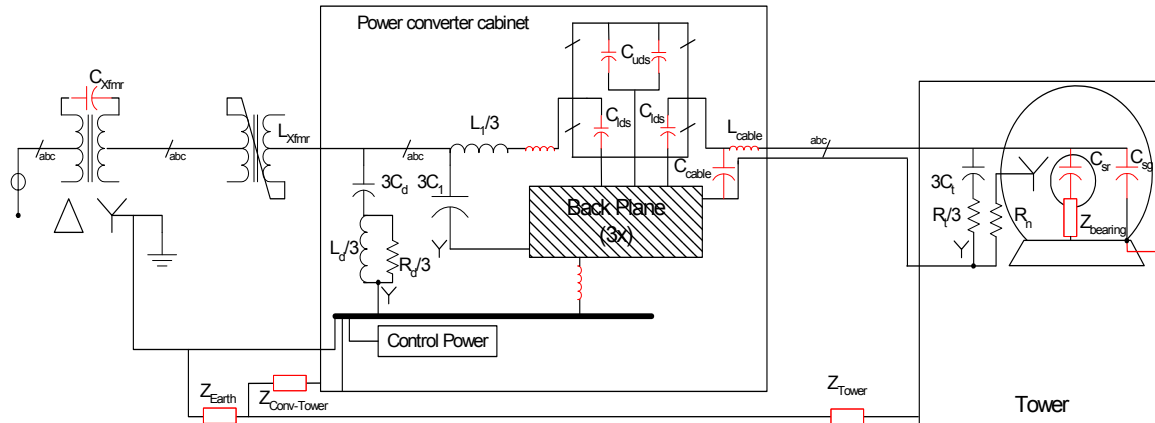


Figure 3-4. A common-mode circuit model of the generator and power electronics determined the magnitude of voltages in the system caused by the IGBT switching noise.

3.3.5 Design Control

Design control issues involved the discussion of roles and responsibilities between GDEB and Northern. It was decided that GDEB would have responsibility for the rotor and wound stator assemblies. Northern would have responsibility for the balance of the generator, and the creation of interface documents.

All of the component drawings produced at Northern were created with Solidworks. Methods were established to organize and control the drawings. Drawings produced by GDEB were created with AutoCAD. Hardcopies of the Northern and GDEB drawings were used for fabrication.

3.4 Detailed Design Verification

Every component and system was analyzed to determine that it would function to the requirements of the design specification. This section describes the analysis results and the details of the design.

3.4.1 Structural

Each critical structural component was analyzed to determine its safety and function when subjected to the applied loading. The structural analysis is divided into four categories: stress analysis, deflection analysis, bolted joint analysis, and vibration analysis. The analysis was performed using a variety of tools. Finite element models were used for most major structural components. The stresses from the models were input to spreadsheets to determine static and fatigue reserves. Bolt analysis following the VDI 2230 standard was done with a spreadsheet.

3.4.1.1 Stress Analysis

The static and fatigue analysis of the major structural components was done using finite element models. In most cases, these were welded structures. To simplify the analysis, full-penetration welds were specified, so the same fatigue category could be used throughout the part. The finite element model of the spindle is shown in Figure 3-5. It shows a maximum stress of 89.7 MPa for the most severe ultimate load case. Spreadsheet analysis, utilizing the partial load factors for loads and materials, and the material yield stress, indicate a static reserve of 2.53 (greater than 1.0 being a safe design). Also, unit loads were applied to the finite element model, and these stress functions were input to a fatigue analysis, based on the load spectrums for pitch and yaw bending moments. The analysis showed a fatigue reserve of 1.44 (1.0 being a safe design). Thus the design is safe for both static and fatigue loads. Note that the highest stress is near the end of the bearing land. Particular attention was paid to the relief of this corner in the design to avoid a stress concentration.

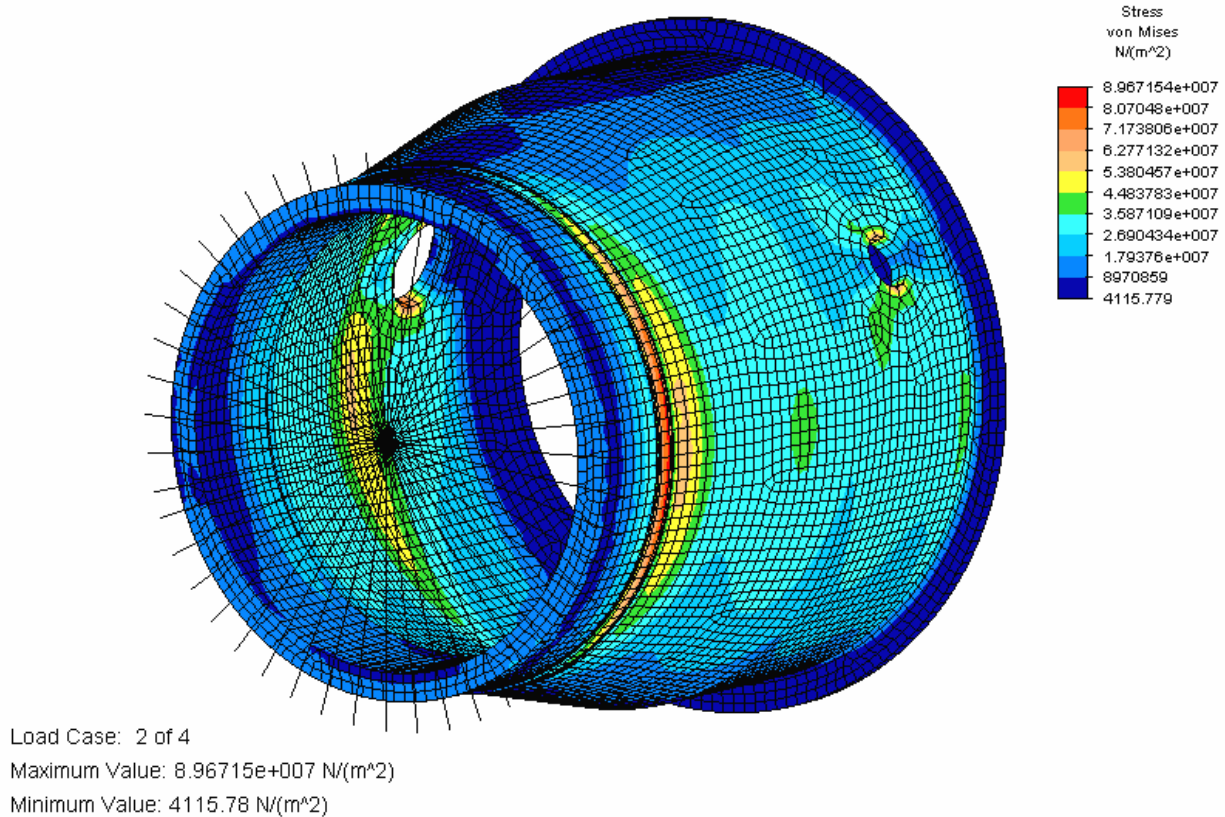


Figure 3-5. The spindle was analyzed using finite element analysis to determine the correct thickness and geometric details to carry blade rotor moment loads.

A similar stress analysis was done for other structural components. The details are provided in Appendix C. The results are summarized in this section. The reserves for the most critical components are shown in Figure 3.6. All static and fatigue reserves are greater than 1.0. There were three critical failure modes (margins close to 1.0). First, the stresses caused by lifting the generator were very high. This design was difficult because of the size of the large lifting bosses

relative to the 1.0-inch plate. Another area of concern was the rotor fatigue. If the rotor is installed eccentric to the stator by 0.5 mm, a fairly large electromagnetic imbalance force is created. This imbalance force is applied for every cycle of turbine rotation. This failure mode was not considered until after the design was completed, thus the rotor was not optimized to minimize stresses due to this load. A third issue in the design was the rotor lock pin in the spider arm. In the high wind speed condition during service, the load from the lock pin is very high, and design changes were required to reinforce this area.

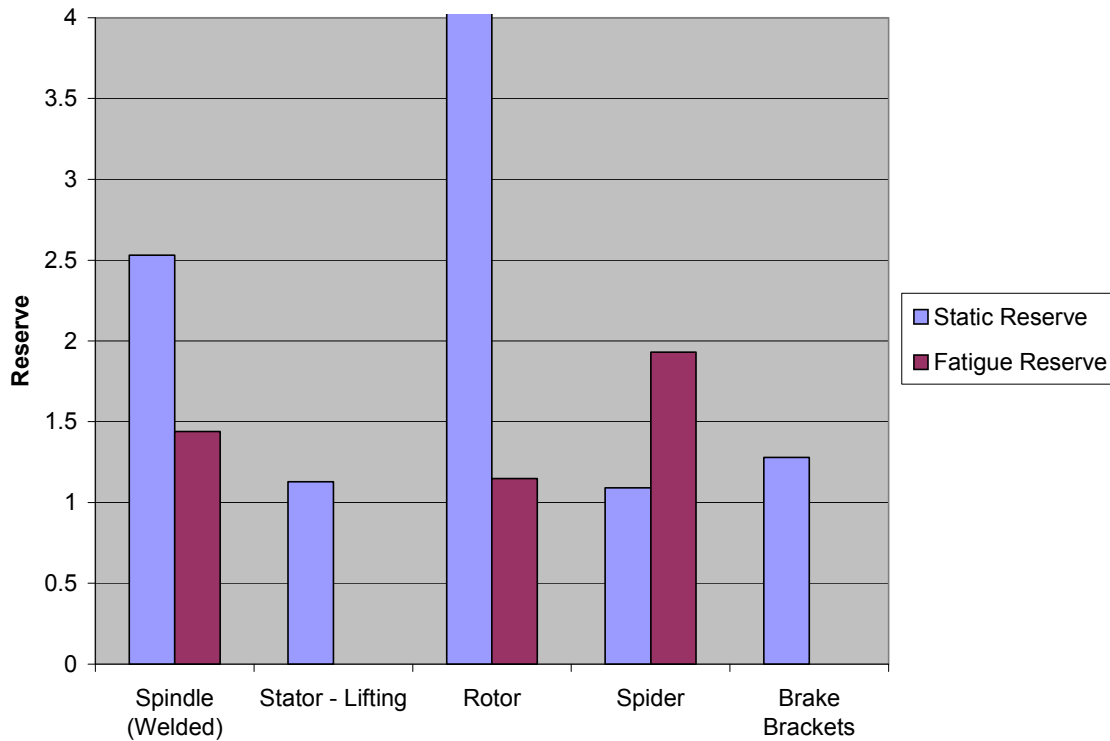


Figure 3-6. The summary of structural analysis shows that margins of safety were adequate (Safe designs >1).

3.4.1.2 *Deflection Analysis*

The generator performance is highly dependent on the size of the air gap between the rotor and the stator. If the air gap is too large, the torque will be diminished. If the air gap is too small, the voltage may be too high. If the air-gap is too non-uniform, the imbalance forces may cause excessive fatigue loads on the generator. To verify that the design will have an acceptable air gap, deflection analysis is needed. First, the load deflections are predicted using finite element analysis, as shown in Figure 3-7. Second, the positions of the rotor components with respect to the stator are predicted, taking into account dimensional variations due to manufacturing tolerances. These aspects are combined into a unified analysis of the as-built configuration, as compared to the allowable variation of the air gap between the rotor and the stator.

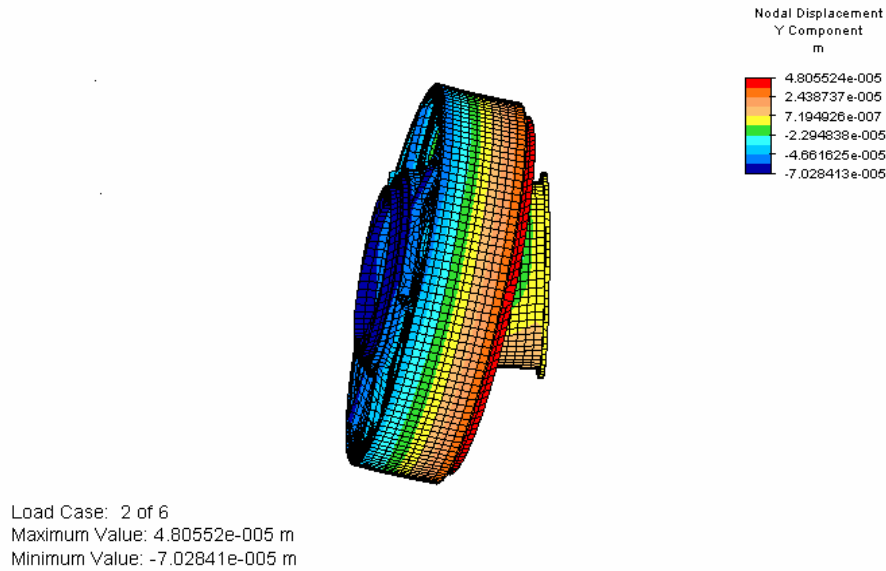


Figure 3-7. The deflection of the rotor was calculated to determine the effect on the gap.

The deflections of the rotor relative to the stator are shown in Figure 3.8. The main source of deflection is caused by the rotor blade moments passing through the spindle of the generator. This causes rotation and translation of the generator rotor. Also, a portion of the deflection is due to gravity (or earthquake) loads on the rotor and stator. It can be seen from Figure 3.8 that there are two allowables for deflections. First, there is an allowable for normal operation of the generator during power production (based on +/- 10% of the mean air gap dimension). This allowable is base on power quality and fatigue loading requirements. Second, there is an allowable for extreme winds, when the generator is not producing power. In this case, the allowable is based on keeping the rotor from touching the stator. Figure 3.8 clearly shows that the deflections are less than the allowables in all cases.

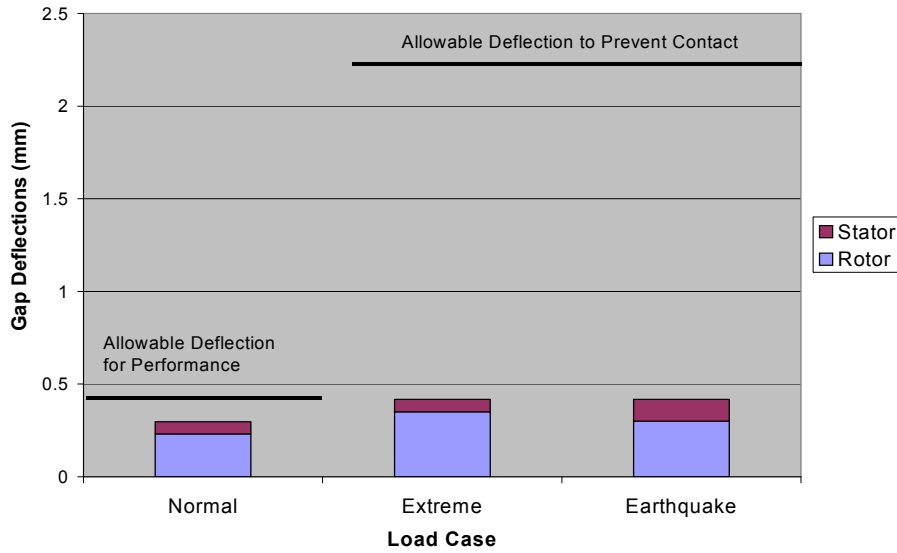


Figure 3-8. Analysis shows that the deflections are within specified limits when manufacturing tolerances are neglected.

Another issue relative to the air gap is the manufacturing tolerances required to maintain the air gap within specifications. The manufacturing method for the generator calls for the bearing land on the spindle to be machined concentric to the inner diameter of the stator. Thus the major contributors to variation are the stator inner diameter, spindle (bearing land) concentricity, bearing concentricity, rotor concentricity, the rotor hub outer diameter, and the pole thickness, as shown in Figure 3-9. This analysis shows that the variation caused by manufacturing tolerances is also less than the allowable, which is +/- 10% of the mean air gap dimension.

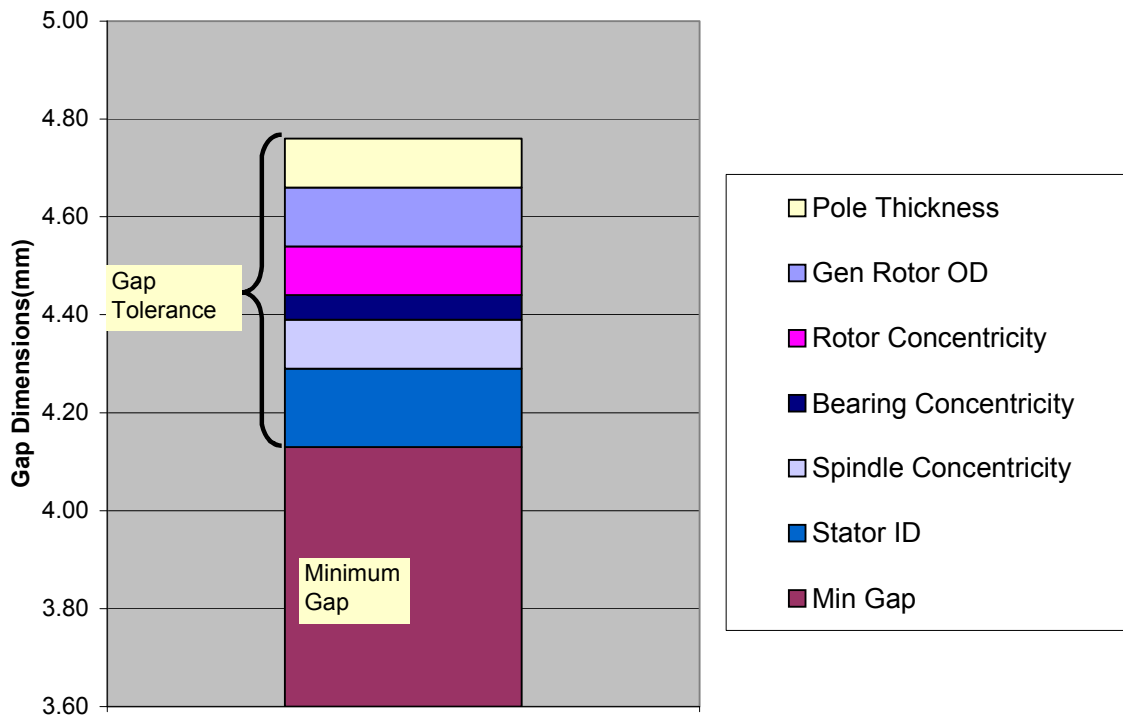


Figure 3-9. The stackup analysis of the gap showed the major sources of variation.

The resulting gap variation for operational deflections and manufacturing variations is +/-14%. The target was +/-10%. This design was accepted because it was unlikely that the gap variation could be improved without adding significant additional cost. It was also possible that the power quality issues and imbalance loads due to a +/- 14% air gap could be insignificant.

3.4.1.3 *Bolted Joint Analysis*

The bolted joints were analyzed with a VDI2230 spreadsheet. Static and fatigue reserves, shown in Figure 3.10, indicate that all designs are safe. The joints that carry a large torque load, to prevent slipping, require a wire brush or flame treatment to achieve a coefficient of friction of 0.3. All torque joints were analyzed with regard to the tightening system. The more accurately the bolt can be preloaded, the safer the design. All joints that carry torque only (generator rotor to main bearing, stator to spider) are designed to be safe using torque wrench tightening. All joints in bending require hydraulic tension or controlled rotation tightening to be safe. Washers are required for all bolts and nuts to prevent denting of the substrate material. Thread friction coefficient of 0.12 is assumed for all bolts. This means that lubrication of the fastener must be in place during tightening. The fatigue reserve is mainly based on the bolt tensile force caused by fatigue loading. Because torque joints do not have a tensile fatigue loading, no fatigue reserve is calculated. For the bending joints, the reserve mainly depends on the relative stiffness of the flanges and the bolt. Thicker flanges are better. The main bearing fatigue reserves are a little

lower than for the Spindle-Turret due to the rotating loads on the main bearing. The static reserve for bolts is difficult to define. Failure is defined as a one-sided separation of the two flanges. The static reserve is defined as the yield force of the bolt divided by the sum of the preload and bolt load. Because the preload for a given bolt is normally much larger than the bolt load, and the preload for a bolt is 70% of the ultimate tensile load, the static reserves for a passing bolt are usually about 1.3.

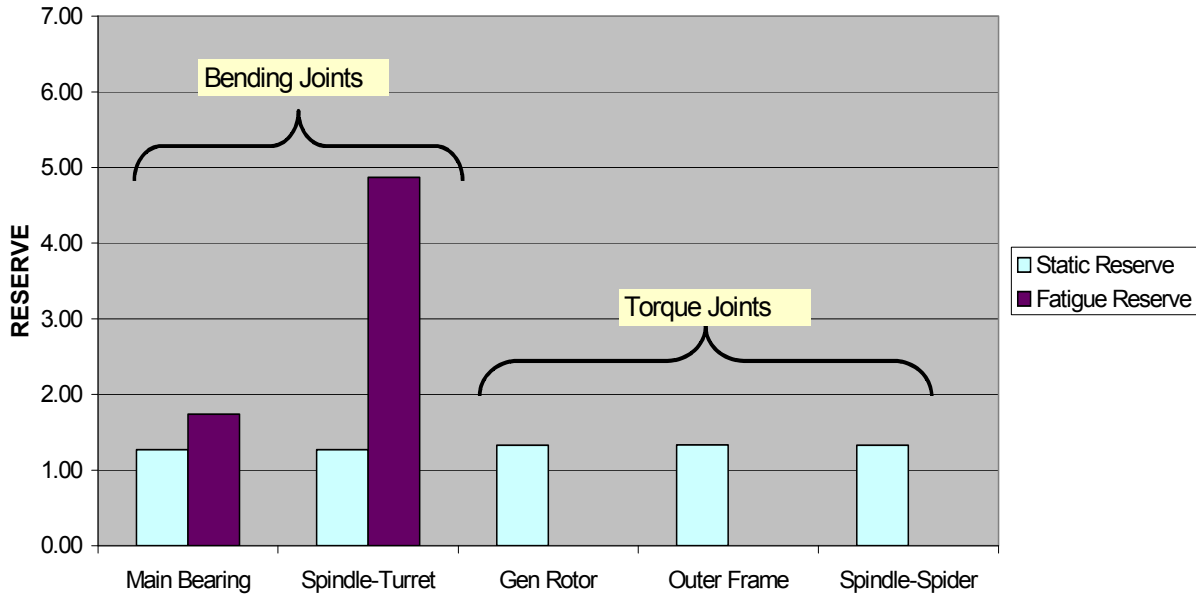
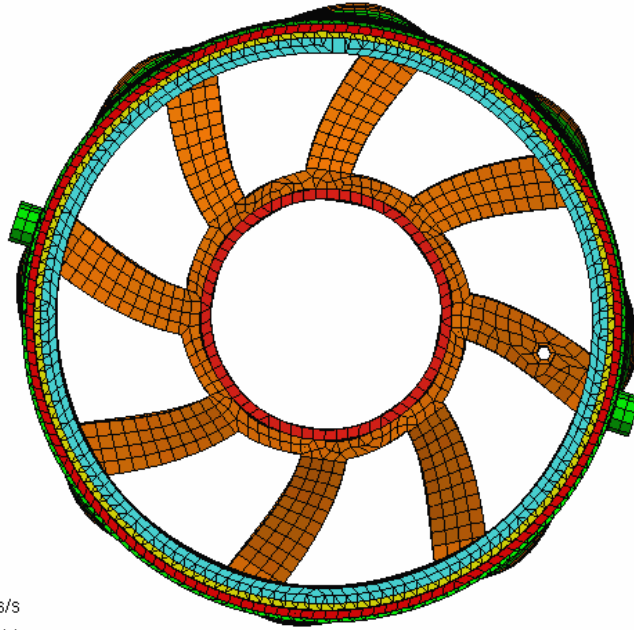


Figure 3-10. The bolted joints for all major structural connections were safe.

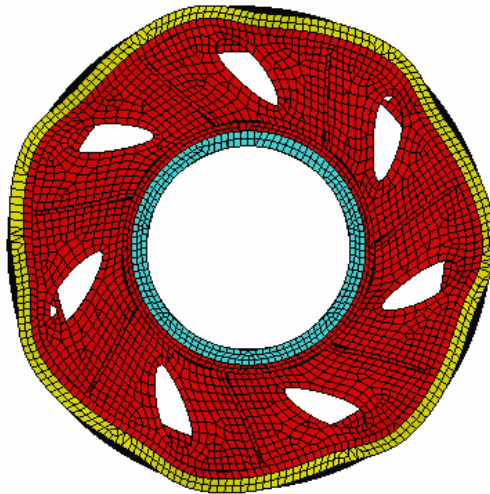
3.4.1.4 *Vibration Analysis*

A normal modes analysis was performed to ensure that the generator would not have damaging vibration during operation. This analysis was performed on the rotor and stator independently. The fundamental torsional mode shapes for the stator and rotor are shown in Figures 3.11 and 3.12. The main forcing functions of the generator are radial and torsional in nature, and are related to the rotational frequency, generator electric frequency, and slot passing frequency. These values for rated conditions are shown in Table 3.7. It seems that the rotor frequency and electric frequency are far below the natural frequencies of the rotor and stator, and should not cause any problems. The slot passing frequency is on the same order of magnitude with the rotor and stator natural frequencies, and thus may be of concern. The analysis shows a wide degree of separation of the forcing and natural frequencies. Vibration issues are very difficult to foresee, however, because of the effects of the stiffness of mating structures, and the possibility of forcing functions due to electromagnetic sources. This situation was monitored closely in the dynamometer tests. Results are in Section 5 of this report.



Mode: 3 of 10
Frequency: 46.5345 cycles/s
Maximum Value: Not Available
Minimum Value: Not Available

Figure 3-11. The normal modes analysis of the stator showed a torsional natural frequency of 46.5 Hz.



Mode: 6 of 10
Frequency: 149.935 cycles/s
Maximum Value: Not Available
Minimum Value: Not Available

Figure 3-12. The normal modes analysis of the rotor showed a torsional natural frequency of 149.9 Hz.

Table 3-7. Forcing and Torsional Natural Frequencies at Rated Conditions

Parameter	Value
Rotor Speed	19.65 rpm
Rotor Frequency	0.33 Hz
Electric Frequency	9.17 Hz
Slot Passing Frequency	110.0 Hz
Rotor Torsional Natural Frequency	149.9 Hz
Stator Torsional Natural Frequency	46.53 Hz

3.4.2 Mechanical

3.4.2.1 Main Bearing

Two main bearings were designed. The Timken bearing was designed for the wind turbine application, and the Avon bearing was designed for the dynamometer test only.

The loads for the Timken bearing were specified in the loads document. The loading histogram for the wind turbine application was binned by thrust level, radial force level, moment level, and speed. For each of 114 bins, the thrust, radial force, moment, speed, and duration was input into the life calculation model.

The Timken bearing and Avon bearing is shown in Figure 3-13.

For the Avon bearing, the static and fatigue loads are the same as shown in Table 3-8. This is because the only loading is caused by the overhanging moment caused by the weight of the main shaft. Static capacity and fatigue life were calculated by the supplier. The static loads are insignificant relative to static capacity. Predicted life is based on continuous operation at 20 rpm. The life of 2.1 years is considered sufficient for the dynamometer testing

Table 3-8. The Avon Bearing Was Analyzed to Determine that the Life Would Be Adequate for the Duration of the Dynamometer Test.

Parameter	Value
Static & Fatigue Loads	
Radial	23.5 kN (52804 lb)
Moment	115.5 kNm (85,200 ft-lb)
Static Capacity	
Radial	1,432 kN (321,556 lb)
Moment	945 kNm (828,139 ft-lb)
Life at 20 rpm	18,460 hr (2.1 years)

The main bearing for the turbine is a double-row, tapered roller bearing. The life of each row is calculated separately, given the loads for a Class II turbine. Timken calculated the life, using the SYSx calculation program. Results are shown in Table 3-9. Catalog L10 life is typically

calculated for a bearing, but it corresponds to a reliability of 90%. Thus 10% of the bearings can be expected to fail before the L10 life is complete. The Timken bearing can be expected to have a 97.7% reliability at 20 years for Class I loads, and a 98.0% reliability at 20 years for Class II loads. Thus, less than 3% of the bearings are expected to fail before 20 years.

Table 3-9. The Timken Double-Row, Tapered Roller Bearing Was Designed to Meet the 20-year Life Requirements of the Turbine Application.

	Bearing Position	Catalog Life L10 Hours (yr)	20 year Reliability %
Class I Loads	Outboard	731,000 (83.4)	97.9
	Inboard	938,000 (107.1)	99.8
	System	516,000 (58.9)	97.7
Class II Loads	Outboard	793,000 (90.5)	98.1
	Inboard	1,125,000 (128.4)	99.9
	System	582,000 (66.4)	98.0

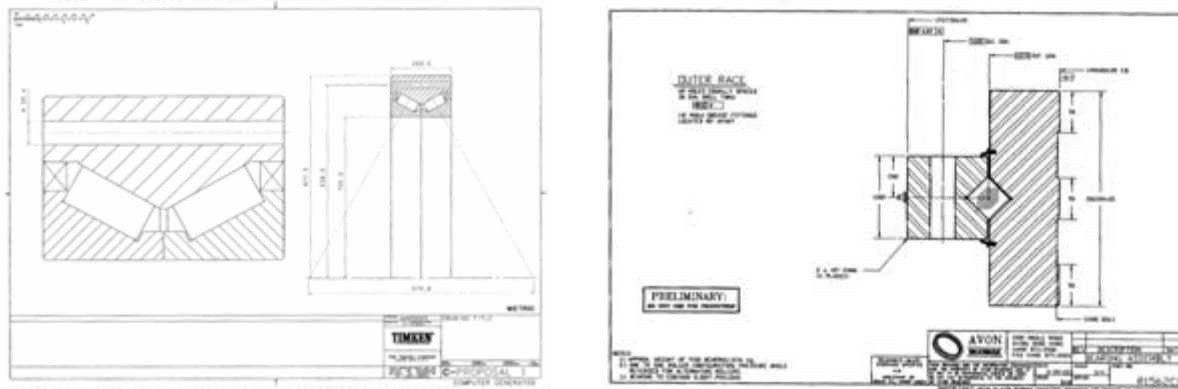


Figure 3-13. The crossed roller bearing was used instead of the double-tapered roller bearing to reduce the cost of the dynamometer prototype.

3.4.2.2 Parking Brakes

The verification of the parking brakes was performed by Svendborg. Calculations were made to ensure that the selected brake caliper could safely carry the required torque at the pressures delivered by the selected hydraulic system. The brake brackets were also analyzed using finite element analysis, and determined to have an acceptable margin of safety.

3.4.2.3 Generator Cooling System

The cooling system was analyzed by GDEB. For rated conditions, the temperatures are as shown in Table 3-10. Of critical concern is the temperature of the windings. To obtain the required life of 20 years, the temperatures were kept below those specified for Class F insulation.

This is because the typical class rating for insulation is based on a life of 20,000 hours (about 2.5 years), which is insufficient for a wind turbine. The magnet temperature must be kept low to obtain adequate efficiency, because the magnetic flux is reduced with higher temperatures. At a temperature of 155°C, the magnet becomes permanently demagnetized; however, this is well above normal operating temperatures for this generator. The maximum desired coolant temperature is specified at 50°C for this analysis, but the actual coolant flow rate will probably be higher than 40 GPM, providing additional safety for the overall cooling system design.

Table 3-10. The Generator Cooling System was Designed to Keep the Winding Temperatures Lower than 155°C.

Parameter	Value	Allowable Value
Heat Rejected	109.25 kW	N/A
Winding Temperature in Stator Slot	114°C	155°C (Class F)
Winding Temperature in Coil Extension	126.4°C	155°C (Class F)
Magnet Temperature	50°C	155°C (Magnet Material)
Coolant Temperature at Inlet	40°C	N/A
Coolant Temperature at Outlet	50°C	N/A
Coolant Flow Rate	40 GPM (2.52 liter/s)	N/A
Coolant Pressure Drop	19 psi (1.31 bar)	N/A

The generator was designed to produce rated power in a 30°C ambient air environment. This condition was chosen so that the generator would not be overly expensive, and would not waste power by shutting down on hot days. In a typical application, hot days do not correlate with windy days. Also, the machine is designed to provide at least 84% of rated power when the ambient air temperature rises to 50°C. Also, the generator is protected with numerous thermocouples, so the generator will even run in ambient temperatures above 50°C at lower power levels.

3.4.3 Electromagnetic

GDEB performed electromagnetic analysis to estimate the performance of the generator. Northern also performed some electromagnetic analysis to confirm GDEB results and provide data for this report. Shown in Figure 3-14 is a flux plot for rated conditions, assuming a 50°C magnet temperature. The yellow and white areas have the highest flux density, and are most susceptible to saturation. For an optimized design, these locations will be near saturation at rated conditions. This analysis is nonlinear. The properties of the material as a function of flux and temperature are calculated to ensure that the generator will perform within specifications. Given the flux, the torque can be calculated and compared to specifications. Similar analyses were conducted for no-load and short circuit conditions. Most of the analysis was done on the unskewed generator, because this is easier to analyze. Some adjustments of the unskewed results to determine skewed results are made, based on experience from similar generators.

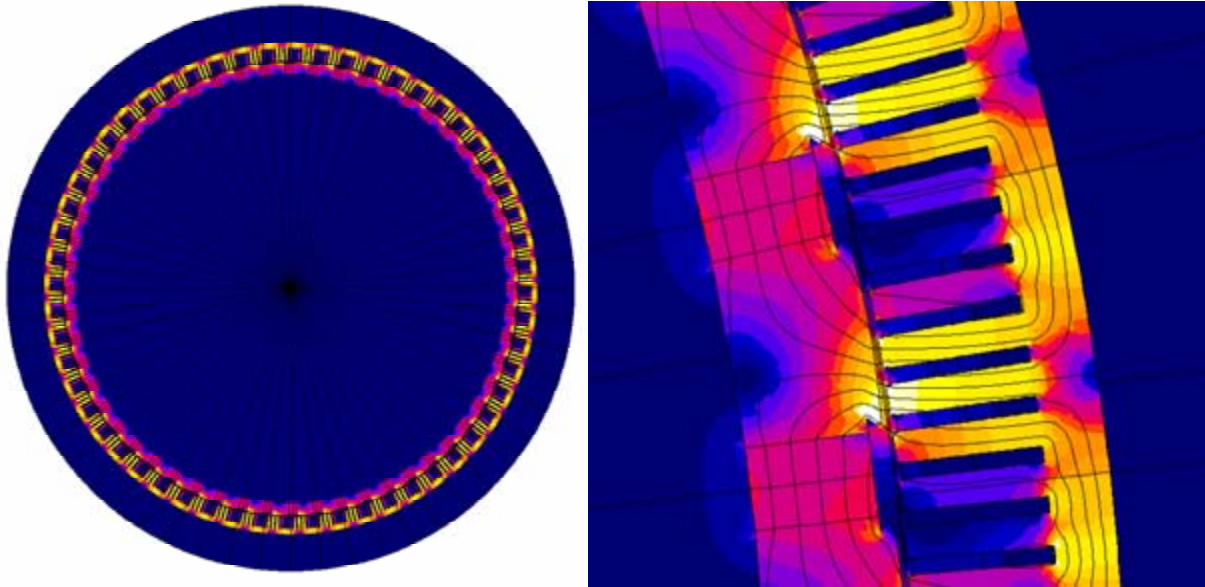


Figure 3-14. Electromagnetic finite element analysis was used to determine the operating characteristics of the generator.

The torque will not be constant, due to variations in geometry. The no-load torque indicates the fluctuations due to the slot geometry (See Figure 3-15). The unskewed cogging torque (P_k) is 2.4%. This is also known as the cogging torque. The harmonic content of the no-load torque is also shown in Figure 3-16. The results indicate that the 12th and 24th harmonic orders have the most energy, relative to the electrical frequency. Note that this calculation was based on an unskewed analysis. Because the actual generator has skew, the results will be smoother than the analysis. Results were used in comparison to the natural frequencies of the generator rotor and stator.

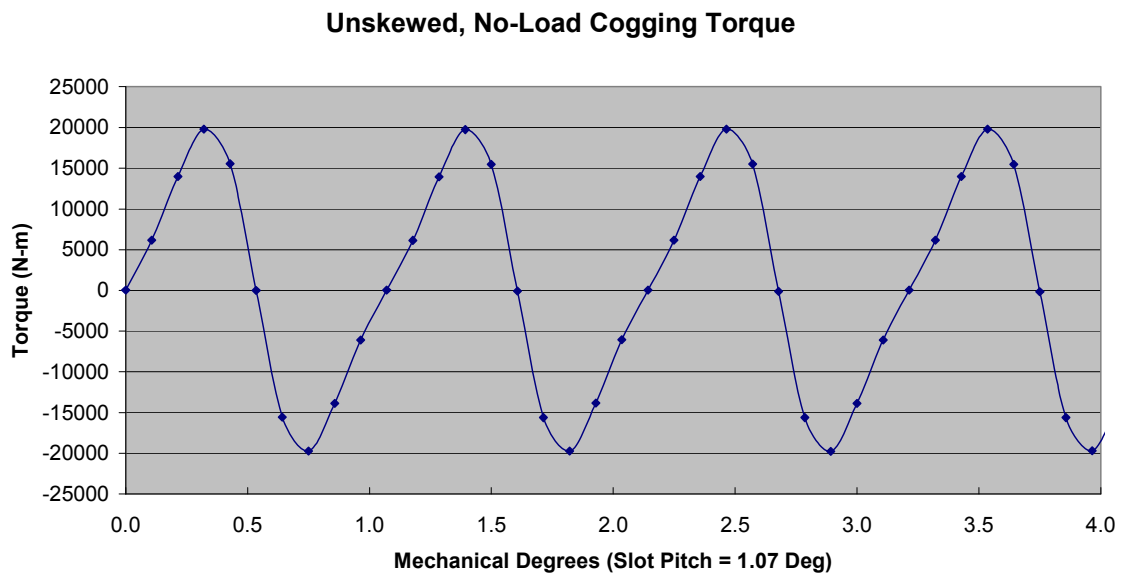


Figure 3-15. The no-load torque of the generator was calculated for input into dynamic analysis of generator components.

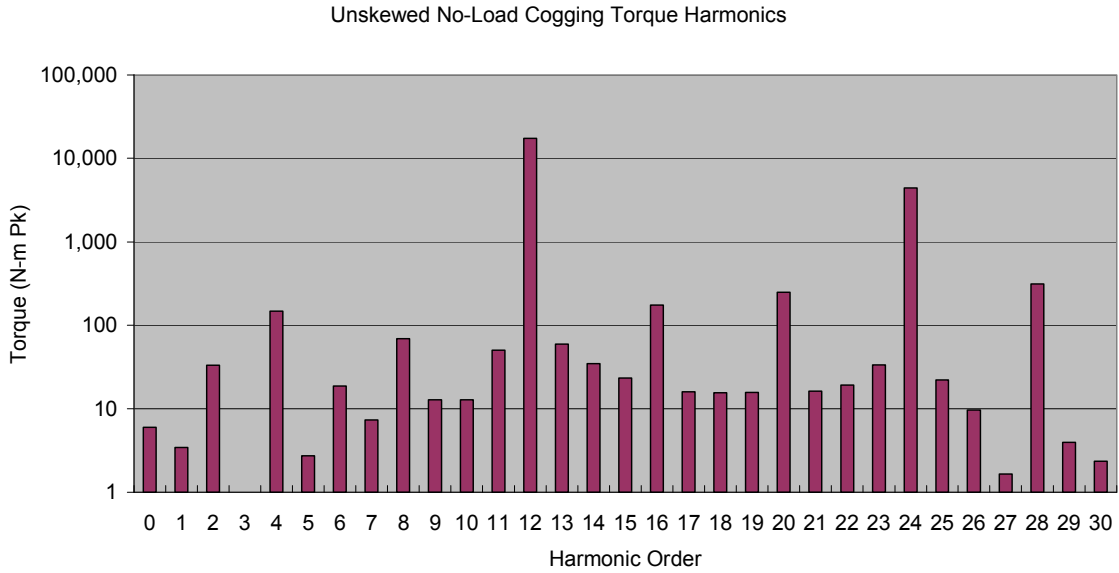


Figure 3-16. The harmonic content of the unskewed no-load cogging torque is at the 12th and 24th, relative to the electrical fundamental frequency.

Similar torque results were calculated for rated conditions, and are shown in Figures 3-17 and 3-18. The results indicate that the 6th, 12th and 24th harmonic orders have the most energy, relative to the electrical frequency. The unskewed ripple torque (Pk) is 5.4% of full-load torque.

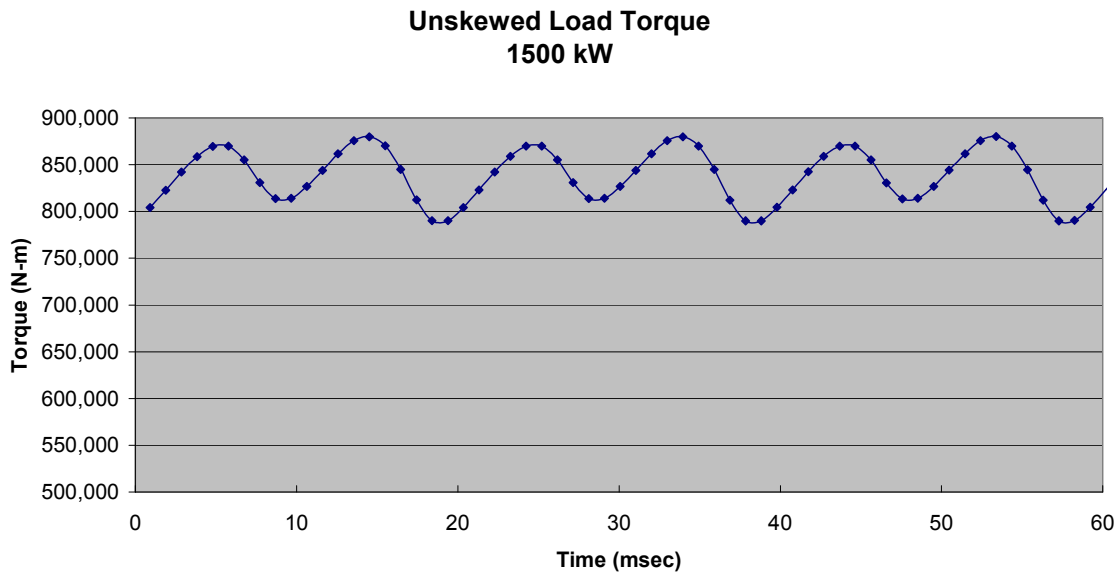


Figure 3-17. The unskewed torque at rated conditions and 0.9 power factor had a larger ripple than the no-load cogging torque.

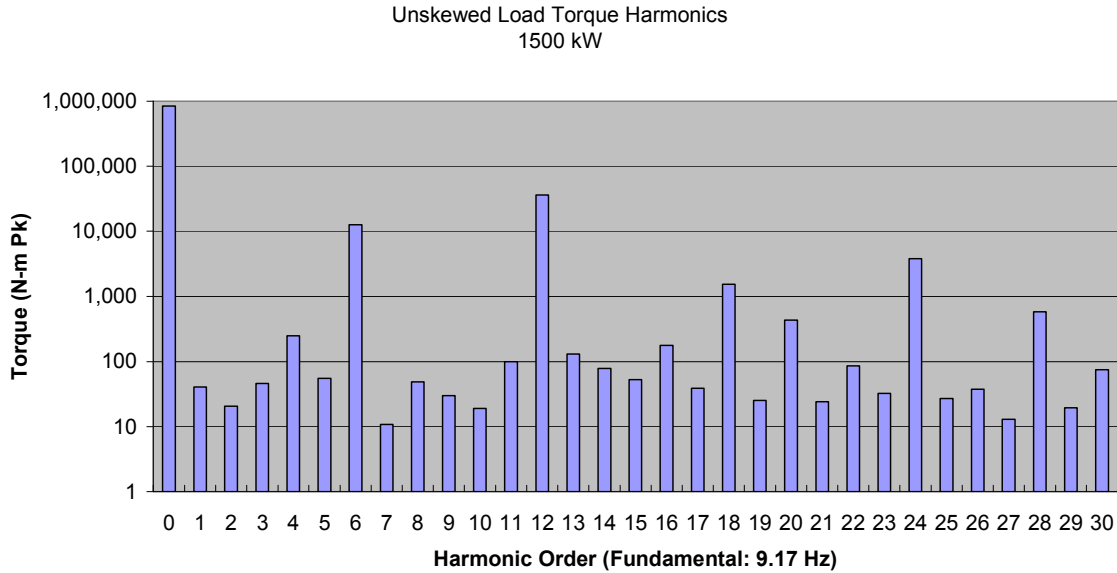


Figure 3-18. The torque harmonics at rated conditions and 0.9 power factor were similar to no-load harmonics.

The open circuit line-line voltage is shown in Figure 3-19. The waveform had some distortion caused by cogging and the shape of the rotor pole. The voltage harmonics are shown in Figure 3-20 and Table 3-11. Total harmonic distortion is 5.1%, which is close to the specification of 5%. It is expected that skewing will reduce the harmonic distortion slightly. The unskewed line-line voltage is 812.46 Vrms. Adjusted for the skew of the stator, the line-line voltage is 803.21 Vrms. Adjusted for 5/6 winding pitch, the line-line voltage is 775.90 Vrms.

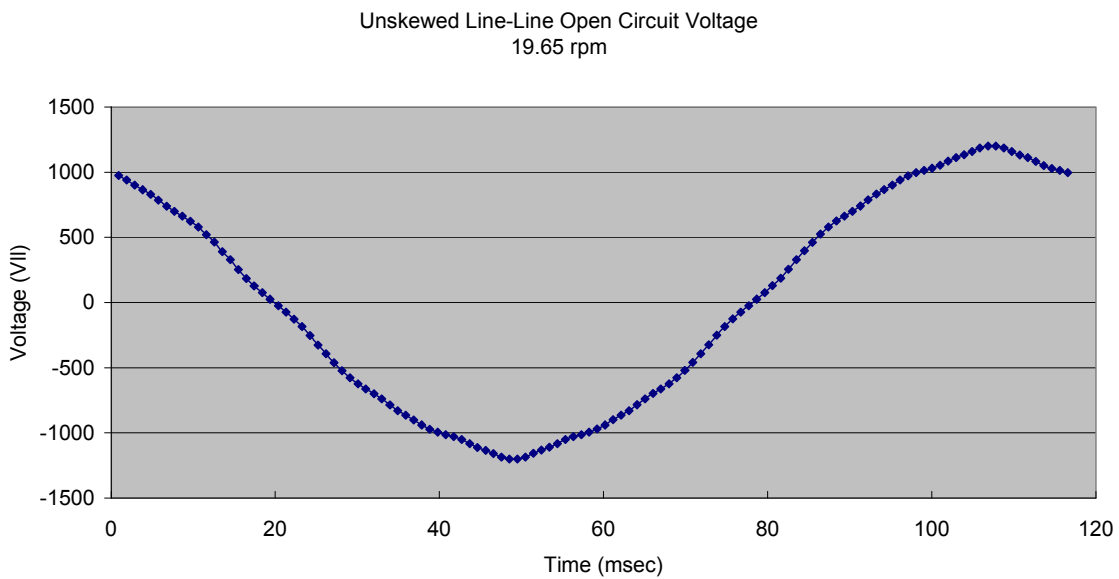


Figure 3-19. The unskewed open circuit voltage had some distortion due to the cogging effects.

Unskewed Line-Line Open Circuit Voltage
19.65 RPM

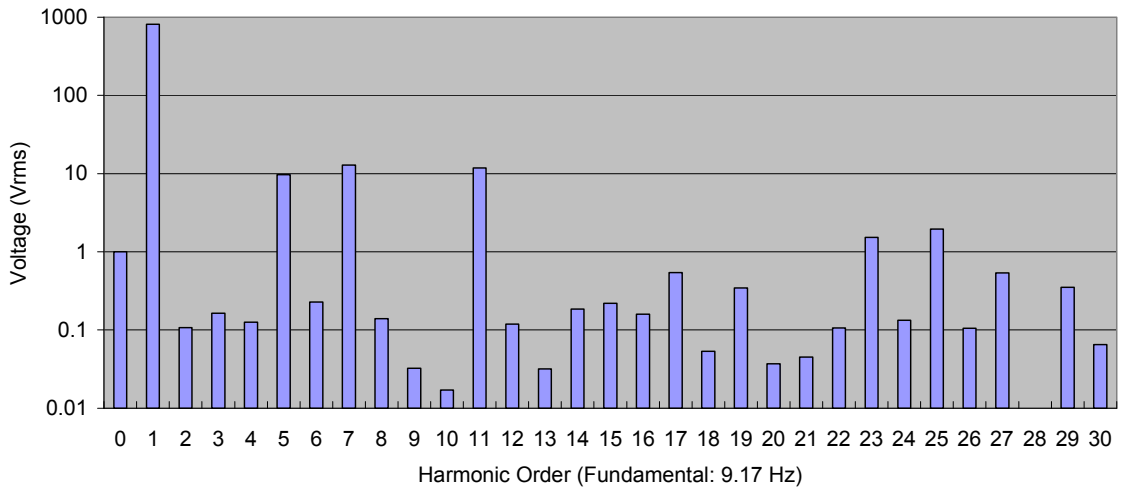


Figure 3-20. The harmonic content of the open-circuit voltage showed the most distortion at the 5th, 7th, and 11th harmonics.

Table 3-11. The Total Harmonic Distortion of the Unskewed Open-Circuit Voltage was 5.1%.

Harmonic Order	Magnitude (Vrms)	%
0	0.000	
1	812.213	
2	0.107	0.0%
3	0.163	0.0%
4	0.127	0.0%
5	9.704	1.2%
6	0.228	0.0%
7	12.811	1.6%
8	0.140	0.0%
9	0.032	0.0%
10	0.017	0.0%
11	11.821	1.5%
12	0.120	0.0%
13	0.032	0.0%
14	0.185	0.0%
15	0.220	0.0%
16	0.159	0.0%
17	0.544	0.1%
18	0.053	0.0%
19	0.345	0.0%
20	0.037	0.0%
21	0.045	0.0%
22	0.106	0.0%
23	1.523	0.2%
24	0.134	0.0%
25	1.948	0.2%
Total	41.665	5.1%

The line voltage for the generator at rated conditions is shown in Figure 3-21. The waveform is not exactly sinusoidal, but this is not expected to be a problem for the wind turbine application. The voltage value corresponding to this waveform, 835.8 Vrms, can be adjusted to account for skewing in the stator. The predicted skewed line voltage is 825.3 Vrms. Voltage waveform harmonics are shown in Figure 3-22. Current in the analysis is assumed to be sinusoidal with amplitude 1,320 A rms. The current is commanded by the power electronics, so this assumption is reasonable.

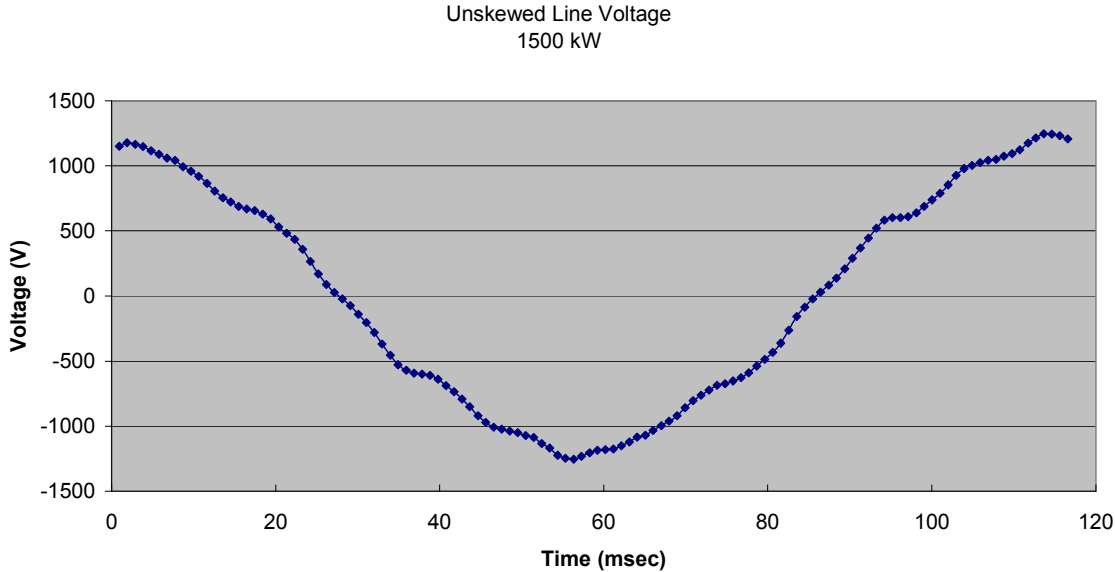


Figure 3-21. The predicted voltage magnitude at rated condition and 0.9 power factor exceeded the specification requirement.

**Unskewed Line Voltage Harmonics
1500 kW**

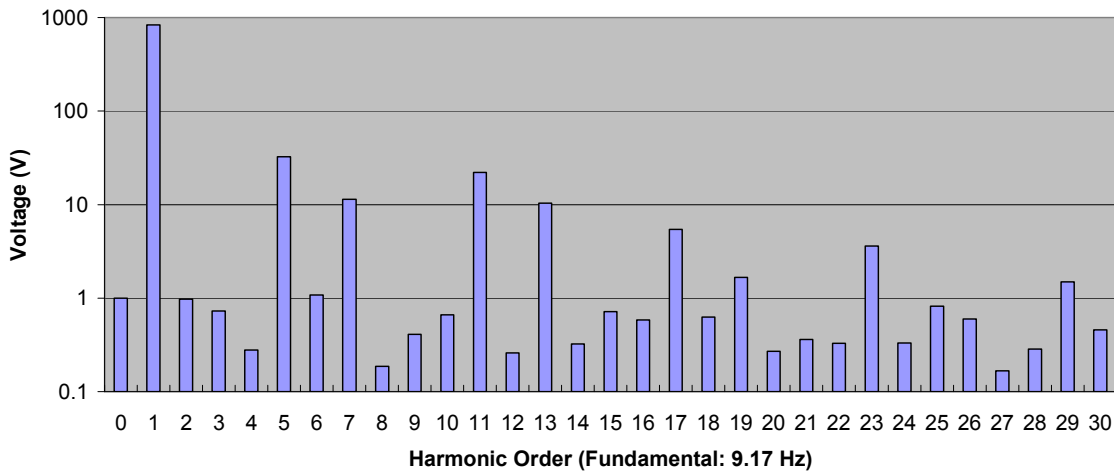


Figure 3-22. Total harmonic distortion of the line voltage at rated conditions was dominated by 5th, 7th, 11th, and 13th order harmonics.

Efficiency of the generator was calculated with a spreadsheet analysis. Results are shown in Table 3-12. The main sources of power loss are associated with the copper resistance losses, and the stator core resistance and magnetic losses. Smaller losses are associated with windage, and permanent magnet and rotor pole resistance and magnetic losses. For simplicity, these are lumped into the copper losses. The predicted efficiency of 93.4% is slightly less than the 93.8% specification, but was considered to be close enough. At the time of the analysis, no data was available for accurate prediction of the bearing friction losses.

Table 3-12. The Predicted Efficiency of the Generator was Very Close to the Target of 93.8%.

Parameter	Value
Output Power	1550 kW
Copper Loss	103.5 kW
Core Loss	5.75 kW
Total Loss	109.25 kW
Efficiency	93.4%

3.4.4 Power Electronics

The verification of the power electronics performance is based on the prediction of operating temperatures, efficiency, and power quality.

The semiconductors have sufficient life if operated at a junction temperature lower than 120°C. Figure 3-23 shows the predicted IGBT junction temperatures (for 40°C coolant) are significantly cooler than requirements. The filter inductors are designed to be within class H temperature rise

(180°C) and are each designed to carry rated current with a cooling of 1.0 m/s airflow. The predicted maximum temperature is 174°C. Actual airflow in the application is expected to be larger than 1.0 m/s.

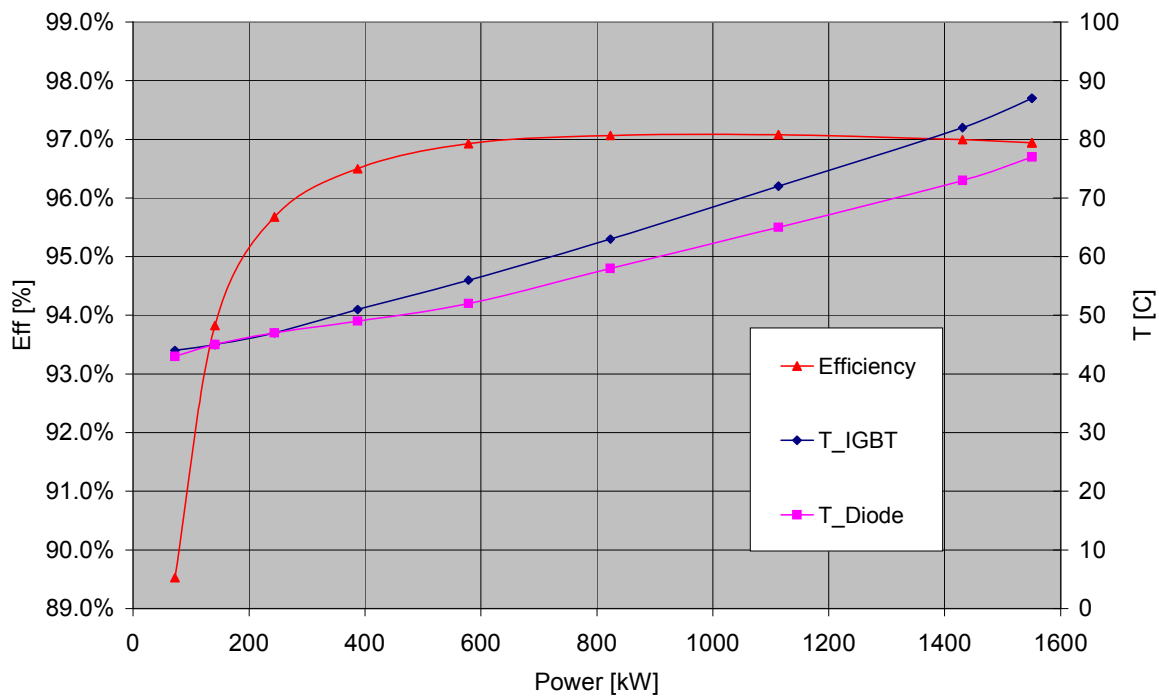


Figure 3-23. Thermal models were used to calculate the temperatures of critical components and the resulting efficiency of the power converter.

Efficiency is calculated using electric current data from the circuit model (described in Section 3.3.4) and operating temperature data from the thermal model. This data was incorporated into a spreadsheet. Figure 3-24 shows that the efficiency meets the target of 97% efficiency for the majority of the operating range. Efficiency is lower at low power levels because of fixed parasitic loads for control and start-up. Because the cooling system is good, the efficiency drops off only slightly at higher power levels.

Insulation life of the generator was predicted for both the conditions expected in a wind turbine application and for the dynamometer test conditions. However, the prediction of the insulation life in a wind turbine will depend on the length of cable between the generator and power electronics, and the filtering. The filter will be chosen to provide a life greater than 20 years for a given insulation system. For the unfiltered system to be used in the dynamometer, the voltage spike magnitude was $2.5 \text{ pu} \times 724 = 1,810 \text{ V}$. Given the insulation thickness, the voltage stress is 4,114 kV/mm. Based on the data in Figure 3.24, the expected life for dynamometer conditions is 2.3 years of continuous operation at rated conditions. However, extrapolation is required to obtain this result, making the results uncertain. Physical testing at this voltage stress level is highly recommended.

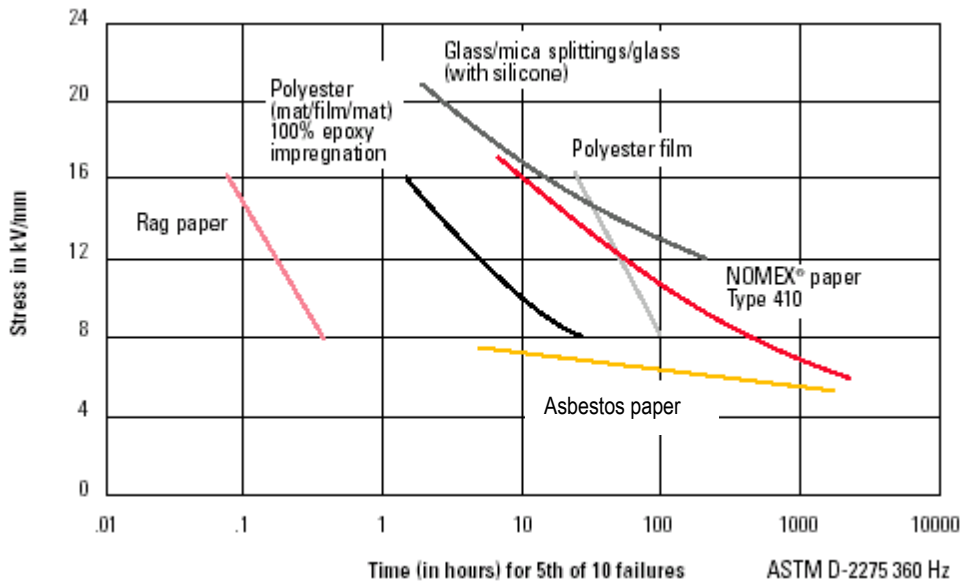


Figure 3-24. The power electronics produces a voltage stress in the generator of 4 kV/mm, but little data exists to accurately predict NOMEX insulation life for the generator.

The bolts used in the power electronics were analyzed using VDI 2230 or similar analysis. The critical loads are for transportation. Overhung masses were calculated, and loads were determined for upright transportation. Particular components evaluated were fasteners for the circuit breakers, IGBTs, contactors, and bus bars. The loads were based on FMCSA 49 CFR Parts 392 and 393 (2002). In all cases, the fasteners recommended by the electronics component manufacturers were extremely safe.

Table 3-13. Power Electronics Cooling System (Rated Conditions)

Parameter	Predicted Value	Allowable Value
Heat Rejected	45 kW	N/A
Inverter IGBT Hot Spot Temp	87 °C	120 °C
Rectifier Diode Hot Spot Temp	77 °C	120 °C
Inductor Hot Spot Temp	174 °C	180 °C (Class H)
Coolant	80% Water, 20% Propylene Glycol	N/A
Coolant Temp Inlet	40 °C	N/A
Coolant Temp Outlet	48 °C	N/A
Ambient Air Temp.	30 °C	N/A
Coolant Flow Rate	29 GPM (1.83 liters/s)	N/A
Calculated Pressure Drop – Electronics	34 psi (1.31 bar)	N/A

3.5 Cost Estimation

The cost of the generator increased compared with the Phase I study. This is shown in Figures 3-25 and 3-26. The main reason for the cost increase was the increased mass of the structure supporting the rotor and stator. Also, the production cost of the bearing increased from the preliminary estimation. It is recommended that further scaling studies involving generators be based on the following principles. If the generator air gap between rotor and stator is assumed to be constant for varying mean gap diameter, then the structure should be sized to maintain a constant deflection of the rotor and stator. Otherwise, one should assume the generator gap is proportional to the mean air gap diameter.

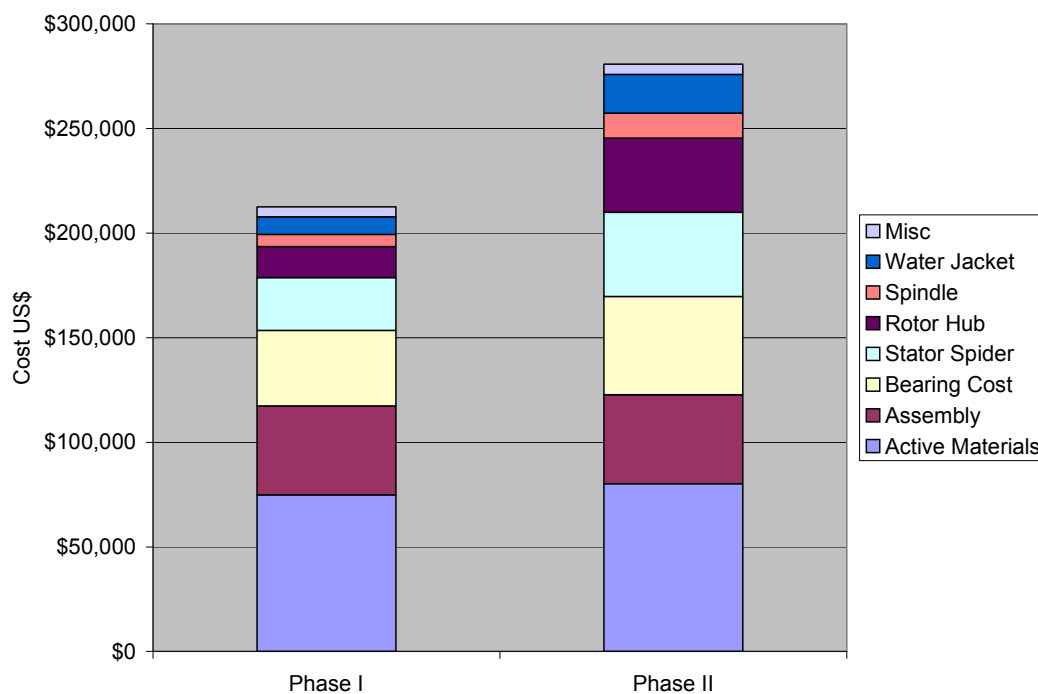


Figure 3-25. The generator cost breakdowns showed significant cost increases for the stator spider, rotor hub, spindle, and water jacket.

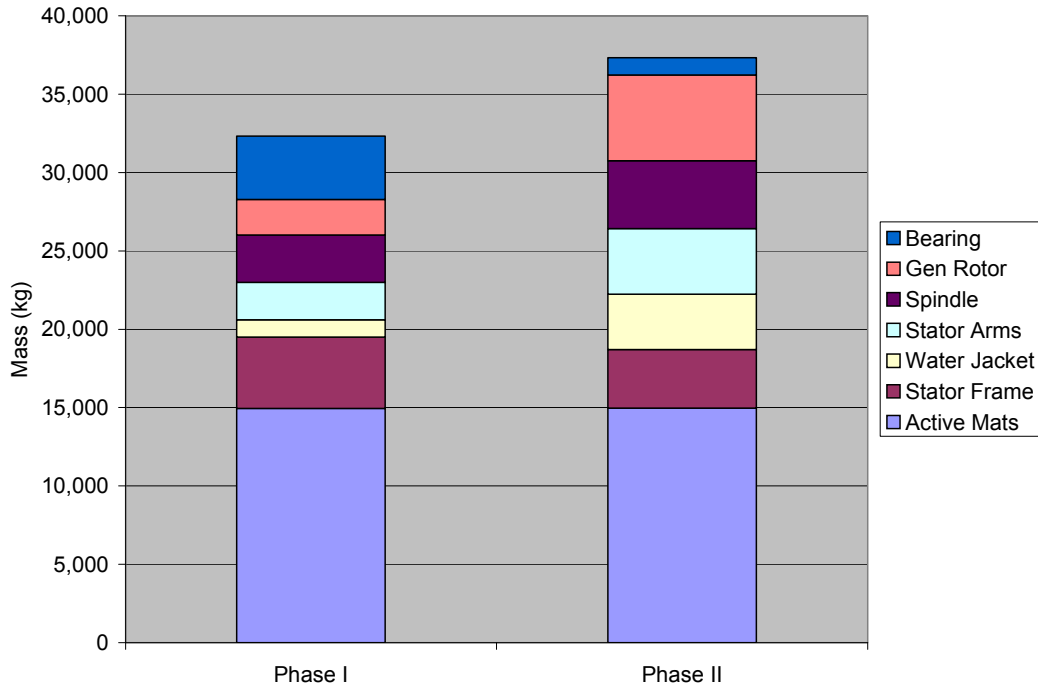


Figure 3-26. The generator mass breakdowns showed significant mass increases for the water jacket, stator arms, spindle, and generator rotor.

3.6 Dynamometer Assembly Design

Some modifications to the generator design were made for the dynamometer assembly. First, the front seal on the generator was eliminated. This seal is not necessary for an indoor environment. Also, the removal allows the passage of wires needed for test sensors. Second, the double-tapered roller bearing was replaced with a crossed roller bearing. This was done simply as a cost saving measure.

Several parts were designed to mate the generator with the existing dynamometer components. Instead of a blade rotor hub, a hub adapter component was connected to the main shaft of the dynamometer. Also, a test turret connects the downwind side of the generator to the test bedplate. These parts are shown in Figure 3-27. Lifting plates were designed to attach to the generator bosses to allow lifting and rotating the generator. A finite element analysis, such as that shown in Figure 3-28, was performed on these parts to determine a reserve for both static loading and fatigue loading. Resulting static and fatigue reserves are shown in Figure 3-29.

The main issue to resolve with the design for the dynamometer was the alignment and positioning of the generator. It is very important not to overload the coupling by misalignment. Oversized holes were used in the base of the test turret to allow some adjustment of position to be made. Special thick washers were made to bridge the large holes. A separate set of loads was used to size the hub adapter and turret. The weight of the overhanging shaft and the applied torque were considered. The fatigue loads were based on the operating torque of the generator applied for 1 year of continuous testing. Also, deflections of the shaft during loading were

calculated to ensure that the coupling would not be overloaded. The predicted deflection of the shaft is less than the allowable shaft misalignment.

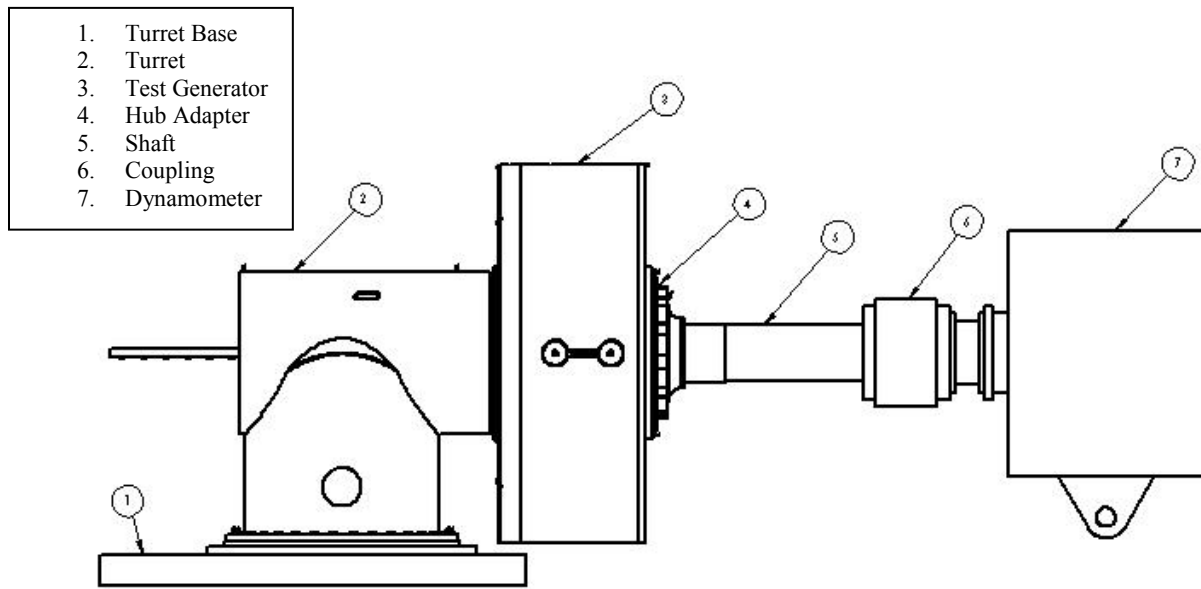


Figure 3-27. Dynamometer test layout.

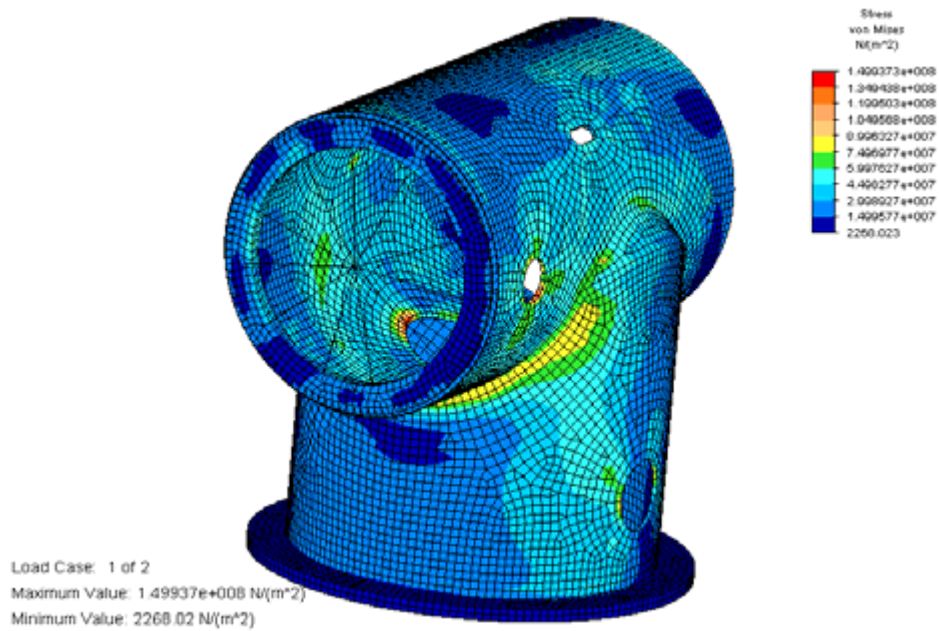


Figure 3-28. Finite element analysis was performed on the dynamometer test turret to ensure it would survive test loads.

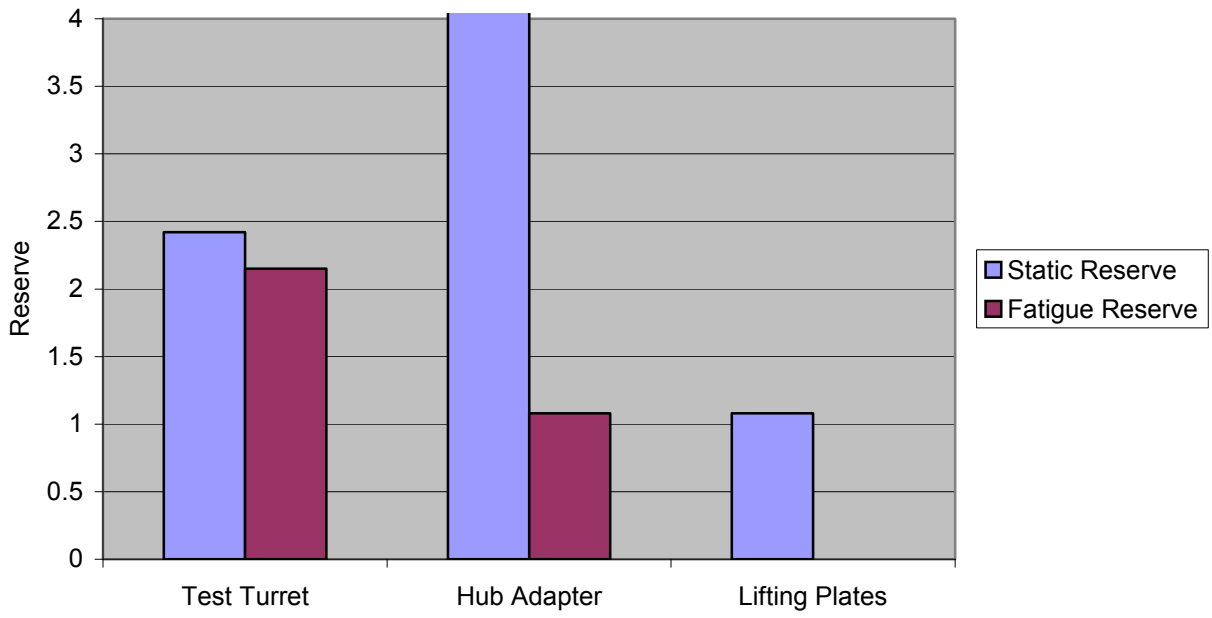


Figure 3-29. The static and fatigue reserves of components in the dynamometer assembly were acceptable (Reserve > 1.0).

3.7 Detailed Design Summary

A generator design method was developed to incorporate GDEB permanent magnet expertise into a direct-drive wind turbine.

Goals were set for cost and performance to ensure that we had a good idea of the project requirements.

Overall, this design was predicted to be acceptable in all areas of safety and performance.

The gap variation was predicted to be larger than the original specification; however, it was not expected that this variation would prevent critical overall power performance goals from being met.

Cost targets were not met, but could not be improved without building a prototype and learning more about the manufacturing process.

This design represented the state of the art in direct-drive generator design when fabrication was started. However, we knew that additional improvements could be made based on the experience of fabrication and test.

4 Fabrication

The large size of the 1.5-MW, direct-drive generator, combined with a very small gap between the rotor and stator made the manufacture of this machine especially challenging. Every effort was made to create a design that was easy to manufacture, but as with most new designs, fabrication issues were confronted and solved during the manufacturing and assembly process. Lessons were also learned during the fabrication of the power electronics, and during the dynamometer installation. However, because the power electronics and dynamometer installation were more conventional, these fabrication tasks involved fewer challenges.

The three major fabrication efforts were:

- Generator
- Power Electronics
- Dynamometer Installation.

In each of the following sections, the issues relating to components and quality control will be explained.

4.1 Generator

4.1.1 Generator Component Issues

The generator is composed of a number of mechanical, structural, and electromagnetic parts. The issues relating to these components follow.

The main bearing was originally planned to be a Timken double-tapered roller bearing. The problem was the tooling cost. Also, the first prototype would never be exposed to full dynamic loading conditions on the dynamometer. For these reasons the decision was made to purchase a less-expensive crossed roller bearing from Avon, saving more than \$100,000 in project costs. The Avon bearing had the same inner and outer diameter as the Timken bearing. The Avon bearing was a stock item that was sufficient for the dynamometer test.

The Neodymium-Iron-Boron magnets were purchased from Shin-Etsu. In production, we would probably have the magnets delivered from Japan unmagnetized. This makes shipping much less expensive. The problem was that we didn't have the tooling required to magnetize them in the factory. This would be a big expense for equipment that would be used only once. Thus we shipped the magnets magnetized. Special packaging had to be used to shunt the magnets and prevent them from being dangerous to the shipper. These magnets could be damaged or cause injury if two magnets get too close together during handling. The packaging was well designed to allow the magnets to be removed one at a time for insertion into the rotor. Another issue with the magnets was the epoxy coating. The coating prevents oxidation of the magnet material. On some magnets, the coating had some small drip marks. After inspection at the factory, some of the magnets were rejected because there was a concern that the dried epoxy drips might cause some physical interference during insertion.

The large weldments, such as the component shown in Figure 4-1, were subcontracted to Felguera, a large steel fabricator in Spain used by Cantarey. Felguera makes wind turbine towers and bedplates. This company has a good quality system for manufacturing large weldments, which are its specialty. All types of welds and stress-relieving methods used in the generator were tested prior to fabrication. This included welding of low-carbon steel to low-carbon steel, welding of low-carbon steel to stainless steel, welding thin and thick plate, and using manual and semi-automatic methods. Welds were inspected visually at the factory and were found to be very uniform. No ultrasonic inspection was specified for these welds for the prototype, but would be specified for weldments subject to long-term fatigue loading.

A few issues complicated weldment machining. First, the spindle weldment was found to be a little short axially and did not clean up to the machined dimension. This might have been caused by machining too much material off the back before attempting to machine the front. To solve the problem, weld material was added to the front of the spindle. Also, the back of the spider arms was supposed to be left as welded. This was machined to make the surface flat enough to provide a good mating surface for the back panels. Unfortunately, too much machining of this surface, which removed too much material, caused subsequent dimensions to be axially misaligned. This issue mainly affected the location of the brakes relative to the rotor. Eventually, this problem was resolved by shimming the brake bracket.



Figure 4-1. The weldment vendor, Felguera, has equipment such as this vertical lathe for machining large parts.

The assembly order was determined in cooperation with Cantarey and Felguera. There were two main assembly order choices:

Assembly Order Option #1

- Assemble stator core, water jacket, and outer frame (stator core and frame assembly) at Felguera.
- Ship stator core and frame assembly to Cantarey.
- Insert coils, connect coils, attach terminals, and impregnate.
- Ship wound stator assembly back to Felguera.
- Attach wound stator assembly to spindle and spider.
- Machine spindle to be concentric to stator inner diameter.
- Ship stator to Cantarey
- Assemble rotor into stator.

Assembly Order Option #2

- Assemble stator core, water jacket, and outer frame (stator core and frame assembly) at Felguera.
- Attach stator core and frame assembly to spindle and spider.
- Machine spindle to be concentric to stator inner diameter.
- Ship stator core and frame assembly and spindle and spider to Cantarey.
- Separate stator from spindle and spider.
- Insert coils, connect coils, attach terminals, and impregnate.
- Attach wound stator assembly to spindle and spider.
- Assemble rotor into stator.

It was decided to use Option #2 because it required less shipping back and forth. Also, in Option #1 there is a machining operation on the spindle after the stator is wound and impregnated. The machining operation can leave small metal particles in the windings, which could damage the generator.

The most serious issue with the welded parts was maintaining the roundness of the stator outer frame. This ring was very thin relative to its large diameter. Thus it was flexible, and after machining to a dimension within specified tolerances, the part distorted. The distortion was aligned with the lifting bosses, as shown in Figure 4-2. The residual stresses due to the large welds in this area are a likely source for the distortion. It is unlikely that this residual stress can be eliminated. The part was properly stress relieved after welding. To resolve the problem, a special spider was attached to the stator on the downwind side, and a stiffening ring was added on the upwind side, as shown in Figure 4-3. This was not sufficient to keep the stator within the original tolerances, but it was good enough to provide a working prototype. The special spider and ring were kept in place during the winding and impregnation process. After impregnation, the wound stator assembly, which includes the stator, water jacket, and outer frame, was stiff enough to stay round without the special spider. The special spider was removed and the regular spider was put in its place.

Location	Diameter (mm)	Variation From Nominal (mm)
A	3,486.85	+0.70
B	3,485.18	-0.97
C	3,484.15	-2.0
D	3,485.90	-0.25

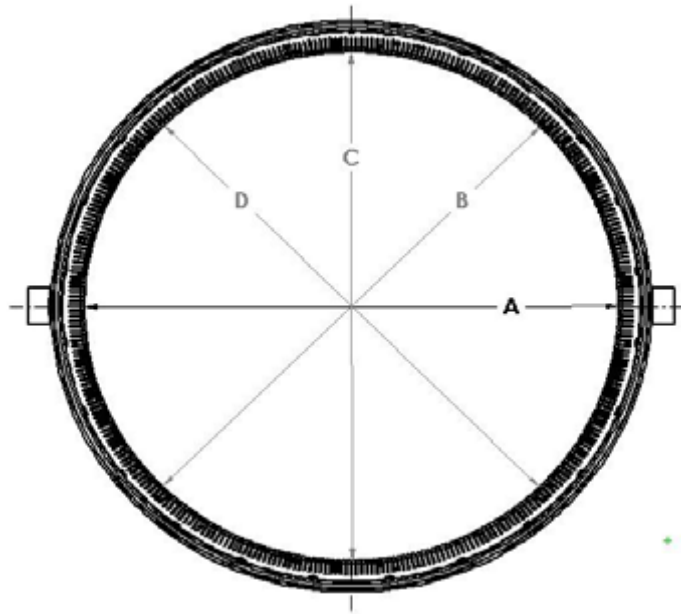


Figure 4-2. Distortion of the outer frame was aligned with the lifting bosses. These values are for the stator inner diameter after assembly into the water jacket and outer frame.

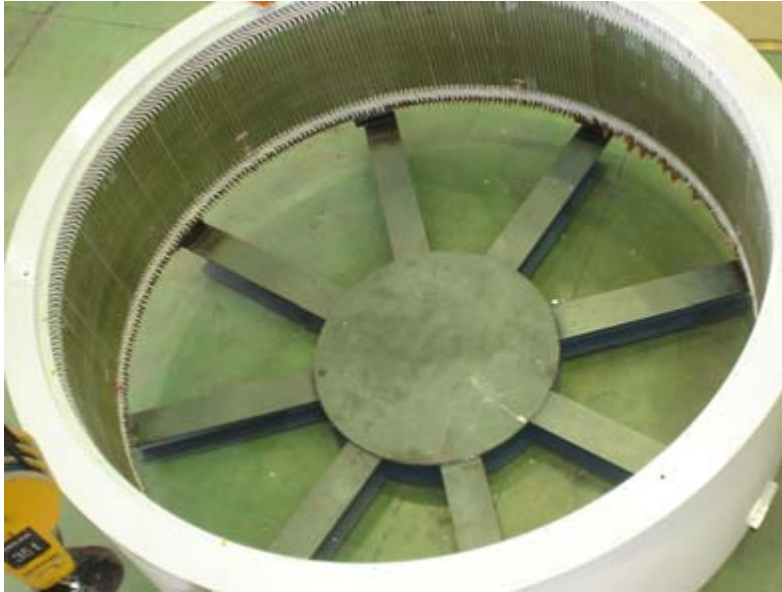


Figure 4-3. A special spider and front ring was attached to the stator to keep it round during winding and impregnation.

Once the regular spider was attached, inspection showed that the spindle was not concentric to the stator. The dowel pins that located the spider to the stator were removed, and the stator was moved to make it concentric. New dowel pin holes were drilled and new dowels inserted to locate the stator in the correct position. The stator outer frame was welded to the spider in several locations to be sure that no further movement or misalignment occurred.

The stator laminate manufacturing required the use of an assembly tool. This tool had removable pillars establishing the inside diameter of the stator and the slot skew of the stator. Band clamps around the outside diameter of the laminate pushed the laminations to the center. After completion of the lamination stacking process, the outside diameter was welded. The outside diameter of the tool was selected to be 0.5 mm less than the nominal inner diameter of the stator. This was to account for expected springback from the tool. In fact, the stator inner diameter was very close to the tool outer diameter after fabrication. Next time, the tool diameter will be selected to be the nominal diameter.

No major problems were encountered when winding the stator. The wire is rectangular. It is wound around a tool and formed to the shape required for the generator. This tool was specially developed for this project. The stator is unusual because it uses a single turn coil. Cantarey developed a frog-leg coil system, shown in Figure 4-4, and modified the stator connection diagram to use it. The connections between the coils, which were also unusual due to the single turn, caused some delays. The main problem was that they took more time to connect than a normal connection. The durability of the connection is expected to be outstanding. Cantarey noted that some extra room between the coils and the housing ends would make the winding process go faster.

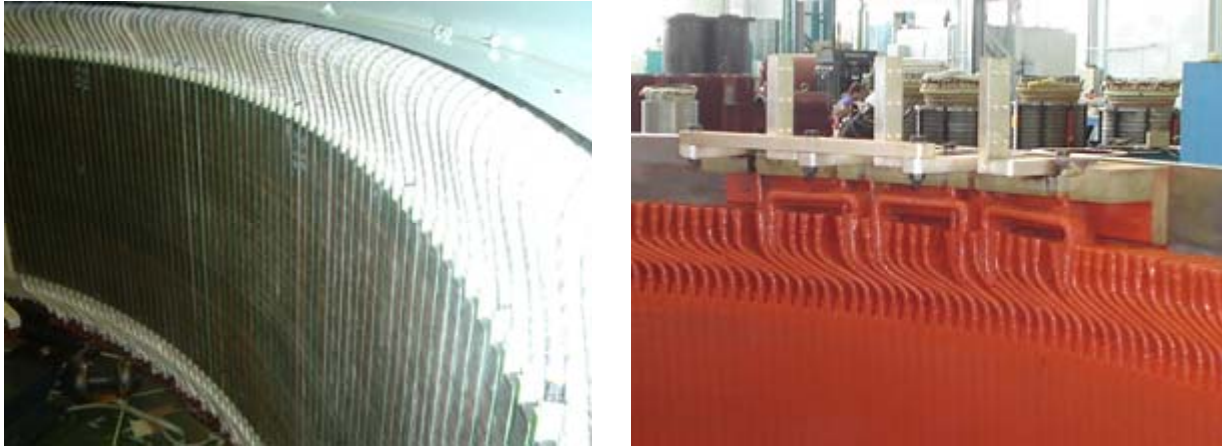


Figure 4-4. The stator winding process was more time consuming than expected.

The impregnation and painting of the stator was changed during the manufacturing process. The original design called only for vacuum impregnation of the stator after winding. There was no vacuum impregnation tank in Spain, however, that was large enough for the 1.5-MW stator. Also, the stator was too large for the manufacturer's electric oven. Because of the flammability of the varnish, a standard oven couldn't be used. Thus a room-temperature, air-drying varnish was used by Cantarey. This varnish was also used by Cantarey on similar large wind turbine generators for another customer. A special tank was fabricated to immerse the stator in the varnish with the axis vertical. Also, the stator inner diameter was painted with an anti-flash paint that has especially good resistance to chemicals. This is a good option because the stator may be contaminated with brake fluid or bearing grease.

In retrospect, this impregnation system was probably inadequate and may have harmed the performance of the generator in three ways. First, the stator stiffness was reduced because of incomplete drying of the varnish. Second, the generator thermal performance was reduced. Third, the generator had two shorts, and it is likely that the possibility of shorts would be reduced with a better varnish system using vacuum pressure impregnation.

The assembly of the rotor was accomplished in three steps. First, the laminated rotor poles were attached to the outside diameter of the rotor with fasteners. This was done with the rotor axis vertical. Second, the rotor wedges were inserted between the poles. This created a space in which to place the magnets. Third, the rotor was rotated to axis horizontal, and fixtured so that it could be rotated about its axis. A tube was attached to the rotor to guide the magnets into position, as shown in Figure 4-5. This process worked very well. No problems were encountered; however, the outside diameter was a little out of tolerance. This was mainly due to the variation in the rotor poles. Another problem was the difficulty measuring the assembled diameter. No equipment to do this measurement accurately was available at the manufacturer's site. The only reliable measurement was obtained by measuring the gap.



Figure 4-5. The magnets were inserted into the rotor using a proprietary method developed by General Dynamics.

Assembly of the rotor into the stator was difficult for two main reasons. First, the assembly tool was too flexible. It did not have enough stiffness to adequately guide the rotor, and prevent it from hitting the stator during the insertion process. Also, there was slightly too much clearance between the tool and the inner diameter of the rotor. A second problem was the front ring of the stator. This was added to the design to solve the stator stiffness problem, but it is a large magnetic component that has an inner diameter dimension similar to the stator. The insertion tool should have been made several inches longer to compensate for this fact. Also, the ring could have been made with an inner diameter slightly larger than the stator inner diameter, to allow easy passage, but the actual dimension was actually slightly smaller than the stator inner diameter, making it hard to pass. Also, the flexibility of the insertion tool caused the machining tool to chatter and thus the surface was rougher than specified. These problems were addressed by using 2-mm-thick fiberglass strips to protect the rotor from rubbing against the stator during insertion. Also, the rotor was covered in a thin mylar sheet. The rotor was inserted in a long and difficult process taking about 10 hours.

Insertion of the bearing on the spindle was very easy. The dynamometer test bearing, a crossed roller bearing, is designed for a slight clearance fit at the inner and outer diameter. The bearing was heated in a furnace, and lifted with a crane to the spindle. The bearing was dropped on to the spindle and fixed with the bearing retainer.

After insertion the gap between the rotor and stator was checked. Table 4-1 shows a comparison of the original specification and the actual results.

Table 4-1. The As-Manufactured Gap was Smaller and had More Variation than Originally Specified, but was Considered Acceptable for the First Article.

Tangential Location	Measured Gap Upwind (mm)	Measured Gap Downwind (mm)
0°	3.4	4.1
45°	2.8 (Min)	2.9
90°	3.1	3.0
135°	3.6	4.5 (Max)
180°	3.2	4.2
225°	3.1	4.0
270°	3.0	3.5
315°	3.6	4.2

Gap Specification (mm)	Measured Gap (mm)
4.44 +/- .45 (4.0 to 4.9)	3.65 +/- .85 (2.8 to 4.5)

4.1.2 Generator Quality Control

First article inspection data were required for all fabricated parts. This was absolutely necessary for the generator components because of the tight gap tolerance between the rotor and the stator. This data was used to determine that everything would fit together correctly before final assembly. In addition, mechanical inspection of the final assembly was done to determine the overall length, brake function, dimensions of the gap, and the cogging torque.

A factory acceptance test document was written to evaluate the electric performance of the generator before shipping. This was somewhat complicated by the fact that a dynamometer was not available at the plant for such a large generator. A factory dynamometer test would have provided a much better ability to evaluate performance prior to shipping. Also, if a problem had been found, the personnel, tools and equipment for fixing the problem would have been readily available. The tests that were performed at the factory are as follows:

- Dielectric
- Insulation Resistance
- Stator Resistance
- Standstill Frequency Response.

The generator during the factory acceptance test is shown in Figure 4-6. Most of these tests were repeated as part of the dynamometer test procedure, to ensure that the generator was not damaged during shipping. The results are included in Section 5. Note that the plastic, vacuum-sealed covering of the generator leaked during shipment, and water entered the interior of the generator. The generator was allowed to dry for a few weeks before testing.

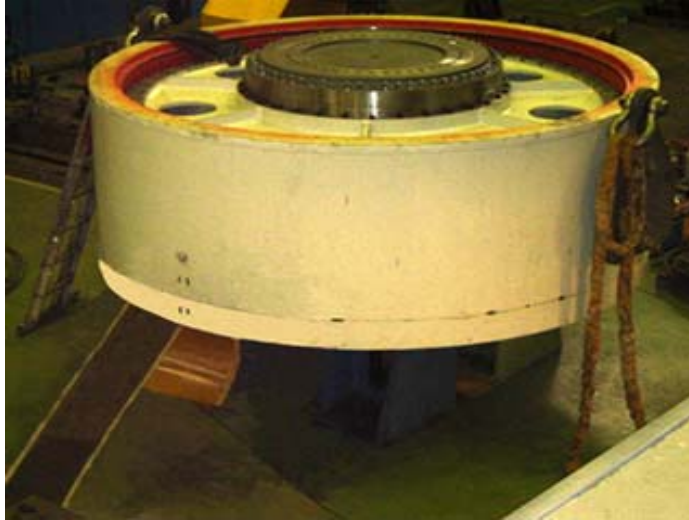


Figure 4-6. A final acceptance test was performed at the generator manufacturing facility, but the generator was too large for the facility's dynamometer.

4.2 Power Electronics

4.2.1 Power Electronics Component Issues

The fabrication of the power converter was commenced at the completion of the electromagnetic and thermal design of the converter. The long-lead items for the power converter are the IGBT assemblies and alternating current (AC) filter components. The power electronics lead time is much shorter, however, than the generator lead time. Thus the power electronics assembly was completed several months before the generator. The IGBTs were produced by SemiKron (See Figure 4-7). The AC filter components were produced by NWL and Electronic Concepts. The DSP control board was an internal NPS product. The PR1 DSP is a general-purpose power converter controller based on the fixed point TI2407 DSP. The inverter and rectifier units have independent PR1 controllers.

To assemble the power electronics, first the major components were installed on the back panels, doors, and floors. Then the back panels were installed into the cabinets. Then the plumbing, wires, and connections were completed.

During initial testing, some of the gate drives (part of the IGBT assemblies) failed. These were replaced, and spares were purchased. Some of the capacitors in the power converter were not adequate, based on additional information obtained from the component manufacturer. So these were replaced with adequately rated components. To prepare the converter for shipment, a stiff steel skid was fabricated. The skid had fork pockets for easy loading and unloading on the truck. Also, capacitor brackets that were not stiff enough were replaced. These modifications were deemed adequate for transportation of the power converter to NREL.

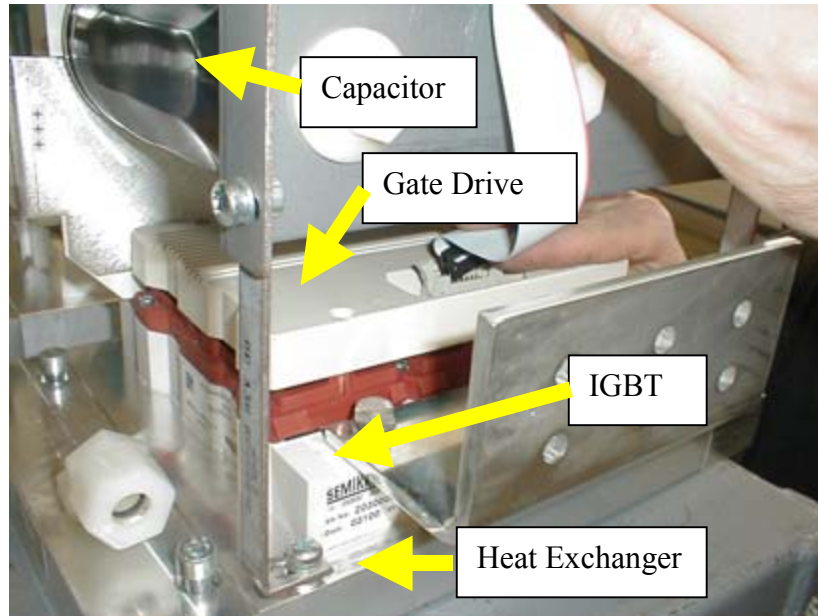


Figure 4-7. The IGBT's were attached to a water-cooled heat exchanger.

To reduce EMI, the back panels of the power modules were insulated from the cabinet by attachment with fiberglass studs. These studs are not suitable for transportation loads. Thus they had to be removed for shipment, and re-inserted after installation.

4.2.2 Power Electronics Quality Control

After the fabrication of the power electronics, a complete wiring check was performed to ensure that all connections were made according to design. The components have been high pot tested to 3,400 V dc to verify that there were no unintentional shorts to ground or defects during fabrication. An ohmmeter test was done prior to the high pot test to ascertain that there was good confidence in passing the high pot test. The DSP and PLC controllers were powered up to verify that they would operate properly. All the power converter alarms were tested to ensure that they work. The unit was tested with a 100-kW generator on the Northern dynamometer in Vermont, and the system control algorithm was verified to operate according to the design objectives. Also, the unit was connected to a 690-V grid connection, to ensure that all grid-powered components would work properly.

Electromagnetic interference was tested by operating a computer near the power electronics. The computer worked normally, indicating that EMI leakage from the cabinets was small.

The power availability at Northern's facility is lower than the total power rating of the power electronics. Hence a complete thermal test could not be completed. However, each 500-kW section of the power electronics has been tested at its full current rating for adequate time duration to verify that the temperature rise is consistent with the design. To perform the test, we connected the generator-side (rectifier) to the grid, and connected the grid-side (inverter) to a resistive load. Tests indicate that we expect the power converter to function properly during the

NREL dynamometer tests. Test results are shown in Figure 4-8. Temperatures of all critical components were cooler than specifications.

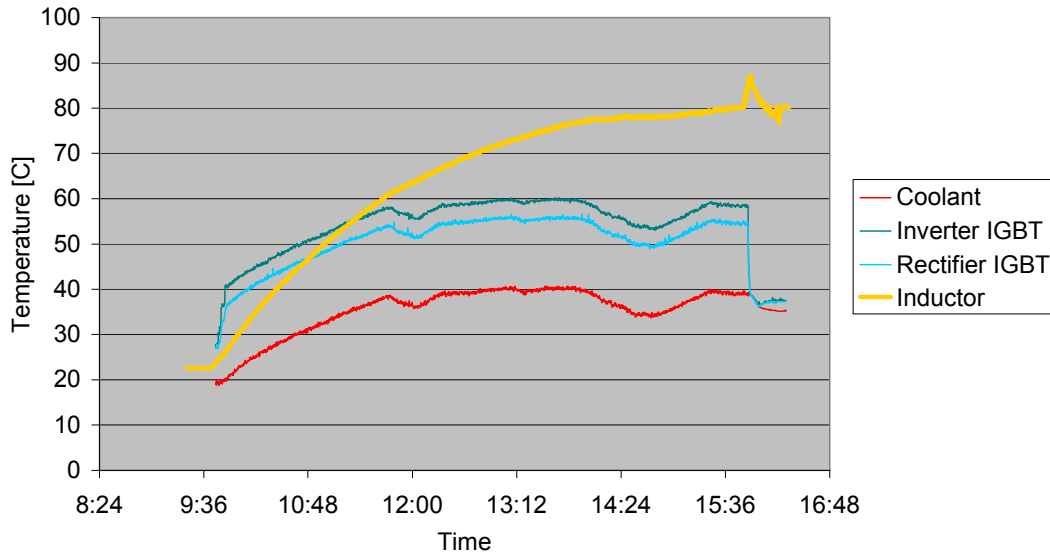


Figure 4-8. Each 500-kW section of the power electronics was tested at full current and all temperatures were within specifications.

4.3 Dynamometer Installation

4.3.1 Dynamometer Installation Issues

The first issue with the dynamometer installation was shipping to the NWTC. The generator is large and heavy. To get from Spain, it first had to be lifted on to a large flatrack. A flatrack is a large steel structure similar to the bed of a flatbed truck. The generator stayed on the flatrack from the factory to the port in Houston to avoid the risk of overloading the stator outer frame. The frame is strong enough to carry the lifting load when a spreader bar is used, but without supervision, the dock personnel might try to lift it with the straps at an angle. This could bend the stator toward the rotor and cause poor performance. Lifting with a flatrack avoids this risk. The generator was loaded on a roll-on, roll-off ship. This type of ship is normally used for transport of vehicles. After unloading in Houston, the generator was put on a lowboy truck and driven to the NWTC.

At the NWTC, the generator was loaded on a cart and rolled into the facility. The force to roll the generator up the driveway slope was provided by the gantry crane, which was connected to the cart via pulleys, as shown in Figure 4-9.



Figure 4-9. The generator was rolled into the dynamometer facility on a cart, which was pulled by cables connected to the gantry crane.

The rotation of the generator from axis vertical to axis horizontal was a difficult lift, and it required a significant planning effort. A three-point lift was performed, using two cranes, to achieve the highest level of safety possible. The gantry crane lifted the generator from the equalizer plates, using a spreader bar provided by the rigging vendor. The third point of lift was from the point on the generator that would be at 6:00 (bottom) in the installed position. However, there was nothing to connect the crane to at that point, so a special shackle plate was attached to the stationary generator flange, and the strap attached to the shackle plate was routed to the third lift point. To prevent the strap from slipping, a section of C-channel was welded on to the generator at the critical point. The critical lift setup is shown in Figure 4.10.



Figure 4-10. The generator was rotated into position using a three-point lift, to be as safe as possible.

Assembly of the generator on the dynamometer was straightforward. The alignment of the generator to the dynamometer shaft was difficult and time consuming. The position of the generator along the shaft axis and in the horizontal plane was adjusted by loosening the bolts between the turret and base plate, or by loosening the bolts between the base plate and the T-slots in the floor. Hydraulic jacks were used to move the structure, and the crane was used to prevent the assembly from tipping when the bolts were loosened. Once the generator and dynamometer were in the correct location, the coupling was installed as shown in Figure 4-11.



Figure 4-11. The coupling was installed after the generator and dynamometer shafts were aligned.

Electrical cable assembly was done mainly using the existing cable tray. For proper system operation, the cables had to be 20 m long, which is longer than the run of cable tray from the generator to the converter. Droop loops of cable were hung from the tray to take up the slack, as shown in Figure 4-12.



Figure 4-12. Droop loops were hung from the cable tray to take up the slack.

The generator cooling system was mostly implemented with steel pipe, which was routed along the floor to a nearby pump, open-air reservoir, and radiator. The converter required a much longer run to the radiator and pump, and utilized flexible tubing. The flexible tubing worked well for routing through the existing trench network at NWTC.

4.3.2 *Dynamometer Quality Control*

To ensure that the dynamometer testing would be safe and successful, a test plan document was written. This test plan covered the following subjects:

- Test objectives
- Test milestones
- Description of the test article
- Instrumentation plan
- Test conditions
- Procedures
 - Safe operating procedures
 - Operating procedures
 - Installation, maintenance, and decommissioning procedures.
- Interface documents
- Personnel plan.

This plan was reviewed by the NWTC, and personnel involved in the testing were trained with the plan. Revisions were made as needed during the test process, and were reviewed by Northern and NWTC personnel.

4.4 Conclusions and Recommendations

Many things were learned in the manufacturing process of the generator. We have resolved issues relating to the manufacturing and have produced a good prototype. We have learned which parts of the manufacturing process are straightforward, and which are not. We have learned which dimensions are easy to get within tolerance, and which need to be loosened. We have proven tooling concepts for stator lamination, stator stiffening, coil winding, impregnation, magnet insertion, and rotor insertion.

The key recommendations for the next prototype are:

- Stiffening the stator
 - Add a stiffening ring to the front of the generator
 - Press fit the water jacket to the outer frame for more stiffness
 - Impregnate the stator lamination before inserting coils.
- Increase the stator lamination tool OD to stator nominal inner diameter (ID).
- Decrease the rotor cost
 - Eliminate stainless steel
 - Make the rotor ring thinner.
- Increase the rotor insertion tool stiffness and length
- Increase the space for end turns and connections
- VPI the stator after coil insertion.

The power electronics manufacturing process was relatively smooth. The main recommendations for the future are:

- A greater integration of mechanical and electrical design is needed to ensure that the parts will have mechanical structural integrity, and that components will fit together reliably.
- Fabrication in a facility with a dynamometer, test generator, and full-power grid connection will increase the reliability of future designs.
- Ordering of spare parts will prevent delays caused by occasional defective parts.

The dynamometer assembly was very smooth. The safety procedures were adequate and the personnel were trained well for their duties.

5 Dynamometer Testing

The dynamometer test was done to verify that the generator met the design goals. These goals mainly address the power performance and efficiency of the generator. The test was performed at the National Wind Technology Center (NWTC). A special thanks goes to Hal Link, Vahan Gevorgian, Ed Overly, and other personnel at the NWTC who were vital to the completion of the test program.

5.1 Test objectives

The test objectives are divided into three sections: structural, cooling, and electrical.. This section presents the test results only, without any comparisons to predicted values. Comparisons to the predicted values will be summarized in Section 6. Also, not all of the objectives were accomplished because of damage in the power converter from an accidental overspeed. The completion status of each objective is provided below. The assessment of the performance of the generator, based on the accomplished objectives, will also be addressed in Section 6.

5.1.1 Structural Objectives

- Measure spindle deflection and the gap between rotor and stator when the generator is stationary and the main shaft is unweighted by the hydraulic jack. Gap will be measured every 45° around the circumference and at the front and back of the machine.
- Measure spindle deflection and the gap between rotor and stator when the hydraulic jack force is zero. Measure strain in the spindle relative to the unweighted condition.
- Measure strain in the spider arms when torque is applied.
- Measure natural frequencies of stator and rotor and vibration of rotor and stator as speed is slowly increased throughout normal range.
- Measure main bearing temperature during rated speed and power operation.

5.1.2 Cooling Objectives

- Measure flow rate of cooling system.
- Check temperatures during rated speed operation to ensure proper cooling system function.

5.1.3 Electrical Objectives

- Tests without the generator connected to the power converter
 - Measure back electromagnetic force (EMF).
 - Measure X_d and X_q .
 - Perform a short circuit test.
 - Measure Line to neutral impedance with an impedance analyzer for different positions of the rotor.
 - Measure zero sequence impedance using the impedance analyzer. – Not done.
 - Measure cogging torque when spinning the machine. This is measured by looking at the power ripple on the machine that is used to spin the generator. Measurements for strain gauges will also be used if available with sufficient resolution.

- Study bearing impedance at different turbine speeds. Also, measure any induced rotor voltages.
- Perform tests with the generator connected to the power converter.
 - Perform initial tests with just the power converter switching with the generator at no load.
 - Measure peak voltages and currents, the rate of change of voltage, (dv/dt) and the rate of change of current (di/dt) on the generator.
 - Measure effectiveness of the generator terminations. Measure dv/dt and di/dt with and without the generator terminations. (This test will only be performed if there is sufficient common mode damping on the power converter without terminations.)
 - Measure bearing currents induced by the power converter with generator at zero speed.
 - Perform tests with the generator along the turbine speed torque curve. – Done at 19 rpm.
 - Measure generator torque-speed characteristics along the turbine operating curve. Generator voltage and current waveforms along the operating curve. Root mean squared (rms) voltages and currents and harmonics will be measured.
 - Determine generator electrical parameters and compare with prediction.
 - Determine torque ripple of the generator.
 - Measure bearing voltage and current in the generator. Study the effectiveness of shorting the bearing.
 - Measure generator efficiency – Not done at rated temperature.
 - Estimate the loss in the rotor and stator, including iron and copper losses.
 - Measure the temperature rise in stator windings, end windings, stator iron, and in the rotor.
 - Measure generator transient thermal time constants.

5.2 Test Milestones

The schedule of actual tasks completed is shown in Figure 5-1. The tests were first performed on individual components such as the generator and power electronics to ensure that each was working correctly before they were connected together. In this way, risk of damage due to a problem was minimized. During the component testing, two shorts occurred in the generator. These caused delays, but the shorts were repaired. The main deviation from the original test plan was the elimination of full-power performance testing. This was cancelled after a short circuit occurred in the power converter. The power converter was damaged and its replacement would have taken several weeks and cost \$80,000. NREL decided to terminate full-power testing after the occurrence of the converter short. Also, some extra tests were performed on the generator, including a thermal imaging test, and a frequency response test. These tests enhanced our understanding of the generator, and did not require a working power converter.

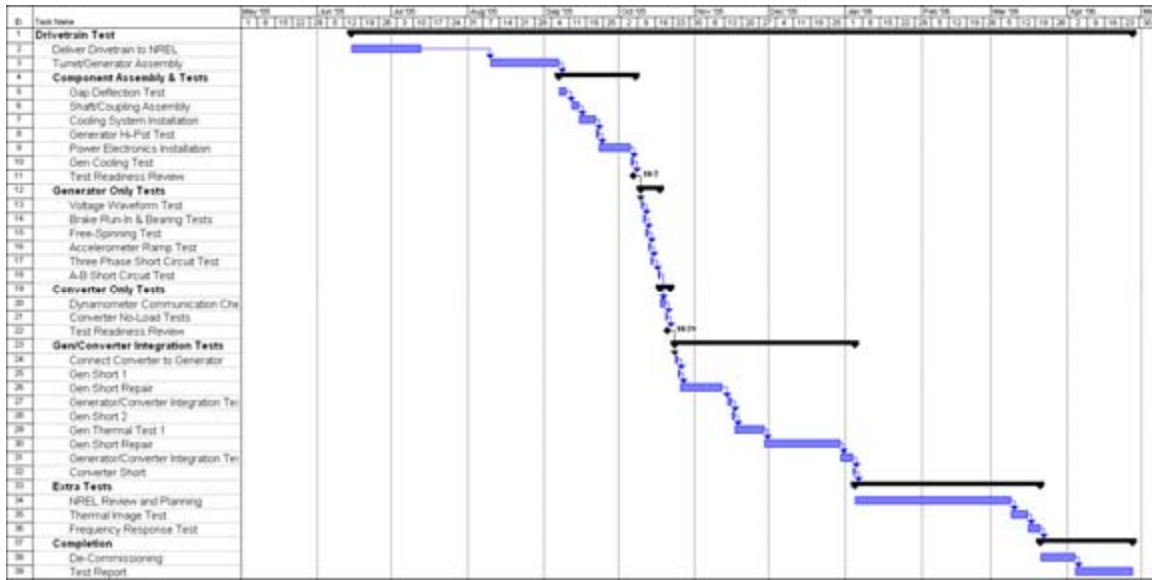


Figure 5-1. NW1500 actual test schedule.

5.3 Description of the Test Article

The test article is shown in Figures 5-2 to 5-4. The test article was a 1.5-MW direct-drive, permanent magnet generator. There was no gearbox. The generator was mounted on a turret, which connects it to the existing turret base, which sits on the floor. The generator rotor was directly connected to the main shaft of the dynamometer. The generator was connected to a power electronics and control unit, shown in Figure 5-5. An overhead cable tray supported power cables. Additional cables connected the power electronics to the transformer disconnect box.

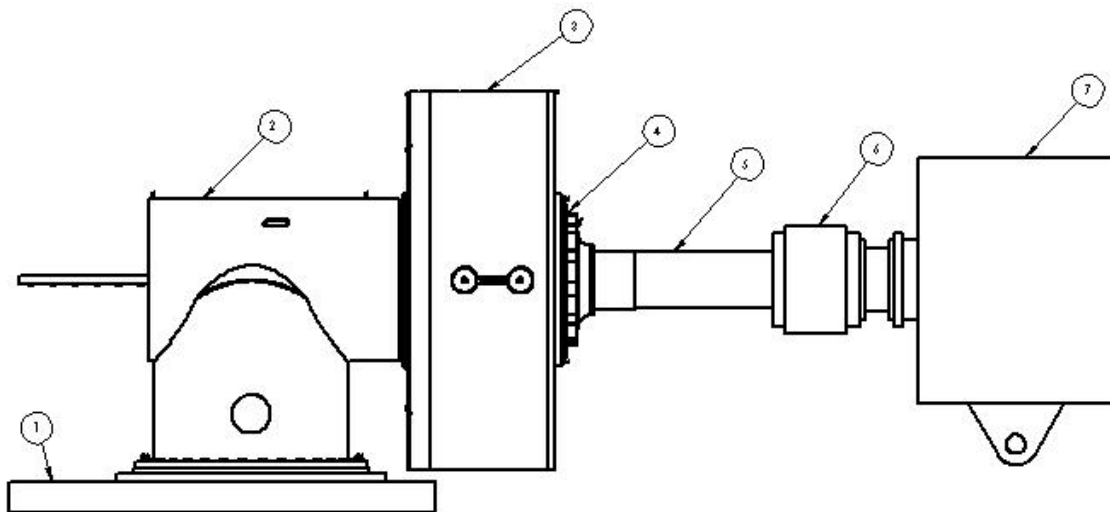


Figure 5-2. Dynamometer test article



Figure 5-3. The generator was attached to the bedplate with a turret, and had removable covers for access to the active materials.



Figure 5-4. The generator connects to the dynamometer using a long shaft and coupling, as shown here viewed from the control room.



Figure 5-5. The power electronics connected to the generator via overhead trays, and connected to the grid via trays on the floor.

5.4 Test Results

5.4.1 Gap Deflection Test

The Gap Deflection Test was performed by loading the rotor with the weight of the dynamometer shaft. First, the shaft weight was unloaded by lifting with the crane with force (F) at a point 1.4 m from the end of the shaft. Once F at the lifting point was equal to the weight of the shaft, the displacement (d) was zeroed. The gap was measured at 8 points at the upwind and downwind ends of the generator. Then the shaft was slowly released by the crane, and the loaded conditions were measured. Results are shown in Table 5-1. Data is numbered clockwise looking at the generator on the side of the generator indicated in each column.

Table 5-1. Air Gap Measurements

Unloaded			Loaded		
F=64,413 N d=0 mm	Upwind (mm)	Downwind (mm)	F= 0 N d=2.47 mm	Upwind (mm)	Downwind (mm)
0° (12:00)	3.81	5.21	0° (12:00)	3.94	5.21
45	2.92	4.83	45	2.79	4.70
90	2.92	3.30	90	2.92	3.43
135	3.94	3.68	135	4.06	3.81
180	3.94	4.32	180	4.06	4.57
225	3.81	4.06	225	3.68	3.94
270	2.67	2.41	270	2.67	2.41
315	3.68	3.81	315	3.68	3.81

5.4.2 Cooling System Test

The Cooling System Test was very straightforward. The cooling system for the generator was connected, and the pump was started. The bypass valve was adjusted to obtain the minimum flow rates, measured in gallons per minute (GPM), as required by the cooling loop drawing. The system was checked for leaks, and the generator pressure drop, measured in pounds per square inch (psi), was measured. Results are shown in Table 5-2. Note that the converter cooling loop flow rate was not measured. This loop was run with the bypass loop closed to obtain the maximum flow rate possible. Coolant temperatures were within specification for all subsequent testing.

Table 5-2. Cooling Loop Test Results

	Generator	Converter
Flow Rate	64 GPM	Not Measured
Pressure Drop	10 psi	25.6 psi

5.4.3 Generator High Pot Test

The Generator High Pot Test was performed after generator assembly to ensure that no damage occurred during shipping of the generator. A similar test was also performed as part of the Factory Acceptance Test. This test was performed with a 1-kV Megger owned by NWTC. The test was performed with the high voltage connected to Phase 1, and the remaining two phases were grounded. The neutral ends of the phases were not connected to each other. The test was repeated for each phase and the resulting resistances are shown in Table 5-3.

Table 5-3. Generator High Pot Test Results

Measurement	Voltage	NREL Resistance	Pass/Fail
DC for 60s P1	1.0 kV	2,000 MOhm	Pass
DC for 60s P2	1.0 kV	2,000 MOhm	Pass
DC for 60s P3	1.0 kV	2,000 MOhm	Pass

5.4.4 Generator Free Spinning Tests

The Generator Free Spinning Tests were performed with the power electronics disconnected. The generator was mechanically connected to the dynamometer. A thermocouple was attached to the bearing in a threaded hole underneath the inner race. The power cables from the generator were connected to the volts open circuit (VOC) and short circuit current (ISC) test fixture. Some issues occurred during testing that caused deviations from the original plan. Mainly, it was found that the brake was rubbing, creating a parasitic drag. Two extended free-spinning tests were performed to cause some brake wear, and reduce the parasitic drag. These tests produced a lot of brake dust.

5.4.5 Voltage Waveforms

First, the open circuit voltage was measured. Voltage waveforms were measured at 5, 10, 15, and 20 rpm. The three phase voltages, neutral voltage, and bearing voltage were measured at 1,000 Hz data acquisition rate (data from 10/10/05). The line-to-line voltage, neutral voltage, and bearing voltage are shown in Table 5-4. Bearing voltage was measured at the outer race using a slip ring. A plot of line-to-line voltage as a function of rotor speed is shown in Figure 5-6. Phase and neutral voltage and Fourier transform of the phase voltage for operation at 20 rpm are shown in Figures 5-7 and 5-8. The phases were well balanced, and the neutral voltage was small. The voltage spectrum showed little harmonic distortion.

Table 5-4. Generator Free Spinning Test - Voltage

Speed (rpm)	Vll (Vrms)	Vneutral (Vrms)	Vbearing (Vpk)
5	194.6	5.4	2.4
10	382.1	8.1	2.4
15	570.9	9.6	2.5
20	764.2	11.9	2.4

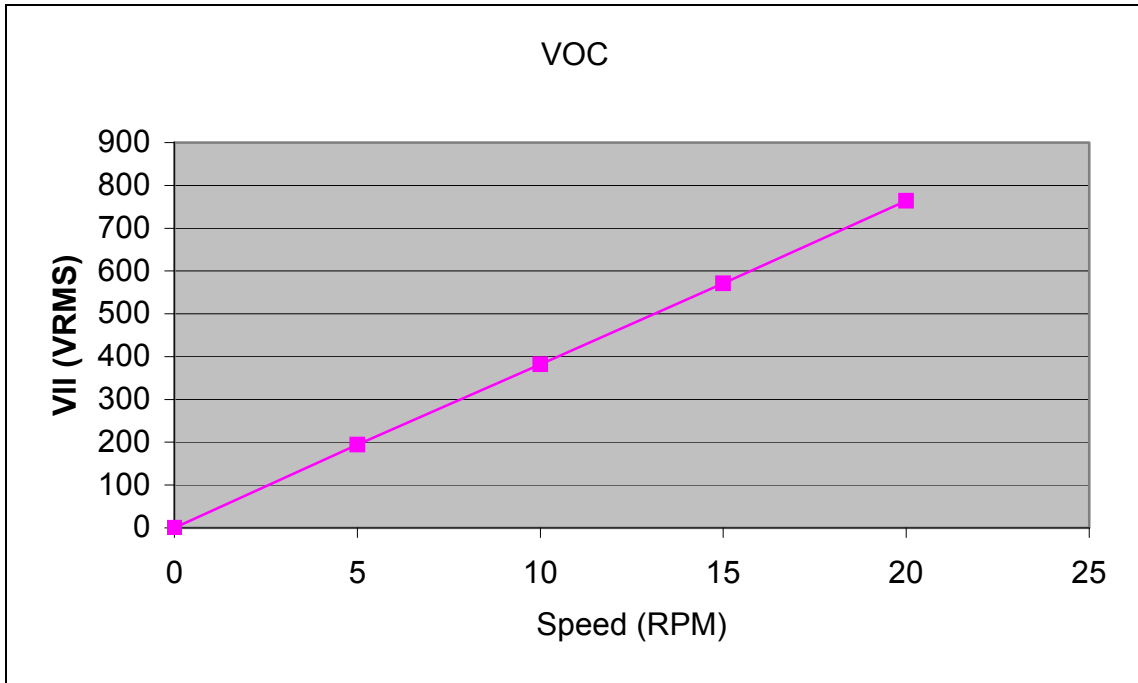


Figure 5-6. The line-to-line voltage for free spinning test was linear.

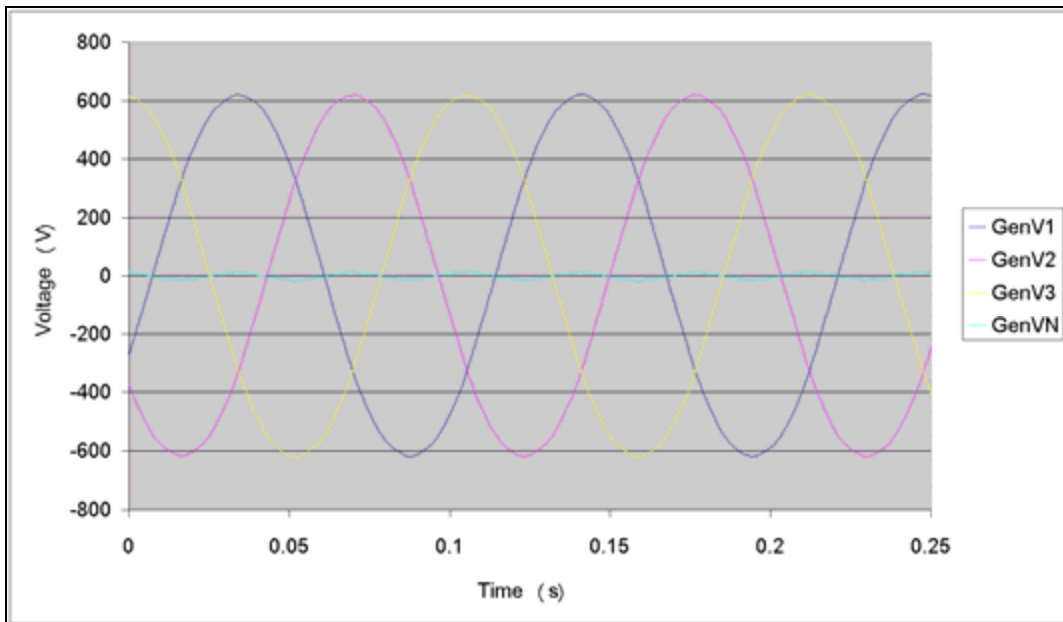


Figure 5-7. The open circuit voltage at 20 rpm was well balanced, and the neutral voltage was near zero.

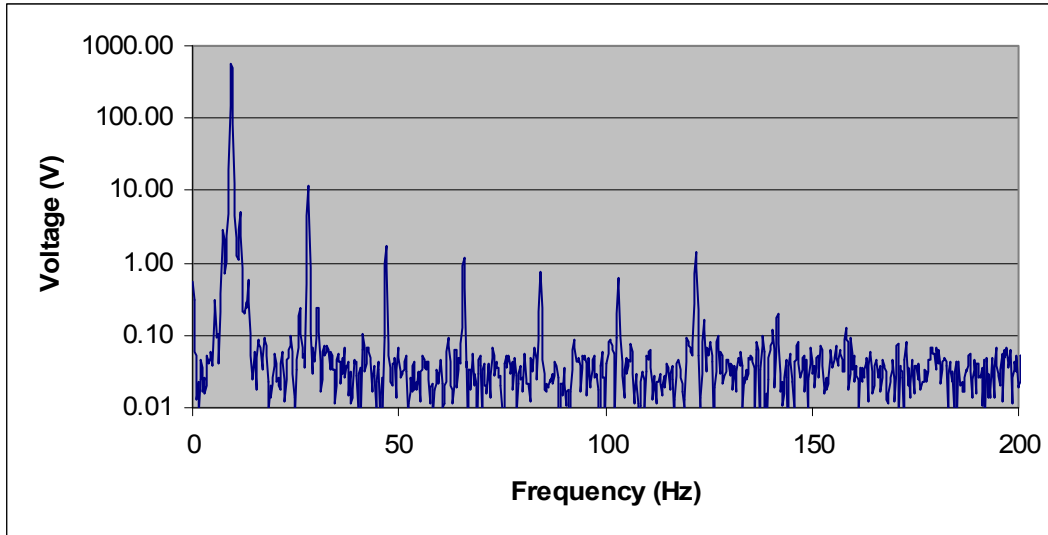


Figure 5-8. The phase voltage spectrum at 20 rpm showed a small amount of harmonic distortion.

The phase voltage harmonic distortion at 20 rpm is summarized in Table 5-5. The overall harmonic distortion is 3.09%. Voltage imbalance is shown in Table 5-6.

Table 5-5. Harmonic Distortion of Open Circuit Voltage at 20 rpm.

Frequency (Hz)	Voltage Magnitude (V)	Order	Distortion (%)
9.27	563.4	1	
28.08	11.5	3	2.04
46.88	1.7	5	0.30
65.67	1.2	7	0.21
84.47	0.8	9	0.14
103.03	0.6	11	0.11
121.83	1.4	13	0.25
141.84	0.2	15	0.04
Total	17.4	NA	3.09

Table 5-6. Voltage Imbalance of Open Circuit Voltage at 20 rpm.

Phase	Voltage (Vrms)	Imbalance (%)
A	441.2	0.15
B	440.6	0.14
C	441.9	0.01
Average	441.2	NA

5.4.6 Brake Run-In and Bearing Tests

Because the brake was rubbing, the generator was rotated (Data from 10/10/05) at 18 rpm for about 30 minutes with the brake applied (150 psi brake pressure). Then the generator was rotated at 18 rpm for 105 minutes without the brake applied to determine if there was still rubbing and if the bearing would overheat (data from 10/12/05). The measured drag torque during this test was -1.91 kNm, which is essentially zero on the full scale of $\pm 1,400$ kNm. Unfortunately, the small amount of parasitic drag and large scale of the load cell prevented accurate measurement of the parasitic drag. The bearing temperature rise, shown in Figure 5-9, was very small, indicating that the bearing parasitic losses were very low. During this test, the brake generated dust that was deposited on the windings. It is possible that a short circuit was caused by this dust. It was removed by vacuuming and wiping with a cloth.

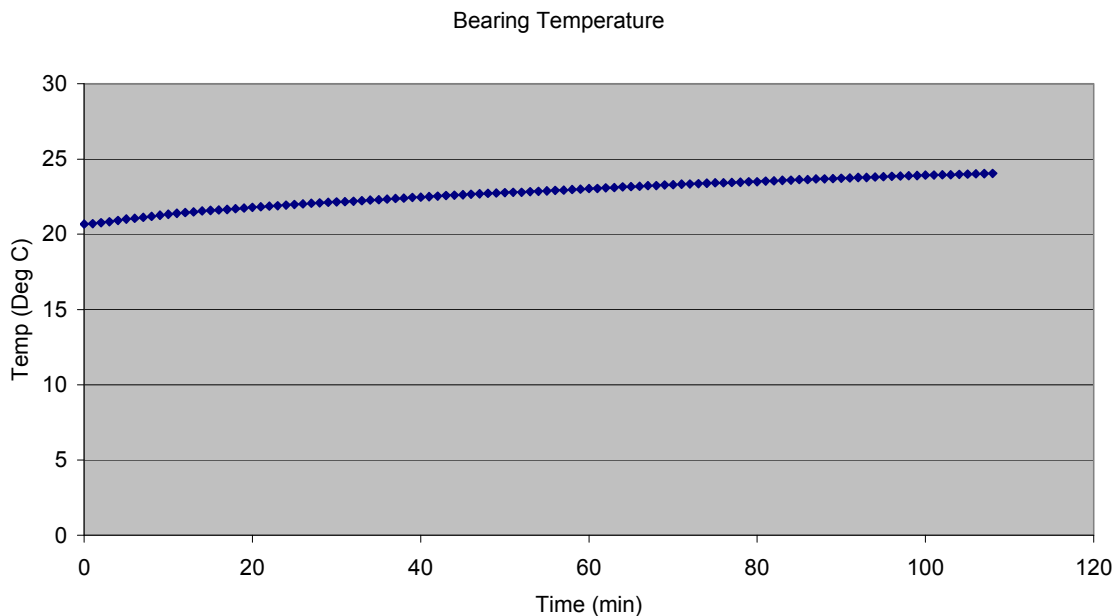


Figure 5-9. The bearing temperature for free spinning test (18 rpm) stayed low, indicating that the drag torque of the bearing is small.

5.4.7 Accelerometer Ramp Test

A ramp test from 0 to 20 rpm was performed, and accelerometer data was taken at 500 Hz to determine if excessive vibration occurred at any speed (data 10/13/05). Results are shown in Figures 5-10 through 5-12. This test was of limited use. The object of the test was to provide a steady input speed to the generator, and measure the vibrations of the rotor and stator. The dynamometer controller, however, could not hold the speed steady, especially at or near 20 rpm. Three natural frequencies of the stator are apparent, however. The stator torsional mode is most visible in the y-direction accelerations (tangential), which were measured at the 12:00 position upwind on the stator housing. The accelerations in Figure 5-10 show peaks at shaft speeds of 1.6 rpm, 3.6 rpm, and 6.15 rpm. The slot passing frequencies

corresponding to these shaft speeds are 9.13 Hz, 20.14 Hz, and 34.4 Hz. These correspond to the stator being excited at a slot passing frequency of 1, 2, and 3 times the lowest natural frequency.

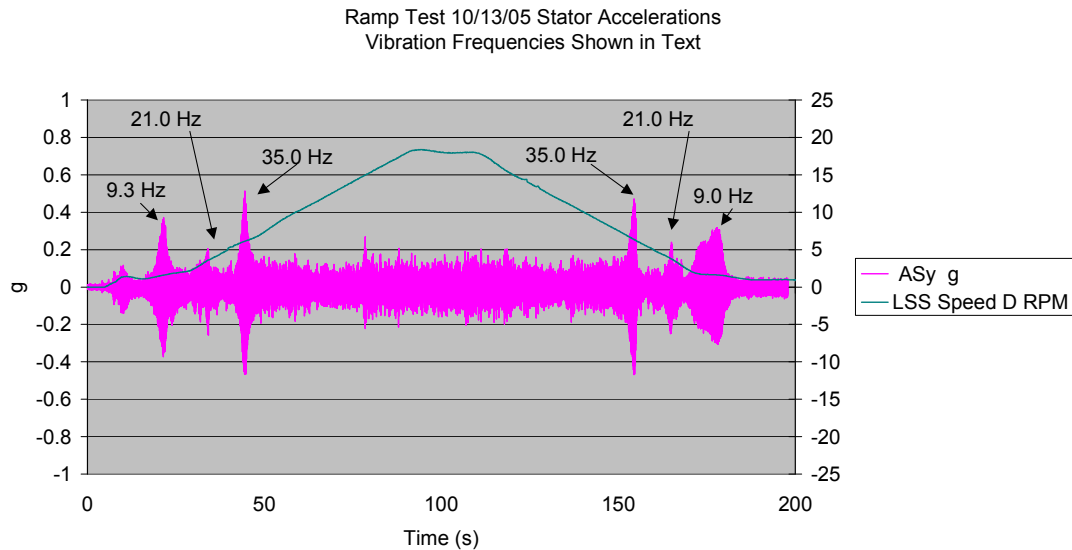


Figure 5-10. The stator had high y-accelerations at rotor speeds of 1.6, 3.6, and 6.1 rpm, when the shaft was accelerating and decelerating.

The z-direction accelerations (radial), shown in Figure 5-11, also seem to be excited at the same frequency as the slot passing frequency; however, the mode of vibration is not purely torsional. The accelerations show peaks at shaft speeds of 3.6 rpm while the shaft is accelerating, and 5.0 rpm while the shaft is decelerating. The reason for the difference in the natural frequencies is not clear. The slot passing frequencies corresponding to these shaft speeds are 20.1 Hz, and 28.0 Hz.

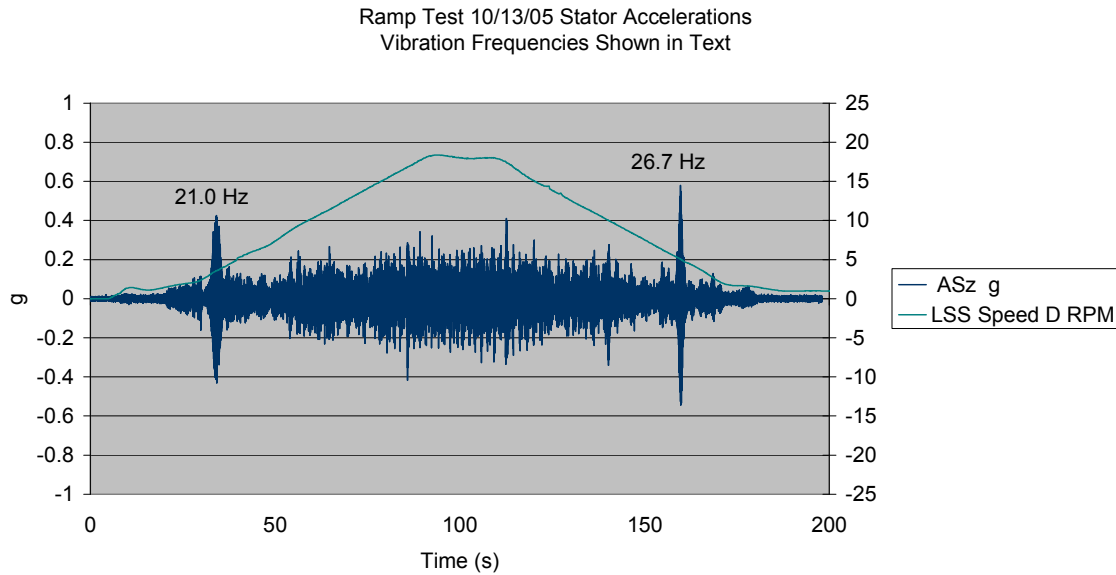


Figure 5-11. The stator had high z-accelerations at rotor speed 3.6 rpm as the rotor speed increased, and at 5.0 rpm as the rotor speed decreased.

The stator x (axial) and rotor x (axial), y (tangential), and z (radial) accelerations were not useful. The vibrations that occurred were associated with shaft speed control issues. For example, some vibration would occur at the transition point between constant speed and decelerating shaft speed. Also, the vibrations visible during acceleration were not apparent at the same speed while decelerating. An example of this behavior is shown in Figure 5-12. Spider strains were also measured, but the strains caused by vibration were very small, and could not be discriminated from noise.

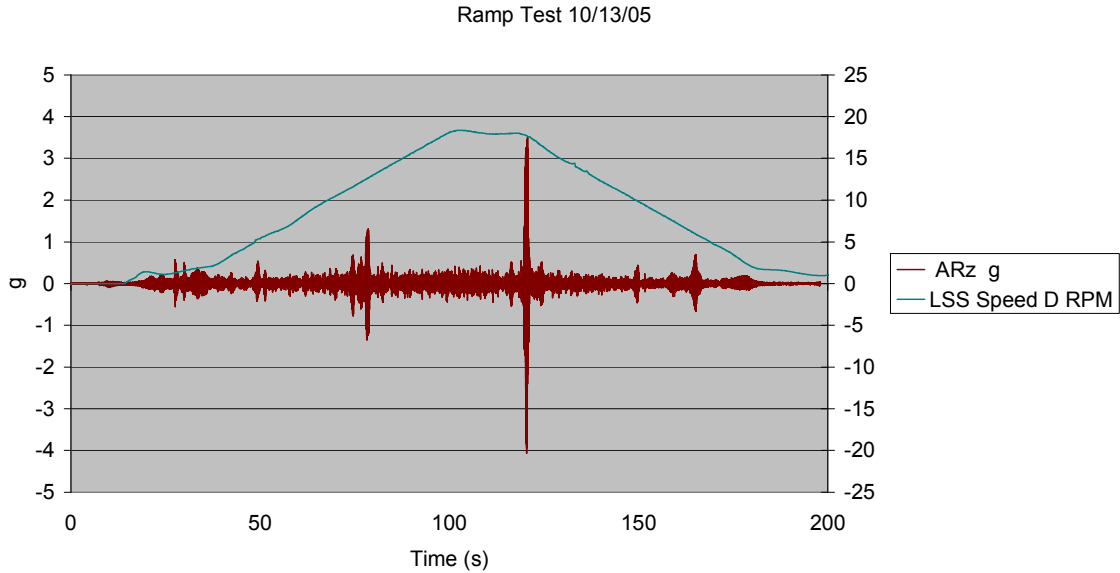


Figure 5-12. The rotor x acceleration (in shaft direction) did not indicate any natural frequencies, because the vibrations did not occur while the shaft was both accelerating and decelerating.

5.4.8 Generator Short Circuit Test

The Generator Short Circuit Test was performed with the generator cooling system in operation. The power electronics were not connected. The power leads were connected to the VOC and ISC test fixture and all three phases were shorted. Current measuring devices were installed. The dynamometer was started three times at 0.5, 0.7, and 0.95 rpm. Three-phase short circuit currents are shown in Table 5-7.

A two-phase short circuit test was performed at 0.5 rpm with the terminations A and B shorted. Short circuit current and max temperatures for these conditions are shown in Table 5-8. The torque and phase A and B currents are shown in Figure 5-13. The torque cycled from zero to approximately rated torque during every electrical cycle. This test was more severe than was originally thought, so the test was terminated to avoid damage to the test system.

Table 5-7. Short Circuit Current (Three Phase Short)

Speed (rpm)	Average Phase Current (Arms)
0.5	861.7
0.7	1097.3
0.95	1326.1

Table 5-8. Short Circuit Current (Two Phase Short)

Phases	Speed (rpm)	Max Phase Current (A)	Max Stator Temp (°C)
A-B	0.5	1213	33

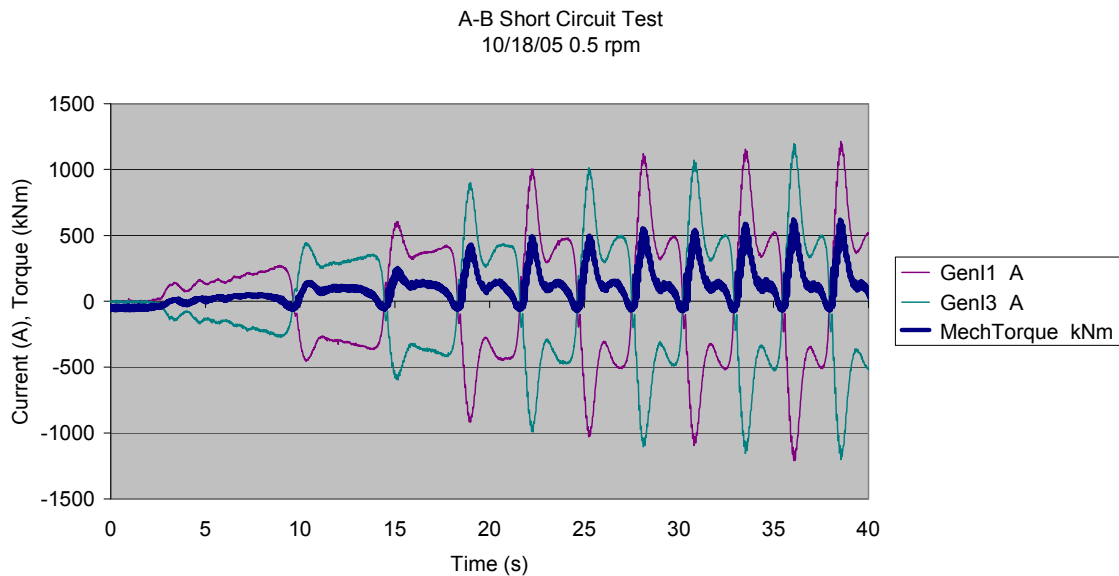


Figure 5-13. The torque in the two phase short circuit test was severe, so the test was terminated.

5.4.9 Bearing Impedance Test

First the resistance of the main bearing was measured with a slip ring connection while the generator was stationary. A 9-mV drop was measured for a 0.1-A DC excitation. This test was repeated with the slip ring shorted and the same result was obtained, confirming that the slip ring impedance was insignificant. With the generator rotor slowly rotating, the voltage drop for a 0.2-A DC excitation was measured. The results are shown in Table 5-9. The bearing resistance is low, so the rotor is effectively grounded during operation. Further testing was done without a ground wire connected to the rotor through the slip ring.

Table 5-9. The Bearing Resistance was Low, and Independent of Rotor Position.

Rotor Position (Deg)	Current (A)	Voltage (mV)	Resistance (Ohm)
0	0.2	18.0	.090
90	0.2	17.8	.089
180	0.2	17.9	.090
270	0.2	18.3	.092

5.4.10 Converter No Load Test

The Converter No Load Test was performed after the converter was connected to the grid, and before the converter was connected to the generator. The cooling system for the converter was connected and operating during the test. During this test, the setpoints and alarms were checked, and the ability for the converter control to work from 690-V grid connection was verified. It was found that Phase B and C in the cables connecting the converter to the grid had to be changed to obtain the correct phase rotation. The DC link voltage was set to 1,070 V. The dynamic brake system was checked by temporarily setting the DC link voltage above the limit. During this test, the communication link to the dynamometer system was debugged so that the systems could enable each other to start a test.

5.4.11 Generator Converter Integration Test 1

The Generator Converter Integration Test starts with a pulse test of the generator. This test applies a voltage to each phase sequentially to detect if there are any shorts. When the phase test was performed, a short was detected which caused a shutdown. The shutdown was not immediately detected, however, because the short circuit current was not larger than the limit setpoint. The test was repeated several times until the problem was diagnosed. A few weeks were spent repairing the generator and testing it to make sure that the generator converter integration tests could continue.

5.4.12 Generator Converter Integration Test 2

The Generator Converter Integration Test was continued after fixing the short in the generator windings. The generator was connected to the converter and the pulse test of the generator windings was completed without incident. The generator was rotated at low speed (4 rpm), and the converter tried to determine the position and speed of the generator from the encoder signal. The signal had a great deal of noise, however, which caused a fault. This situation was fixed by grounding the shield of the cable at the generator, rather than at the converter. After clearing all the faults, 200 amp Q-axis current (I_q) was commanded by the converter. This worked well.

The generator rotor speed was increased to 8 rpm and the current was increased to 400 amp I_q . After running for about 0.5 hours at these conditions, a second short occurred in the generator windings. This short was subsequently located and a jumper was used to take the affected coil out of the circuit to allow testing to continue. The jumper was installed after the short circuit test of Section 5.4.13. A single short to ground does not affect operation of a short circuit test.

5.4.13 Generator Short Circuit Thermal Test

A three-phase short circuit test was performed with the intention of testing the cooling system for the generator. The rotation speed was selected to obtain a current similar to the

current at rated conditions. The generator terminations were shorted with three 0000 cables connected from Phase A to B, and three 0000 cables from phase B to C. The VOC and ISC test fixture was not used, because it would require unfastening all the cable terminations in the power converter. The water/glycol coolant temperature was also controlled to be as close to rated conditions (40°C generator inlet) as possible, as shown in Figure 5-14. The stator slot and end turn temperatures were monitored to determine the hot spot temperature under these conditions. The rotor speed had to be increased twice during the test, because as the stator heated up, the generator became less efficient, and the current dropped. The speed started at 0.95 rpm, increased to 1.15 rpm at 70 minutes, then to 1.35 rpm at 187 minutes. At the end of the test, the current was 1,324.3 Arms, which is 6% less than the expected current of 1,404.7 Arms at rated conditions. Assuming a winding resistance of 15.86 milliOhm (mOhm), the resistance losses were 83.4 kW. The test was terminated at 300 minutes (5 hrs) when the temperatures had approximately equalized. Also, at the end of the test, it was clear that varnish vapors were coming from the generator, which created a potentially unhealthy working environment in the dynamometer facility. Also, at 180 minutes, the torque signal was lost due to a radio communication error. The dynamometer needed to be shut down for about a minute to restart the load cell communication device. It is expected that the highest RTDs were reading higher than actual temperatures, because of the long length of the leads to the data acquisition equipment. Still, the maximum temperatures, shown in Figure 5-15, were below the limits of 155 °C set for this design.

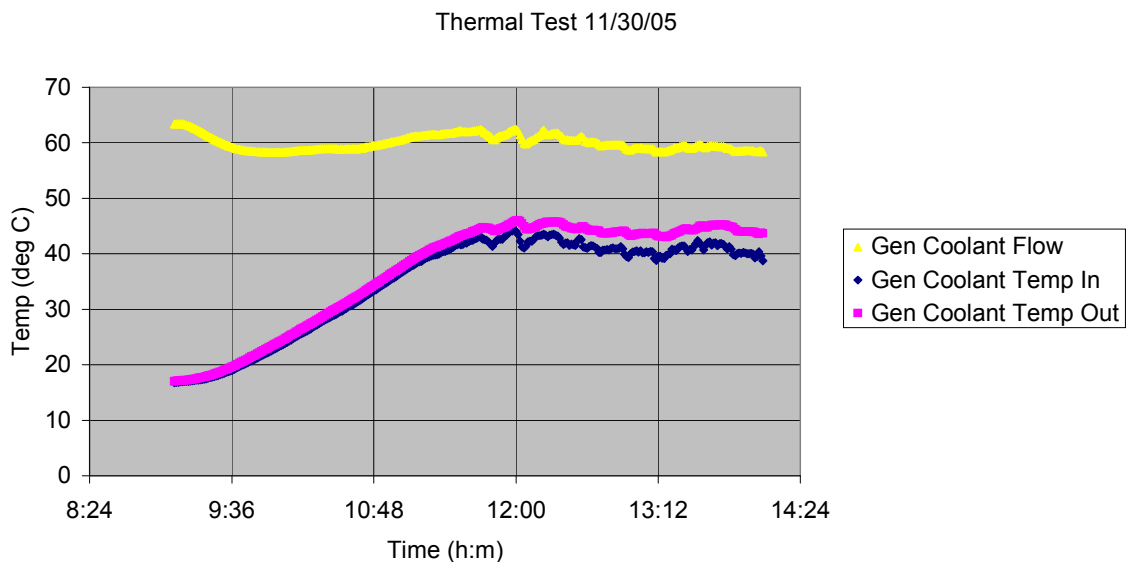


Figure 5-14. The coolant inlet temperature was controlled to maintain a 40°C temperature.

Thermal Test 11/30/05

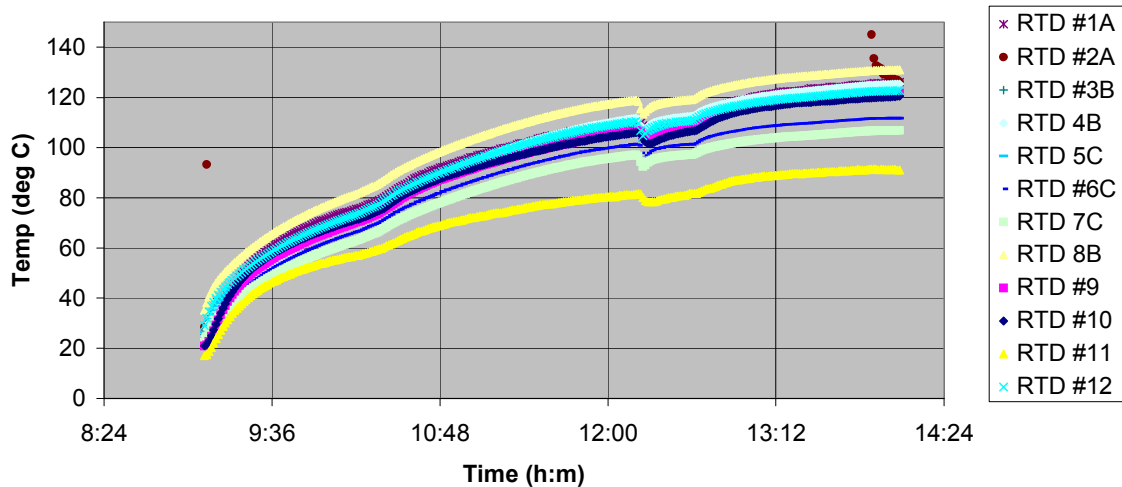


Figure 5-15. The temperatures measured in the thermal test were within the limits of a class H insulation system (155 °C), but they caused some out-gassing of vapors due to incomplete curing of the varnish.

5.4.14 Generator Converter Integration Test 3

The Generator Converter Integration Test was continued after fixing the second short in the generator windings.

Tests were carried out at 25%, 50%, and 100% power at 19 rpm for 30 minutes at each power level. The dynamometer was unstable at higher rpm and so the test was limited to 19 rpm. It was found that limits for the real current command based on DC bus voltage were not sufficient at 1.2 MW. This resulted in a DC overvoltage shutdown as the power was raised up from the 75% level. Once the current limits were widened, the converter reached 1.5 MW. There were a number of other trips related to the dynamometer shutting down because of line voltage imbalance and voltage sags on the 690-V bus. At this point, the generator and converter performance was as expected. These tests, however, did not run long enough to reach the temperatures associated with rated conditions. The generator phase voltages are very jagged, due to the neutral point modulation technique employed in the converter. The neutral point was adjusted to reduce the peak phase voltages at the generator and reduce switching losses in the converter. A generator phase voltage and neutral voltage chart is shown in Figure 5-16. The dv/dt , measured in volts (V) per microsecond (μs), for the phase voltage is shown in Figure 5-17. The generator line-to-line voltage is much closer to a sinusoid, but was noisy, as shown in Figure 5-18. This noise does not significantly affect performance. The spectrum of the generator line-to-line voltage is shown in Figure 5-19, and the harmonic distortion is shown in Table 5-10. Total harmonic distortion was calculated by summing the amplitudes at harmonic orders up to the switching frequency. The generator phase current is shown in Figure 5-20, and the spectrum of the phase current is shown in Figure 5-21. Total harmonic distortion is 1.26%, as shown in

Table 5-11. The utility interface voltage, shown in Figure 5-22, is very smooth. The utility interface harmonic distortion and spectrum are shown in Table 5-12 and Figure 5-23. Other parameters pertaining to 1,500-kW power production are shown in Table 12. Note that the power factor in the table was based on the phase angle between the line-to-line voltage and current (32°). The inductance was calculated by using the aforementioned phase angle and the phase angle between the current and the Q-axis. The latter phase angle is 10° . Thus the total angle between the electromotive force and the generator voltage is 42° . Figure 5-24 shows the stator RTD results. Many of the stator temperature signals were affected by noise during power production, and those results are not shown. Power production at 1,500 kW was reached at 800 seconds into the test, so the average stator temperature during power production was around 50°C .

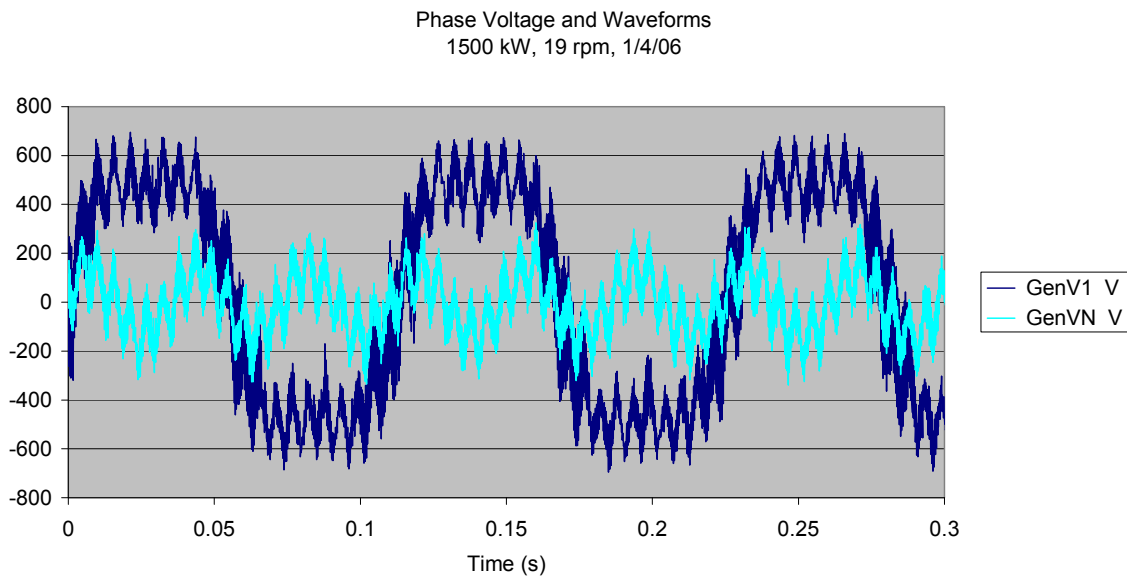


Figure 5-16. The generator phase voltage is jagged because of neutral-point-modulation, which decreases peak voltage.

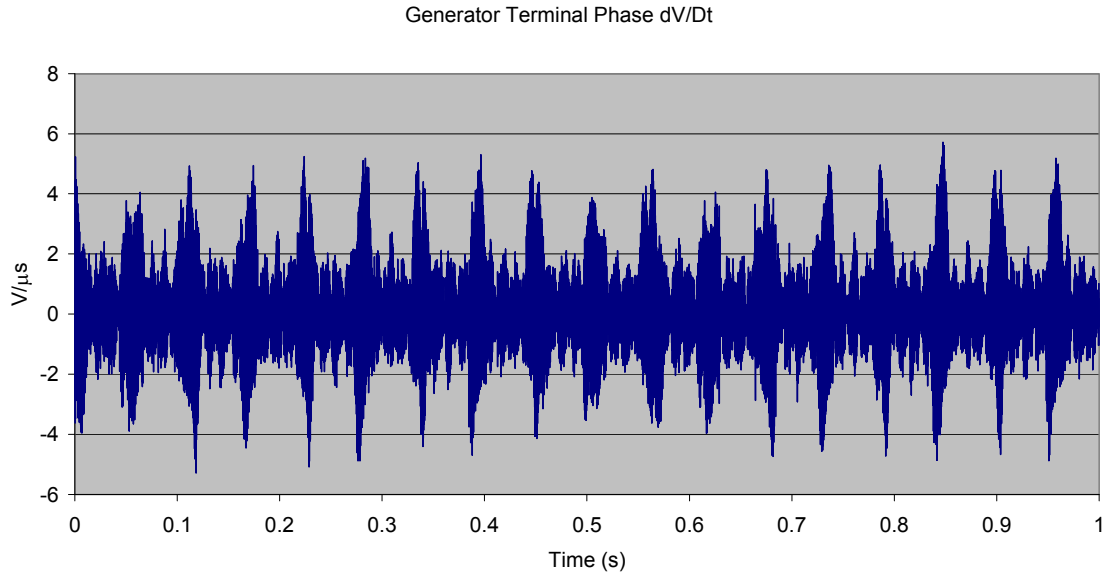


Figure 5-17. The generator phase voltage dv/dt was less than $6V/\mu s$.

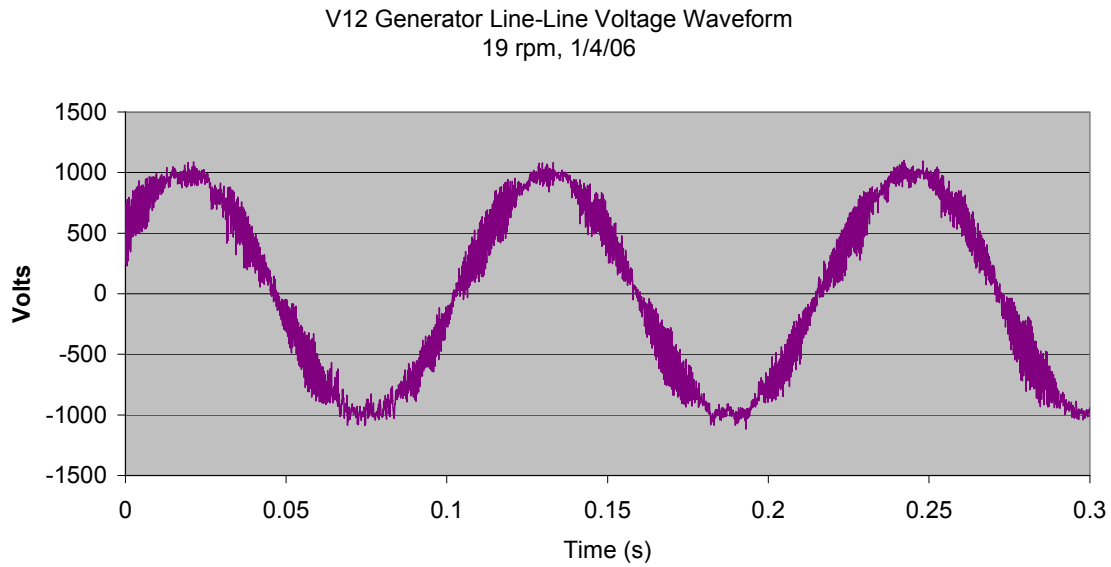


Figure 5-18. The generator line-to-line voltage was noisy due to active rectifier switching effects.

Generator Line-to-Line Voltage Spectrum
1500 kW, 19 rpm, 1/4/06

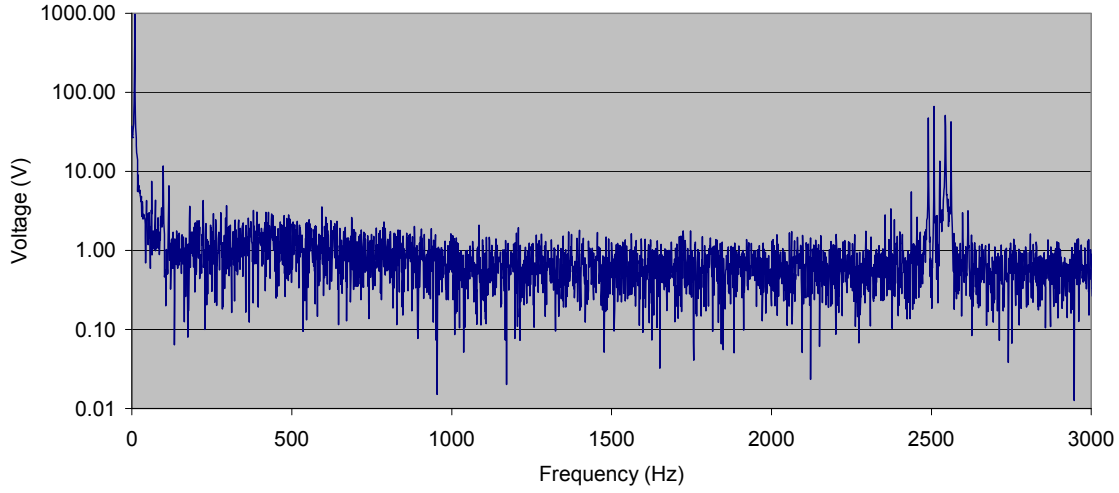


Figure 5-19. The spectrum of the generator line-to-line voltage is dominated by 2.5 kHz switching noise.

Table 5-10. Total Harmonic Distortion of the Generator Line-to-Line Voltage at 1,500 kW was Dominated by Switching Noise at 2.5 kHz.

Frequency (Hz)	Voltage Magnitude (V)	Order	Distortion (%)
8.89	973.14	1	
17.77	0.00	2	0.00
26.66	0.00	3	0.00
35.54	0.00	4	0.00
44.43	4.28	5	0.44
53.32	0.00	6	0.00
62.20	7.49	7	0.77
71.09	0.00	8	0.00
79.97	0.00	9	0.00
88.86	0.00	10	0.00
97.75	11.68	11	1.20
106.63	0.00	12	0.00
115.52	6.62	13	0.68
124.40	0.00	14	0.00
133.29	0.00	15	0.00
142.18	0.00	16	0.00
2,532.21	67.15	285	6.90
Total			7.12

Rated Generator Current Waveform, I1
1500 kW, 19 rpm, 1/4/06

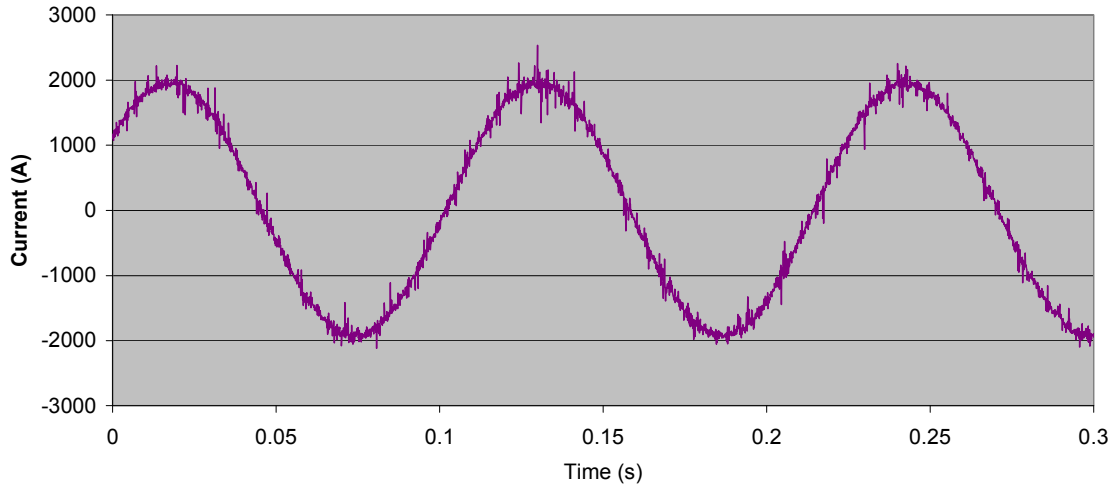
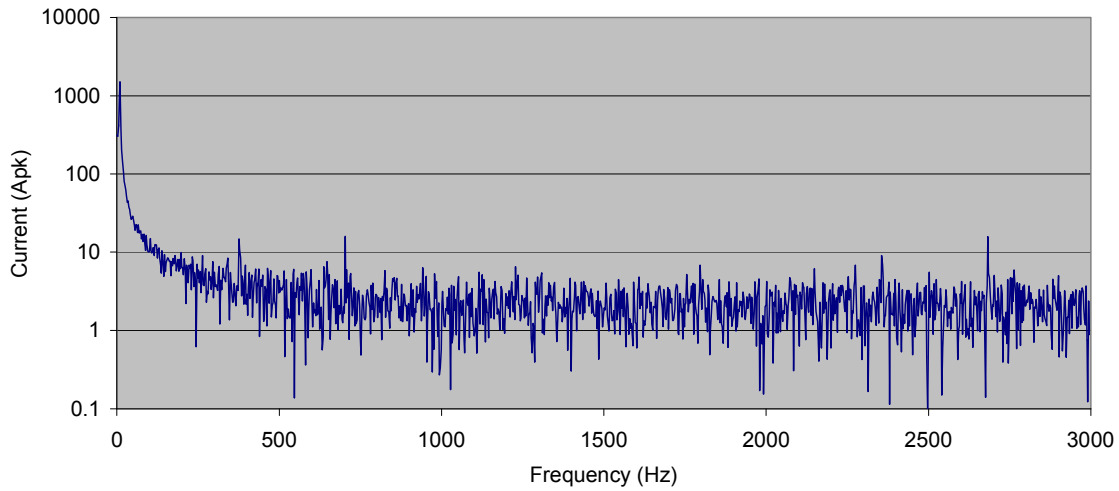


Figure 5-20. The phase current was also noisy, but this did not affect the function of the

Generator Phase Current Spectrum
1500 kW, 19 RPM, 1/4/06



generator.

Figure 5-21. The phase current spectrum shows very little harmonic distortion.

Table 5-11. The Total Harmonic Distortion of the Phase Current was 1.26%.

Frequency (Hz)	Current Magnitude (A)	Order	Distortion (%)
8.89	1908.99	1	
17.77	0.00	2	0.00
26.66	0.00	3	0.00
35.54	0.00	4	0.00
44.43	0.00	5	0.00
53.32	0.00	6	0.00
62.20	0.00	7	0.00
71.09	0.00	8	0.00
79.97	0.00	9	0.00
88.86	0.00	10	0.00
97.75	0.00	11	0.00
106.63	0.00	12	0.00
115.52	0.00	13	0.00
124.40	0.00	14	0.00
133.29	0.00	15	0.00
142.18	0.00	16	0.00
373.21	16.42	42	0.86
701.99	12.22	79	0.64
2,532.21	12.60	285	0.66
Total			1.26

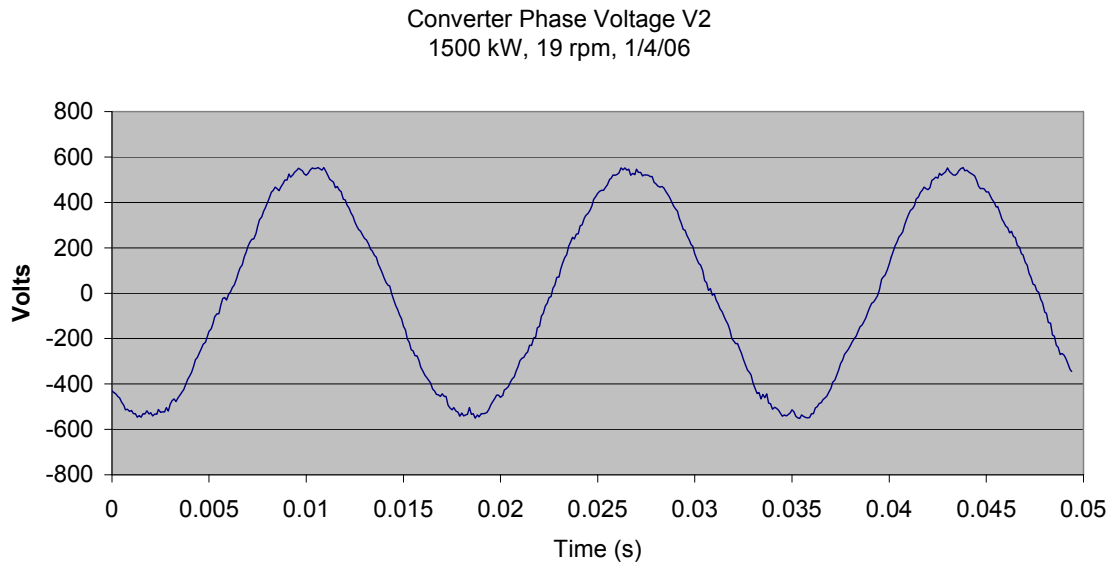


Figure 5-22. The converter phase waveform at rated conditions was very smooth.

Table 5-12. The total Harmonic Distortion of the Converter Phase Voltage at 1,500 kW was 3.15%.

Frequency (Hz)	Voltage Magnitude (V)	Order	Distortion (%)
60	543.61	1	
120	1.69	2	0.31
180	5.82	3	1.07
240	1.85	4	0.34
300	9.78	5	1.80
360	1.90	6	0.35
420	1.09	7	0.20
480	0.00	8	0.00
540	0.00	9	0.00
600	0.00	10	0.00
660	0.87	11	0.16
720	1.74	12	0.32
780	9.95	13	1.83
840	0.00	14	0.00
900	0.60	15	0.11
960	0.00	16	0.00
Total			3.15

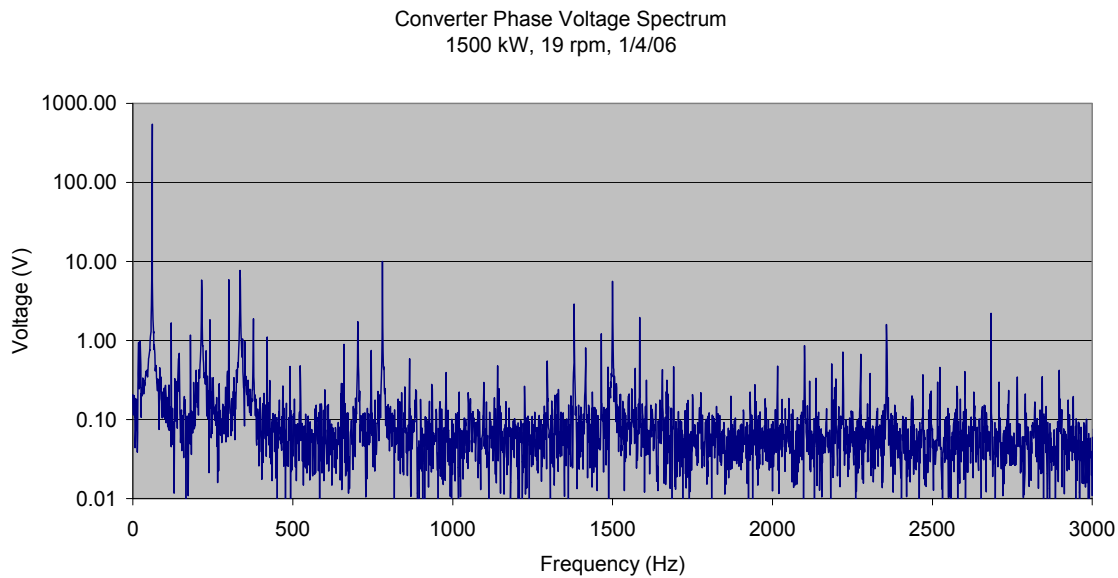


Figure 5-23. The converter phase voltage spectrum showed little harmonic distortion and switching noise.

Table 5-13. Generator/Converter Data at 19 rpm, 1,500 kW

Measurement	Value
D-Axis Current Command (A)	-337
Q-Axis Current Command (A)	-1914
Power to Grid	1503.5 kW
Shaft Speed	19.0 rpm
Power Factor	0.84
Generator Voltage THD	7.12 %
Q-Axis Inductance (mH)	3.9
Utility Inverter Current (Arms)	Phase A -1303.8 Phase B -1294.5 Phase C - 1306.2
Active Rectifier Current (Arms)	Phase A -1373.8 Phase B -1381.4 Phase C - 1352.1
Active Rectifier Voltage (Vllrms)	722.8
DC Voltage Average (V DC)	1149.0
Converter Line-Line Voltage THD	3.15%
Generator Peak Temperature (°C)	58.9
IGBT Peak Temperature (°C)	61.0
Coolant Peak Temperature (°C)	28.4

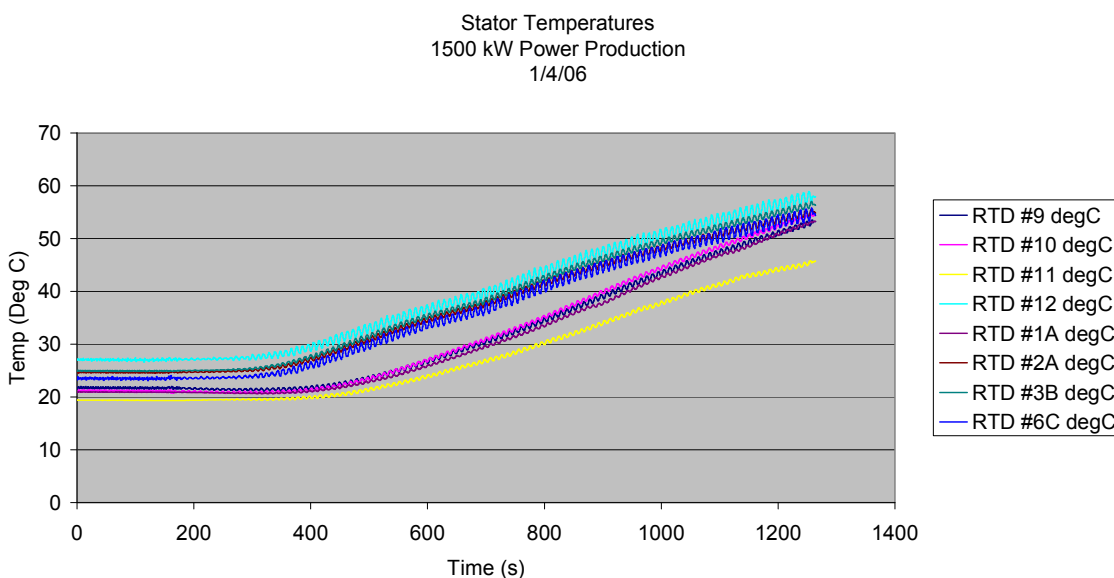


Figure 5-24. Stator temperatures during 1500 kW power production reached about 55 °C.

The generator efficiency was difficult to determine because the voltage signals at the generator terminals were inaccurate. These transducers were calibrated before the start of testing, but were probably damaged by the second short circuit in the windings. This was not discovered until after the test was completed. The voltage transducers at the utility interface worked fine,

however, so the overall efficiency (generator and converter) could be measured directly. Calculated losses of the converter and cable losses were subtracted from the total losses to determine the generator losses and the efficiency of the generator. This is shown in Table 5-14. Also, these values can be adjusted for temperature to predict the efficiency at rated steady-state temperature conditions. A small change in current is expected at rated temperature, because the magnet temperature increases, reducing field strength. The major change is the winding resistance, which increases as a function of temperature, and thus increases the losses. This calculation is shown in Table 5-15. In this calculation the stator temperature drop is assumed to be proportional to the losses.

Table 5-14. The Generator Efficiency was Calculated Using the Estimated Converter Efficiency, Because the Generator Voltage Transducer was Damaged.

Parameter	Value	Units
Rated Torque	826.1	KNm
Rated Speed	19	rpm
Rated Speed	1.99	rad/s
Rated Mech Power	1643.8	kW
Rated Grid Power	1503.5	kW
System Efficiency	91.5%	
Est. Converter Efficiency	97.0%	
Conv.. Input Power	1550.0	kW
Conv. Losses	46.5	kW
Cable Losses	4	kW
Gen Out Power	1554.0	kW
Gen Efficiency	94.5%	

Table 5-15. The Generator Efficiency at Rated Temperature Conditions was Estimated by Calculating Winding Resistance at 120 °C.

Parameter	Value	Units
Current (Measured)	1369.1	Arms
Current (Rated)	1404.7	Arms
Resistance (Measured)	12.67	mOhm
Resistance (Rated)	15.86	MOhm
Gen Losses (Measured)	89.8	kW
I ² R Losses (Measured)	71.24	kW
I ² R Losses (Rated)	93.85	kW
Gen Losses (Rated)	112.4	kW
Gen Efficiency (Rated)	93.2%	

5.4.15 Natural Frequency Test

The Natural Frequency Test was performed after the generator and converter were working properly. Accelerometers were placed on the rotor and stator for the test. The rotor accelerometer was placed on the downwind end of the rotor inner diameter, near the brake disk. The stator accelerometer was placed on the upwind end at 12:00. For each of these accelerometers, x is the direction along the shaft axis, and y is the tangential direction. The coordinate z direction is up for the stator and radially outward for the rotor. The test was done in two parts. First, vibrations were measured as the normal speed range of the generator was spanned (10-19 rpm). For this test, the current in the rectifier was fixed at 313 Arms. Power level at each speed is shown in Figure 5-25. Maximum acceleration as a function of shaft speed is shown in Figure 5-26. The acceleration increases with speed, but the values are relatively low, and no unusual vibration noises were heard during this test. A second part of this test was done to determine the vibrations at 19 rpm at various power levels. The acceleration as a function of power is shown in Figure 5-27. The accelerations were low, but increased with increasing power. The largest acceleration was the rotor x-direction acceleration (Figure 5-28), which had a frequency of twice the electrical frequency. The x-direction is an axial vibration.

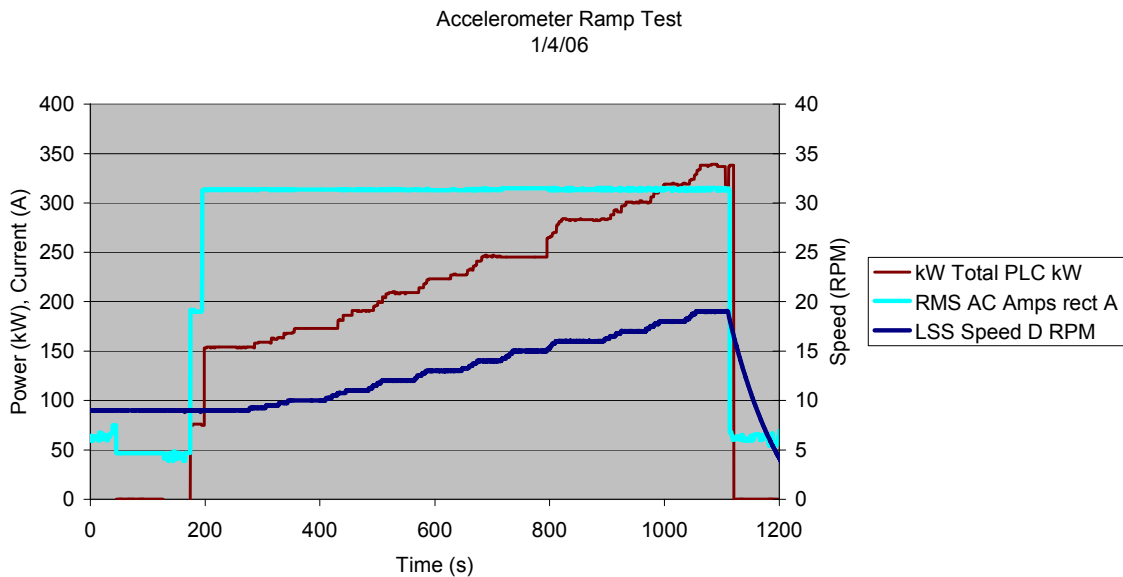


Figure 5-25. In the ramp test, the current in the rectifier was kept at 313 Amps, while the speed was increased from 10 to 19 rpm.

Stator and Rotor Maximum Acceleration
Accelerometer Ramp Test
1/4/06

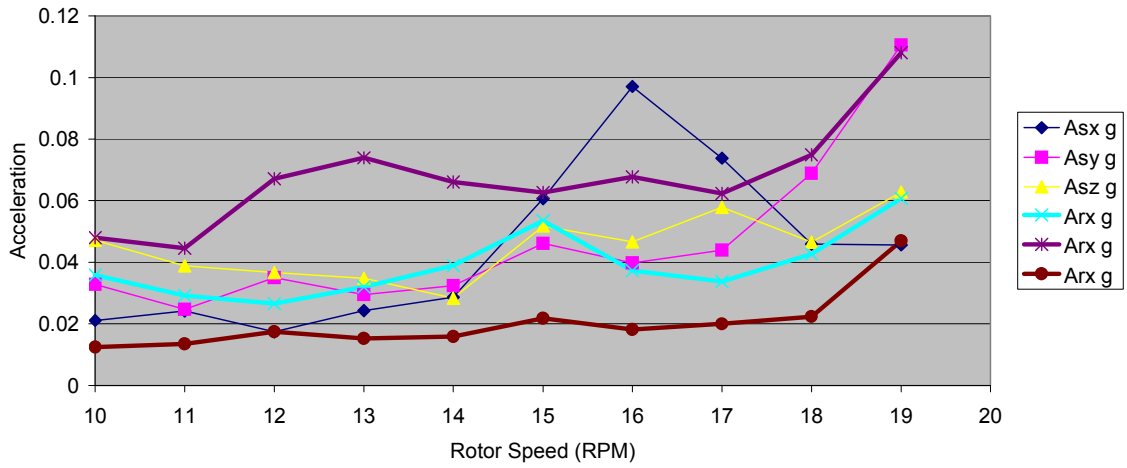


Figure 5-26. In the ramp test, the rotor and stator acceleration was small, but increased with rotor speed.

Rotor and Stator Acceleration
19 RPM, 1/04/06

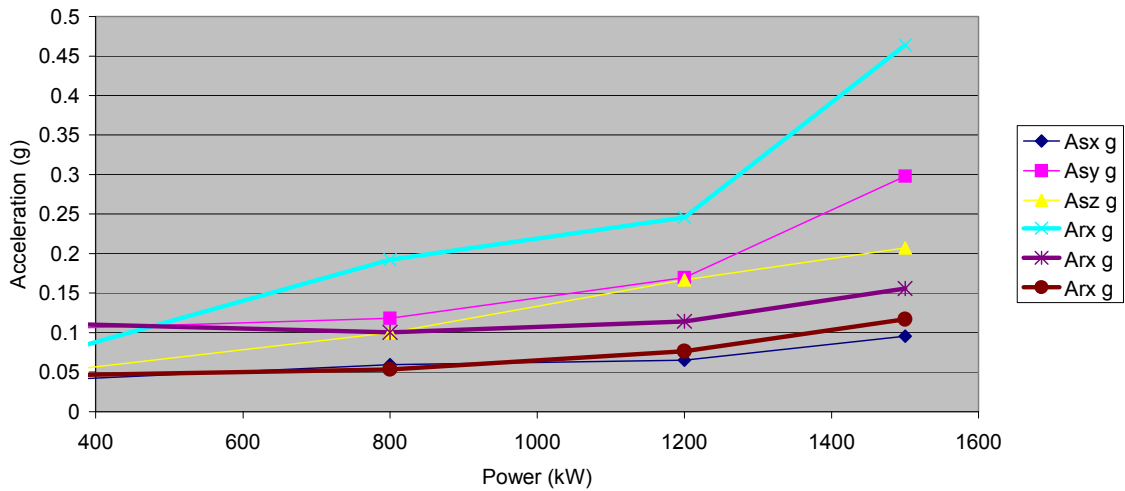


Figure 5-27. At 19 rpm, the rotor and stator accelerations were small, but increased with increased power production.

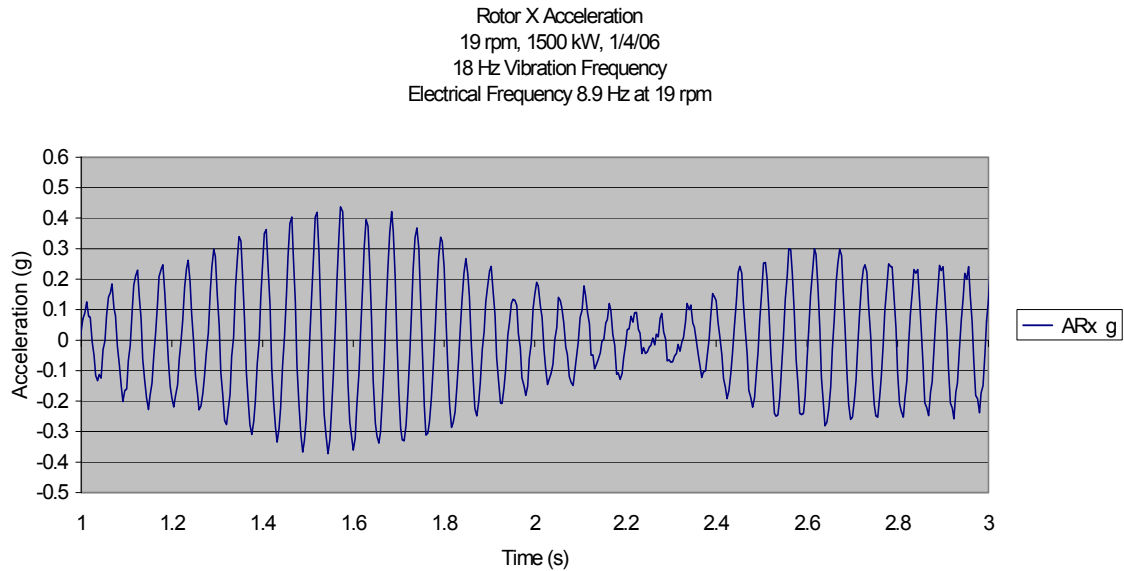


Figure 5-28. At 1,500-kW power production, the largest acceleration was an 18-Hz vibration of the rotor in the x-direction. This is twice the electrical frequency.

Note that after the natural frequency test, a short occurred in the converter. The sequence of events was as follows: First, the dynamometer accidentally sped up to over 22 rpm. Second, the active rectifier lost control of the terminal voltages. Third, the dynamic brake system activated to limit excessive voltages on the DC bus. Fourth, a converter variable wrapped over because of error accumulation. Fifth, the inverter reversed power flow due to the numerical error sending power back to the generator. Sixth, the inverter shut down. Seventh, the stored energy in the generator overcharged the DC bus and caused a capacitor to short circuit and fail. No further testing could be done using normal power production. Due to short-circuit and heat damage to many components, the cost of repairs would have been about \$80,000. Two additional tests were done, a thermal image test, and a frequency response test, to gain as much understanding of the generator as possible.

5.4.16 Thermal Image Test

A thermal image test was done to look for hot spots on the stator or rotor that could not be determined with the RTDs. The procedure for this test was the same as the first short circuit thermal test, except that the speed started out at 0.95 rpm and was increased to 1.2 rpm after 1 hour. The speed was kept at 1.2 rpm for the remainder of the test. The test was performed twice. First, the test was done with the front and rear panels off to get an overall view of the generator. At the end of the first test, the current was 1,297 Arms. Then the front and rear panels were replaced to determine the effect of the panels on the temperatures. A 300-mm x 300-mm hole

was cut into the front and rear end covers to allow the camera to view the end turns. At the end of the second test, the current was 1,315 Arms.

Overall, the thermal image test showed that the temperature of the end turns was very uniform, and not very sensitive to the placement of the front and rear covers. At the currents specified in these tests, it takes about three hours to reach steady-state conditions. The temperatures measured are well within the temperature rating of the stator insulation system. Stator RTD and coolant temperatures are shown in Figures 5-29 to 5-32. Images of the generator with the covers off, at the end of the first test, are shown in Figures 5-33 to 5-40. An image of the generator windings with the covers on, at the end of the second test, is shown in Figure 5-41. The thermal image hot spot temperatures match the RTD hot spot temperatures very well.

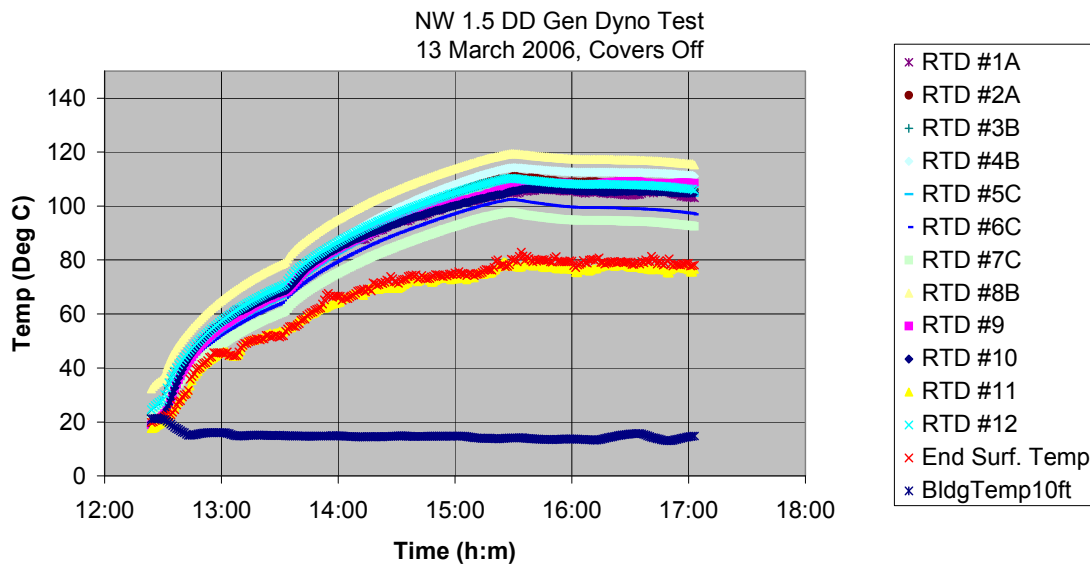


Figure 5-29. The first generator thermal image test was done with the covers off, and reached a hot-spot temperature of about 120°C.

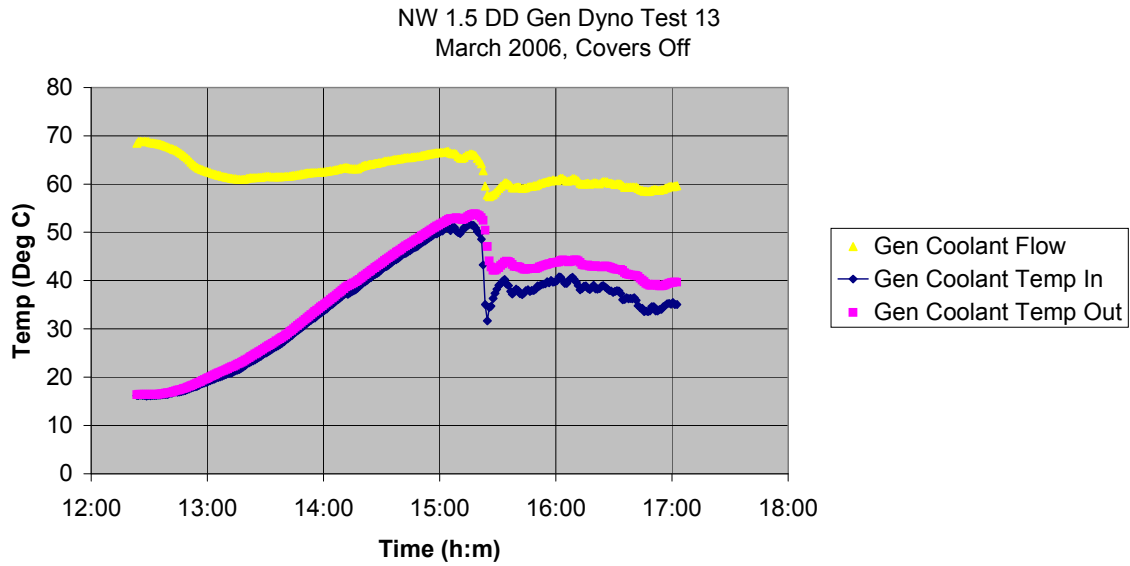


Figure 5-30. The coolant temperature was controlled manually to an inlet temperature of about 40°C.

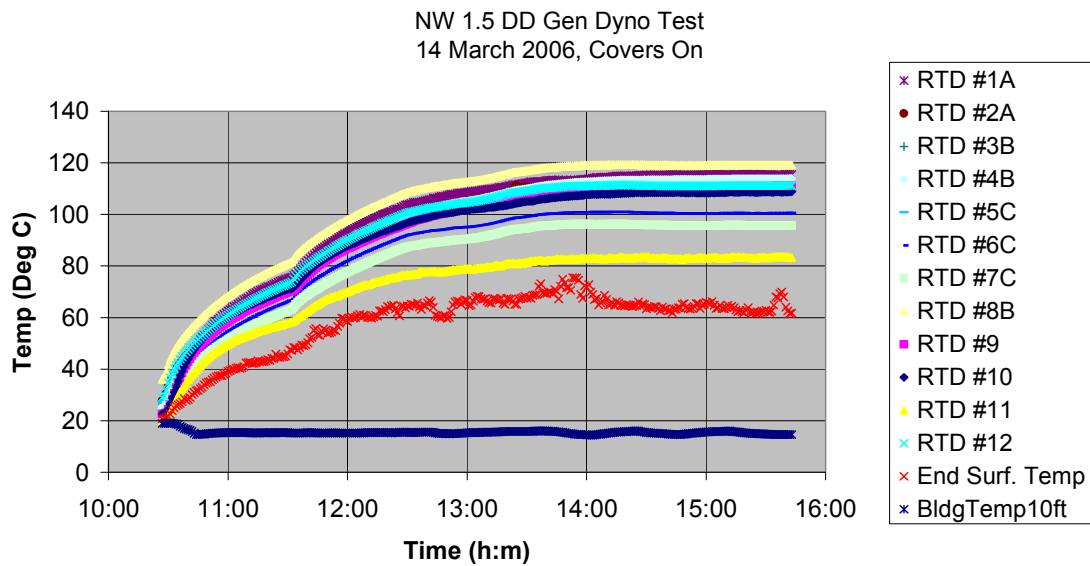


Figure 5-31. The thermal test was repeated with the covers on and reached a hot-spot temperature of 120°C.

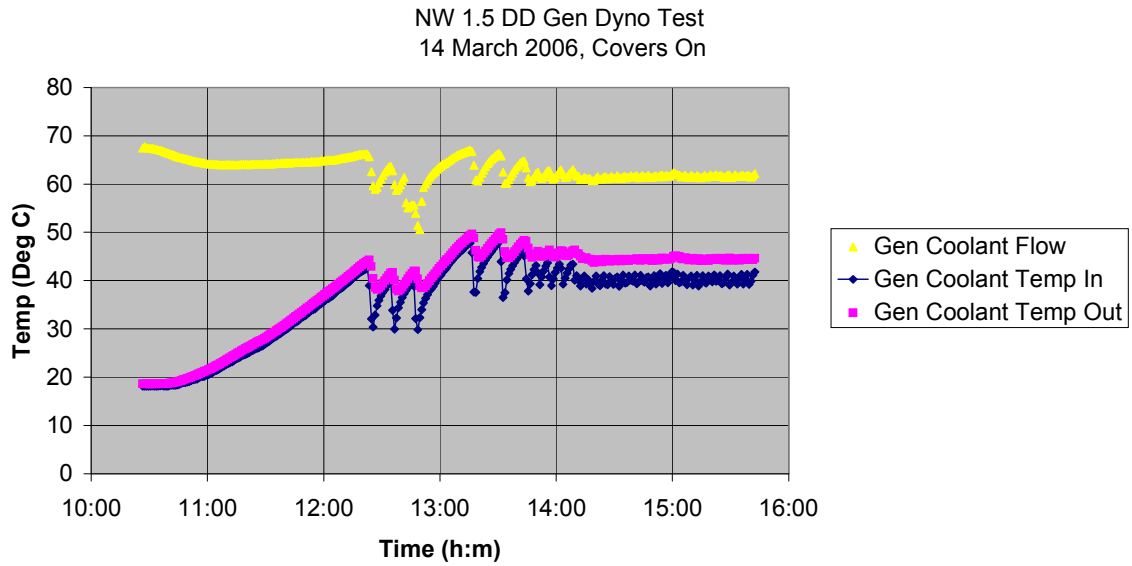


Figure 5-32. When the test was repeated, coolant temperature at the generator inlet was about 40°C.

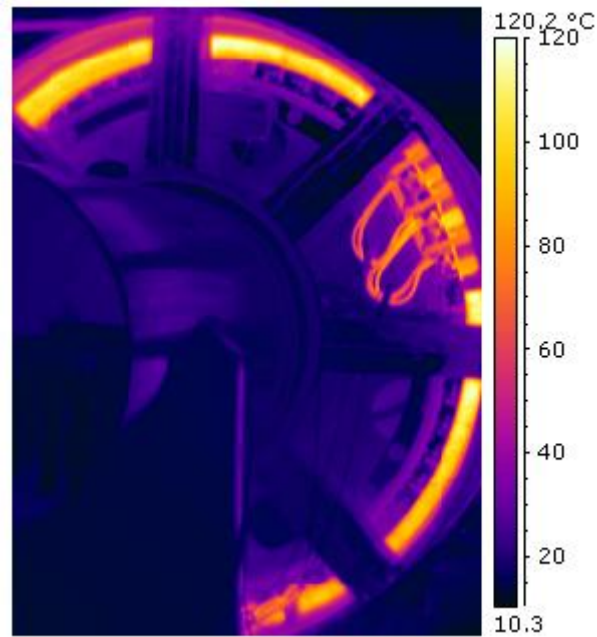


Figure 5-33. The thermal image of the end turns at the downwind end showed slightly hotter temperatures (121.6°C) at 12:00.

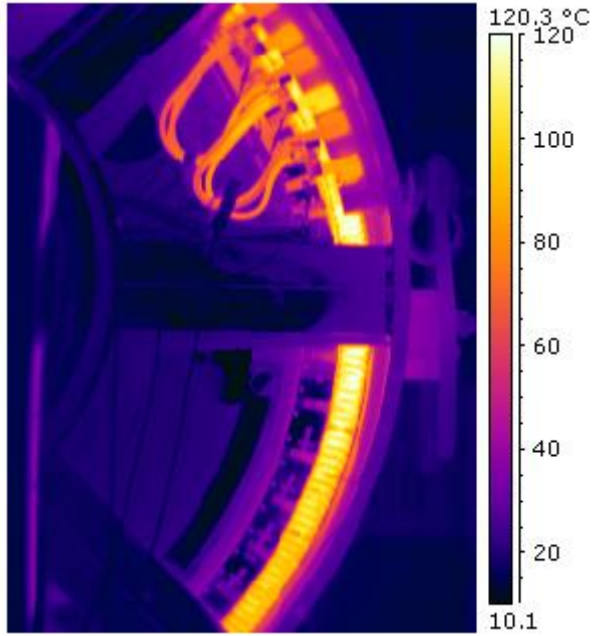


Figure 5-34. The thermal image of the short circuit jumpers shows a hot spot of 123.5°C.

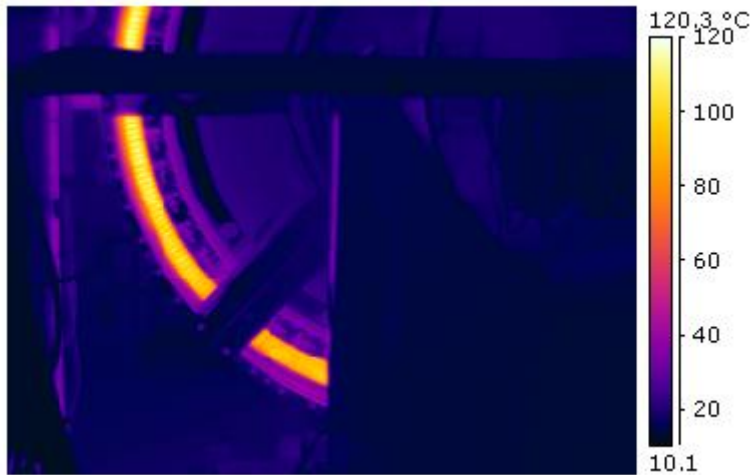


Figure 5-35. A thermal image of the downwind end of the generator shows a hot spot of 112.6°C.

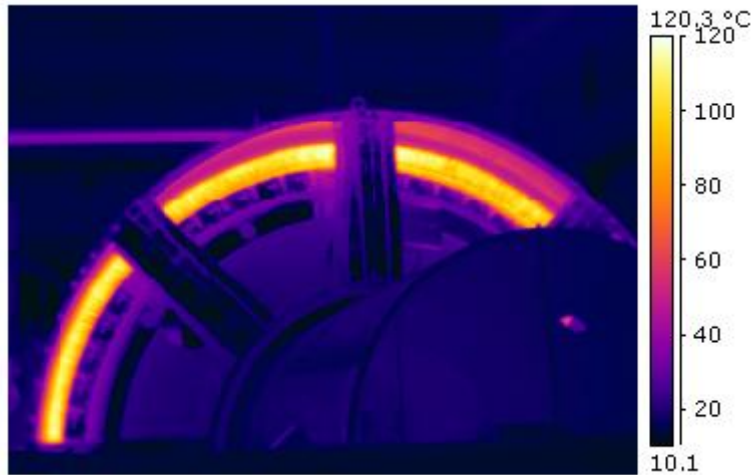


Figure 5-36. A hot spot (121.7°C) is visible at 12:00 on the downwind end of the generator.

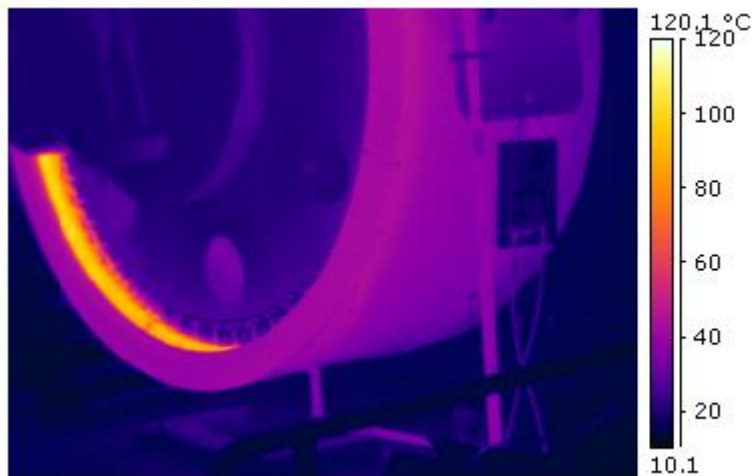


Figure 5-37. The upwind end turn temperatures were partially obscured by the front ring of the generator (103.7°C).

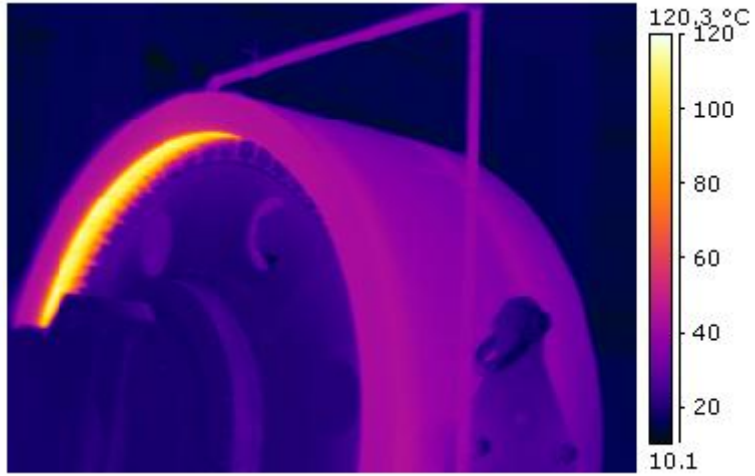


Figure 5-38. The hottest spot on the upwind end of the generator (118.3°C) was about 5°C less than the hottest spot on the downwind side.

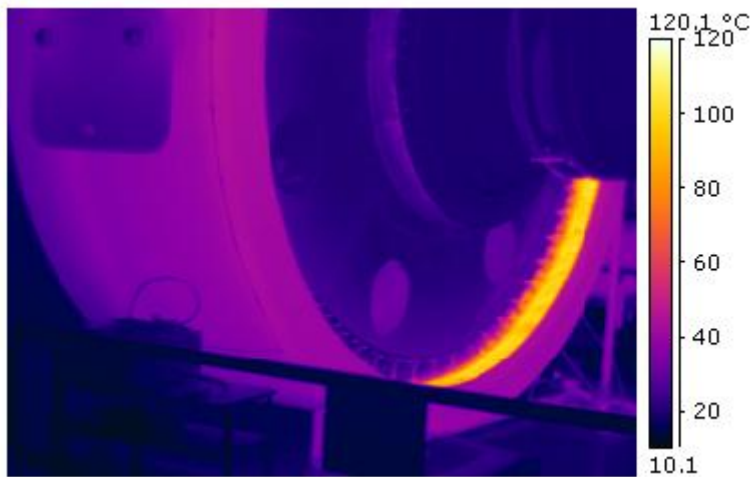


Figure 5-39. The stator housing temperature was very uniform at the temperature of the coolant.

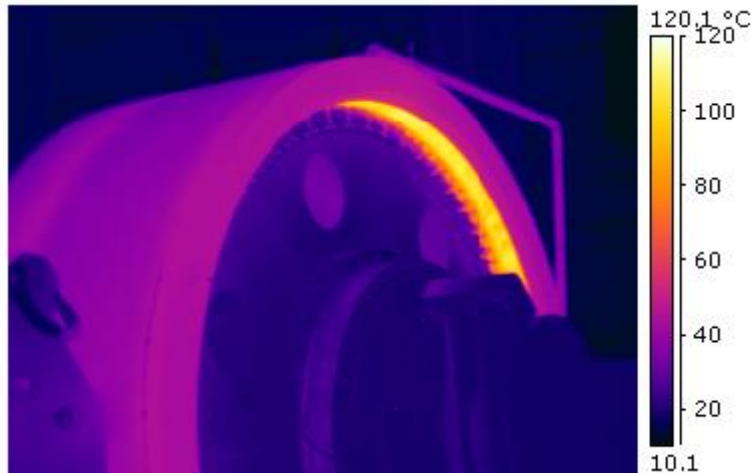


Figure 5-40. The hottest spot (120.1°C) on the upwind end of the generator was near 12:00.

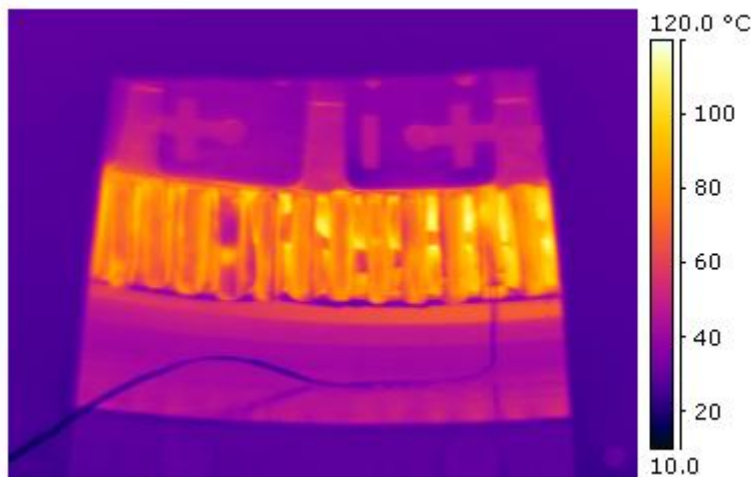


Figure 5-41. The hot spot temperatures were similar with the covers on (117.8°C), and a close-up shows that the rotor was at approximately the same temperature as the housing.

5.4.17 Frequency Response Test

The frequency response tests consist of a measurement of X_d and X_q , performed at the NWTC dynamometer facility, and a measurement of zero sequence impedance performed at the generator manufacturer's facility. Test instruments and equipment used were:

- HP3562A dynamic signal analyzer
- BOP20-20M power amplifier
- 20A LEM current sensor, with power supply, etc.
- 200A DC power supply.

Note that the 200-A DC power supply was used at NWTC to align the rotor. A similar current supply was used at the generator manufacturer's facility.

The two portions of this test are:

- D – axis impedance characteristics
- Q – axis impedance characteristics.

To measure the D-axis characteristics, the rotor must be aligned with the appropriate slot. This was done by releasing the brake on the rotor, applying a DC current from the Phase A termination to the Phase B termination. The DC current from the DC power supply was about 135 A when connected to the generator. The neutral bus bar was connected. After alignment, the rotor was locked with the brake (1,000 psi hydraulic pressure).

Using the analyzer source signal as an excitation command signal, the power amplifier excited the windings with variable-frequency AC test current. The current was varied in frequency from 10 Hz down to 0.001 Hz. Voltage and current sensor outputs were connected into the analyzer input ports. The analyzer measured the winding voltage and current to derive impedance. The Xd impedance data is shown in Figure 5-42. Corresponding inductance is shown in Figure 5-43.

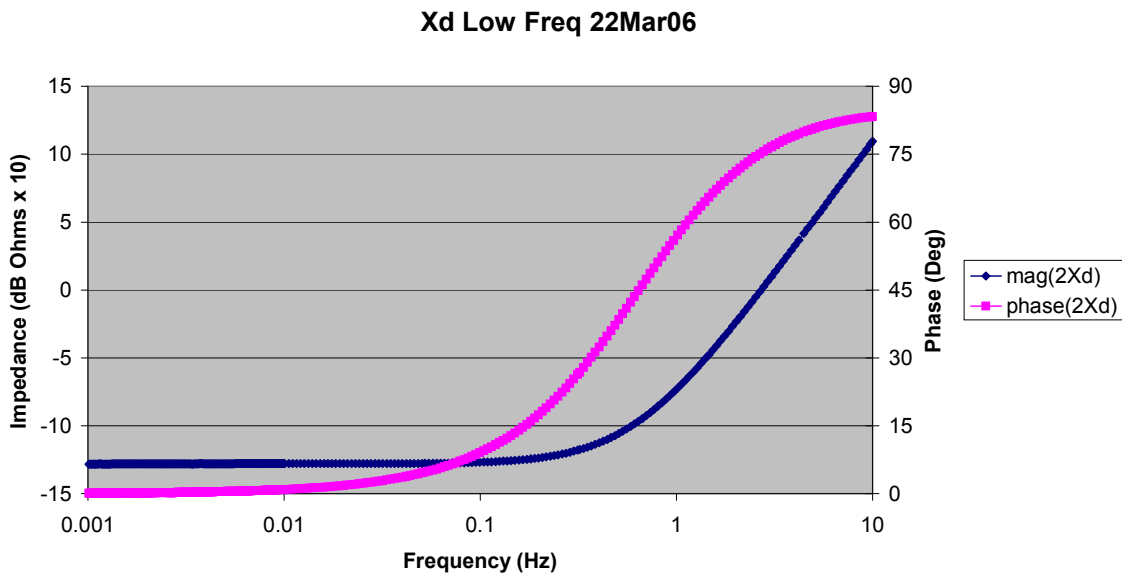


Figure 5-42. The D-axis impedance was obtained from 0.001 Hz to 10 Hz.

Ld Low Freq 22Mar06

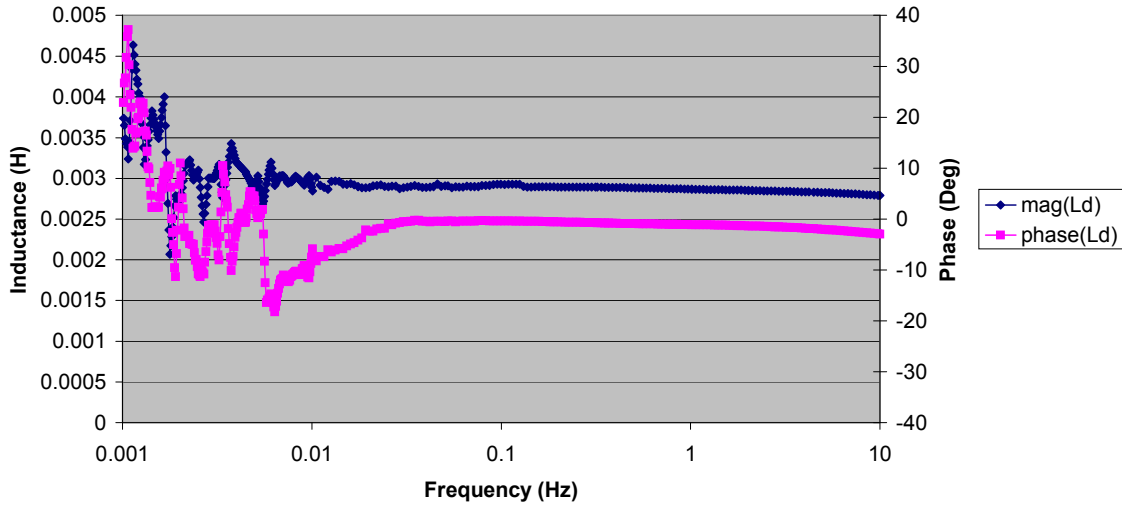


Figure 5-43. The DC D-axis inductance was 2.9 millihenry (mH).

To align the rotor for the Q-axis inductance, the current source is connected at one end to the C termination, and at the other end, phase A and phase B terminations shorted together. The brake is released, current is applied, and after the rotor has moved to its final position, the brake is applied. Results are shown in Figures 5-44 and 5-45. Data near 10 Hz was noisy due to a resonance at this frequency, and was eliminated from the plotted results. Note that this value for Q-Axis inductance is significantly higher than that calculated during the operation of the machine at rated conditions. It is well known that the value of the inductance drops as the current increases and as magnetic saturation of the stator is approached.

Xq Low Freq 22Mar06

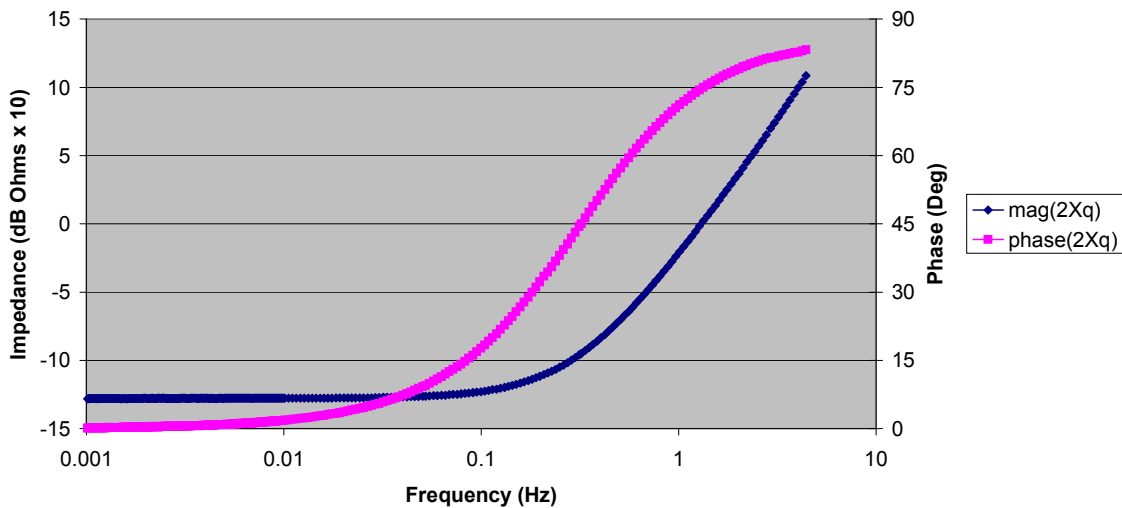


Figure 5-44. The Q-axis impedance was recorded up to 4.4 Hz to avoid noise caused by resonance near 10 Hz.

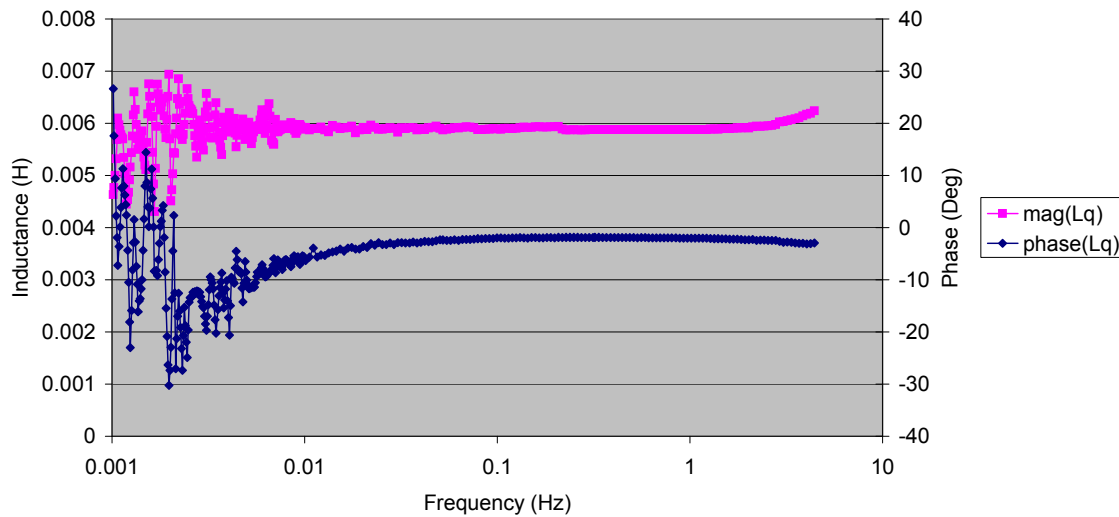


Figure 5-45. The DC Q-axis inductance was 5.9 mH.

Additional frequency response testing was done at the generator manufacturing facility as part of the Factory Acceptance Test. The Factory Acceptance Test included the X_d and X_q measurements, and common mode response measurements. In the common mode test, the phases are all excited with a current and the voltage response of the phases to ground is measured. The common mode results are shown in Figure 5-46. The response has a phase angle close to 90° , which indicates that the phases are acting like a capacitor. The response at high frequencies is important for the design of the generator termination filter and neutral point modulation system. Power converter switching excites the neutral point at the switching frequency and harmonics of the switching frequency. This test helped determine the termination filtering requirements for the generator.

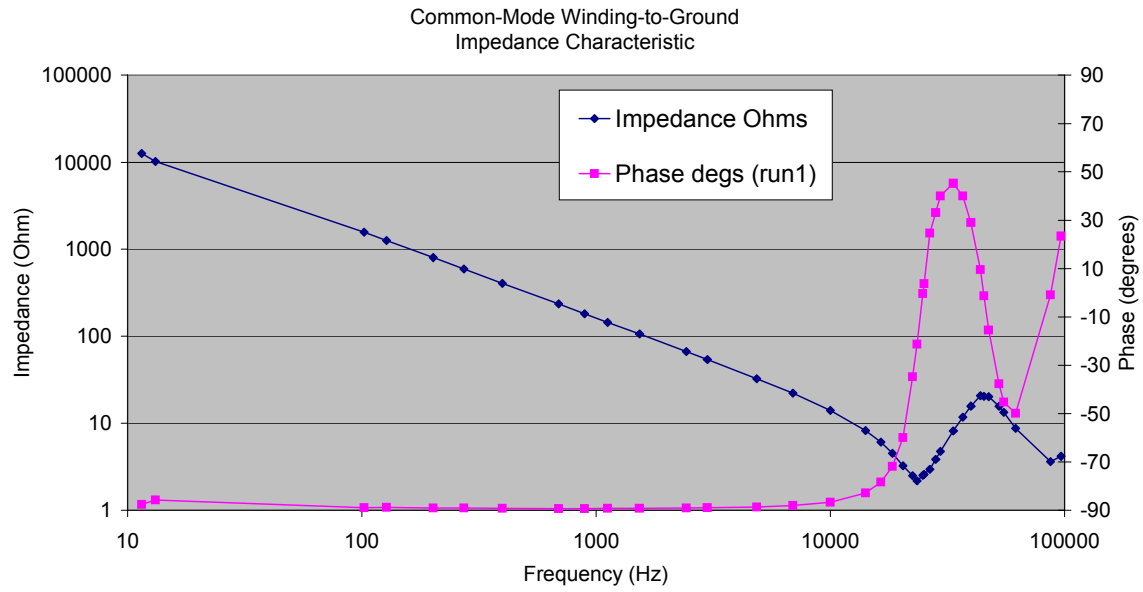


Figure 5-46. The common mode impedance was sufficiently large at the switching frequency and at the first several harmonics of the switching frequency.

6 Conclusions and Recommendations

A great deal was learned as a result of the work reported here. This learning is being applied to the next generation production design. This design, when applied in a full turbine system, will prove to be the lowest overall life cycle cost drivetrain configuration available.

6.1 Trade Study

- Two configurations were identified and designed that showed lower life cycle costs as compared to the baseline configuration: the medium-speed/single-output (MS-1) design, and the permanent magnet direct-drive (PMDD) design.
- The 5.3 m diameter PMDD design shows the lowest COE of all investigated configurations.
- The 4.0 m diameter PMDD design shows a lower COE than the baseline configuration, and may be more appealing than a 5.3 m diameter design in some markets due to shipping limitations.
- Economies of scale favor increased turbine sizes for all configurations as compared to the 1.5MW baseline configuration.
- In selecting a drivetrain configuration for further development, Northern also considered trends in material cost and the maturity level of the technology. The Northern team reached the conclusion that there was more opportunity for ongoing cost reductions for the PMDD configuration as compared to the more mature gear driven configurations, further strengthening the life cycle cost advantage of the PMDD configuration over time.
- Based on the Trade Study, Northern selected the 4.0m PMDD drivetrain configuration to build and test under this program.

6.2 Generator Performance

A comparison of predicted and measured generator performance is shown in Table 6-1. The following are general conclusions based on the results.

- The generator electrical performance was in generally good agreement with the predicted final design values, with the open circuit voltage, short circuit current, generator inductance, and output harmonic distortion within expected levels of performance.
- The generator produced its specified rated output power at 19 rpm.
- The thermal performance of the generator rotor assembly met the design requirements, with magnet and rotor temperature rise close to predictions.
- The thermal performance of the generator stator assembly was slightly below specified levels, with slightly higher temperature rise at rated output than predicted. This deviation in stator thermal performance we believe is related to the use of a simple dip coating as opposed to a complete VPI impregnation process on the completed stator due to manufacturing limitations, which reduced the thermal conductivity of the stator assembly.

- The power converter met its efficiency and harmonic distortion specifications, and was a valuable step in Northern’s development of a commercial wind power converter product.
- No vibration problems were encountered with the generator during normal operation, but the normal modes predicted for the generator did not match well with the experiments. This may be due to poor solidification of the stator/varnish system. Going forward, the models should be re-evaluated to look for possible modeling assumptions that cause the natural frequencies to increase.
- No problems were encountered with the bearing, and the bearing stiffness was close to predictions.

Table 6-1. Test Results Showed that Measured Values were Close to Design Predictions.

Parameter	Prediction or Specification	Measured Value
Open Circuit Voltage (Vrms)	437.0	441.2
Open Circuit Voltage Harmonic Distortion (%)	5% Max	3.09%
Rated Condition Hot Spot Temp (°C)	155 Max (126 prediction)	157.4 (estimated)
Rated Condition Losses (kW)	109.3	122.4 (estimated)
Rated Condition Efficiency (%)	93.8% Min	92.7% (estimated)
Rated Condition Current (Arms)	1320	1404.7 (estimated)
Rated Condition Terminal Voltage (Vllrms)	724.5	722.8
Rated Converter Harmonic Distortion (%)	None	3.15%
Rated Power Factor	0.90	0.85
Rated Q-Axis Inductance (mH)	3.9	4.1

6.3 Generator Recommendations

Northern has developed a number of generator design refinement recommendations for implementation into a production wind turbine and is currently in the process of implementing the recommendations listed here. The recommendations address two specific generator issues that arose during the WindPACT design and test program, as well as the general ongoing effort to optimize cost and performance as the DDPM configuration is scaled to larger wind turbine capacity ratings.

One issue encountered during the fabrication and test program was the difficulty in maintaining air gap concentricity during construction and transport of the generator. While we were able to overcome these issue to successfully operate the generator, this issue needs to be addressed to increase manufacturability and to reduce costs. Recommendations and current design changes underway include:

- Increasing the generator air gap.
- Stiffening and optimization of the stator structure

- Incorporation of the ability to adjust the concentricity of the rotor to the stator at final assembly.
- Using a more rigid rotor insertion fixture.

Another major issue during the test program was two separate incidents where there was a stator insulation fault, causing winding shorts to ground. The test team was able to repair the first fault, and to isolate the second fault to allow data collection to complete testing. The design team has thoroughly analyzed these faults to improve the current generator design. In this regard, the following steps are recommended:

- Using vacuum pressure impregnation on the stator.
- Design the stator assembly for cost effective vacuum pressure impregnation, which was not possible with the WindPACT design at the manufacturing facility used for that program.
- Design the stator for a cost effective post impregnation baking process; the WindPACT stator had to use an air dry varnish due to lack of availability of a suitably sized curing oven.
- Slightly reduce stator slot fill factor to increase manufacturability.
- Improved design details for the stator coil insulation system, and for the stator slot liner system.
- Improve design to allow repair of individual faulted coils.

In addition, results from the program led to specific improvements and refinements to optimize the cost of the generator. These changes include:

- Stator design modifications to allow easy transportation of generators larger than the 4.0m WindPACT design.
- Improved rotor magnet configuration that eliminates need for a stainless steel spider structure.
- Optimization of stator design to reduce required active materials, and fabrication labor cost.
- Improvements in the water jacket design that both reduce costs and increase thermal performance.

6.4 Power Converter Recommendations

The power converter prototype designed and built by Northern in support of this program was a useful stepping stone for further power converter development. Based on the work under this program and a subsequent LWST Phase I program, Northern developed a specification for an advanced MW class power converter with the following design attributes:

- High Power Density of 1,000 kVA/m³

- High Efficiency Approaching 98%
- Modular Design with Rack-out Modules
- Partial Power Operation
- Zero Voltage Ride Through Capability
- VAR Support
- Low THD < 1.5%

Northern subsequently has designed and is now commercializing a MW class power converter based on these design requirements.

6.5 *Dynamometer Assembly and Test Recommendations*

To improve the dynamometer control we recommend:

- Modifying the control system to provide better speed control.
- Modifying the safety system to prevent overspeed.

To improve dynamometer measurements we recommend:

- Calibrating the power electronics measurements as a backup to official test measurements.

The converter had voltage and current measuring devices, however, these are typically purchased uncalibrated to reduce cost. By calibrating them before the test, the accuracy of other measuring instruments can be assessed.

6.6 *Final Comments*

This program has shown that a permanent magnet direct drive generator can be produced that satisfies the requirements of a multi-megawatt wind turbine. The resulting wind turbine will have very favorable life cycle economics.

A production version of this machine is currently being designed that incorporates all of the changes noted in the recommendations with a focus on reduced production cost, and in addition is being scaled up to the 2MW power level. Concurrently, a full turbine system is being developed in the 2MW class, and a prototype will be erected in 2008. This full turbine design will prove to be the lowest overall life cycle cost drivetrain configuration available.

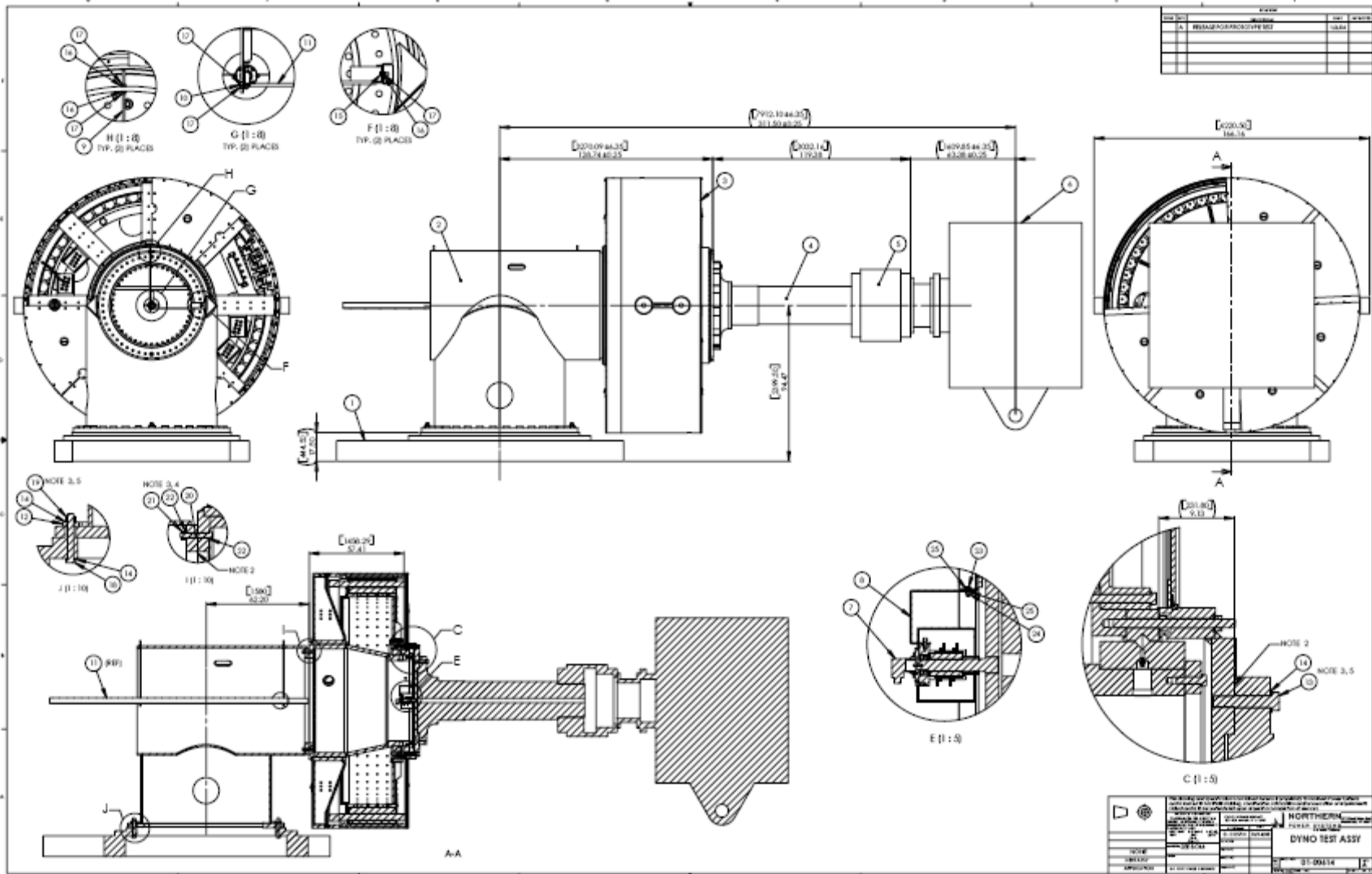
Finally, a PMDD design should be considered for marine (subsurface) applications as many of the features that make it attractive for wind turbine use also improve economics in marine applications: primarily reliability and efficiency. In addition, since thermal management is far easier underwater, a relatively more compact design may be realized.

7 References

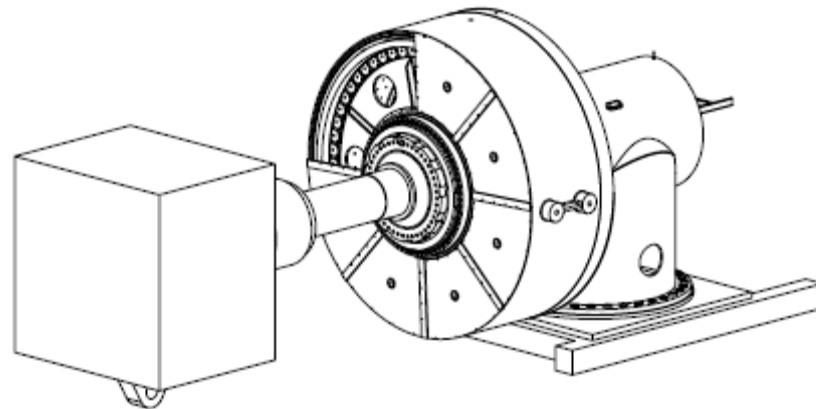
- Akagi, H. (2002). "Prospects of New Technologies for Power Electronics in the 21st Century." Presented at the Transmission and Distribution Conference and Exposition 2002: Asia Pacific, New York, NY: Institute for Electrical and Electronics Engineers (IEEE).
- Anacona, D.; McVeigh, J. (2001) *Wind Turbine: Materials and Manufacturing Fact Sheet*. Rockville, MD: Princeton Energy Resources International.
http://www.perihq.com/WindTurbine-MaterialsandManufacturing_FactSheet.pdf.
- ANSI C84.1-1995 (1995). *Electrical Power Systems and Equipment—Voltage Ratings (60Hz)*, Washington, DC: American National Standards Institute. <http://www.ansi.org/>.
- ANSI/AGMA 2001-C95 (2001). *Fundamental Rating Factors and Calculation Methods for Involute Spur and Helical Gear Teeth*, Washington, Alexandria, VA: American Gear Manufacturers Association. <http://www.agma.org//AM/Template.cfm?Section=Home>.
- ANSI/AGMA/AWEA 6006-A03 (2003). *Standard for Design and Specification of Gearboxes for Wind Turbine Generator Systems*. Alexandria, VA: American Gear Manufacturers Association. <http://www.agma.org//AM/Template.cfm?Section=Home>.
- Bauer, E. for Allianz Center for Technology (August 2001). "Risks and Damages." *Wind-Kraft Journal*. Grevenburg, Germany: Verlag Natürliche Energie. (2); pp. 66-71.
- Bohmeke, G.; Boldt, R. for Aerodyn and LDW/AEG (1997). "Direct Drive, Geared Drive, Intermediate Solutions: Comparison of Design Features and Operating Economics", Prepared for 1997 European Wind Energy Conference, Dublin, Ireland.
- BTM Consult (2001). *International Wind Energy Development: World Market Update 2000; Forecast 2001–2005*. ISBN 87-987788-1-1. Rinkobing, Denmark: BTM Consult.
<http://www.btm.dk/>.
- Buhl, M. (October, 2003). *Crunch User's Guide*. NREL/EL-500-30122. Golden, CO: National Renewable Energy Laboratory. <http://www.nrel.gov/>
- Bywaters, G. et al. (May 2004). *Northern Power Systems Alternative Design Study Report*. NREL/SR-500-35524. Work performed by Northern Power, Waitsfield, VT. Golden, CO: National Renewable Energy Laboratory. <http://www.nrel.gov/>
- Dahlgren, M. et al. (2000). "Windformer™: Wind Power Goes Large-Scale." *ABB Review* (3/2000); p.31-37. <http://www.abb.com/>.
- Electric Power Research Institute (December 1997). *Renewable Energy Technology Characterizations*. EPRI TR-109496. Palo Alto, CA: Electric Power Research Institute.
<http://my.epri.com/portal/server.pt?>
- FMCSA 49 CFR Parts 392 and 393 (2002). *Development of a North American Standard for Protection Against Shifting and Falling Cargo, Final Rule*. Washington, DC: Federal Motor Carrier Safety Administration. <http://www.fmcsa.dot.gov/cargosecurement.pdf>
- Gardner, P. et al. (1998). *Wind Energy—The Facts. Volume 1, Technology*, Brussels, Belgium: European Wind Energy Association. <http://www.ewea.org/>.
- Germanischer Lloyd (1999). *Non-Marine Technology, Part 1: Regulations for the Certification of Wind Energy Conversion Systems. Rules and Regulations, IV*. Hamburg, Germany: Germanischer Lloyd. <http://www.gl-group.com/start.htm>
- Grauers, A. (September 1994). *Design of Direct-Driven Permanent-Magnet Generators for Wind Turbines*. PhD Thesis. Goteborg, Sweden: Chalmers University of Technology. Technical Report No. 292.

- Griffin, D. (April 2001). *WindPACT Turbine Design Scaling Studies, Technical Area 1: Composite Rotors for 80 to 120m Rotor*. NREL/SR-500-29492. Work performed by Global Energy Concepts, Seattle, WA. Golden, CO: National Renewable Energy Laboratory. <http://www.nrel.gov/>
- Hau, Erich (2000). *Wind-Turbines Fundamentals, Technologies, Application, Economics*. New York, NY: Springer-Verlag.
- Hava, A. et al. (1999). "Simple Analytical and Graphical Methods for Carrier-based PWM-VSI Drives." *IEEE Transactions on Power Electronics* (14:1); pp. 49–61.
- Heffernan, R. et al. (April 1996). *Direct-Drive Wind Turbine Feasibility Study. Final report to Electric Power Research Institute*. TR-104911. Palo Alto, CA: Electric Power Research Institute. <http://my.epri.com/portal/server.pt?>
- Hendershot, J. Jr.; Miller, T. (1994). *Design of Brushless Permanent Magnet Motors*. Monographs in Electrical and Electronic Engineering, London: Clarendon Press.
- IEC 61400-1 (1999). *Wind Turbine Generator Systems, Part 1: Safety Requirements*. Geneva, Switzerland: International Electrotechnical Commission (IEC). <http://www.iec.ch/>
- IEEE 519-1992 (1992). *IEEE Recommended Practices and Requirements for Harmonic Control in Electrical Power Systems*. New York, NY: Institute for Electrical and Electronics Engineers (IEEE). <http://www.ieee.org/portal/site>
- ISO 2394 (1998). *General Principles on Reliability for Structures*. Geneva, Switzerland: International Organization for Standardization. <http://www.iso.org/iso/en/ISOOnline.frontpage>
- Jaecklin, A. (1997). "Integration of Power Components—State of Art and Trends." Paper presented at the 7th European Conference on Power Electronics and Applications. Trondheim, Norway. (1) pp. 1-6.
- Kerkman, R. et al. (1999). "AC Drives: Year 2000 (Y2K) and Beyond." Paper presented at the 14th Annual Applied Power Electronics Conference and Exposition, March 1999. Dallas, Texas. Vol. 1. pp. 28–39. New York, NY: Institute for Electrical and Electronics Engineers (IEEE). <http://www.ieee.org/portal/site>
- Lorenz, L. (1997). "Systems Integration—A Milestone for Future Power Electronic Systems." Paper presented at the 7th European Conference on Power Electronics and Applications. Trondheim, Norway. (1) pp. 10-16
- Lubas, M., U.S. Patent No. 5,952,755 (September 14, 1999).
- Pullen, A (2006). *Global Wind Energy Report*. Brussels, Belgium: Global Wind Energy Council.
- VDI2230 (1988). *Systematic Calculation of High Duty Bolted Joints with One Cylindrical Bolt*. Translation of Ed. 7. Dusseldorf, Germany: Verein Deutscher Ingenieure (VDI) Society for Product Development, Design and Marketing. <http://www.vdi.de/vdi/english/index.php>
- Weh, H.; May, H. (1988). "Achievable Force Densities for Permanent Magnet Excited Machines in New Configurations." Technical paper presented at ICEM, September 1988. Braunschweig, Germany: Technical Institute of Braunschweig.
- Windstats Newsletter, (Autumn, 2002). "Direct Drive Turbines." *Windstats Newsletter*, Knebel, Denmark. pp. 6. <http://www.windstats.com/>

Appendix A – Generator Design Drawing



ITEM NO.	QTY.	PART NO.	WEIGHT(kg)	DESCRIPTION
1	1	NONE		TURRET BASE
2	1	01-00624	5546	TEST TURRET ASSEMBLY
3	1	01-00632	41006	TEST GENERATOR ASSEMBLY
4	1	900033E	6397	MAINSHAFT
5	1	MB-220265	3277	COUPLING
6	1	NONE		DYNO MOTOR
7	1	01-00626	12	SLIP ENCODER ASSY
8	1	02-00425	1	ANTI-ROTATE TAB
9	2	05-00854	1	TRAY HANGER ROD, M12X1.75X1m.
10	2	38-01484	0	HANGER CLAMP, P-W# 9985-1899-01
11	1	01-00633	46	CABLE TRAY ASSY
12	34	02-00407	3	WASHER
13	44	05-00929		M36X4X180 HEX CAP, GR. 8.8, BLK.
14	112	05-00928		M36 FLAT WASHER, CASE HARD, BLK.
15	2	05-00893		M12X1.75X35 HEX CAP, 18-8 SS
16	8	05-00876		M12 FLAT WASHER, 18-8 SS.
17	10	05-00803		M12X1.75 HEX NUT, 18-8 SS
18	34	05-00926		M36X4X280 HEX CAP, GR. 8.8, BLK.
19	34	05-00927		M36X4 HEX NUT, GR. 8.8, BLK.
20	48	05-00925		M27X3X180 HEX CAP, GR. 8.8, BLK.
21	48	05-00857		M27X3 HEX NUT, GR. 8.8, BLK.
22	96	05-00856		M27 FLAT WASHER, CASE HARD, BLK.
23	2	05-00574		M8X1.25X25 HEX CAP, 18-8 SS
24	2	05-00405		M8X1.25 HEX NUT, 18-8 SS
25	4	05-00795		M8 FLAT WASHER, 18-8 SS



REV.	DESCRIPTION	DATE	APPROVED
A	RELEASE FOR PROTOTYPE TEST		

NOTES:

1. FULL FASTENER PATTERNS NOT SHOWN FOR CLARITY.
2. THE FLANGE MATING 'FACES' MUST BE CLEANED WITH WIRE BRUSH TO ROUGHEN SURFACE AND SOLVENT CLEAN PER SSPC-SP1 TO REMOVE ANY OIL OR WATER FROM THE SURFACE PRIOR TO JOINING
3. OIL REQUIRED ON SCREW THREAD AND UNDER HEAD OF FASTENERS. WIPE OFF EXCESS OIL TO PREVENT DRIPS FROM PENETRATING INTO FLANGE.
4. TORQUE 27 mm FASTENERS TO 1550 Nm.
5. TORQUE 36 mm FASTENERS TO 2600 Nm.
6. TORQUE 12 mm FASTENERS TO 51 Nm.
7. TORQUE 8 mm FASTENERS TO 15 Nm.

	This drawing and specifications contained herein is proprietary to Northern Power Systems and is loaned to facilitate bidding, construction, fabrication and/or execution of requirements stated and it to be surrendered upon request or completion of services.	
	INTERPRET DIMENSIONS & TOLERANCES PER ANSI Y14.5 UNLESS OTHERWISE SPECIFIED DIMENSIONS ARE IN MILLIMETERS TOLERANCES ARE AS SHOWN FINISHES: GR. 8.8, BLK. N/A 20-02 20-03	CAD-DRAWING ORIGNAL DO NOT MANUALLY EDIT
NONE	SEE BOM	NORTHERN POWER SYSTEMS DYN0 TEST ASSY
NEXT ASSY	APPROVALS: DATE: 10/14/00 DESIGNED: D. COSTIN	PART NO. 01-00614 REV. A
APPLICATION: DO NOT SCALE DRAWING	CHECKED:	DRAWN:

Appendix B – Dynamometer Test Assy Drawing

Appendix C - Detailed Design Document

This appendix includes a detailed structural summary for the generator and the dynamometer assembly. It will include data that we would like to keep proprietary. Every major component and system was analyzed in order to determine that it would function in the design. This section describes the analysis results and the details of the designs.

C.1 Generator Structural Design

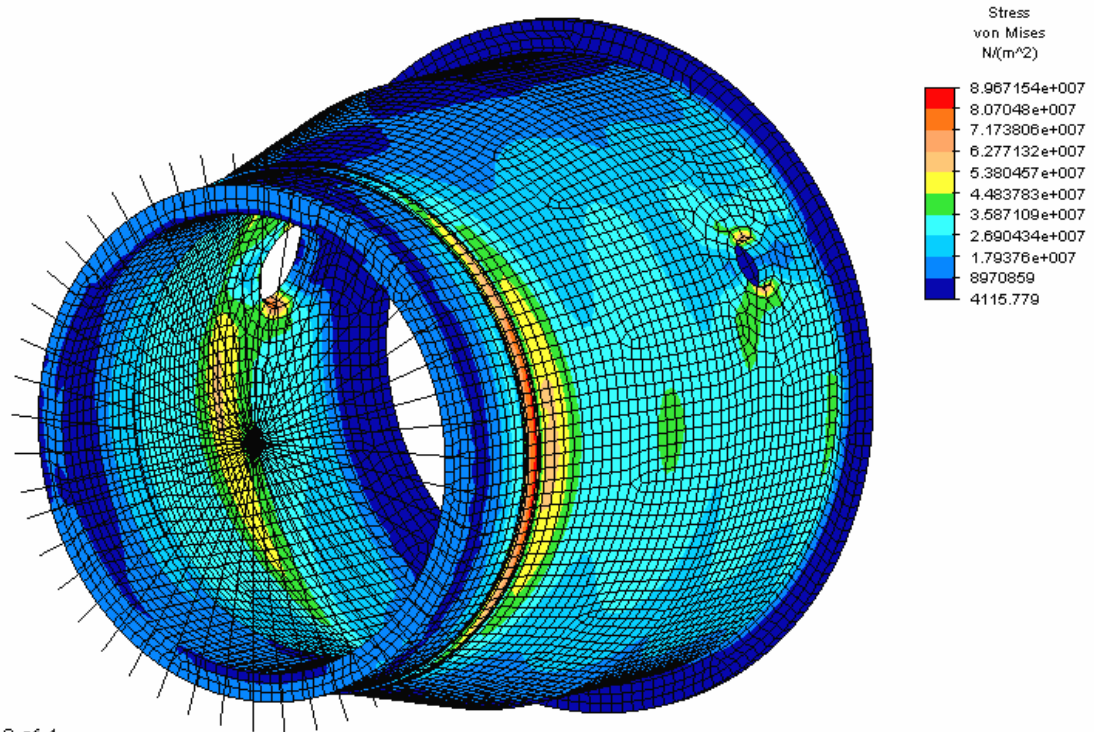
Each critical structural component was analyzed to determine its safety and function when subjected to the applied loading. The structural analysis is divided into four categories: stress analysis, deflection analysis, bolted joint analysis, and vibration analysis. The analysis was performed using a variety of tools. Finite element models were used for most major structural components. The stresses from the models were input to spreadsheets to determine static and fatigue reserves. Bolt analysis following the VDI 2230 standard was done with a spreadsheet. Analysis was done for the following parts and systems:

- Structural Analysis
 - Spindle Stress Analysis
 - Stator Stress Analysis
 - Rotor Stress Analysis
 - Spider Stress Analysis
 - Brake Bracket Stress Analysis
- Stackup and Deflection Analysis
- Bolted Joint Analysis
- Vibration Analysis
- Bearing Analysis
- Generator Cooling System Analysis.

C.1.1 Structural Analysis

C.1.1.1 Spindle Stress Analysis

The static and fatigue analysis of the major structural components was done using finite element models. In most cases, these were welded structures. To simplify the analysis, full-penetration welds were specified so the same fatigue category could be used throughout the part. The finite element model of the spindle is shown in Figure 3-5. It shows a maximum stress of 89.7 Megapascals (MPa) for the most severe ultimate load case. Spreadsheet analysis, utilizing the partial load factors for loads and materials and the material yield stress, indicate a static reserve of 2.53 (1.0 being a safe design). Also, unit loads were applied to the finite element model, and these stress functions were input to a fatigue analysis, based on the load spectrums for pitch and yaw bending moments. The analysis showed a fatigue reserve of 1.44 (1.0 being a safe design). Thus the design is safe for both static and fatigue loads. Note that the highest stress is near the end of the bearing land. Particular attention was paid to the relief of this corner in the design to avoid a sharp corner.



Load Case: 2 of 4
 Maximum Value: 8.96715e+007 N/(m²)
 Minimum Value: 4115.78 N/(m²)

Figure C-1. The spindle was analyzed using finite element analysis to determine the correct thickness to carry blade rotor moment loads.

C.1.1.2 Stator Stress Analysis

The critical loading for the stator outer frame is the lifting of the generator. The generator can be lifted with the axis vertical or horizontal. With the axis vertical, it can be lifted with the spider side up or down. Thus there are three major load cases to evaluate. All of these load cases are for ultimate loads only. No fatigue failures are expected for this part. The torque load is very small relative to the overall section thickness of the part. Based on finite element analysis, the lifting with axis horizontal is most critical. A maximum stress of 139.5 MPa was calculated, leading to a margin of safety of 1.13 relative to the yield stress of A36 material. This analysis was calculated with no contribution of stiffness due to the waterjacket or stator, making the analysis conservative. The body force of the stator and waterjacket were applied with a surface force on the inside diameter of the stator outer frame.

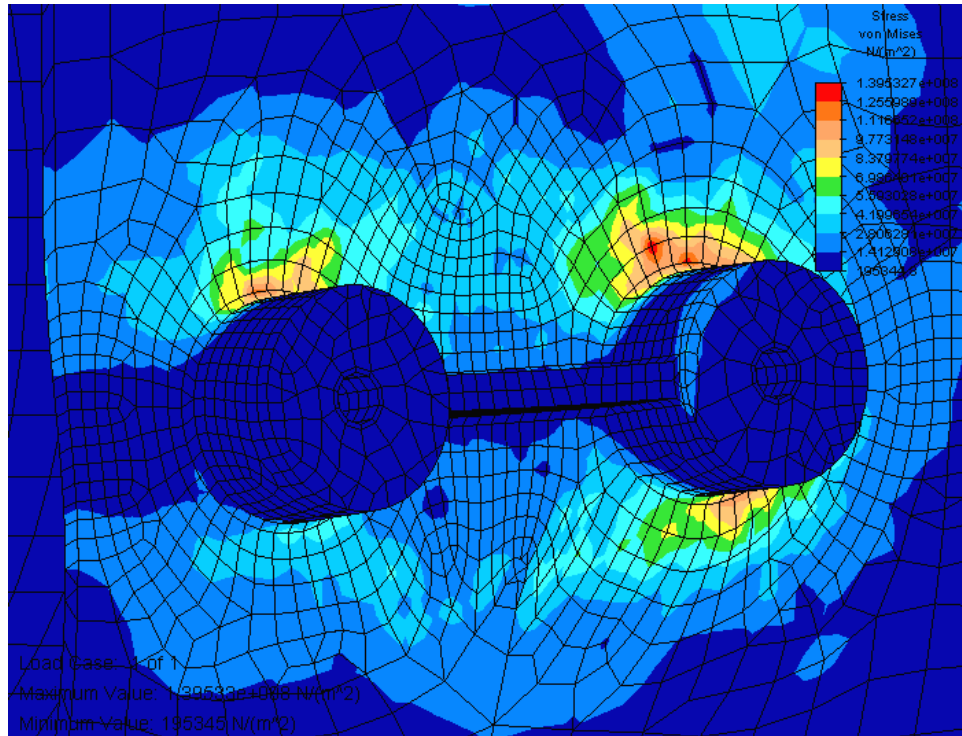


Figure C-2. The generator frame was sized based on the stresses due to lifting.

C.1.1.3 Rotor Stress Analysis

For the rotor, extreme and fatigue torque loading is nearly equally critical. Extreme loading is caused by short circuit conditions. The fatigue loading for the rotor is the torque applied during normal operation at rated conditions. No mechanical brake loading is allowed during operation. Ultimate and unit stresses were calculated with a finite element model, shown in Figure C.3. Ultimate loads created a stress of 28 MPa with a margin of safety of 8.12. Unit stresses were input into a spreadsheet containing the rotor torque load spectrum, and the expected life was calculated. The resulting fatigue reserve is 9.39. Thus the rotor is very safe for both extreme and fatigue loads. This part is not necessarily over-designed, however, because deflection of the rotor from imbalanced magnetic forces is more critical. This loading was calculated using an electromagnetic model that predicted the rotor radial imbalance force associated with a 0.5-mm offset of the rotor to the stator. This represents that worst-case gap condition that is within the specified air gap tolerance of the generator. Because this load is applied once per revolution, regardless of the speed or power level, the number of cycles is very large (>20 million). Thus calculation of fatigue margin relative to the cut-off limit of the material is appropriate. The margin of safety relative to the cut-off limit is 1.15.

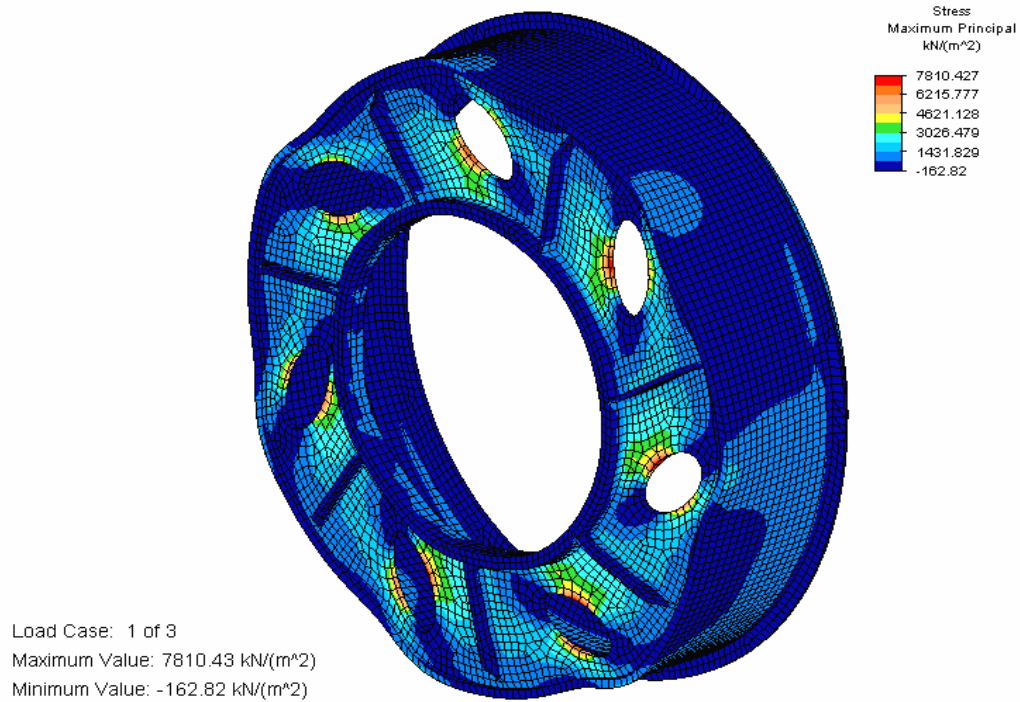


Figure C-3. The rotor was analyzed using finite element analysis to determine the proper sizing of the structure.

C.1.1.4 Spider Stress Analysis

The spider is subject to extreme torque due to dynamic braking, extreme torque due to rotor lock pin loads, and fatigue torque loading due to normal operation. Ultimate and unit stresses were calculated with a finite element model, shown in Figure C.4. The rotor lock ultimate stress was 196 MPa with a margin of safety of 1.09. This margin is safe, but relatively low due to localized stresses near the lock pin. Stresses due to extreme operating torque were lower. Unit stresses were input into a spreadsheet containing the rotor torque load spectrum, and the expected life was calculated. The resulting fatigue reserve is 1.93. Thus the spider is safe for both extreme and fatigue loads.

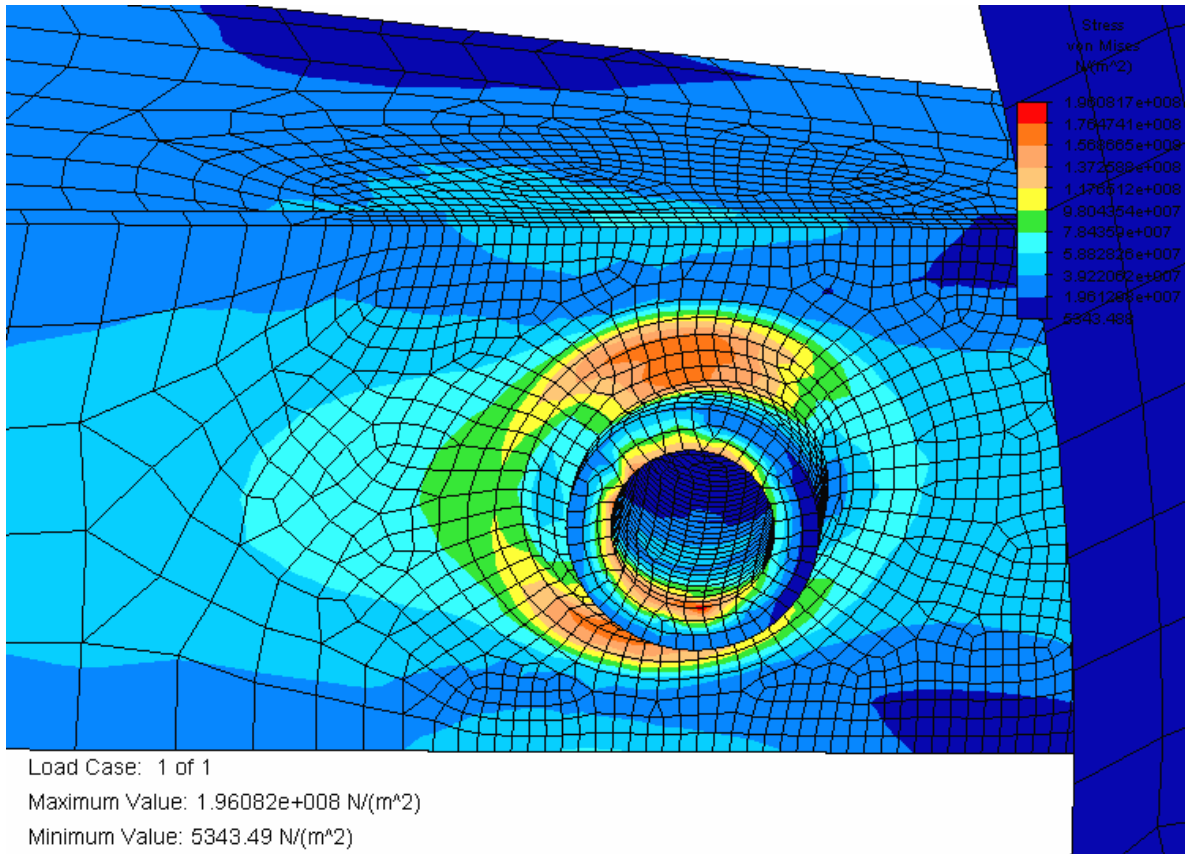


Figure C-4. The spider was analyzed using finite element analysis to determine proper sizing of the spider arms.

C.1.1.5 Brake Stress Analysis

The spider and service brake brackets are subject to extreme torque due to service brake loads. A finite element model was created and individual loads were applied to each brake bracket, as shown in Figure C.5. The service brake ultimate stress was 167 MPa, with a margin of safety of 1.28. This stress was located at the interface between the brake bracket and the spider arms. Thus the spider and brackets are safe for this failure mode.

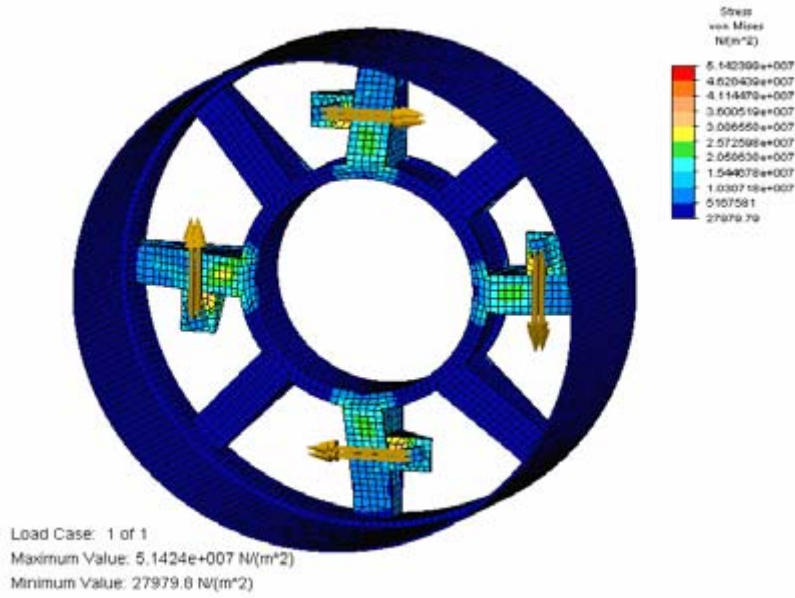


Figure C-5. The brake system was analyzed with finite element analysis to determine proper sizing of the brackets and spider arms.

The reserves for the most critical components are shown in Figure 3.6. All static and fatigue reserves are greater than 1.0. There were three critical failure modes (reserves close to 1.0). First, the stresses due to lifting the generator were very high. This design was difficult due to the size of the large lifting bosses relative to the 1.0-inch plate. Another area of concern was the rotor fatigue. If the rotor is installed eccentric to the stator by 0.5 mm, a fairly large electromagnetic imbalance force is created. This imbalance force is applied for every cycle of turbine rotation. This failure mode was not thought of until after the design was completed, thus the rotor was not optimized to minimize stresses due to this load. A third issue in the design was the rotor lock pin in the spider arm. In the high wind speed condition during service, the load from the lock pin comes close to yielding the stator.

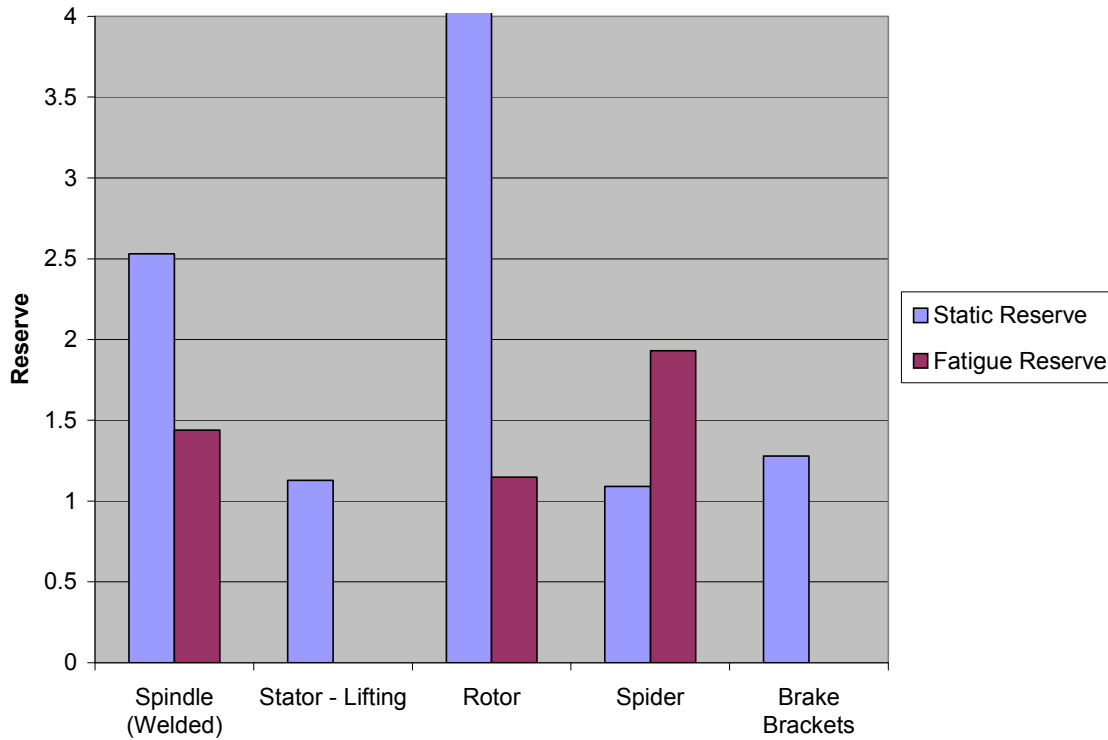


Figure C-6. The summary of structural analysis shows that static and fatigue reserves were adequate (Safe designs >1).

C.1.2 Stackup and Deflection Analysis

The generator performance is highly dependent on the size of the air gap between the rotor and the stator. If the air gap is too large, the torque will be low. If the air gap is too small, the voltage may be too high. If the air gap is too non-uniform, the power quality may be poor, and the imbalance forces may cause excessive fatigue loads on the generator. To verify that the design will have an acceptable air gap, deflection analysis is needed. First, the load deflections are predicted using finite element analysis, as shown in Figure C-7. Second, the position of components due to manufacturing variation is predicted. These aspects are combined into a unified analysis of the as-built configuration, as compared to the allowable variation of the air gap between the rotor and the stator.

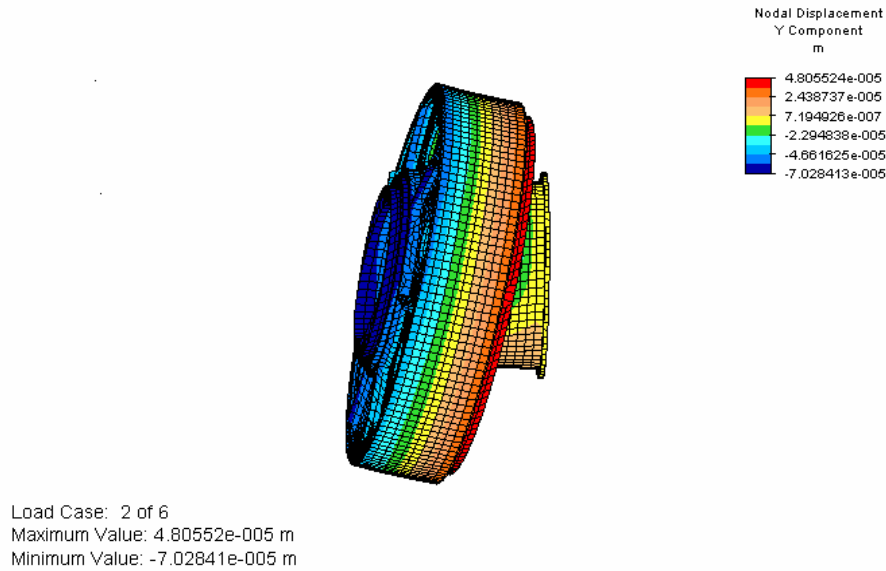


Figure C-7. The deflection of the rotor was calculated to determine the effect on the gap.

The deflections of the rotor relative to the stator are shown in Figure C.8. The main source of deflection is due to the rotor blade moments passing through the spindle of the generator. This causes rotation and translation of the generator rotor. Also, a portion of the deflection is due to gravity (or earthquake) loads on the rotor and stator. It can be seen from Figure C.8 that there are two allowables for deflections. First, there is an allowable for normal operation of the generator during power production (based on +/- 10% of the mean air gap dimension). This allowable is based on power quality and fatigue loading requirements. Second, there is an allowable for extreme winds, when the generator is not producing power. In this case, the allowable is based on keeping the rotor from touching the stator. Figure C.8 clearly shows that the deflections are less than the allowables in all cases.

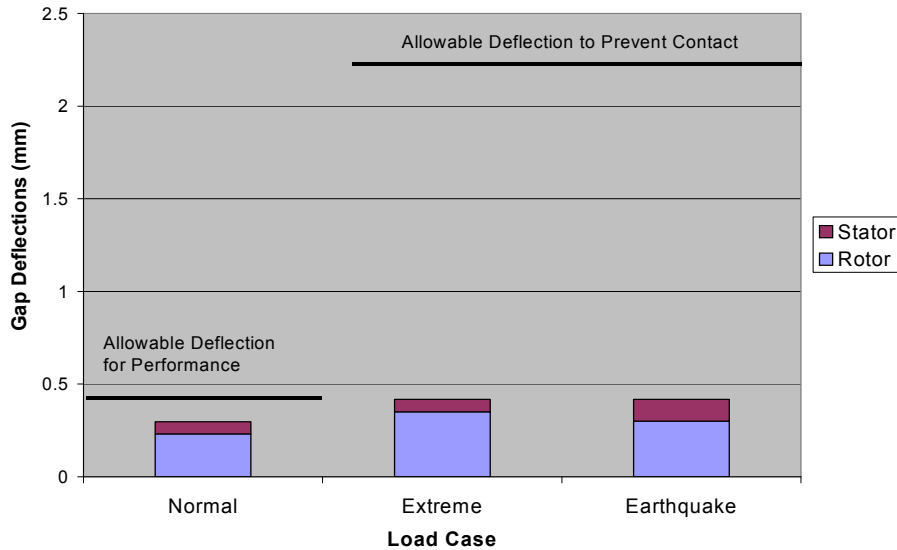


Figure C-8. Analysis shows that the deflections are within specified limits when manufacturing tolerances are neglected.

Another issue relative to the air gap is the manufacturing tolerances required to maintain the air gap within specifications. The manufacturing method for the generator calls for the bearing land on the spindle to be machined concentric to the inner diameter of the stator. Thus the major contributors to variation are the stator inner diameter, spindle (bearing land) concentricity, bearing concentricity, rotor concentricity, the rotor hub outer diameter, and the pole thickness, as shown in Figure C-9. This analysis shows that the variation due to manufacturing tolerances is also less than the allowable, which is +/- 10% of the mean air gap dimension.

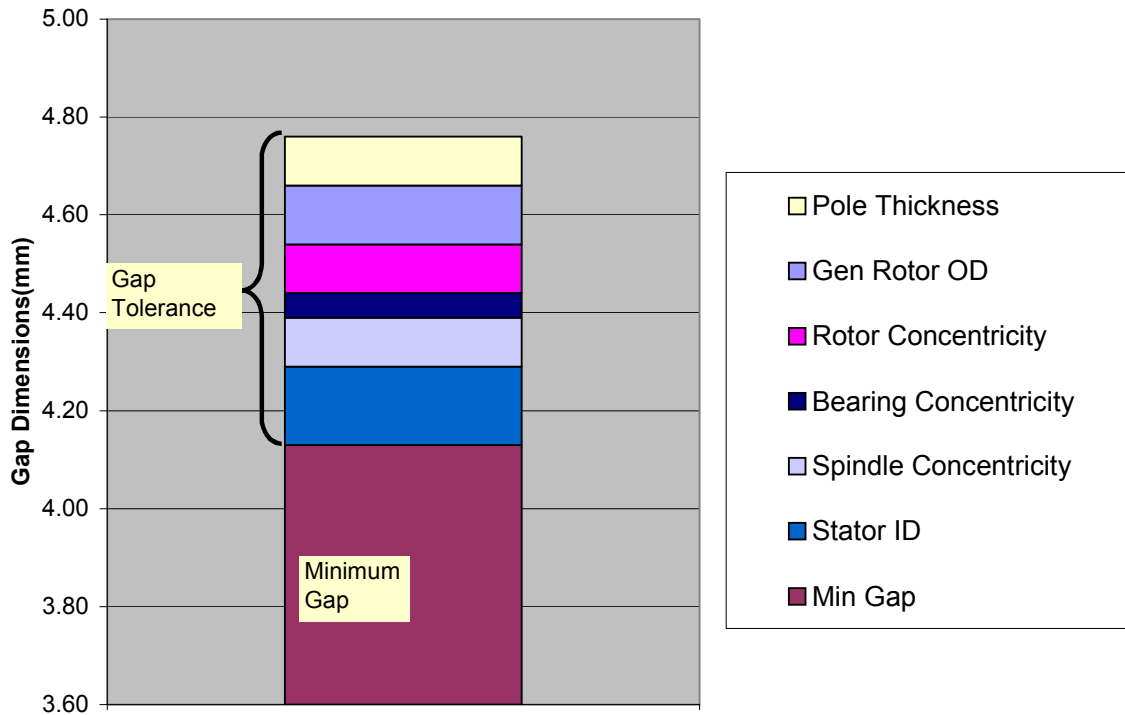


Figure C-9. The stackup analysis of the gap showed the major sources of variation.

The resulting gap variation for operational deflections and manufacturing variations is +/-14%. The target was +/-10%. This design was accepted because it was unlikely that the gap variation could be improved without adding significant additional cost. It was also possible that the power quality issues and imbalance loads due to a +/- 14% air gap could be insignificant.

C.1.3 Bolted Joint Analysis

The bolted joints were analyzed with a VDI2230 spreadsheet. Static and fatigue reserves, shown in Figure C-10, indicate that all designs are safe. The joints that carry a large torque load, in order to prevent slipping, require a wire brush or flame treatment to achieve a coefficient of friction of 0.3. All torque joints were analyzed with regard to the tightening system. The more accurately the bolt can be preloaded, the safer the design. All joints that carry torque only (generator rotor to main bearing, stator to spider) are designed to be safe using torque wrench tightening. All joints in bending require hydraulic tension or controlled rotation tightening in order to be safe. Washers are required for all bolts and nuts in order to prevent denting of the substrate material. Thread friction coefficient of 0.12 is assumed for all bolts. This means that lubrication of the fastener must be in place during tightening. The fatigue reserve is mainly based on the bolt tensile force due to fatigue loading. Because torque joints do not have a tensile fatigue loading, no fatigue reserve is calculated. For the bending joints, the reserve mainly

depends on the relative stiffness of the flanges and the bolt. Thicker flanges are better. The main bearing fatigue reserves are a little lower than for the Spindle-Turret due to the rotating loads on the main bearing. The static reserve for bolts is difficult to define. Failure is defined as a one-sided separation of the two flanges. The static reserve is defined as the yield force of the bolt divided by the sum of the preload and bolt load. Because the preload for a given bolt is normally much larger than the bolt load, and the preload for a bolt is dependent on the bolt more than the load, the static reserves for a passing bolt are usually about 1.3.

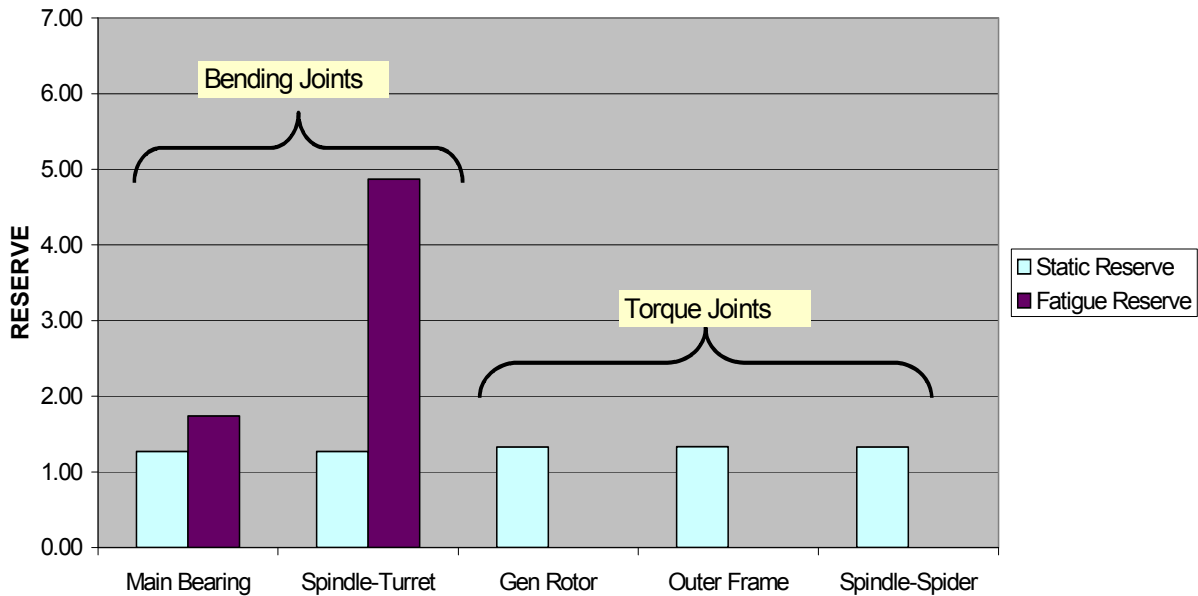
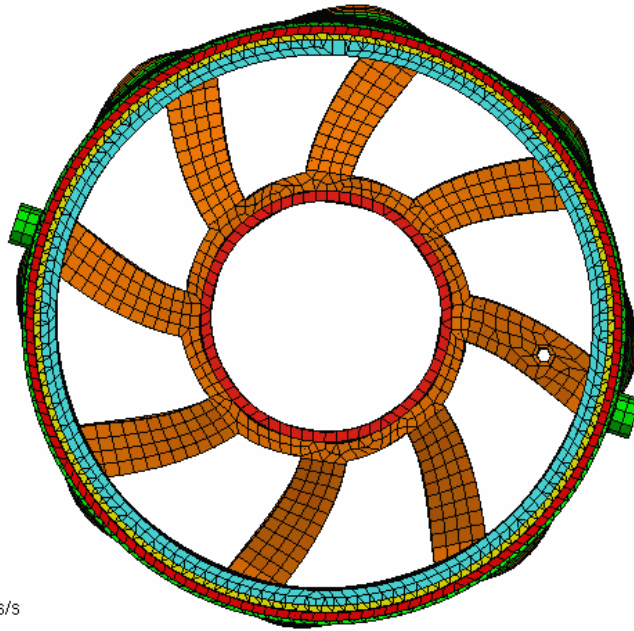


Figure C-10. The bolted joints for all major structural connections were safe.

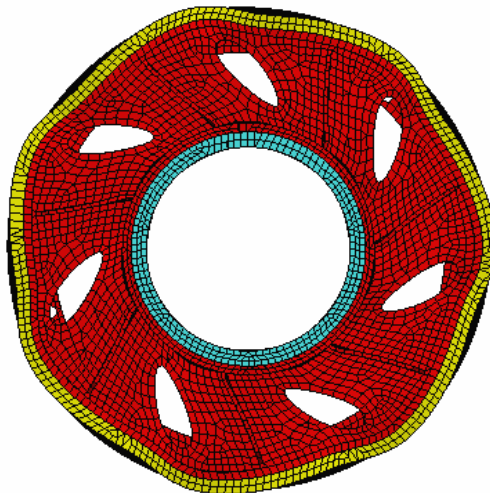
C.1.4 Vibration Analysis

A normal modes analysis was performed to ensure that the generator would not have damaging vibration during operation. This analysis was performed on the rotor and stator independently. The fundamental torsional mode shapes for the stator and rotor are shown in Figures C-11 and C-12. The main forcing functions of the generator are radial and torsional in nature, and are related to the rotational frequency, generator electric frequency, and slot passing frequency. These values for rated conditions are shown in Table C-1. It seems that the rotor frequency and electric frequency are far below the natural frequencies of the rotor and stator, and should not cause any problems. The slot passing frequency is on the same order of magnitude with the rotor and stator natural frequencies, and thus may be of concern. The analysis shows a wide degree of separation of the forcing and natural frequencies. Vibration issues are very difficult to foresee, however, due to the effects of the stiffnesses of mating structures, and the possibility of forcing functions due to electromagnetic sources. This situation will be monitored closely in the dynamometer tests.



Mode: 3 of 10
Frequency: 46.5345 cycles/s
Maximum Value: Not Available
Minimum Value: Not Available

Figure C-11. The normal modes analysis of the stator showed a torsional natural frequency of 46.5 Hz.



Mode: 6 of 10
Frequency: 149.935 cycles/s
Maximum Value: Not Available
Minimum Value: Not Available

Figure C-12. The normal modes analysis of the rotor showed a torsional natural frequency of 149.9 Hz.

Table C-1. Forcing and Torsional Natural Frequencies at Rated Conditions

Parameter	Value
Rotor Speed	19.65 RPM
Rotor Frequency	0.33 Hz
Electric Frequency	9.17 Hz
Slot Passing Frequency	110.0 Hz
Rotor Torsional Natural Frequency	149.9 Hz
Stator Torsional Natural Frequency	46.53 Hz

C.1.5 Main Bearing Analysis

Two main bearings were designed. The Timken bearing was designed for the wind turbine application, and the Avon bearing was designed for the dynamometer test only.

The loads for the Timken bearing were specified in the loads document. The loading histogram for the wind turbine application is complicated because events need to be binned by thrust level, radial force level, moment level, and speed. For each of 114 bins, the thrust, radial force, moment, speed, and duration were input into the life calculation model.

The Timken bearing and Avon bearing are shown in Figure C-13.

For the Avon bearing, the static and fatigue loads are the same as shown in Table C-2. This is because the only loading is due to the overhanging moment caused by the weight of the main shaft. Static capacity and fatigue life were calculated by the supplier. The static loads are insignificant relative to static capacity. Predicted life is based on continuous operation at 20 RPM. The life of 2.1 years is considered sufficient for the dynamometer testing.

Table C-2. The Avon Bearing was Analyzed to Determine that the Life Would be Adequate for the Duration of the Dynamometer test.

Parameter	Value
Static & Fatigue Loads	
Radial	23.5 kN (52804 lb)
Moment	115.5 kNm (85,200 ft-lb)
Static Capacity	
Radial	1432 kN (321,556 lb)
Moment	945 kNm (828,139 ft-lb)
Life at 20 RPM	18,460 hrs (2.1 years)

The main bearing for the turbine is a double-row, tapered roller bearing. The life of each row is calculated separately, given the loads for a Class II turbine. Timken calculated the life, using the SYSx calculation program. Results are shown in Table C-3. Catalog L10 life is typically calculated for bearings, but it corresponds to a reliability of 90%. Thus 10% of the bearings can

be expected to fail before the L10 life is complete. The Timken bearing can be expected to have a 97.7% reliability at 20 years for Class I loads, and a 98.0% reliability at 20 years for Class II loads. Thus less than 3% of the bearings are expected to fail before 20 years.

Table C-3. The Timken Double-row Tapered Roller Bearing was Designed to Meet the 20-year-life Requirements of the Turbine Application.

	Bearing Position	Catalog Life L10 Hours (yr)	20 year Reliability %
Class I Loads	Outboard	731,000 (83.4)	97.9
	Inboard	938,000 (107.1)	99.8
	System	516,000 (58.9)	97.7
Class II Loads	Outboard	793,000 (90.5)	98.1
	Inboard	1,125,000 (128.4)	99.9
	System	582,000 (66.4)	98.0

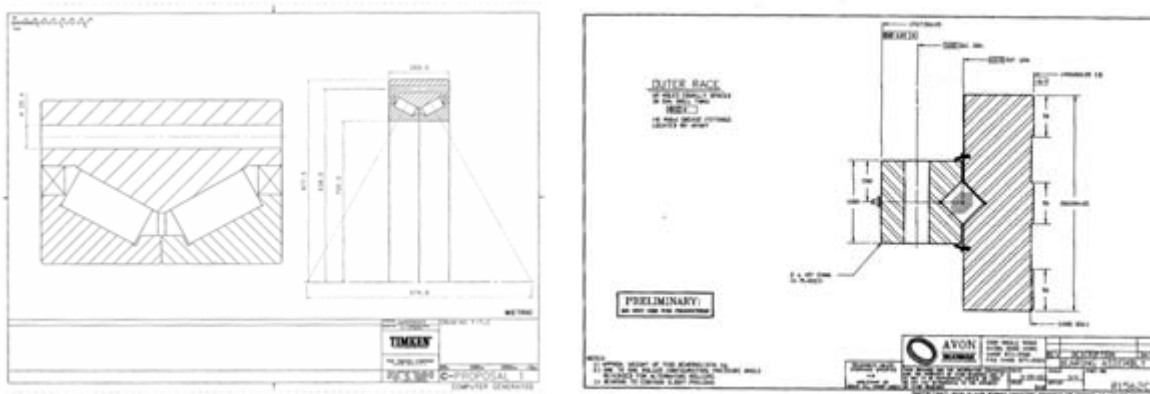


Figure C-13. The crossed roller bearing was used instead of the double-tapered roller bearing to reduce the cost of the dynamometer prototype.

The verification of the parking brakes was performed by Svendborg. Calculations were made to ensure that the selected brake caliper could safely carry the required torque at the pressures delivered by the selected hydraulic system. The brake brackets were also analyzed using finite element analysis, and determined to have an acceptable margin of safety. See section C.1.5.

C.1.6 Generator Cooling Analysis

The cooling system was analyzed by GDEB. For rated conditions, the temperatures are as shown in Table C-4. Of critical concern is the temperature of the windings. To obtain the required life of 20 years, the temperatures were kept below those specified for Class F insulation. This is because the typical class rating for insulation is based on a life of 20,000 hours (about 2.5 years), which is insufficient for a wind turbine. The magnet temperature must be kept low to obtain adequate efficiency because the magnetic flux is reduced with higher temperatures. At a temperature of 155°C, the magnet becomes permanently de-magnetized; however, this is well

above normal operating temperatures for this generator. The maximum desired coolant temperature is specified at 50°C for this analysis, but the actual coolant flow rate will probably be higher than 40 GPM, providing additional safety for the overall cooling system design.

Table C-4. The Generator Cooling System was Designed to Keep the Winding Temperatures Lower than 155°C.

Parameter	Value	Allowable Value
Heat Rejected	109.25 kW	N/A
Winding Temperature in Stator Slot	114 °C	155 °C (Class F)
Winding Temperature in Coil Extension	126.4 °C	155 °C (Class F)
Magnet Temperature	50 °C	155 °C (Magnet Material)
Coolant Temperature at Inlet	40 °C	N/A
Coolant Temperature at Outlet	50 °C	N/A
Coolant Flow Rate	40 GPM (2.52 liter/s)	N/A
Coolant Pressure Drop	19 psi (1.31 bar)	N/A

The generator was designed to produce rated power in a 30°C ambient air environment. This condition was chosen so that the generator would not be overly expensive, and would not waste power by shutting down on hot days. In a typical application, hot days do not correlate with windy days. Also, the machine is designed to provide at least 84% of rated power when the ambient air temperature rises to 50°C. Also, the generator is protected with numerous thermocouples, so the generator will even run in ambient temperatures above 50°C at lower power levels.

C.2 Dynamometer Structural Design

Some modifications to the generator design were made for the dynamometer assembly. First, the front seal on the generator was eliminated. This seal is not necessary for an indoor environment. Also, the removal allows the passage of wires needed for test sensors. Second, the double-tapered roller bearing was replaced with a crossed roller bearing. This was done simply as a cost saving measure.

Several parts were designed to mate the generator with the existing dynamometer components. Instead of a blade rotor hub, a hub adapter component was connected to the main shaft of the dynamometer. Also, a test turret connects the downwind side of the generator to the test bedplate. These parts are shown in Figure C-14. Lifting plates were designed to attach to the generator bosses to allow lifting and rotating the generator. A finite element analysis, such as that shown in Figure C-15, was performed on these parts to determine a reserve for both static loading and fatigue loading. Resulting static and fatigue reserves are shown in Figure C-19.

The main issue to resolve with the design for the dynamometer is the alignment and positioning of the generator. It is very important not to overload the coupling and bearing by misalignment. Oversized holes were used in the base of the test turret to allow some adjustment of position to be made. Special thick washers were made to bridge the large holes. A separate set of loads was

used to size the hub adapter and turret. The weight of the overhanging shaft and the applied torque were considered. The fatigue loads are based on the operating torque of the generator being applied for 1 year of continuous testing. Also, deflections of the shaft during loading were calculated to ensure that the coupling would not be overloaded. The predicted deflection of the shaft is less than the allowable shaft misalignment.

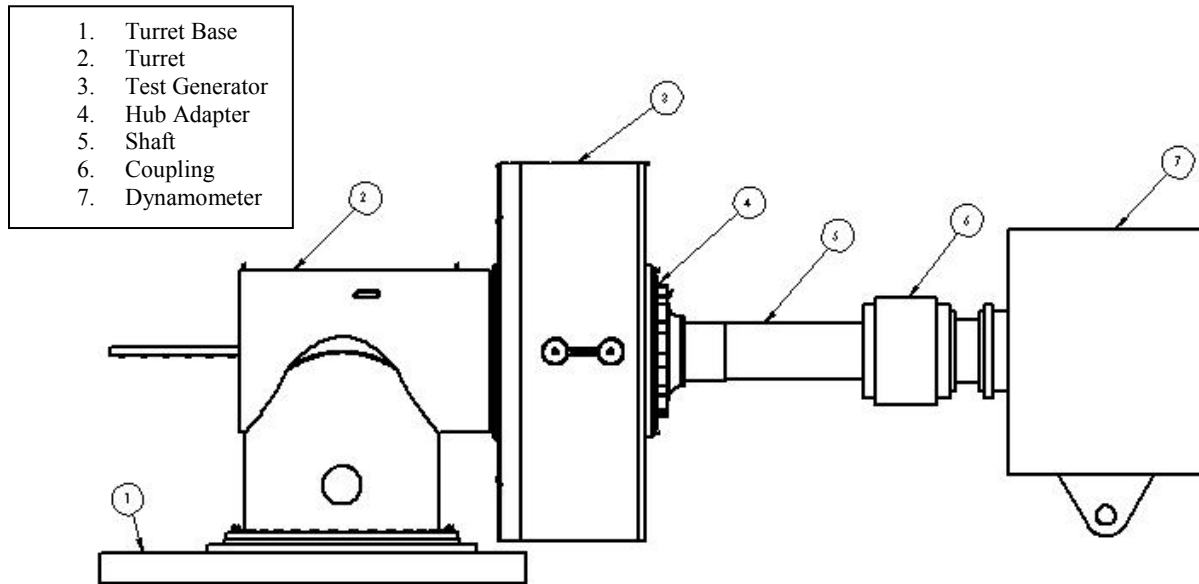


Figure C-14. Dynamometer test layout.

C.2.1 Test Turret Stress Analysis

The test turret was analyzed for extreme loads due to the weight of the generator and shaft, and for torsional fatigue loads due to testing. The von-mises stress for extreme loads was 150 MPa, providing a margin of safety of 1.42, as shown in Figure C-14. Fatigue loads led to a fatigue reserve of 2.15, based on a 20-year life. Displacements were calculated based on the deflection and rotation at the center of the flange connecting to the generator. Assuming a rigid shaft, the deflection of the end of the shaft was calculated, as shown in Figure C-15. The deflection at the coupling was 7.3 mm. This compares to the allowable coupling misalignment of 5.2 mm; however, the extreme loads are mainly due to gravity, so the coupling can be aligned to the deflected shape.

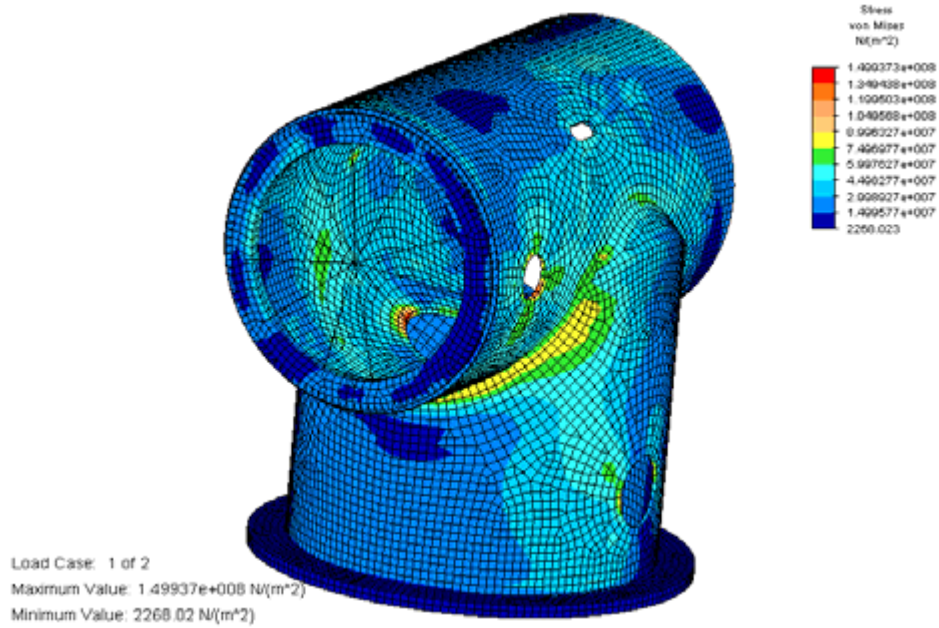


Figure C-15. Finite element analysis was performed on the dynamometer test turret to ensure it would survive test loads.

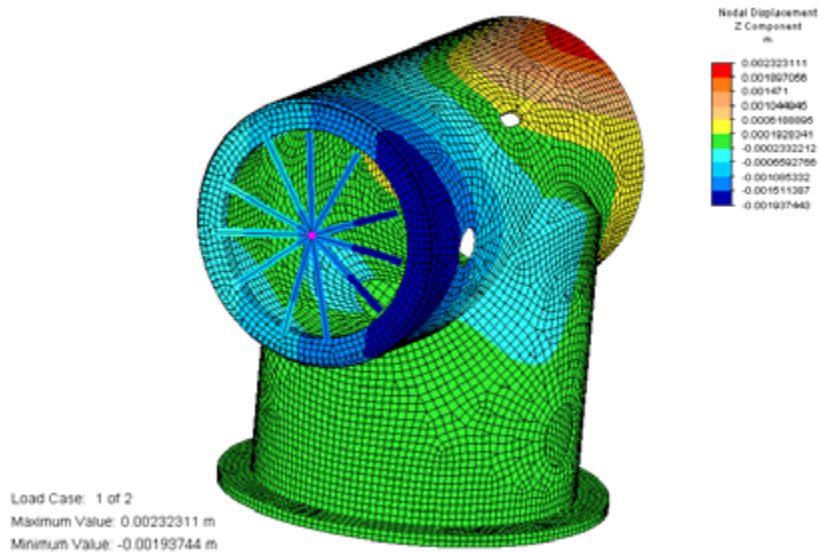


Figure C-16. Displacement and rotation of the turret was extrapolated to the end of the shaft to determine coupling misalignment.

C.2.2 Hub Adapter Stress Analysis

The hub adapter is subject to extreme loads due to the overhung weight of the main shaft and the applied torque. It is also subject to fatigue loads from applied torque, and from the overhung weight. A finite element model was created and loads were applied, as shown in Figure C.17. The ultimate stress was 19 MPa, with a static reserve of 19.0. The fatigue stress from torque was very low, and was neglected. The fatigue stress from the overhung weight was comparatively

high, due to the complete reversal for every revolution. The expected life is 1.5 years of continuous operation, and the fatigue reserve is 1.08, based on a 1-year life. Thus the hub adapter is safe.

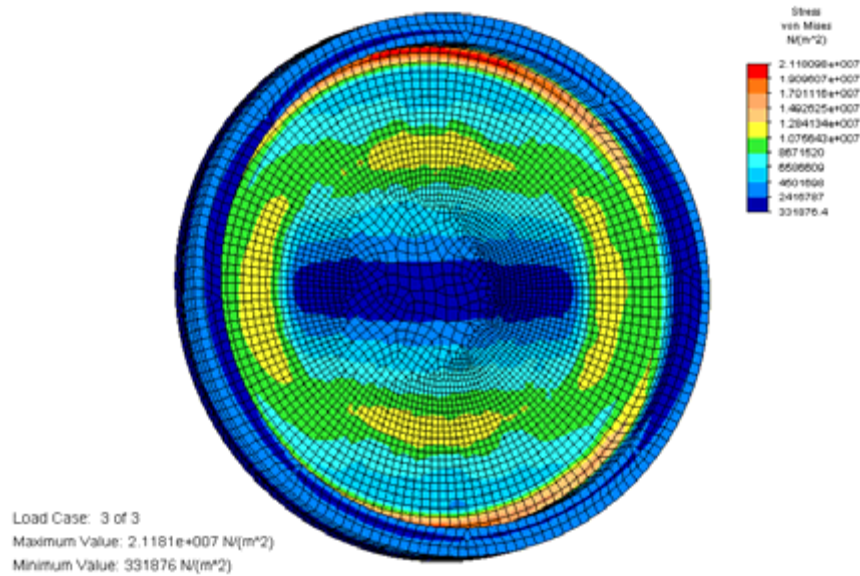


Figure C-17. The hub adapter analysis was dominated by fatigue loading from the overhung mass of the main shaft.

C.2.3 Lifting Plate Stress Analysis

The lifting plate is subject to extreme loads only. Loads are applied to the generator with axis vertical, and with the axis horizontal. The lifting cables were assumed to be 10% off from vertical. A finite element model was created and individual loads were applied, as shown in Figure C.18. The critical ultimate stress was 147 MPa, with a static reserve of 1.08, corresponding to the axis vertical load case. The maximum stress was at the closest hole to the load. The lifting plate is safe for this failure mode.

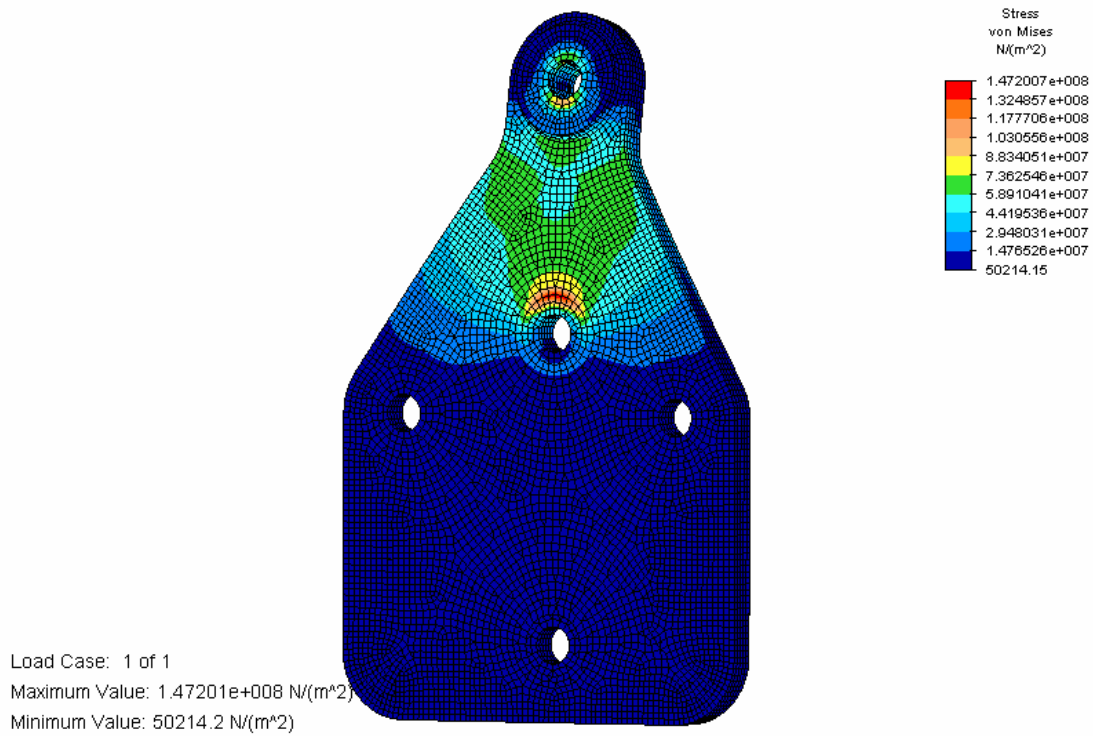


Figure C-18. The lifting plate was analyzed and is safe, even including unbalanced loading due to nonvertical rigging.

The summary of reserves for the test equipment is shown in Figure C-19. All components are safe.

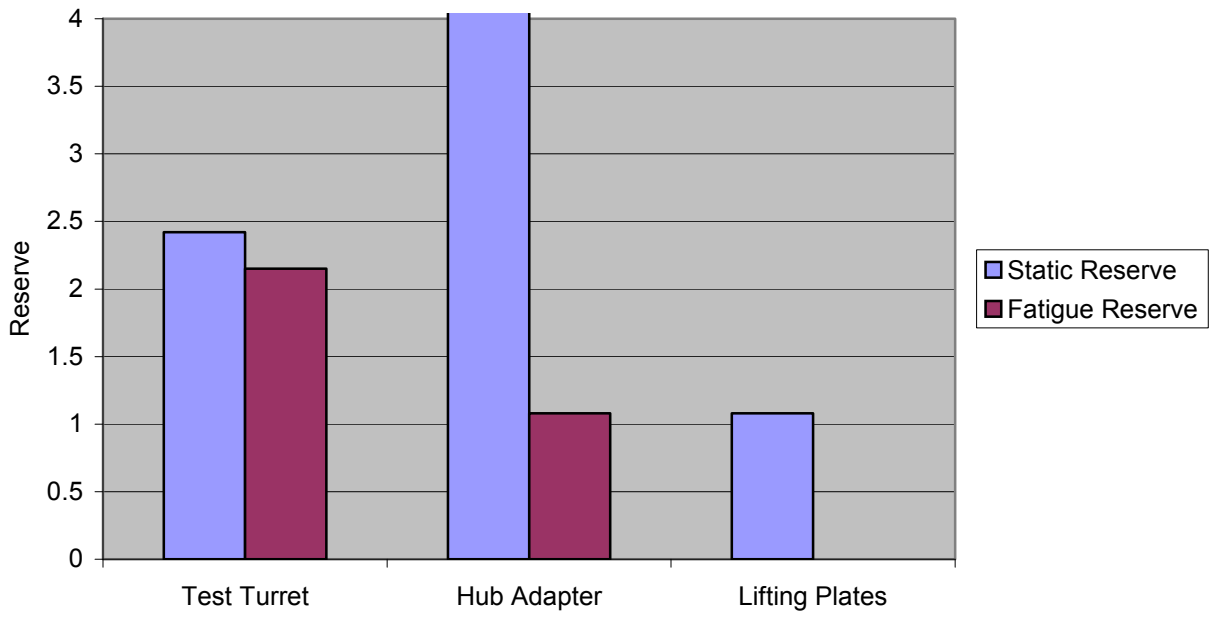


Figure C-19. The static and fatigue reserves of components in the dynamometer assembly were acceptable (Safe Designs > 1.0).

REPORT DOCUMENTATION PAGE

Form Approved
OMB No. 0704-0188

The public reporting burden for this collection of information is estimated to average 1 hour per response, including the time for reviewing instructions, searching existing data sources, gathering and maintaining the data needed, and completing and reviewing the collection of information. Send comments regarding this burden estimate or any other aspect of this collection of information, including suggestions for reducing the burden, to Department of Defense, Executive Services and Communications Directorate (0704-0188). Respondents should be aware that notwithstanding any other provision of law, no person shall be subject to any penalty for failing to comply with a collection of information if it does not display a currently valid OMB control number.

PLEASE DO NOT RETURN YOUR FORM TO THE ABOVE ORGANIZATION.

1. REPORT DATE (DD-MM-YYYY) October 2007		2. REPORT TYPE Subcontract Report		3. DATES COVERED (From - To) April 12, 2001 – September 30, 2006		
4. TITLE AND SUBTITLE Northern Power NW 1500 Direct-Drive Generator			5a. CONTRACT NUMBER DE-AC36-99-GO10337			
			5b. GRANT NUMBER			
			5c. PROGRAM ELEMENT NUMBER			
6. AUTHOR(S) G. Bywaters, P. Mattila, D. Costin, J. Stowell, V. John, S. Hoskins, J. Petter, J. Lynch, T. Cole, A. Cate, C. Badger, and B. Freeman			5d. PROJECT NUMBER NREL/SR-500-40177			
			5e. TASK NUMBER WER6.2201			
			5f. WORK UNIT NUMBER			
7. PERFORMING ORGANIZATION NAME(S) AND ADDRESS(ES) Northern Power Systems, Inc. 182 Mad River Park Waitsfield, VT 05673				8. PERFORMING ORGANIZATION REPORT NUMBER YCX-1-30209-02		
9. SPONSORING/MONITORING AGENCY NAME(S) AND ADDRESS(ES) National Renewable Energy Laboratory 1617 Cole Blvd. Golden, CO 80401-3393				10. SPONSOR/MONITOR'S ACRONYM(S) NREL		
				11. SPONSORING/MONITORING AGENCY REPORT NUMBER NREL/SR-500-40177		
12. DISTRIBUTION AVAILABILITY STATEMENT National Technical Information Service U.S. Department of Commerce 5285 Port Royal Road Springfield, VA 22161						
13. SUPPLEMENTARY NOTES NREL Technical Monitor: Scott Schreck						
14. ABSTRACT (Maximum 200 Words) This report describes work conducted under a subcontract between NREL and Northern Power Systems to identify, design, and test a megawatt-scale wind turbine drivetrain with the lowest overall life-cycle cost.						
15. SUBJECT TERMS wind energy; wind turbine; direct-drive generator; WindPACT						
16. SECURITY CLASSIFICATION OF:			17. LIMITATION OF ABSTRACT UL	18. NUMBER OF PAGES	19a. NAME OF RESPONSIBLE PERSON	
a. REPORT Unclassified	b. ABSTRACT Unclassified	c. THIS PAGE Unclassified			19b. TELEPHONE NUMBER (Include area code)	